Finite Element Modelling for Earthquake Loads on Dykes

Master of Science thesis

Hendrik Pieter Winde

Delft University of Technology
Deltares

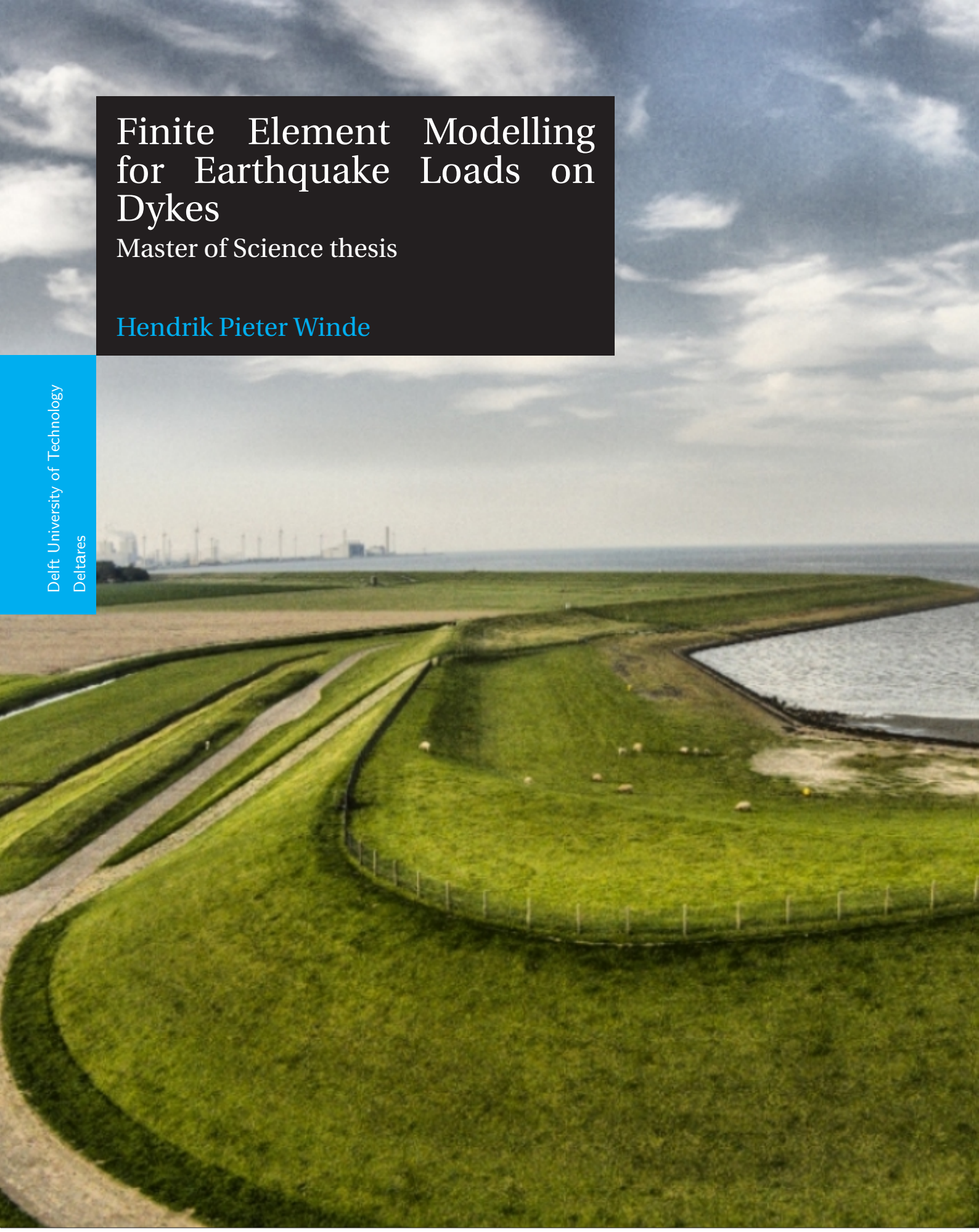

TU Delft Delft University of Technology

Challenge the future

Deltares

Enabling Delta Life

Photo cover page: taken by Emile Wiersum (Wiersum, 2014)

Finite Element Modelling for Earthquake Loads on Dykes

By

Hendrik Pieter Winde

in partial fulfilment of the requirements for the degree of

Master of Science
in Civil Engineering

at the Delft University of Technology,
to be defended publicly Thursday 20th of August 2015 at 16:00.

Thesis committee:	Prof. dr. ir. S.N. Jonkman,	TU Delft
	Dr. ir. R.B.J. Brinkgreve,	TU Delft & Plaxis bv
	Dr. ir. T. Schweckendiek,	TU Delft & Deltares
	Ir. M.A.T. Visschedijk,	Deltares

Email address: erikwinde@hotmail.com

Preface

This report is the result of my master thesis research and can be considered as the last requirement to finish my master Hydraulic Engineering at the Faculty of Civil Engineering and Geosciences of Delft University of Technology.

Over the last few years, a lot of discussion has arisen on consequences of induced earthquakes in Groningen; as consequence of gas extraction. In the nineties, it was assumed that the Dutch flood defence system was not vulnerable to earthquake loading (Lindenberg, 1996). However, the magnitudes of these earthquakes increased as well as the frequency of occurrence. In 2014, Deltares issued a report concluding that earthquakes could damage the flood defences in Groningen (Deltares, 2014). Earthquakes, especially in combination with flood defences, are a rather uncharted territory in the Netherlands. Hence, I am delighted that I had the opportunity to contribute to this topical discussion and hope that with this research I can contribute to the safety of Groningen and its inhabitants.

First of all, I am very grateful to Ryan Phillips of C-CORE for his enthusiastic reponse and provision of the centrifuge test data. In addition, I would like to thank Dharma Wijewickreme and Bronwyn Smyth of University of British Columbia for providing the laboratory test data. Without both datasets, the research could have been conducted the way it has been. Moreover, the availability of the datasets enabled a good comparison between the laboratory results and both constitutive models.

Secondly, I would like to thank the members of my graduation committee Bas Jonkman, Ronald Brinkgreve, Timo Schweckendiek and Marcel Visschedijk for their supervision, criticisms and knowledge in their professional fields. Thanks to my colleagues of Deltares for their great help and the pleasant time I had.

Finally, I would like to thank my family and girlfriend for their support throughout my entire study. Without them, this result would not have be possible.

Hendrik Pieter Winde

Delft, July 2015

Contents

Summary

In the last decades, induced earthquakes were caused by the extraction of gas in the Dutch province of Groningen. Both magnitude and frequency of these earthquakes are expected to increase in the following years, causing a threat for the flood defence system. To guarantee the safety against flooding, it is required to take the influence of earthquake loads on dykes into account.

One of the most important mechanisms that can damage a dyke during an earthquake is liquefaction. The earthquake motion induces an increase of pore water pressure. Consequently, the effective stress decreases. Hence, the shear strength of the soil is reduced; since the shear strength is related to the effective stress. Liquefaction occurs in case of significant development of excess pore water pressure. The soil may lose its strength and act like a fluid. This can result in settlements, increasing the vulnerability to overflow and wave overtopping, and macro instability.

Currently, most methods to determine water pressures are based on tectonic earthquakes; which typically have a deeper hypocentre and larger magnitudes than induced earthquakes in Groningen. Also the EERI MNO-12 monograph, providing probably the most commonly used method to determine the safety against liquefaction, is based on tectonic earthquakes. It is less complicated to include the difference between tectonic and induced earthquakes when using the finite element method. Furthermore, the method according to EERI MNO-12 gives conservative results in terms of excess pore water pressure, which may be predicted more precisely in the finite element method. Lastly, deformations are difficult to predict with EERI MNO-12; whereas this is one of the main purposes of the finite element method.

When applying the finite element method for the prediction of cyclic behaviour, it is required to use a so-called constitutive model. Such models describe the strength and stiffness behaviour of the soil mathematically. These models are based on a constitutive relation, which describes the relation between stress and strain.

For this research, it is required to have a constitutive model that is able to handle cyclic behaviour and development of excess pore water pressures, a so-called effective stress model. Such models are able to take into account the gradual loss of strength as a consequence of pore water pressure build-up; whereas total stress model are not. This research focussed on two constitutive models, which are both able to handle cyclic behaviour: UBC3D-PLM and the Hypoplastic model. Both models are used in PLAXIS 2D AE.02.

The goal of this research is to gain insight in the value and applicability of both the UBC3D-PLM and the Hypoplastic constitutive model for the design of dykes, regarding induced earthquakes; particularly with respect to excess pore water pressure development. The research focuses on the determination of the earthquake load for the Dutch flood defences, the parameter determination for UBC3D-PLM and the Hypoplastic model and it compares the results of both models with centrifuge tests to evaluate their accuracy.

Earthquake loading is relatively new in the Netherland, so currently no guidelines are available for earthquake loading on dykes. The earthquake load, in terms of peak ground acceleration *PGA*, is based on a failure probability requirement. Currently, no earthquake specific values are available for this calculation, so mainly values of other failure mechanisms are adopted; although earthquake loading is significantly different. Moreover, the current calculation method results in extremely large *PGA*s, which are physically not possible. Most researchers agree on the assumption that there must be a physical upper boundary for the *PGA*. However, which value this upper boundary has or how it should be determined is still subject to debate.

Besides, the research describes how to determine the input parameters for both constitutive models. The input parameters of UBC3D-PLM are determined with a correlation with SPT values; the input parameters of the Hypoplastic model are based on sets of Hypoplastic parameters from literature, by comparing three void ratios at zero pressure. The input parameters of both models are calibrated on cyclic DSS tests performed by University of British Columbia. In the research, it is concluded that:

- None of both constitutive models was able to distinguish itself; both models have advantages and disadvantages and their accuracy is similar.
- The SPT relation for UBC3D-PLM parameters is a major advantage.
- A similar relation with CPT values for both constitutive models would be useful.
- Both models need another parameter set in case of static shear.
- The Hypoplastic model is more sensitive to minor changes of the input parameters; considering the predicted amount of cycles to liquefaction.

To evaluate the applicability of both constitutive models, a finite element model is created for each of the two constitutive models to simulate the consequences of an earthquake on an embankment. The predicted accelerations, excess pore water pressure development and settlements are compared with a centrifuge model scale test performed by C-CORE. The conclusion of this validation is that:

- Both models have spurious oscillations in the predicted accelerations. With the Hypoplastic model these oscillations are excessive after the first large acceleration peaks.
- The development of excess pore water pressure is not or hardly influenced by the spurious accelerations.
- The predicted excess pore water pressure development is accurate further away from the slope. Beneath the slope, it is inaccurate and unreliable.
- The displacements are overestimated. The displacement pattern is realistic for UBC3D-PLM, for the Hypoplastic model only till the first large peaks. Hereafter, it is affected by the spurious accelerations.

Based on the validation, it is concluded that both constitutive models are only applicable for horizontal layers beneath a dyke; since the predicted excess pore water pressure development beneath the slope was not satisfactory. Furthermore, both models are not applicable for post liquefaction analysis. The fact that the model parameters can be obtained relatively easily and the cyclic DSS tests can be simulated accurately forms a solid base for future development of both models. However, significant improvement is required to obtain reliable and applicable results. The most important improvement that is required for practical situations is the implementation of static shear stresses in combination with excess pore water pressure development.

1 Introduction

1.1 General introduction

In 1959, the Nederlandse Aardolie Maatschappij (Dutch Petroleum Company, NAM) discovered significant quantities of natural gas in Groningen, near Slochteren. The Dutch government and its population benefited from the gas revenues for several decades, but in the meanwhile two major side effects occurred. Firstly, subsidence caused by compaction of the reservoir (NAM, 2013) and secondly, earthquakes induced by the extraction of gas (Begeleidingscommissie Onderzoek Aardbevingen, 1993). The first recorded induced earthquake occurred on December 26th 1986 (KNMI, 2014). In the years hereafter, both the frequency and magnitude of these earthquakes increased. It is expected by the KNMI that this trend will continue in the next years (Muntendam-Bos & De Waal, 2013).

Hitherto, it was assumed that the impact of earthquakes on flood defences in the Netherlands could be disregarded (Lindenberg, 1996). This opinion became questionable (Verheij et al., 2002) and finally, in 2014, Deltares published a report concluding that earthquakes indeed could be a threat for flood safety in Groningen (Deltares, 2014). In addition, the parties involved with the extraction of gas did not consider earthquakes as safety issue till 2013 (Onderzoeksraad voor Veiligheid, 2015).

Owing to fact that this is a recent development, earthquakes are not taken into account in standard safety assessments for dykes (Ministerie van Verkeer en Waterstaat, 2007). Consequently, there is ignorance how to include earthquakes and which loads should be applied. It is nevertheless required to come up with appropriate design rules as soon as possible; since local water board Noorderzijlvest has decided to advance the reinforcement of the dyke between Eemshaven and Delfzijl (Waterschap Noorderzijlvest, s.a.).

One of the most important mechanisms that can damage a dyke during an earthquake is liquefaction. When liquefaction occurs, saturated loose sand behaves like quicksand; losing its strength and stiffness. Overflow & wave overtopping and macro instability are the dominant failure mechanisms for dykes that are prone to earthquake loading (Deltares, 2014). These mechanisms can be caused by liquefaction.

Currently, most methods to determine water pressures are based on tectonic earthquakes; which typically have a deeper hypocentre and larger magnitudes than induced earthquakes in Groningen. Furthermore, there is little experience with finite element modelling of excess pore water pressures due to earthquakes. In most cases, the predictions are only satisfactory for loading similar to the one that is used to calibrate the model and not for other practical applications (CIRIA, 2013).

1.2 Problem definition

Hitherto, there are no Dutch design rules for earthquake loading on dykes. Hence, it is unknown how to include earthquake loading in the design of flood defences. In addition, it is unknown which design earthquake load should be applied.

One of the consequences of an earthquake might be liquefaction of sand layers in or beneath a dyke. Worldwide, monograph MNO-12 of Earthquake Engineering Research Institute (EERI) (Idriss & Boulanger, 2008) is used to predict liquefaction. This method provides a semi-empirical approach relating the load by means of cyclic stress ratio *CSR* to the resistance of the soil by means of cyclic resistance ratio *CRR.* However, this approach gives conservative results in terms of *CSR* and excess pore water pressure. If the development of excess pore water pressure could be modelled more precisely in the finite element method, it would result in more accurate estimations. This might lead to a more favourable limit state and more efficient designs for dykes.

Moreover, the EERI MNO-12 approach is based on tectonic earthquakes, whereas the earthquakes in the Netherlands are induced. This results in a substantially different earthquake signal; which are shorter in time and hava fewer loading cycles (Deltares, 2013b). This distinction can be made using the finite element method.

Lastly, deformations are difficult to predict with the current semi-empirical approach; while this is one of the main purposes of the finite element method. Using the finite element method could give better insight in the failure process and the appurtenant deformations.

When applying the finite element method for the prediction of cyclic behaviour, it is required to use a so-called constitutive model. Such models describe the strength and stiffness behaviour of the soil mathematically (University of Luxembourg, 2015). These models are based on a constitutive relation, which describes the relation between stress and strain (Puzrin, 2012). Many different constitutive models have been developed due to the large amount of soil types and the many different types of behaviour. One should use the constitutive model that fits best with one's particular question.

For this research, it is required to have a model that is able to handle cyclic behaviour and development of excess pore water pressures, so-called effective stress models. Such models are able to take into account the gradual loss of strength as a consequence of pore water pressure build-up; whereas total stress model are not (Liyanapathirana & Poulos, 2002). Both the UBC3D-PLM and Hypoplastic constitutive model are able to do so (Brinkgreve, 2015).

1.3 Research goal

The goal of this research is to gain insight in the value and applicability of both the UBC3D-PLM and the Hypoplastic constitutive model for the design of dykes, regarding induced earthquakes. In order to evaluate the applicability of both constitutive models, a finite element model is created for each of the two constitutive models to simulate the consequences of an earthquake on an embankment. The results of both finite element models as constitutive models used in the finite element method are compared with a centrifuge model scale test as described in paragraph 6.1. The focus of the research is on the prediction of excess pore water pressures. In addition, the report describes how finite element models could be used for the design of dykes within the Dutch safety standards.

1.4 Research question

The main research question of this study is:

To what extent are the UBC3D-PLM and Hypoplastic constitutive model applicable to modelling the generation of pore pressures and liquefaction in dykes with earthquake loading?

The sub-questions of this study are:

- How can finite element models be applied within the Dutch design approach?
- How to determine the design earthquake load according to the Dutch standards?
- How to obtain the model parameters for the UBC3D-PLM model and Hypoplastic model?
- To what extent are the investigated material models able to reproduce relevant centrifuge tests?

1.5 Research approach & thesis outline

The complete outline of the report is depicted in Figure 1.1. Firstly, relevant information dyke design with earthquake loading is gathered and summarised in chapter two. Paragraph 2.5 describes the calculations that are required for earthquake loading on dykes, whereas paragraph 2.6 describes which of these steps can be done with finite element modelling.

Hereafter, the design earthquake load is determined according to Ontwerpinstrumentarium 2014 (IO2014) (Jongejan, 2014); as described in chapter 3. This chapter elaborates on which parameters should be used to obtain the design earthquake load, how the design earthquake signal should be obtained. This chapter also contains an example for determining the design earthquake load in Groningen.

The principles of finite element modelling and constitutive models are explained in chapter 4. In addition, the constitutive models that are used during the research, UBC3D-PLM and Hypoplastic model, are described in this chapter; as well as their input parameters.

How these parameters should be obtained is stated in chapter 5. The parameters are calibrated on cyclic direct simple shear tests performed by University of British Columbia. Moreover, this chapter provides a sensitivity analysis of the input parameters. This is done by increasing and decreasing all input parameters individually; comparing the amount of cycles to liquefaction.

The next step is to evaluate how accurate the UBC3D-PLM and Hypoplastic constitutive model perform in comparison with practical cases where dykes were subject to earthquakes. However, the data that is required for such calculations is scarce; since it is too difficult and too costly to position measuring equipment in a dyke and wait for an earthquake. Hence, it was decided to use centrifuge tests, performed by C-CORE. In this test, a horizontal acceleration similar to an earthquake was applied on a small embankment in a centrifuge. Measuring equipment was monitoring the horizontal acceleration, excess pore water pressure development and settlement in several different points. A finite element model is created for each of the two constitutive models, to evaluate if the constitutive models are able to reproduce the centrifuge test. Chapter 6 describes the centrifuge tests, the used model input and the results of the validation.

The outcomes of aforementioned chapters come together in chapter 7, which contains the conclusions regarding the research questions. Based on the conclusions, some recommendations for further research are given in chapter 8.

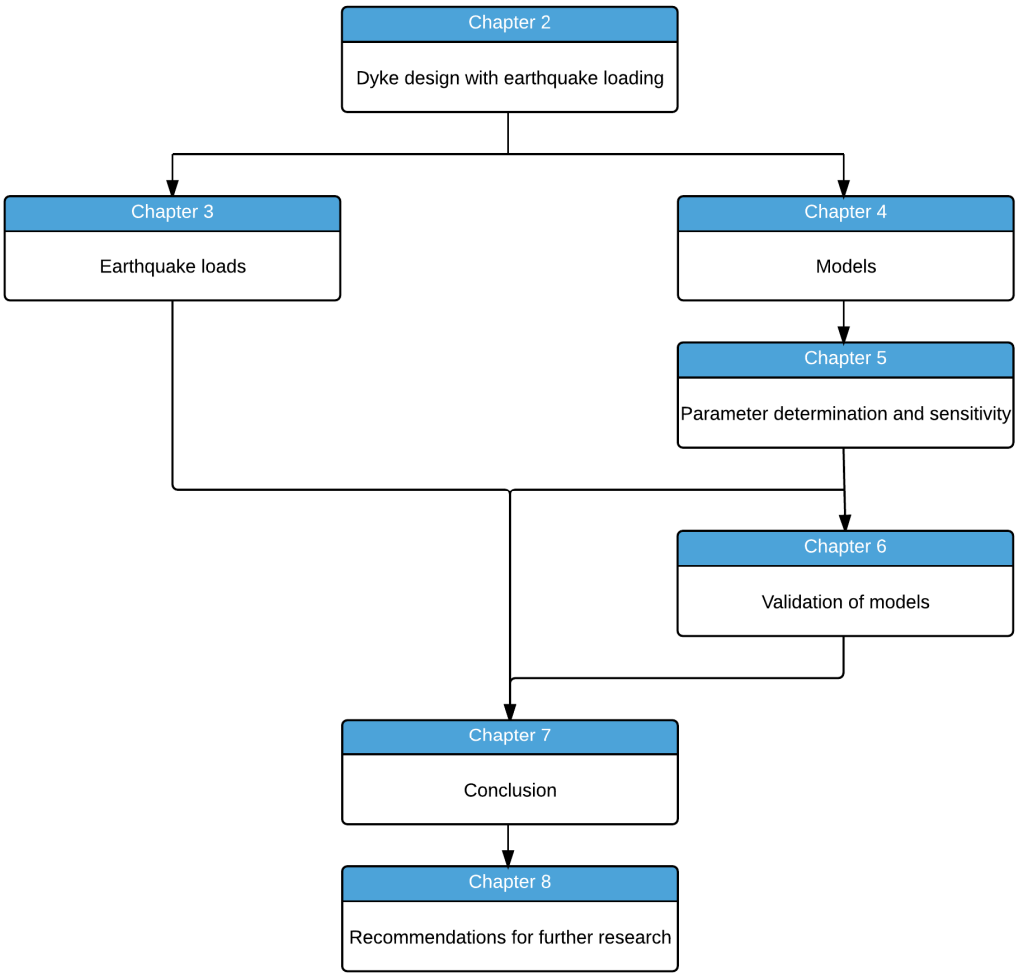

Figure 1.1 Flowchart depicting report outline

1.6 Assumptions

This research focuses on the consequences of earthquakes induced by the production of gas in Groningen. The expression *"induced earthquake"* is therefore related to this type of induced earthquakes in this research; other types of induced seismicity, for instance as a consequence of mining, are not considered.

This research focuses on UBC3D-PLM and Hypoplastic model, because these models are able to handle cyclic/dynamic calculations (Brinkgreve, 2015). Furthermore, they are the closest to application in practice. The Von Wolffersdorff version of the Hypoplastic model is used for this research (Von Wolffersdorff, 1996); extended with the intergranular strain concept (Niemunis & Herle, 1997).

2 Dyke design with seismic loading

2.1 Earthquakes

2.1.1 Mechanisms of induced earthquakes

Several different mechanisms are able to cause induced seismicity related to producing hydrocarbon reservoirs (Grasso, 1992; Green, Styles, & Baptie, 2012; Mulders, 2003; Ottemöller, Nielsen, Atakan, J.Braunmiller, & Havskov, 2005; Van Eijs, Mulders, Nepveu, Kenter, & Scheffers, 2006):

1 Injection of fluids. Increased pore pressures and thus reduction of normal stress may result in fractures.
2 Extraction of fluids. The changes in pore pressure lead to changes in the geological structure.
3 Extraction of hydrocarbon. Massive load removal causes stress pattern changes, resulting in crustal adjustments.
4 Stress diffusion through salt layers.

In the Netherlands, seismicity is primarily caused by reactivation of normal faults at reservoir level (Mulders, 2003; Van Eijs et al., 2006). These faults are mainly reactivated by differential stress development and differential reservoir compaction. Extraction of gas causes reduction in pore pressure, resulting in compaction.

Figure 2.1 shows a schematic cross section of this process. Because the reservoir is coupled to the surrounding rock, it is not able to contract as much as it wants. When differential stress is developed in a reservoir, the vertical effective stress increases more than the horizontal effective stress.

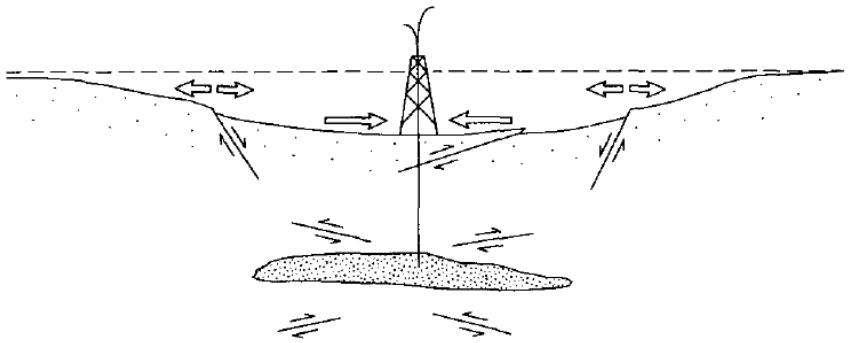

Figure 2.1 Schematic cross section summarising surface deformation and faulting associated with fluid withdrawal (Segall, 1989)

Differential stress development advances frictional sliding on pre-existing normal faults within the reservoir, caused by an induced relative horizontal tension within the reservoir. When reservoir compartments on the same level on either side of a fault plane compact differently, id est not in the same direction or with the same quantity, differential reservoir compaction takes place. (Van Eijs et al., 2006).

Mostly, only differential stress development is not sufficient for reactivation of existing faults. Generally, geometrical anisotropy and differential compaction behaviour on either side of the reservoir is required (Mulders, 2003).

All earthquakes in the northern part of the Netherlands have taken place at a relative shallow depth with respect to tectonic earthquakes. No earthquakes occurred at depths larger than 4 km and most of the earthquakes occurred around a depth of 2.5 km ± 0.5 km (KNMI, 2014; Van Eck, Goutbeek, Haak, & Dost, 2004, 2006).

2.1.2 Magnitudes

Normally, empirical relations are used for ground-motion predictions. These predictions show a large variability, caused by factors like focal mechanism, rupture process, site response and unknown details of 3D crustal structure (Van Eck et al., 2004, 2006). Van Eck et al. state in both reports that small, shallow earthquakes are able to cause large peak ground accelerations (*PGA*). In case of Groningen, this is mainly due to the fact that the hypocentre is much closer to the surface than in case of tectonic earthquakes. The energy released by the earthquake is then dispersed over a smaller area, resulting in larger accelerations.

To obtain the *PGA*, Koninklijk Nederlands Meteorologisch Institutuut KNMI proposed an Ground Motion Prediction Equation GMPE for Groningen (KNMI, 2013b). This GMPE is based on a model for Europe and the Middle East (Akkar, Sandikkaya, & Bommer, 2013) and modified by Bommer after evaluation of the available Groningen data (KNMI, 2013b). Consequently, the GMPE is only valid in Groningen, for magnitudes M_w smaller than 4.2. The applicability of the GMPE for larger magnitudes is uncertain, since no relevant data is available for Groningen. However, KNMI states that this GMPE is currently the best available model.

The proposed GMPE for Groningen is given in equation (2.1) and consist of an earthquake related part, given by equation (2.2), and a soil related part, given by equation (2.3). In the GMPE, ε is the standard normalised residual and σ is the standard deviation. According to KNMI, the standard deviation of the relation is 0.4. The units of *PGA* and PGA_{REF} are g.

Equation (2.2) determines reference peak ground acceleration PGA_{REF}, based on the magnitude M_w and hypocentral distance R_{hyp}. Equation (2.3) takes the soil behaviour into account, with the ratio shear wave velocity between 0 and 30 metres depth V_{S30} and references velocity V_{REF}. V_{S30} is assumed to be 200-300 m/s in Groningen; V_{REF} is defined as 750 m/s.

$$\ln\left(PGA\right) = \ln\left(PGA_{REF}\right) + \ln\left(S\right) + \varepsilon\sigma \tag{2.1}$$

$$\begin{aligned}\ln\left(PGA_{REF}\right) &= -3.161825 + 1.5029M_w - 0.04846\left(8.5 - M_w\right)^2 \\ &+ \left[0.55634M_w - 4.460575\right]\ln\left(\sqrt{R_{hyp}{}^2 + \left(2.593M_w - 3.389\right)^2}\right)\end{aligned} \tag{2.2}$$

$$\ln\left(S\right) = -0.41997\ln\left(\frac{V_{S30}}{V_{REF}}\right) - 0.28846\ln\left(\frac{PGA_{REF} + 2.5\left(\frac{V_{S30}}{V_{REF}}\right)^{3.2}}{\left(PGA_{REF} + 2.5\right)\left(\frac{V_{S30}}{V_{REF}}\right)^{3.2}}\right) \tag{2.3}$$

The *PGA* increases significantly for lower probabilities. This may result in estimations with *PGA*s that are physically impossible; since the *PGA* is limited by the damping in the soil layers at the surface; which is related to shearing of these layers (Bommer et al., 2004). This phenomenon is described by Bommer et al. as: *"Once failure is reached at a given depth within the soil profile, the incident motion is filtered and no motion larger than the motion reached at the failure stage can be transmitted to the upper strata."* This provides an upper boundary for the *PGA*, based on the conditions of the soil layer. Assuming that vertical propagation of SH waves is responsible for the main part of the horizontal motion and that the vertical propagation of P waves causes the main part of the vertical motion, Bommer et al. state that the soil strength limits the horizontal ground motion. This assumption has two requirements. Firstly, the soil has to be practically horizontal layered and secondly, the motions propagate vertically.

Although it is known that the *PGA* is limited, the actual value of the upper boundary is still not unambiguous. Several researches result in different values, from 0.15g for very soft marine deposits to 1.89g for overconsolidated clays (Bommer et al., 2004).

Most induced earthquakes in the Netherlands are between 1.0 and 2.0 on Richter scale and a few earthquakes had a magnitude larger than or equal to 3.0 on Richter scale; the largest induced earthquake to date took place in Huizinga on August 16th 2012 and had a magnitude of 3.6 on Richter scale (KNMI, 2014).

It is unclear what the maximum magnitude of an induced earthquake could be. Grasso says: *"For a minimum of 80% of commercially productive basins, most of the local deformation is reported as aseismic, i.e., there is no evidence for $M_L \geq 3$ earthquakes"* (Grasso, 1992). Other literature estimates the maximum M_L for the Netherlands to be 3.8 with an 85% confident limit and an maximum M_L of 4.0 for a confident limit of 95% (De Crook, Haak, & Dost, 1998). Van Eck et al. continued this research in 2004 with all earthquake data up to mid-October 2003. With the same method as De Crook et al., they came up with a mean M_{max} of 3.6 and an 84% confidence limit at a M_{max} of 3.9 (Van Eck et al., 2004). For the Bergermeer field, a maximum magnitude of 3.8 is expected (Logan, Higgs, & Rudnicki, 1997). For the construction of the NUON energy plant in Eemshaven, $M_L \geq 2.3$ and $M_L \geq 4.0$ are assumed, with an annual probability of 0.6 and 0.001, respectively (Van Eck, Goutbeek, & Dost, 2007). Due to the large uncertainties, the KNMI estimates a conservative upper limit at $M_{max} = 5.0$ (KNMI, 2013a). Minister Kamp states that for the short term, the next three years, the maximum magnitude is 4.1, with a probability of exceedance of 10% (Kamp, 2014). For 2013-2023, the NAM predicts a maximum magnitude of 4.2, 4.9 or 5.4, for a probability of exceedance of 50%, 10% or 1%, respectively (NAM, 2013). Summarising, the actual maximum magnitude is unclear and the trend over the last two decades is that the predicted maximum magnitude increases.

The KNMI states that, since the beginning of seismicity, the seismicity rate of the Groningen field has been increasing significantly. Furthermore, the KNMI says that there is no evidence for a maximum magnitude, based on the distribution of magnitudes (Muntendam-Bos & De Waal, 2013).

The largest *PGA* measured in the north of the Netherlands till the end of 2003 was 3.04 m/s^2 in Roswinkel in 1997 (Dost, Van Eck, & Haak, 2004). Based on van Eck et al. (2006), it is concluded that the *PGA* for the Eemshaven ranges from 0.15g to 0.25g for a probability of exceedance of 0.1 or 0.01, respectively (Van Eck et al., 2007). It should be taken into account that these values are associated with large uncertainties (Van Eck et al., 2006).

Minister Kamp assumes for the short term, the next three years, a maximum ground acceleration of 0.12g; with a probability of exceedance of 10% (Kamp, 2014). Verheij et al. recommended in 2002 to use a maximum *PGA* of 3.2 m/s^2, with a return frequency of 1/100 year (Verheij et al., 2002). The KNMI states a maximum *PGA* value of 0.42g with a probability of exceedance of 10% in 50 years (KNMI, 2013b). Lastly, the NAM predicts a maximum *PGA* of 0.57g, 5.6 m/s^2, for 2013-2023 with an average annual probability of exceedance of 0.2%. This is equivalent to the value stated by Eurocode 8, but for an assessment period of 10 years (NAM, 2013).

2.1.3 Site response

Site response or site effect is the phenomenon that properties of the earthquake are influenced by shallow soil layers. This effect depends on a several parameters (Wassing, Maljers, Westerhoff, Bosch, & Weerts, 2003):

- shear modulus G or shear wave velocity V_s in the top soil layers;
- damping ratio β occurring in the top soil layers;
- the eigenfrequency of the site, f_{site}, or the site period, T_{site}, and the occurrence of large impedance ratios I in the soil, which could lead to amplification or resonance;
- depth till bedrock
- strength, frequency content and duration of the earthquake signal and the amount of cycles N;
- topographic effects;
- 3D variation in soil structure.

Geologists ascertain that soft clays can amplify ground motions, resulting in larger ground motions for softer soil types (Ashford, Jakrapiyanun, & Lukkunaprasit, 2000; Booth & Key, 2006; Sun, Chang, Bray, & Mejia, 1993; U.S. Geological Survey; Wassing et al., 2003). According to Wassing et al., soft, low consolidated soil, like peat and clay, has a lower shear modulus and shear wave velocity than densely packed sand and gravel layers or rock. Wave amplitudes, and with that peak velocities, are larger for peat or clay than it would be in sand, gravel or rock; assuming the same dynamic load and damping.

Wassing et al. reports that a higher damping ratio results in a larger decrease in amplitude. The damping ratio has a non-linear relation with the shear deformation; it increases significantly with increasing shear deformation. Furthermore, the damping ratio decreases with an increasing amount of cycles. This means that the damping factor also depends on the time scale of the earthquake. Moreover, the damping ratio depends on:

- mean effective soil stress;
- depth;
- *OCR*;
- void ratio;
- plasticity index.

When the eigenfrequency of the site, f_{site}, or the eigenfrequency of a soil layer with a large impedance contrast with respect to adjacent layers is close to the dominant frequency of the earthquake, the site response is large (Wassing et al., 2003).

In general, the most important condition for impedance contrast is the transition from bedrock to overlying sediment layers. This is of minor importance in the Netherlands, since this transition normally occurs at much larger depths. An important impedance contrast is found in the northern part of the Netherlands on the boundary of the soft cohesive Holocene deposits and the more stiff Pleistocene deposits (Verheij et al., 2002; Wassing et al., 2003).

For small *PGA*s, the amplification factor is relatively large. Figure 2.2 and Figure 2.3 depict that the amplification factor decreases for larger *PGA*s; approaching an amplification factor of 1.0 or even smaller. In 2013, Stewart and Seyhan derived updated NEHRP site amplification values, based in a reference V_{s30} of 760 m/s, instead of 1050 m/s. It is expected that these values appear in the 2015 version of the NEHRP *Provisions.*

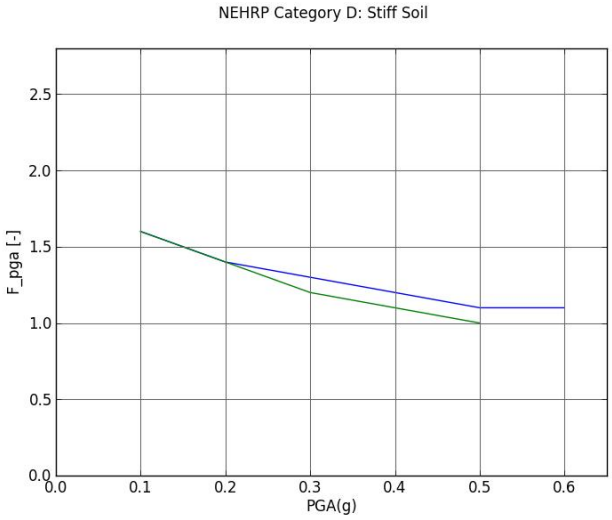

Figure 2.2 Amplification factor as function of PGA, for stiff soils [based on (Stewart & Seyhan, 2013)]. The blue line represents the original values; the green line represents the updated values of Stewart and Seyhan (2013).

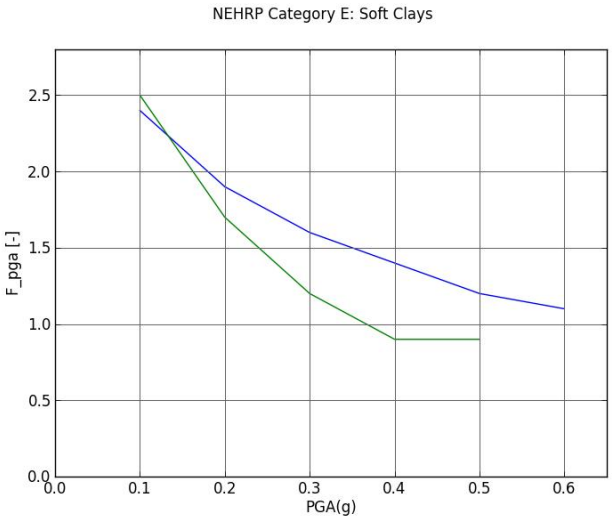

Figure 2.3 Amplification factor as function of PGA, for soft clays [based on: (Stewart & Seyhan, 2013)]. The blue line represents the original values; the green line represents the updated values of Stewart and Seyhan (2013).

2.2 Liquefaction

Liquefaction is the phenomenon that *"loose sand tends to contract under cyclic loading imposed by earthquake shaking, which can transfer normal stress from the sand matrix onto the pore water if the soil is saturated and largely unable to drain during shaking. The result is a reduction in the effective confining stress within the soil and an associated loss of strength and stiffness that contributes to deformations of soil deposit."* (Idriss & Boulanger, 2008). Terzaghi's formula in equation (2.4) shows that the effective stress σ' decreases when soil stress σ remains constant and pore water pressure u increases.

$$\sigma' = \sigma - u \tag{2.4}$$

The Mohr-Coulomb failure criterion states that the shear strength τ depends on the effective stress σ', friction angle φ' and cohesion c; as given in equation (2.5). As a result, the shear strength of the soil decreases when the effective stress is lower due to higher pore water pressures.

$$\tau = \sigma' \tan\left(\phi'\right) + c \tag{2.5}$$

According to Idriss and Boulanger, the stress-strain response of sand to monotonic or cyclic loading strongly does depend on:

- relative density D_R;
- effective confining stress;
- stress history;
- mode of deposition;
- several other factors.

2.2.1 CSR

Idriss and Boulanger state that the excess pore water ratio r_u for undrained cyclic triaxial loading and for standard cyclic simple shear tests can be determined with equation (2.6) and (2.7) respectively; as a function of the excess pore water pressure Δu and either the minor effective consolidation stress σ'_{3c} or the vertical effective consolidation stress σ'_{vc}. The maximum possible value for r_u is 1.0.

$$r_u = \frac{\Delta u}{\sigma'_{3c}} \quad (undrained\ cyclic\ triaxial\ test) \tag{2.6}$$

$$r_u = \frac{\Delta u}{\sigma'_{vc}} \quad (cyclic\ simple\ shear\ test) \tag{2.7}$$

A larger *CSR* means that fewer loading cycles are required to trigger liquefaction. The *CSR* for isotropically consolidated cyclic triaxial tests depends on the cyclic deviatoric stress $q_{cyc}/2$ and σ'_{3c}, as stated in equation (2.8). Similarly, the *CSR* for simple shear tests depends on the cyclic shear stress, τ_{cyc}, and σ'_{vc}, as shown in equation (1.9).

$$CSR = \frac{q_{cyc}}{2\sigma'_{3c}} \quad (undrained\ cyclic\ triaxial\ test) \tag{2.8}$$

$$CSR = \frac{\tau_{cyc}}{\sigma'_{vc}} \quad (cyclic\ simple\ shear\ test) \tag{1.9}$$

2.2.2 CRR

The cyclic resistance ratio *CRR*, as function of the number of loading cycles *N*, is expressed by the coefficients *a* and *b* as shown in equation (2.10) (Idriss & Boulanger, 2008).

$$CRR = a * N^{-b} \tag{2.10}$$

A larger relative density results in a larger coefficient *a* and thus a higher *CRR*. Moreover, the tendency of sand to contract or dilate depends on the effective confining stress and so does the *CRR*. Overburden correction factor K_σ shows the dependence of the *CRR* on consolidation stress; depending on the *CRR* of a soil under a specific value of effective consolidation stress σ'_c, $CRR_{\sigma'c}$ and the *CRR* of the same soil when σ'_c = 1 atm (approximately 100 kPa), $CRR_{\sigma'c=1}$; as shown in equation (2.11) which was developed by H. Bolton Seed 1983. K_σ depends on D_R and the type of test device and its determination is given in paragraph 3.7 of EERI MNO-12.

$$K_\sigma = \frac{CRR_{\sigma_c'}}{CRR_{\sigma_c'=1}} \tag{2.11}$$

Different states of consolidation stresses for cyclic simple shear and cyclic triaxial tests are the cause of differences in the measured *CRR*. In equation (2.12) is the approximation given which relates the *CRR* for anisotropically consolidated specimens, with $K_0 \neq 1$, to the *CRR* for isotropically consolidated specimens ($K_0 = 1$) (Idriss & Boulanger, 2008).

$$CRR_{K_0 \neq 1} = \left(\frac{1+2K_0}{3}\right) CRR_{K_0=1} \tag{2.12}$$

The relation between the *CRR* from a simple shear test, CRR_{SS}, to the *CRR* from the ICU triaxial test, CRR_{TX}, is shown in equation (2.13) (Idriss & Boulanger, 2008).

$$CRR_{SS} = \left(\frac{1+2(K_0)_{SS}}{3}\right) CRR_{TX} \tag{2.13}$$

According to Idriss and Boulanger, this relation is endorsed by several researchers in the 1970s.

EERI MNO-12 also reports that the *CRR* decreases with 10-15% when a second direction of cyclic loading is added. The relation between in-situ CRR_{field} and either CRR_{TX} or CRR_{SS} is given in equation (2.14) and equation (2.15), respectively.

$$CRR_{field} = 0.9\left(\frac{1+2(K_0)_{field}}{3}\right)CRR_{TX} \tag{2.14}$$

$$CRR_{field} = 0.9\left(\frac{1+2(K_0)_{field}}{1+2(K_0)_{SS}}\right)CRR_{SS} \tag{2.15}$$

Similar to K_σ in equation (2.11), H. Bolton Seed developed in 1983 a correction factor K_α, representing the effects of an initial static shear stress ratio α on the cyclic strength. This correction factor depends on the relative density and the confining stress. Moreover, it depends on the used failure criteria for *CRR* and the laboratory test device; a simple shear test gives a more approximate result than a triaxial test. Equation (2.16) gives this relation. The determination of K_α is given in paragraph 3.8 of EERI MNO-12.

$$K_\alpha = \frac{CRR_\alpha}{CRR_{\alpha=0}} \tag{2.16}$$

2.2.3 Safety against liquefaction

The preclude liquefaction in sand layers, the safety factor against liquefaction FS_{liq} should be larger than 1.0. This safety factor is the ratio of the resistance against liquefaction by means of *CRR* over the loading by means of *CSR*; as shown in equation (2.17) (Idriss & Boulanger, 2008).

$$FS_{liq} = \frac{CRR}{CSR} \tag{2.17}$$

The rate of pore pressure generation and the magnitude of the residual pore pressure are both influenced by the presence of sustained static shear stresses ($\alpha > 0$). These stresses can, for example, occur beneath sloping ground and they limit the value for r_u to a value smaller than 100%. This limited value is lower for a larger value of α.

Two other ways to evaluate undrained cyclic loading behaviour are strain-based and energy-based, which are described briefly in chapter 42 and 45, respectively, of the EERI MNO-12 report.

2.2.4 Void redistribution

Idriss and Boulanger state that one of the major difficulties with determining stress loss and deformations is the fact that the excess pore water pressure dissipates over time, since the pore water flows zones of lower excess pore water head. This effect is called void redistribution and it is not replicated with laboratory tests. When this flow is upward into another sand layer, the excess pore water pressure in that layer will increase. These flows result in dilation at the top of the liquefied layer and contraction at the bottom. This might cause liquefaction in this sand layer, while the *CRR* was initially sufficiently large. Moreover, water films or water pockets may be formed, which either slowly dissipate through the overlaying layer or break through and form cracks or piping channels. The consequence of this problem is that the shear strength and stress-strain response do not solely depend on the soil parameters and state. The effects of this phenomenon are still unclear and normally not included in engineering practice.

2.2.5 Triggering of liquefaction

The degree of liquefaction depends on:

- the distribution of cohesionless sediments within the deposit;
- a sufficiently high water table.

Table 1 on page 60 and 61 of EERI MNO-12 gives an overview of susceptibility of soil deposits to liquefaction. Normally, liquefaction occurring at depths of less than approximately 15 meters is noticeable at ground surface level. Figure 2.4 depicts the cyclic stresses during horizontal shaking.

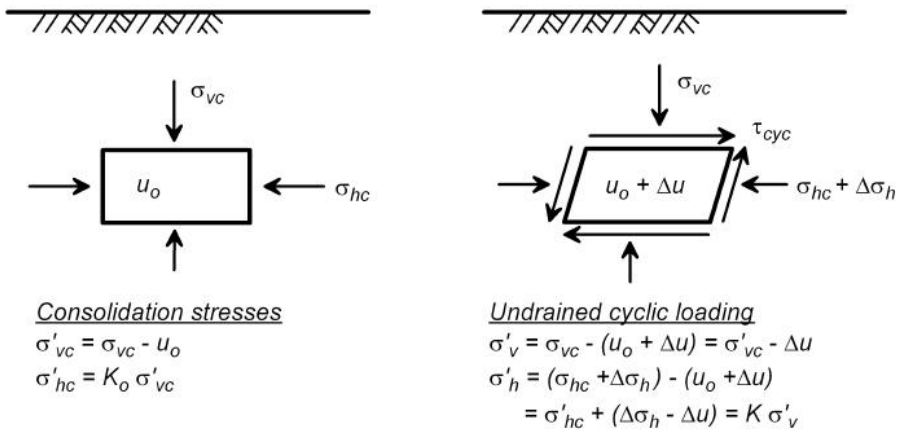

Figure 2.4 Cyclic stresses on a soil element beneath level ground during horizontal shaking (Idriss & Boulanger, 2008)

2.2.6 Correction of in-situ test results

Penetration resistances measured with SPT and CPT increase with increasing confining stress. This means that the N_{60} and q_c values from different locations and depths cannot directly be compared with each other in case of different vertical effective stresses. Paragraph 3.5 of EERI MNO-12 describes how to determine the overburden correction of in-situ test results.

2.2.7 MSF

The magnitude scaling factor *MSF* is used to convert the *CSR* and/or *CRR* that belongs to a certain magnitude into a common magnitude; normally $M = 7.5$ is used. Equation (2.18) gives this relation for the *CRR*.

$$MSF = \frac{CRR_M}{CRR_{M=7.5}} \tag{2.18}$$

According to EERI MNO-12, *MSF* can be derived by combining two interdependent relations:

- the laboratory based relation between the *CRR* and the number of uniform stress cycles;
- the correlation of the number of equivalent uniform cycles with earthquake magnitude.

2.2.8 Relation of SPT and CPT to triggering of liquefaction

SPT and CPT results can be related to the triggering of liquefaction, based on their relation with the *CRR*. For clean sands, this relation is stated in paragraph 3.10 of EERI MNO-12, whereas this relation for silty sand is given in paragraph 3.11. Both paragraphs include graphs relating the *CSR* to the $(N_1)_{60}$ or the CPT tip resistance. An example of such a graph is depicted in Figure 2.5.

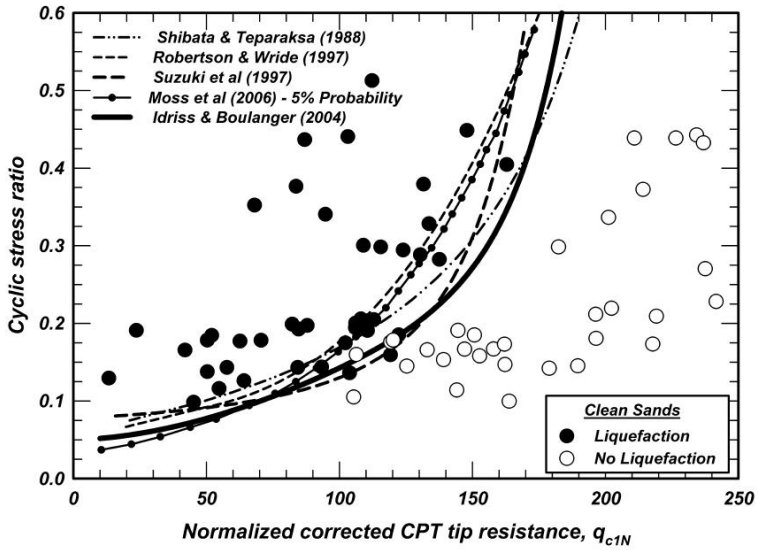

Figure 2.5 Curves relating CRR to q_{c1N} (Idriss & Boulanger, 2008)

2.2.9 Factors that affect liquefaction susceptibility

The liquefaction susceptibility of a soil layer is influenced by many factors. Tsegaye (2009) gives in paragraph 2.4 of his report an extensive description of the influences of a few factors to the liquefaction susceptibility (Tsegaye, 2009). These factors are:

- grain size and gradation;
- soil fabric;
- relative density and definition of state of soil;
- fines content;
- degree of saturation;
- preloading.

2.2.10 Summary of liquefaction consequences

In general, several failure modes can occur due to liquefaction (National Research Council, 1985):

- Sand boils. This is an evidence of excess pore water pressure. Significant amounts of sediment are transported to the surface.
- Flow failures. These failures are normally the most catastrophic ones, since they are able to displace large masses of soil for tens of meters. The failure of the Lower San Fernando Dam during the 1971 San Fernando earthquake is an example of this failure type.
- Lateral spreads. This is the lateral displacement of soil caused by liquefaction in a subsurface layer.
- Ground oscillation. At locations where the slope is too gentle for lateral displacement, liquefaction in the subsoil decouples the overlying soil. This results in soil blocks that can wobble on the liquefied layer.
- Loss of bearing capacity. Liquefied soil loses strength, which could result in settlements of structures.
- Buoyant rise of buried structures. Light weight structures, for instance pipelines, could rise buoyantly when surrounding soil is liquefied.
- Ground settlement. Soil densification due to liquefaction causes subsidence.
- Failure of retaining walls. Increased lateral stresses on the walls could lead to failure.

Table 2.1 gives an overview of liquefaction consequences.

Table 2.1 Overview liquefaction consequences (Rauch, 1997)

In Situ Stress Condition	Soil Behaviour	Typical Field Observation
No driving shear stress	• Volume decrease • Pore pressure increase	• Ground settlement • Sand boils and ejection from surface fissures
Driving shear greater than residual strength	• Loss of stability • Liquefaction	• Flow slides • Sinking of heave buildings • Floating of light structures
Driving shear less than residual strength	• Limited shear distortion • Soil mass remains stable	• Slumping of slopes • Settlement of buildings • Lateral spreading

2.2.11 Mitigation of liquefaction

There are several ways to cope with consequences of liquefaction. Firstly, it is possible to take no measures and either accept the potential damage or abandon the location. Secondly it is possible to modify the design of the soil structure to reduce or preclude damage. Lastly, it is possible to improve the ground. There are many ways to do so, as described in paragraph 5.2 of EERI MNO-12. The main mechanism is to densify the soil. This can be done by vibrating equipment, explosives, deep dynamics compaction, insertion of compaction material like grout and drainage. Another method is soil improvement, by removing loose sand and replacing it with denser sand.

2.3 Earlier work on the influence of earthquakes on Dutch flood defences

The awareness that earthquakes could form a risk regarding safety against flooding has grown in the last two decades. In 1996 was the conclusion that earthquakes do not threaten the Dutch flood defence system, whereas in 2014 it was concluded that earthquakes are a major risk.

2.3.1 Lindenberg (1996)

In 1996, there was no reason to take earthquake loads into account for the Dutch flood defences (Lindenberg, 1996). This assumption was based on calculations on stability, excess pore water pressure and upper limits for slope displacements. However, this report is focussing on the tectonic earthquakes in Limburg. The induced earthquakes in Groningen were less significant at that time. Lindenbergs reports states that the probability on a severe earthquake in the south-eastern part of the Netherlands is significantly higher than in other parts of the Netherlands.

2.3.2 Verheij et al. (2002)

In later research it was concluded that the probability on a decreased safety against flooding was negligible when only taking into account the frequencies of the combined occurrence of significant earthquakes and high water; corresponding to mean high water or the water level required by the norm (Verheij et al., 2002). The earthquakes could damage the dyke, but this damage is small enough to neglect the probability on inundation. Lastly, this report states that at that moment it could not unambiguously be concluded that the effect of earthquakes is negligible. This is mainly due to several uncertainties like the definition of the design earthquake, amplification factor, applied slope stability model and reserve in slope stability. Moreover, no location specific research was done for this report.

According to Verheij et al., the risk with respect to instability of dykes during earthquakes is determined by (Verheij et al., 2002):

- the magnitude and duration of the earthquake;
- the composition of the Holocene deposits on the older subsoil, principally the contrast between the soft top layer and the denser subsoil;
- the thickness of the soft top layer.

2.3.3 Deltares (2014)

In 2014, Deltares produced a report about the quay walls and dykes in Groningen with induced earthquakes. This report includes (Deltares, 2014):

- collecting basis data;
- formulating safety philosophy;
- strength-analysis without earthquake load;
- analysis of stability and height with earthquake load.

The Deltares report considers three failure mechanisms (Deltares, 2014):

- Macro instability land side (with Bishop and Uplift Van models).
- Macro instability sea side (with Bishop model)
- Lowering of the crest height; due to:
  - macro instability (without collapsing);
  - deformations due to compaction;
  - deformation due to squeezing.

In 2014, it became apparent that earthquakes could be a risk for flood safety. Deltares concluded in 2014 that dykes often have significant reserves with respect to the crest height in situations in which the water level is not normative. Therefore, stability is critical. Approximately 45% of the 90 km primary flood defence system in Groningen does not satisfy the standards when including the earthquake loads. According to Deltares is it not possible to exclude the necessity for improvement for at least 40 km of primary flood defence. It should be noted that this conclusion is based on a rough schematisation, including only a single soil profile for the full seventy kilometres of primary flood defence.

2.4 Design guidelines

2.4.1 Dutch law

The Dutch water law, the “waterwet”, contains the regulations related to water safety and water quality in the Netherlands. The local water boards are responsible for the construction, management and maintenance of the flood defence system (Weijers & Tonneijck, 2009). Article 2.12 states that the water boards report the hydraulic conditions of the primary flood defence to the minister every twelve years.

The present standards are based on the annual probability of exceedance of design hydraulic loads; based on a semi-probabilistic approach. In the future, the standards will be based on the failure probability of a dyke section with a certain length. A failure probability budget divides the accepted combined failure probability (100%) into probabilities for each individual failure mechanism. Furthermore, the length effect will be included. The new water law contains, inter alia, new standards with respect to flood safety and is introduced on January 1st 2017. Hence, the accessory statutory assessment guideline (“Wettelijk Toetsinstrumentarium 2017”; WTI2017) will be introduced in 2017. The concept version of WTI2017 will be finished on January 1st 2017; the final version will be finished on January 1st 2019 (Helpdesk Water, 2014). The fourth safety assessment starts in 2017, according to the new regulations, and will be finished in 2023 (Schultz van Haegen, 2014).

According to the new regulations everyone in the Netherlands should have a safety level of 10^{-5}, corresponding to a probability of decease of 1/100,000 per year. Furthermore, additional safety is required for locations with large groups of casualties, significant economic damage or severe damage due to break down of vital and vulnerable infrastructure which is of national importance (Schultz van Haegen, 2014).

Currently, a proposal for the specifications of standards for primary flood defences is designed in the Delta programme, forming the basis for the preparation of new statutory flood safety standards in 2017. In order to anticipate the new standards, a design guideline (“Ontwerpinstrumentarium 2014”; OI2014) has been introduced (Heijn, 2014).

This guideline provides indicative values for an acceptable failure probability, representing the state of the art with respect to a technical study. These values do not have a legal status, but can be used for a sensitivity analysis regarding the new safety standards; which is likely to fulfil the future safety standards. Three types of probabilities are defined:

- Maximum allowed probability of flooding. This is the probability representing the situation that the costs of improvements are barely equal to the benefits.
- Centre probability. This probability is between the rejection probability and the optimal design probability and related to the average damage between two investments. It can be considered to be a signal. After this value, it takes approximately twenty years before the maximum allowed probability of flooding is exceeded.
- Optimal design probability. This probability is based on a life-cycle cost analysis.

The norms or concept norms are described as centre probability; the design probability is normally a factor two larger (Rijkswaterstaat, 2014). The aim of the new regulations is that all primary flood defences satisfy the new standards in 2050 (Schultz van Haegen, 2014; Staf deltacommissaris, 2014).

Furthermore, the length effect is included in the failure probability calculation. It relates the required failure probability P_j of independent sections to the acceptable failure probability for the entire system P_{req}, with the contribution to the failure probability budget ω, a constant that indicates which part of the trajectory's length is sensitive to the specific failure mechanism a, the considered trajectory length L_t and the typical section for the specific failure mechanism L_j; as shown in equation (2.19) (Jonkman & Schweckendiek, 2015; Rijkswaterstaat, 2014).

$$P_j = \frac{P_{req} \cdot \omega}{1 + \frac{aL_t}{L_j}} \tag{2.19}$$

2.4.2 Eurocode

Currently, the Eurocode 8 part 5 (NEN-EN 1998-5 (en)) norms are not obligatory to use. It can be used to habituate to the new norms when the national appendix is finished.

No national appendix is available yet; this appendix will be introduced within a few years. An interim advice will be used first and later the NPR 9998 is used. Both are elaborated in paragraph 2.4.4 and 2.4.3, respectively.

In paragraph 4.1.3.3 of Eurocode 8 part 5, the methods of analysis are described. It prescribes, for instance, that softening of the response with increasing strain level should be taken into account. Besides, the possible effects of pore pressure increase under cyclic loading should be taken into account. This paragraph describes eight other regulations regarding analyse methods.

According to paragraph 4.1.4 of Eurocode 8 part 5, a shear strength and stiffness reduction should be taken into account, due to the increase in pore water pressures in saturated cohesionless materials during earthquake ground motion. This could lead to significant permanent deformations or liquefaction. Furthermore, thirteen other regulations with respect to potentially liquefiable soils are given in this paragraph.

Similarly, Eurocode 8 part 5 provides regulations about settlements due to cyclic loads. In paragraph 4.1.5, it states that the susceptibility to densification and excessive settlements should be taken into account in case of extended layers or thick lenses of loose, unsaturated cohesionless materials occur at a shallow depth. Moreover, the other regulations regarding settlements and densification are given in this paragraph.

Paragraph 4.2 of Eurocode 8 gives the regulations which are related to ground investigation. It states, inter alia, that "*the profile of the shear wave velocity V_S should be regarded as the most reliable predictor of the site-dependent characteristics of seismic action at stable sites".* Table 4.1 on page 20 gives the average soil damping ratios and average reduction factors for shear wave velocity V_S and shear modulus G within 20 m depth (Nederlands Normalisatie Instituut, 2005).

2.4.3 NPR 9998

To tide over the time before the national appendix to Eurocode 8 is ready, it has been decided to make a so-called Nederlandse Praktijkrichtlijn (NPR; "Dutch practice guideline"): NPR 9998.

The NPR 9998 focusses on earthquake resistant buildings and has the preliminary title "Ontwerp en beoordeling van aardbevingsbestendige gebouwen bij nieuwbouw, verbouw en afkeuren – geïnduceerde aardbevingen", which means "Design and assess of earthquake resistant buildings for the construction of new buildings, renovation and rejection – induced earthquakes". The main difficulty drafting this guideline is the fact that there is a significant difference between the induced earthquakes in Groningen and conventional, tectonic, earthquakes elsewhere in the world (NEN, s.a.). The first version is currently available for consultation; the final version is expected in autumn 2015 (NEN, s.a.).

2.4.4 Interim advice

Until the NPR 9998 is released, an interim advice is used in combination with Eurocode 8; NEN-EN 1998 series. This interim advice is called *"Voorlopige ontwerpuitgangspunten voor nieuwbouw en verbouw onder aardbevingsbelasting ten gevolge van de gaswinning in het Groningenveld"*, which means *"Preliminary design principles for the construction of new buildings and renovation under earthquake loading as consequence of gas production in the Groningen gas field"* (Nederlands Normalisatie Instituut, 2014).

2.5 Failure mechanisms

Failure mechanisms are the different mechanisms describing the way a flood defence could be damaged or even collapse. Some of them are more likely to occur than others and not all of them are vulnerable to earthquake loads. The paragraphs below summarise the most relevant failure mechanisms with respect to earthquake loading. The consequences of earthquake loading on dykes can be divided in three components, as illustrated in Figure 2.6:

1. Squeezing, caused by squeezing of a liquefied soil layer beneath a dyke; resulting in settlements or deformations.
2. Densification, caused by dissipation of excess pore pressures in liquefied soils; resulting in settlements.
3. Macro instability. Reduction of soil strength when the effective stress is reduced by the development of excess pore pressures can result in sliding of either inner or outer slope of a dyke. Liquefaction is not required for this component.

Settlements due to densification or squeezing result in a lower crest level, making the dyke more vulnerable to failure mechanisms overflow and overtopping; as elaborated in paragraph 2.5.1. Naturally, the macro instability component contributes to the failure mechanism macro instability; when sliding of either inner or outer slope results in collapsing of a dyke. This is elaborated in paragraph 2.5.2. Furthermore, this component can contribute to the overflow & overtopping failure mechanism; when the crest of a dyke is lower due to slope sliding, but collapsing did not occur. [Bas]

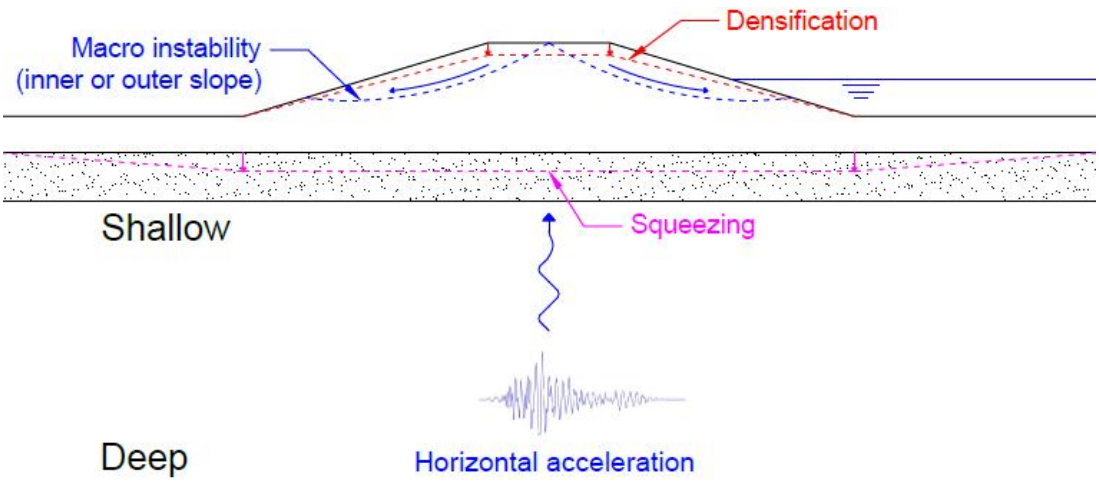

Figure 2.6 Types of failure related to earthquake loading

2.5.1 Overflow & wave overtopping

Overflow occurs when a certain high water level is larger than the height of the dyke, resulting in water flowing over the dyke as illustrated in figure 2.7. The limit state of this failure mechanism is the result of two components:

- the resistance of the inner slope to erosion;
- the amount of water that can be absorbed by the hinterland.

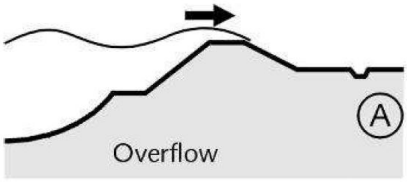

Figure 2.7 Failure mechanism: overflow (Weijers & Tonneijck, 2009)

Wave overtopping is similar to overflow, as illustrated in figure 2.8. The major difference is that in case of wave overtopping, the water level is not larger than the height of the dyke, but a certain discharge over the dyke takes place due to waves. Usually, this discharge is smaller than discharge caused by overflow. The limit state of this failure mechanism is therefore only determined by the resistance of the inner slope to erosion.

Figure 2.8 Failure mechanism: wave overtopping (Weijers & Tonneijck, 2009)

The height of a dyke is highly correlated with both failure mechanisms. In case of earthquakes, overflow and wave overtopping occur when the crest level of the dyke has been decreased due to settlements and the crest level is not sufficiently high any longer. This can be the result of a combination of (Deltares, 2014):

- macro instability (without collapsing);
- deformations due to densification;
- deformations due to squeezing.

The Newmark sliding block method, as described in paragraph 2.5.2, is used for macro instability. This method estimates the total sliding, while only the vertical component is important for the crest level. Therefore, the total displacement is dissolved into a horizontal and vertical component. The direction of the slip circle is assumed to be the slope at the crest.

Regarding densification, Ishihara and Yoshimine report that *"when saturated sand deposits are subjected to shaking during an earthquake, pore water pressures are known to build up leading to liquefaction or loss of strength in the sand deposits. The pore water pressures then start to dissipate mainly towards the ground surface, accompanied by some volume change of the sand deposits which is manifested on the ground surface as settlements."* (Ishihara & Yoshimine, 1992). To summarise, a dyke may settle after an earthquake due to dissipation of excess pore water pressure.

Deltares describes several approaches to determine the settlements due to densification in appendix D.3 of their report and they decided to use an equivalent of the approach of Ishihara and Yoshimine (Deltares, 2014). This approach relates the factor of safety against liquefaction directly to the volumetric strains. Four different ranges of values for the factor of safety are used; each with its own relation. The settlement due to densification can then be described as the product of the volumetric strain and the thickness of the liquefied layer.

It should be noted that normally design of dykes include sea level rise, settlement due to consolidation et cetera. Consequently, most dykes have sufficiently reserves in height. Hence, the probability on overflow or overtopping as a result of only densification is rather small.

The settlements as a consequence of squeezing are difficult to determine accurately (Deltares, 2014). In order to get an estimation of the settlements, Deltares proposed in appendix D4 of their report an approximating relation between the height of the dyke h_{dyke}, the thickness of the liquefied layer d_{liq}, the thickness of the top layer d_{top} (the layer between the liquefied layer and the dyke) and the estimated settlement Δz. This relation is based on several finite element calculations and is given in equation (2.20).

$$\Delta z = 0.2\left(\frac{h_{dyke} \cdot d_{liq}}{d_{top}^2}\right)^{0.4} \tag{2.20}$$

2.5.2 Macro instability

The macro instability failure mechanism is sliding of either inner or outer slope of a dyke, along straight or curved slip planes. The principle of macro instability on the inner slope is depicted in figure 2.9. The same mechanism is possible on the outer slope.

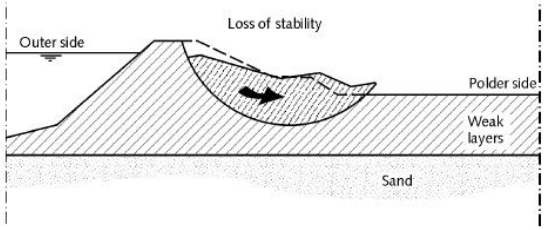

Figure 2.9 Macro instability inner slope due to earthquake loads (Weijers & Tonneijck, 2009)

Macro instability is one of the failure mechanisms that are most vulnerable to earthquakes. Liquefaction caused by earthquakes, which is elaborated in paragraph 2.2, can result in sliding of either the inner or the outer slope.

In the static situation, without any cyclic loading, soil masses tend to slide under gravity loading. However, this is precluded by the equilibrium of the driving force (gravity) with the shear resistance along the slip circle. When soil is liquefied, the effective stress is decreased significantly. Consequently, the strength of the soil decreases and its shear resistance becomes lower. It may happen in that case the shear strength of liquefied soil is not sufficient to maintain stability under solely static loading. The soil mass starts to slide along a slip circle and ground deformations occur. This is what happened with the Lower San Fernando Dam. Moreover, the horizontal acceleration of an earthquake may result in an additional force on the soil mass.

According to EERI MNO-12, the stability of a slope depends on the shear resistance along potential failure surfaces.

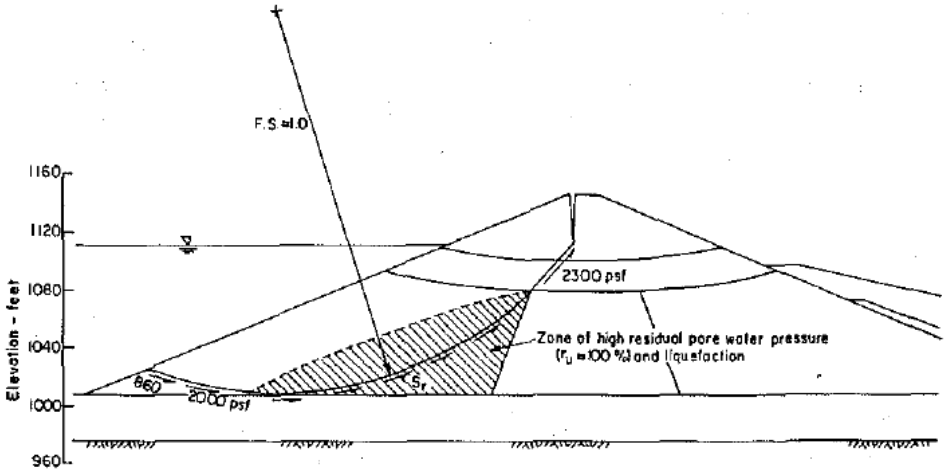

Figure 2.10 Cross-section of the Lower San Fernando Dam at the end of the earthquake (Seed, 1987)

The Newmark sliding block analysis is a method to approximate deformations in soil bodies due to earthquakes. It does not give a very accurate result or, as EERI MNO-12 states, "*sliding block models are a crude approximation of the deformation processes that occur as a consequence of liquefaction. The underlying assumptions of rigid-plastic shear resistance and slip along a discrete sliding surface have little resemblance to the actual deformation mechanisms in most situations."* (Idriss & Boulanger, 2008).

It is required to take into account all of the aspects of the motion when considering the effect of an earthquake. As Newmark says *"in other words, the peak acceleration may not be significant in determining the response of the dam. The effects of the velocities and of the ground displacement, and of the differential displacement of the ground leading to fissures in the ground surface, may be of equal or even greater importance."* (Newmark, 1965). According to Newmark, the most important measure of the intensity is the maximum ground velocity during the earthquake. Figure 2.11 shows the possible motions and deformations for an earth dame in an earthquake. This can be the motion of a block (arcs *a* and *b*), motion of the entire dam (line *c*) or motions that cause fissures (*d* and *e*).

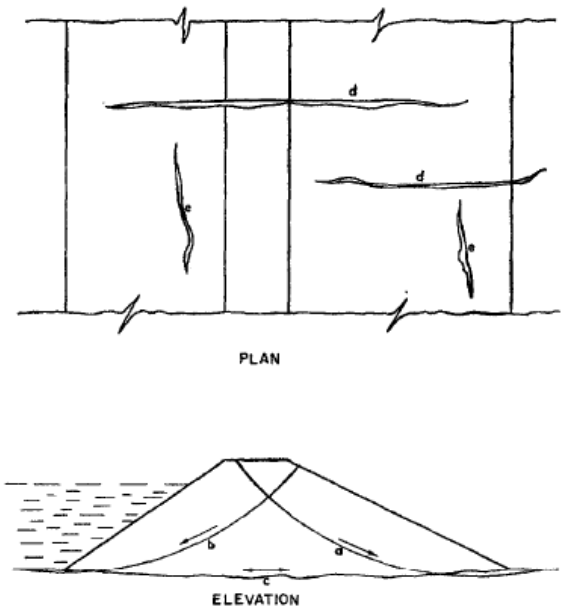

Figure 2.11 Possible motions and deformations of an earth dam in an earthquake (Newmark, 1965)

Newmark states that the resistance for uphill sliding can be taken as infinitely large. This is reasonable, since gravity will cause downhill sliding in case of insufficient shear resistance.

The Newmark sliding block calculation *"is based on the assumptions that the whole moving mass moves as a single rigid body with resistance mobilized along the sliding surface."* (Newmark, 1965). The mass slides when the total shear forces exceed the shear resistance. EERI MNO-12 states: *"The slide mass will slip in relation to the underlying base soils whenever the total shear forces (static plus inertial forces) exceed the available shear resistances from the soils. The inertial force at yield (the onset of the sliding) is described by the yield acceleration (a_y), which is simply the inertial force at yield divided by the slide mass."* (Idriss & Boulanger, 2008). Figure 2.12 gives a schematic of a Newmark sliding block analysis, illustrating that the block only displaces when the acceleration is larger than the yield acceleration.

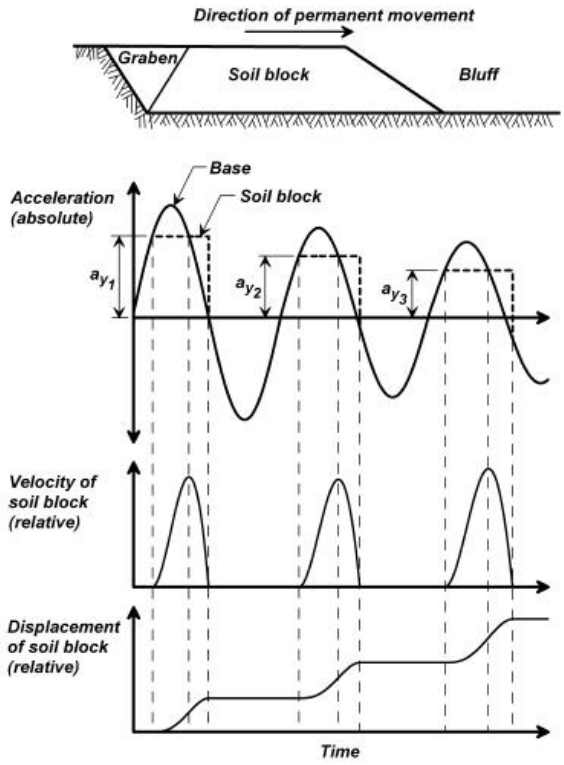

Figure 2.12 Schematic of a Newmark sliding block analysis. (After Idriss 1985, adapted from Goodman and Seed 1966) in (Idriss & Boulanger, 2008)

The complete calculation method of Deltares for macro stability is described in appendix C of their report (Deltares, 2014). Appendix C.2 describes the dynamic deformations with Newmark sliding block calculations. Deltares says that the calculated should be done twice to find the normative case, since the largest (absolute) peak acceleration can be both positive and negative.

For the specific accelerograms that were selected for Groningen, Deltares concluded a line which can be used as maximum boundary for the displacement *x* for a_{yield}/PGA smaller than 0.6; which is shown in equation (2.21). For values larger than 0.75, the result of this equation is closer to a mean or expectation value. The displacements are in that case small and virtually negligible.

$$\log\left(\frac{x}{PGA}\right) = -17\left(\frac{a_{yield}}{PGA}\right)^3 + 20\left(\frac{a_{yield}}{PGA}\right)^2 - 9.5\left(\frac{a_{yield}}{PGA}\right) - 0.6 \qquad (2.21)$$

Afterwards, the displacement should be corrected for scaling the frequency of the earthquake signal.

Several different critical displacements are mentioned in literature, mainly varying from 0.05 to 0.15 metres (Jibson, 2011); based on the comparison of the Newmark sliding block results and the actual damage in different situations. Based on this article, Deltares defines a critical displacement of 0.15 metres for Groningen, since smaller displacements in general did not result in damage (Deltares, 2014). This is in correspondence with the *Guidelines for Evaluating and Mitigating Seismic Hazards in California*, stating that, as a general guideline, *"Newmark Displacements of 0 to 15 cm are unlikely to correspond to serious landslide movement and damage"* (California Geological Survey, 2008).

To take the influence of the earthquake on the drained soil properties into account in pseudo-static analyses, Deltares proposed to reduce the friction angle and cohesion based on the relative excess pore water pressure r_u in the middle of the layer. The reduced friction angle and cohesion are determined with equation (2.22) and (2.23) respectively. Deltares uses a r_u of 0.5 during the Newmark sliding block calculation and a r_u of 1.0 during post-earthquake calculations.

$$\phi_{red} = (1 - r_u)\phi \tag{2.22}$$

$$c_{red} = (1 - r_u)c \tag{2.23}$$

2.6 Conclusion

An overview of the seismic analysis as described in paragraph 2.5 is given in Figure 2.13.

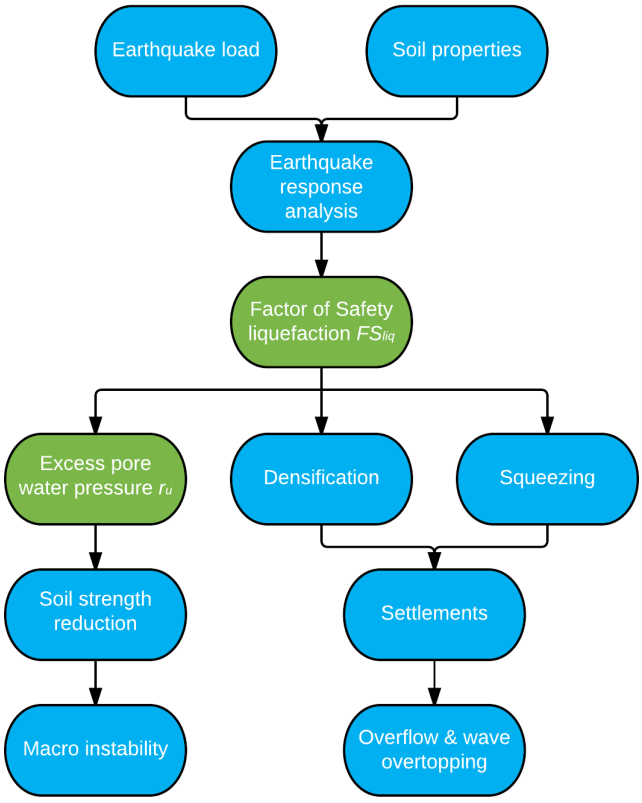

Figure 2.13 Overview of seismic analysis

This research focuses on the development of excess pore water pressure and the onset of liquefaction. The green boxes depict the components that can be done with the excess pore water pressure predicted by the constitutive models; assuming that the prediction is sufficiently accurate:

- Factor of Safety FS_{liq}. This parameters is currently determined with the method of EERI MNO-12 (Idriss & Boulanger, 2008). The results of the constitutive models do not provide the same safety factor, but the liquefaction susceptibility is found by looking at the excess pore water pressure development in relation to the vertical effective stress.
- The excess pore water pressure is currently determined with a relation with FS_{liq} (Deltares, 2014). This parameter can be obtained directly from the results of the finite element calculation to determine the soil strength reduction as given in equation (2.22) and (2.23).

The use of earthquake loading for the design of flood defences is a recent development, which is associated with many unknowns. For instance, the current approaches to determine the safety

factor against liquefaction are mainly based on tectonic earthquakes; which generally have a deeper hypocentre and more cycles than the induced earthquake in Groningen. Consequently, it is questionable to which extend these approaches are applicable for the induced earthquakes in Groningen. Further research is required on the differences between tectonic and induced earthquakes.

Furthermore, it is unknown how earthquake loading should be applied in the Dutch design approach; especially in case of flood defences. Designing with earthquake loading is relatively new in the Netherlands and consequently no guidelines are available. Moreover, it is unknown which values should be used for several parameters, like a maximum *PGA.*

Most researchers agree on the assumption that there must be a physical upper boundary for the *PGA.* However, which value this upper boundary has or how it should be determined is still subject to debate. A decisive answer to this question would lead to a significant lower design load and hence a more feasible design in terms of finances and constructability. On the other hand, it is expected that the *PGA* is limited by the confined shear strength of soft soils when applying the finite element method in combination with base signals.

Moreover, it is hard to predict the situation in Groningen in the next two to four decades. After many political discussions, it was decided to reduce the annual extraction of gas. This trend may continue in the next few years. However, it is not known what the consequences of this decision are with respect to the induced earthquakes. It is generally assumed that both the magnitude and the amount of earthquakes will reduce; but to which extent this happens and how many years it will take before the earthquakes disappear completely is unknown. Even if the extraction of gas is stopped completely, it will take several years before the earthquakes are over (Volkskrant, 2014).

Lastly, earthquake related data is scarce, especially when it comes to pore water pressure development. For the validation of constitutive models, it would be better to have more data; preferably from practical cases. Therewith, one can attempt to reproduce a practical situation with constitutive models, instead of a laboratory test. However, it is difficult to obtain such data; since it is too time consuming, difficult and costly to put measuring equipment in a dyke and wait for an earthquake. Currently, the failure of the Lower San Fernando Dam (U.S. Geological Survey, s.a.-b) is mainly used as reference case.

3 Earthquake loads

Both the earthquake and the hydraulic loads must be determined in accordance with the semi-probabilistic approach of *Ontwerpinstrumentarium 2014 (OI2014)*. This document is used for the transition between the former regulations, *Wettelijk Toetsinstrumentarium 2006 (WTI2006)*, and the new regulations; *Wettelijk Toetsinstrumentarium 2017 (WTI2017).* It is used for a flood probability based design of flood defences from 1 January 2014 (Rijkswaterstaat, 2014). However, this document only considers hydraulic loads; earthquake loads are not considered yet.

3.1 Earthquake loads

3.1.1 Failure probability

According to OI2014, the acceptable failure probability P_T for a certain dyke section and failure mechanism is derived from a preliminary standard in the form of a failure probability (Rijkswaterstaat, 2013). The preliminary standards are expressed as centre probability; since this research focuses on the design of dykes, the optimal design probability is used. Provisionally, a design probability of two times the centre probability may be applied (Rijkswaterstaat, 2014). The semi-probabilistic approach is based on design values for both load (Sd) and strength (Rd), as shown in figure 3.1. The failure probability norm should be satisfied for Sd < Rd, as shown in equation (3.1).

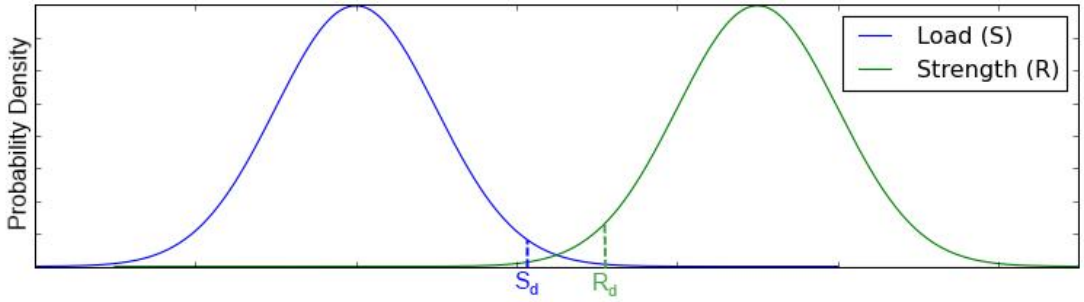

Figure 3.1 Example of probability functions of load (S) and strength (R), S_d and R_d

$$P(R < S) < P_T \tag{3.1}$$

The failure probability requirement for each failure mechanism for a cross-section is based on the failure probability budget. This budget shows the contribution of the different failure mechanisms to the flood probability norm.

3.1.2 Failure probability requirement

The design value for the peak ground acceleration *PGA* is related to the failure probability requirement, by means of return period *T.* This requirement depends on four factors:

- norm, by means of design probability per year P_d;
- contribution to the failure probability budget ω;
- influence factor α;
- length effect, depending on three parameters:
  - constant that indicates which fraction of the trajectory's length is sensitive to earthquakes *a;*
  - length of trajectory considered L_t;
  - length of a typical section for failure mechanism L_j.

The norm is fixed according to OI2014. The centre probability per year P_c for dyke section 6-7 (Eemshaven-Delfzijl) is 1/10000 per year (Ministerie van Infrastructuur en Milieu, 2014). It is recommended to take a design probability per year P_d of twice the centre probability (Jongejan,

2014; Rijkswaterstaat, 2014); resulting in a P_d of 1/5000 per year. By designing this way, it is stated that the failure probability at the end of the lifetime does not exceed the limit state.
The contribution factor ω depends on the failure mechanism. Overflow & overtopping and macro stability are the two most important failure mechanisms with respect to earthquakes (Deltares, 2014). OI2014 prescribes a contribution of 24% for overflow & overtopping and 4% for macro stability (Rijkswaterstaat, 2013), although this may be changed per location if necessary. Deltares proposed to increase the contribution of macro stability with 20% to 24%, for instance at the expense of the piping contribution (Deltares, 2015).

Factor α is the influence coefficient; showing the influence of the earthquake load with respect to the hydraulic load. Although this factor is of major influence, there is currently no regulation prescribing a value for this factor; it is still subject of debate. The CUR recommends a dominant load parameter of 0.7 (CUR, 1997). However, recent studies show that this value may be larger in Groningen; which is also endorsed by Expertise Netwerk Waterveiligheid (Expertise Network for Flood Protection, ENW). Provisionally, Deltares assumes an α value of 0.9 for Groningen (Deltares, 2015).

Parameter a in the length effect represents a constant indicating the fraction of the trajectory's length L_t that is sensitive to the considered failure mechanism; L_j is the length of a typical section for a specific failure mechanism (Jonkman & Schweckendiek, 2015). Currently, the values for stability are adopted for the length effect parameters; which are L_j = 50 m and a = 0.033 m (Rijkswaterstaat, 2014). It is recommended to investigate the validity of these values for earthquakes, since earthquake loading is a specific type of loading. The length of the trajectory L_t is 22.3 kilometres (ENW, 2014).

All proposed values for the acceptable annual failure probability calculation are summarised in Table 3.1.

Table 3.1 Proposed values for the failure probability calculation

Parameter	Value	Unit
P_c	1/10000	year^{-1}
P_d	1/5000	year^{-1}
ω	0.24	-
α	0.9	-
a	0.033	-
L_t	22300	m
L_j	50	m

Regarding the combination of hydraulic and earthquake load, a distinction is made between two situations. Firstly, one in which the earthquake load is dominant to the hydraulic load and secondly a situation with a dominant hydraulic load. This means that in the second situation, the earthquake load is not dominant; therefore the calculation is done with a value of 0.4*α (CUR, 1997).

An important factor that is not included yet is the recovery time and/or residual strength of the dyke; because it is unknown how this should be applied in the current approach. It is provisionally assumed that collapsing of a dyke due to earthquake loading instantaneously results in failure of the flood defence system and therewith inundation of land behind the dyke; although this is not realistic since failure depends on both earthquake and hydraulic loading. In case the residual strength of the dyke is sufficient to withstand the water or the dyke can be restored before the next storm or high water; the flood defence does not necessarily lose its water retaining function.

Deltares proposed a recovery time of one year in 2014 (Deltares, 2014), mainly to be able to work with yearly failure probabilities. However, this is extremely conservative. Expertise Network for Flood Protection (Expertise Netwerk Waterveiligheid, ENW) recommends reducing this period substantially; considering that the *PGA* decreases rapidly with increasing distance to the epicentre (ENW, 2014). Hence, it is not expected that a dyke collapses over the length of tens of kilometres. Moreover, ENW recommends preparing measures in order to be able to recover the dyke quickly in case of failure. This also results in a shorter recovery time. However, ENW does

not propose an improved recovery time. Therefore, further research is recommended, since a shorter recovery time results in a significant lower the probability of simultaneous occurrence of both collapsing and high water. A recovery time of five to six weeks is assumed to be realistic. Within this period, it should be possible to restore the dyke (temporarily). Currently, it is still subject of discussion what would be a proper recovery time. Deltares's most recent assumption is a flood probability of 1/3 during recovery time.

The first step to determine the return period, is to convert the design probability per year P_d in a required probability per year P_{req} by taking into account the length effect of the dyke trajectory and the contribution to the failure probability; as shown in equation (3.2). With the proposed values for Groningen, this results in a P_{req} of $3.054 \cdot 10^{-6}$. Hereafter, the required reliability index β_{req} is determined with equation (3.3); which is, based on this P_{req}, equal to 4.523. This β_{req} is used to obtain the failure probability per year P_f for the case in which earthquake loading is dominant (equation (3.4)) and not dominant (equation (3.5)). This results in failure probabilities of $2.35 \cdot 10^{-5}$ per year and 0.0517 per year, for the case where earthquake loading is dominant and not dominant respectively. Lastly, return period T is determined with equation (3.6) and equation (3.7) for dominant earthquake loading and not dominant respectively. As expected, the return period is much larger when the earthquake loading is dominant, namely 42608 years, than in case of not dominant earthquake loading. The latter has a return period of only 19.32.

$$P_{req} = \frac{P_d \cdot \omega}{1 + \frac{a \cdot L_t}{L_j}} = \frac{1/5000 \cdot 0.24}{1 + \frac{0.033 \cdot 22300}{50}} = 3.054 \cdot 10^{-6}\ year^{-1} \tag{3.2}$$

$$\beta_{req} = -\Phi^{-1}\left(P_{req}\right) = 4.523 \tag{3.3}$$

$$P_{f,dom} = 1 - \Phi\left(\alpha \cdot \beta_{req}\right) = 1 - \Phi\left(0.9 \cdot 4.523\right) = 2.35 \cdot 10^{-5}\ year^{-1} \tag{3.4}$$

$$P_{f,ndom} = 1 - \Phi\left(0.4 \cdot \alpha \cdot \beta_{req}\right) = 1 - \Phi\left(0.4 \cdot 0.9 \cdot 4.523\right) = 0.0517\ year^{-1} \tag{3.5}$$

$$T_{dom} = \frac{1}{P_{f,dom}} = \frac{1}{1.48 \cdot 10^{-4}} = 42608\ years \tag{3.6}$$

$$T_{ndom} = \frac{1}{P_{f,ndom}} = \frac{1}{0.0739} = 19.32\ years \tag{3.7}$$

3.1.3 Peak ground acceleration

The KNMI provided tables with the probability of exceedance of a significant amount of *PGA*s, for multiple locations in Groningen; in order to convert a certain failure probability requirement to a normative *PGA*. Figure 3.2 is based on the table for a location close to the primary flood defence between Eemshaven and Delfzijl and shows the relation between the return period and the *PGA*. The coordinates of this location are 6.90^{o} E, 53.33^{o} N. When applying a return period of 42608 years, as calculated in paragraph 3.1.2, the result is a design peak ground acceleration of 9.51 m/s^2, which is equal to 0.97g. Hitherto, the highest *PGA* measured in Groningen is 0.085g, which is approximately 0.83 m/s^2 (Deltares, 2013a). This earthquake took place on August 16th of 2012 and its epicentre was close to Huizinge, which is approximately 15 kilometres away from the dyke between Eemshaven and Delfszijl. The extremely large design value induces a discussion about a maximum value of the *PGA*; as elaborated in paragraph 3.1.4.

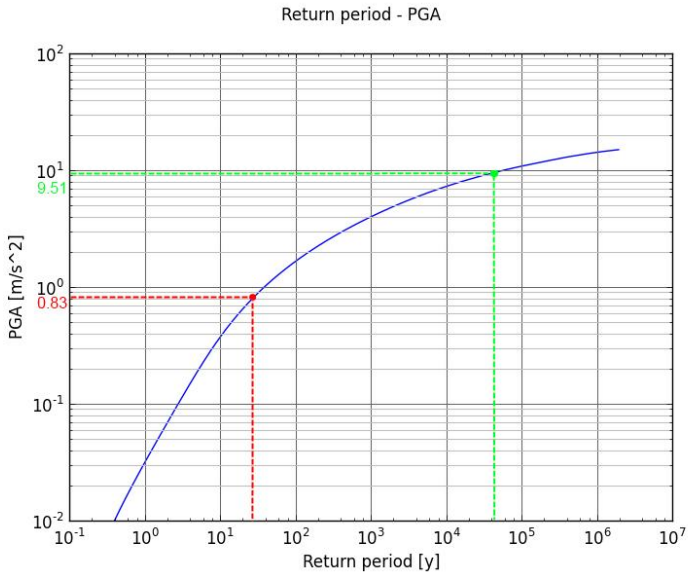

Figure 3.2 Probability of exceedance for the PGA for 6.90° E, 53.33° N (Data source: KNMI). The red points depicts the largest PGA measured and the green point depicts the design PGA belonging to the return period of 42608 years.

The data of Figure 3.2 has been implemented in the failure probability requirement calculation from paragraph 3.1.2, resulting in a relation between the norm, contribution to the failure probability budget and alpha on the one hand and the *PGA* on the other hand. Figure 3.3 illustrates the influence of ω and α on the *PGA* for the dominant situation with a design probability of once in five thousand years. The complete results are shown in appendix A; depicting the influence of each parameter on the normative *PGA*.

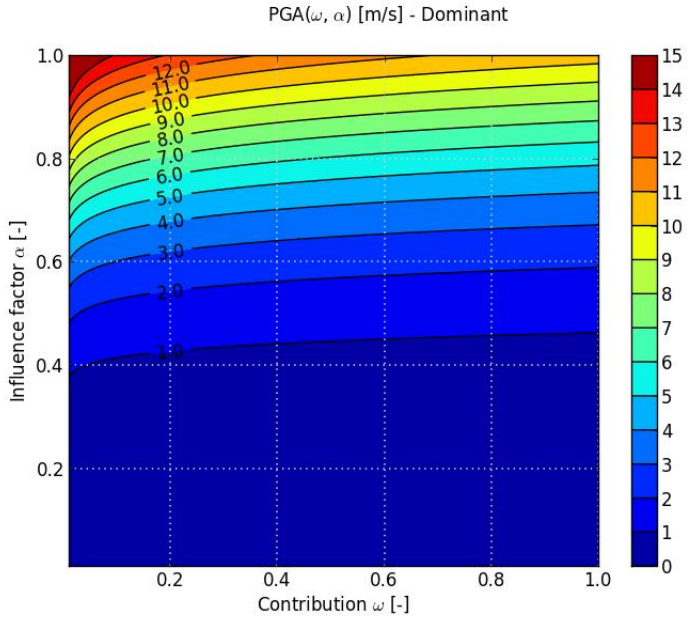

Figure 3.3 PGA as function of contribution and alpha

The main conclusion is that the *PGA* is mostly influenced by coefficient α. Taking together this conclusion and the fact that there is no regulation or guideline for this factor, leads to the conclusion that there is a large uncertainty. Choosing a slightly higher or lower value for α changes the *PGA* significantly, especially for higher values of α. For instance, the *PGA* of 9.51

m/s^2 was based on an α of 0.9. The same calculation, but then with an α of 0.7 would result in a significantly lower *PGA* of 4.31 m/s^2.

3.1.4 Upper boundary *PGA*

Because of physical limitations, it is not realistic to expect peak ground accelerations belonging to extremely small failure probabilities. The soil strength limits the horizontal ground motion, assuming that vertical propagation of shear waves (S waves) is responsible for the main part of the horizontal motion and that the vertical propagation of pressure waves (P waves) causes the main part of the vertical motion (Bommer et al., 2004). This assumption has two requirements. Firstly, the soil has to be practically horizontal layered and secondly, the motions propagate vertically. Bommer et al. (2004) state that *"once failure is reached at a given depth within the soil profile, the incident motion is filtered and no motion larger than the motion reached at the failure stage can be transmitted to the upper strata"*. With other words, the motion that can be transferred by the soil is limited by the soil strength.

On the other hand, geologists ascertain that soft clays are able to amplify ground motions, resulting in larger ground motions for softer soil types (Ashford et al., 2000; Booth & Key, 2006; Sun et al., 1993; U.S. Geological Survey; Wassing et al., 2003). Middelstum, Groningen, has a V_{s30} of 184 m/s (Wassing et al., 2003), corresponding to NEHRP site class D (International Code Council, 2000). However, since site class E comprises soils with V_{s30} smaller than 600 ft/s (approximately 183 m/s) and soil is inhomogeneous, it is concluded that the classification of the soil in Groningen is at the boundary of soil type D and E. This means that *"significant amplification of shaking by these soils is generally expected"* or even *"the strongest amplification of shaking due is expected for this soil type"*, for soil type D and E respectively (U.S. Geological Survey).

In addition, the site amplification factor depends on the *PGA*, as shown in Figure 3.4. This figure depicts that the amplification factor decreases for larger *PGA*s in case of stiff soils (V_{s30} = 180-360 m/s) and soft clays (V_{s30} < 180 m/s); approaching an amplification factor of 1.1. For other soil types, for instance rocks, the amplification factor can be smaller than 1.0 (Stewart & Seyhan, 2013).

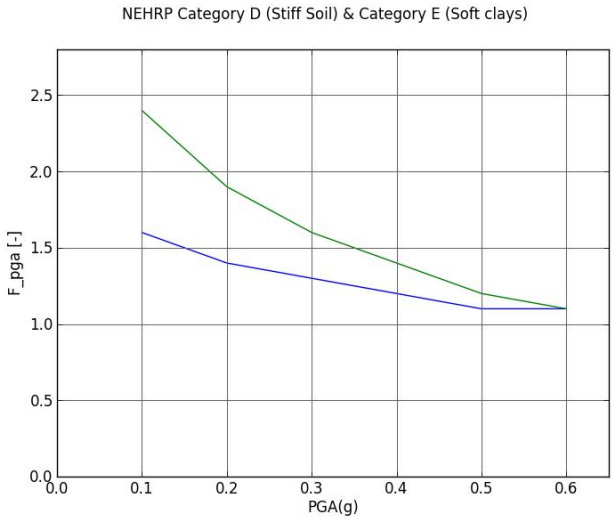

Figure 3.4 Amplification factor as function of PGA, for stiff soils (blue line) and soft clays (green line) [based on (Stewart & Seyhan, 2013)].

Although Bommer et al. (2004) argue that the *PGA* is limited; the actual value of the upper boundary is still not unambiguous. Several researches in the 1970s and 1980s resulted in different proposed upper boundaries, from 0.15 g for very soft marine deposits to 1.89 g for overconsolidated clays.

In conclusion, various factors influencing the propagation of the wave result in a complicated situation to determine an upper boundary for the *PGA*. Further research on this topic is therefore

required. Currently, very low annual frequencies of exceedance result in extremely large accelerations; as shown in paragraph 3.1.3. An upper boundary would be beneficial for engineering projects using these values, since it reduces the maximum load. This would result in lower costs and potentially less complex solutions.

Whether an upper boundary can be used for Groningen, and if so how this should be implemented, is still a matter of discussion. However, designing earthquake resistant dykes without such an upper boundary leads to designs of which the feasibility and costs are doubtful (Deltares, 2015); because of the large *PGA*. This is also endorsed by the calculation in paragraph 3.1.2 and 3.1.3; showing that the *PGA* would be more than ten times the largest observed *PGA*. Deltares argues that it is known from measurements and calculations that low peak base accelerations (*PBA*) lead to amplification in soft soil; whereas the *PGA* due to a larger *PBA* is limited, because of low soil shear strength. In other words, the relation between amplification and ground motion is non-linear. Moreover, Deltares states that it seems KNMI took this effect insufficiently into account.

Initially, Deltares assumed an upper boundary of 4.0 m/s^2, based on literature and *PGA*s measured in Groningen. Later on, Deltares proposed to create a new non-linear transfer function for soft soils. However, this approach was rejected by Expertise Netwerk Waterveiligheid (ENW). ENW opines that such a transfer function is only acceptable if it is generally applied and not only for flood defences (ENW, 2015).

On the other hand, this problem may be solved when KNMI provides the acceleration at the base, so called peak base acceleration *PBA*, instead of accelerations at surface level. In that case, site response analyses that include the confined shear strength of soft soil can be conducted. It is expected that such analyses show that soft soil is not able to transfer large accelerations.

Summarising, applying the current design rules without any upper boundary results in unrealistically large *PGA*s and extremely conservative designs. It is therefore required to define an upper boundary or, preferably, use site response analyses in combination with a suitable base acceleration record. However, it is currently unknown how an upper boundary should be implemented in the current design rules. Further research and discussion with involved parties should give a definite conclusion. Until the upper boundary or new Ground Motion Prediction Equation is available, it is recommended to use the calculated *PGA* without limitation or to apply a conservative upper limit.

3.2 Earthquake signal

The ground motion characteristics of an earthquake consist of three components (Idriss & Boulanger, 2008):

- level of shaking;
- duration of shaking;
- frequency content.

The ground motion is described by an accelerograms, which provides the horizontal acceleration at ground level in time. In order to obtain the design accelerogram, the signal must be scaled; as elaborated in paragraph 3.2.1.

3.2.1 Scaling & site response analysis

Normally, it is recommended to use a signal that was measured in a similar situation to obtain design peak acceleration at ground level PGA_{design}. Unfortunately, this is not possible for Groningen; since both the earthquakes and subsoil in Groningen are really specific (Deltares, 2014). Deltares recommends using signals that have been measured during smaller earthquakes in Groningen and scale the acceleration, amount of cycles and frequency content to obtain the required signal.

Normally, it is required to use a design response spectrum for scaling; this response spectrum is prescribed by the Eurocode. It is generally provided as graph, with the period on the horizontal axis and spectral acceleration on the vertical one. However, since the response spectra in

Eurocode are based on tectonic earthquake, it is not possible to apply these spectra directly. Hence, a specific design response spectrum for Groningen is required. This spectrum is proposed by the NPR. A design response spectrum is used to check if the applied earthquake signal results in a similar response spectrum.

According to Eurocode 8, at least three accelerograms are required for a spatial model (European Committee for Standardization, 2003). Deltares choose four normative signals measured at ground level ($PGA_{measured}$) from the KNMI dataset, based on the characteristic length, the amount of effective oscillations and the expected values of these characteristics for M_w > 5 (Deltares, 2014):

1 Event 1: Westeremden, recorder 060808MID3 – simple signal, one peak
2 Event 6: Huizinge, recorder 120816WSE – complex signal, multiple peaks
3 Event 8: Zandeweer, recorder 130207KANT – intermediate signal
4 Event 5: Hoeksmeer, recorder 110627WSE – larger amount of oscillations

The steps that are required to convert $PGA_{measured}$ into PGA_{design} are depicted in Figure 3.5.

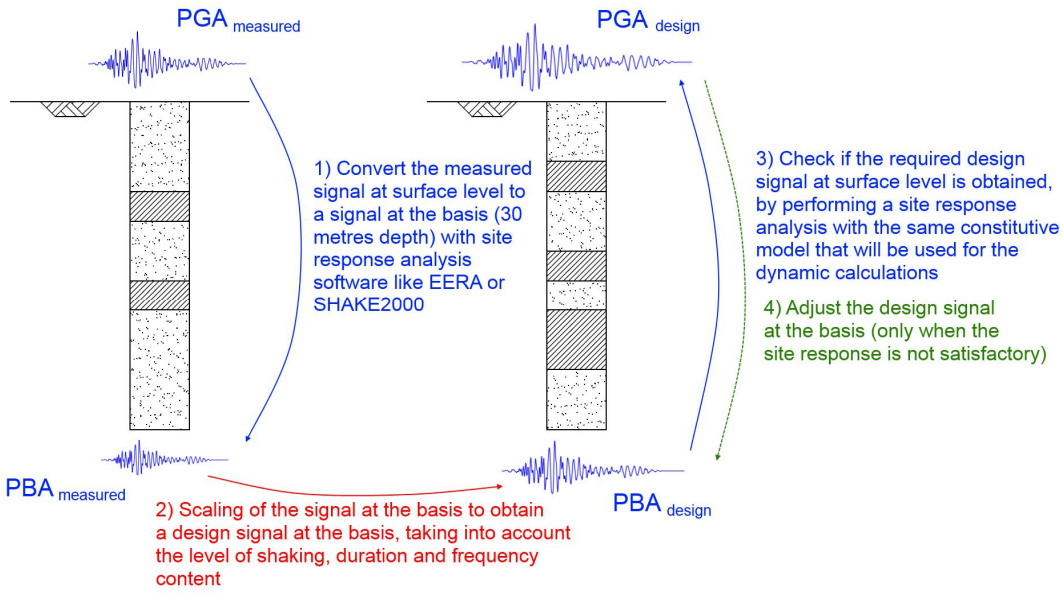

Figure 3.5 Required steps to obtain the design signal

Firstly, the acceleration signal $PBA_{measured}$ at thirty metres depth is determined with the signal measured at surface level $PGA_{measured}$; based on the local soil stratification. This is done with site response analysis software like EERA or SHAKE2000. Afterwards, the level of shaking, duration and frequency content in this signal is scaled to the required design signal at thirty metres depth PBA_{design} at the design location.

The level of shaking is described by the *PGA*, which is scaled to the value that is required according to the failure probability; as explained in paragraph 3.1.3.

The frequency and duration are scaled together. The peak frequency decreases for increasing magnitude; so the peak period increases. Deltares derived a relation between the peak period and *PGA* for the specific situation in Groningen, as given in equation (3.8) (Deltares, 2014).

$$\frac{T_{peak}}{T_{peak,ref}} = -1.036\left(\frac{PGA}{g}\right)^2 + 2.4963\left(\frac{PGA}{g}\right) + 0.63 \tag{3.8}$$

The amount of cycles in the signal is kept constant, so the duration of the signal will increase due to the increase of the periods.

Subsequently, this PBA_{design} is used to check if PGA_{design} is obtained as site response of PBA_{design}, when taking into account the local soil stratification. This should be done with the same constitutive model as the one that will be used during the dynamic calculations. PLAXIS described how such site response analyses should be performed (PLAXIS, 2015). The scaling succeeded if this is the case and PBA_{design} can then be applied as dynamic input signal at the base in PLAXIS.

If the obtained PGA_{design} is not satisfactory, PBA_{design} has to be adjusted till the right PGA_{design} is attained. This is an iterative process that might require some time. PBA_{design} is the signal that is finally used at the base of the finite element model. Note that PGA_{design} is only obtained to check if the site response is correct; this signal is not used during the calculation itself.

4 Models

In this chapter, the principle of finite element models and constitutive models is elaborated. Furthermore, background information about the UBC3D-PLM (PLAXIS Liquefaction Model) and the Hypoplastic constitutive model is given. Regarding both constitutive models, it is assumed that the soil is homogeneous and isotropic.

4.1 Finite element models

The principle of finite element models is that the domain is divided into smaller elements, which are connected to each other by nodal points or nodes on the element boundaries (Mulders, 2003). The smaller the size elements, the more elements and nodes are used. This provides more detailed and accurate results, but it has the drawback that the calculation time increases significantly. The main solution process of a finite element model is (Subramani, Sakthi Kumar, & Badrinarayanan, 2014):

1 Discretisation/meshing: dividing the structure into pieces (elements with nodes).
2 Forming element matrices: connecting (assembling) the elements at the nodes to form a system of equations for the whole structure.
3 Solve the system of equations involving unknown quantities at the nodes (for instance displacements).
4 Calculate desired quantities at selected elements (for instance strains and stresses).

Finite element models have some advantages over the conventional way to predict the onset of liquefaction, with EERI MNO-12. The main advantage is that it can provide insight in the development of excess pore water pressure at any location in the soil. Moreover, it gives an impression of the deformations that might occur. Lastly, when the model has been configured for one specific calculation, it can be used easily for other calculations; for instance other cross-sections or similar cross-sections with slightly different soil parameters. Therefore, it is really useful in case of a dyke with multiple normative cross-sections. Major disadvantage of finite element models is that calculations like this can take several hours. Besides, it is time consuming to obtain the soil parameters and configure the model. Finite element models are therefore less suitable when fast solutions are required.

Because this research focusses on cross-sections of dykes, it was chosen to use a 2D finite element program. The main focus is on the onset of liquefaction in a specific sand layer and failure of a normative cross-section; not considering deformations in longitudinal direction. Therefore, there is no necessity to take the longitudinal direction into account.

PLAXIS 2D AE.02 is used as finite element program in this research. This is a *"special purpose two-dimensional finite element program used to perform deformation and stability analysis for various types of geotechnical applications"* (PLAXIS, 2014). By default, it uses 15-node triangles with twelve Gauss (stress) points, as depicted in Figure 4.1.

Figure 4.1 Position of nodes and stress points in soil elements (PLAXIS, 2014)

4.2 Constitutive models

In constitutive soils models, the strength and stiffness behaviour of soils and rock is described

mathematically (University of Luxembourg, 2015). Constitutive models are based on a constitutive relation, which describes the relation between stress and strain (Puzrin, 2012). Furthermore, these models are formulated with material properties and state variables (Niemunis, 2003). Material properties describe the properties of the soil; these properties are not changing during the calculation. State variables, on the other hand, are related to a particular point in time. Their quantity may change in time; the description of that change should also be part the constitutive model. The void ratio is a good example of a state parameter.

Due to the large amount of soil and rock types and the many different types of behaviour, it is not possible to develop one constitutive model that is able to simulate all different situations. Consequently, many different types of simple and complex constitutive models have been developed in the last years; each model with its own strength and limitations.

Most finite element models are not able to cope with cyclic loading, which is required to predict the onset of liquefaction. It is required to use an effective stress model, since such models are able to take into account the gradual loss of soil strength as a consequence of pore water pressure build-up; whereas total stress model are not (Liyanapathirana & Poulos, 2002). Two models that are able to do so are the UBC3D-PLM and Hypoplastic constitutive model. UBC3D-PLM and the Hypoplastic model are elaborated in paragraph 4.3 and 0 respectively. Considering the most common user defined soil models for PLAXIS, these two models are the only two models that are capable to handle cyclic loading and liquefaction (Brinkgreve, 2015).

4.3 UBC3D-PLM

UBC3D-PLM (PLAXIS Liquefaction Model) is a for PLAXIS adapted 3D version of the 2D UBCSAND constitutive model, which has been developed at the University of British Columbia by Beaty & Byrne. The UBCSAND model was principally developed for seismic liquefiable sand-like soils, like loose sands (relative density smaller than about 80%) (Beaty & Byrne, 2011). This chapter describes the model qualitatively; for the mathematical background it is recommended to read:

- UBCSAND Constitutive Model (Beaty & Byrne, 2011);
- PLAXIS Liquefaction Model (Tsegaye, 2010);
- PLAXIS Liquefaction Model UBC3D-PLM (Petalas & Galavi, 2013).

4.3.1 Model

UBC3D-PLM is a constitutive elasto-plastic model that is able to accumulate plastic strains in case of cyclic loading and accumulate pore pressure in case of undrained cyclic loading (Brinkgreve, 2014b; Waterman, 2015).

The model decomposes strains into two components: elastic and plastic. The elastic behaviour is non-linear and is controlled by two stress dependent parameters: elastic bulk modulus *K* and elastic shear modulus *G* (Petalas & Galavi, 2013). When the stress state has reached the yield surface, irrecoverable deformation occurs. This is plastic behaviour, which is governed by the hardening rule. The hardening rule used in UBC3D-PLM is hyperbolic and relates the increment of the sine of the mobilised friction angle φ_m to the increment of the plastic shear strain (Brinkgreve, 2014b; Petalas & Galavi, 2013; Tsegaye, 2010). The sine of φ_m is defined as the mobilised shear stress divided by the mean effective stress, as shown in equation (4.1) (Brinkgreve, 2014b; Petalas & Galavi, 2013; Tsegaye, 2010). Hence, an increase of the ratio mobilised shear stress versus mean effective stress results in larger plastic strains.

$$\sin\phi_m = \frac{\sigma'_{max} - \sigma'_{min}}{\sigma'_{max} + \sigma'_{min}} \tag{4.1}$$

The direction of the plastic strains is determined by the plastic potential function. A so-called non associated flow rule, where the plastic potential differs from the yield function, is used in UBC3D-PLM (Tsegaye, 2010); because an associated flow rule would lead to large volumetric plastic strains. For 2D situations, the plastic potential function can be similar to the yield function; replacing the mobilised friction angle by the mobilised dilatancy angle. However, this gave unrealistic results for 3D situations according to Tsegaye. Therefore, a Drucker-Prager type plastic potential function is used.

The flow rule, given in equation (4.2), describes the relation between the plastic shear strain and the accumulation of plastic volumetric strain. UBC3D-PLM uses a similar flow rule as UBCSAND, which is based on the simplified version of Rowe's stress dilatancy relation shown in equation (4.3) (Tsegaye, 2010). This flow rule relates the increment of plastic volumetric strain $d\varepsilon_v^p$ to the increment of plastic shear strain $d\gamma^p$ and the sine of the mobilised dilatancy angle ψ_m. The latter is given as the difference between the sine of both the mobilised friction angle φ_c and the friction angle at constant volume φ_{cv}. When this difference becomes larger, the plastic volumetric strain increment will also become larger.

$$d\varepsilon_v^p = \sin\psi_m d\gamma^p \tag{4.2}$$

$$\sin\psi_m = \sin\phi_m - \sin\phi_{cv} \tag{4.3}$$

As depicted in Figure 4.2, UBC3D-PLM uses a failure surface and two yield surfaces (Galavi, Petalas, & Brinkgreve, 2013; Waterman, 2015):

- Mohr-Coulomb failure surface;
- primary shear yield surface for isotropic hardening (remains at maximum mobilised friction angle $\varphi_{m,max}$);
- secondary shear yield surface for kinematic hardening (friction angle can be demobilised).

As shown in the figure, both yield surfaces expand during loading. During unloading, the friction angle is demobilised. The primary surface remains constant during unloading, whereas the secondary surface shrinks. In reloading, the secondary surface expands; resulting in elasto-plastic behaviour. When the mobilised friction angle becomes equal to the maximum mobilised friction angle and loading continues, both surfaces expand together. The current stress ratio is then the highest stress ratio in the loading history of the soil.

Because of the lowering of the secondary surface, plastic strains do not only occur during loading, but also during reloading. Hence, UBC3D-PLM is able to accumulate plastic strains in cyclic loading. Consequently, UBC3D-PLM is able to cope with accumulation of pore water pressure. Unloading, however, is always elastic.

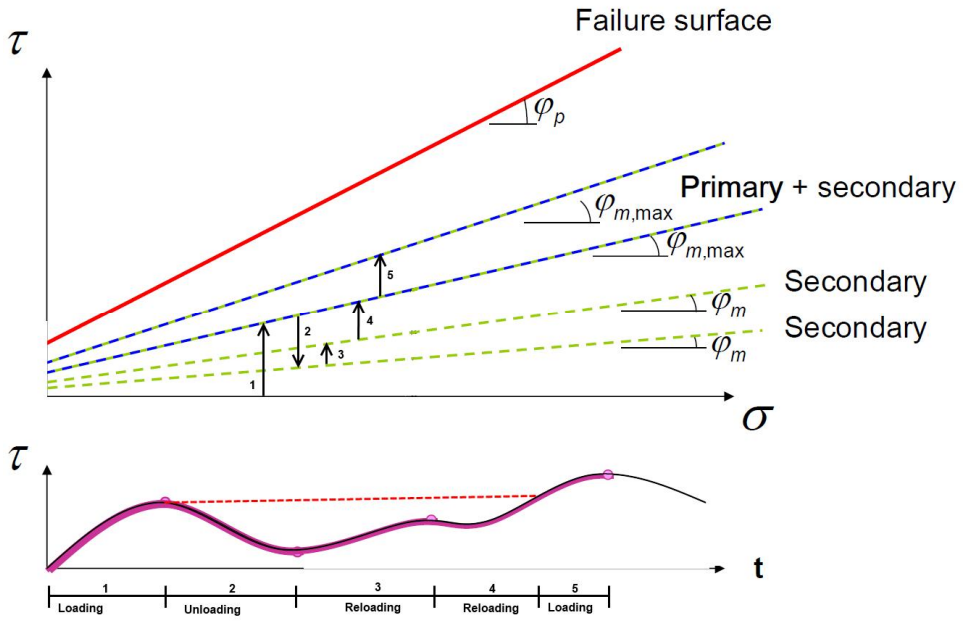

Figure 4.2 Failure and yield surfaces of UBC3D-PLM (modified figure, originally from (Waterman, 2015))

Both the primary and secondary yield surface are defined by a Mohr-Coulomb type yield function. This function is formulated as shown in equation (4.4) (Brinkgreve, 2014b; Petalas & Galavi, 2013; Tsegaye, 2010). It includes the minimum and maximum stress components; whereas it is not influenced by the intermediate stress component. Furthermore, it includes two model parameters: cohesion c, which is zero for sands, and peak friction angle φ_p. Lastly, mobilised friction angle φ_m, which describes the current stress state, is included.

$$f_m = \frac{\sigma'_{max} - \sigma'_{min}}{2} - \left(\frac{\sigma'_{max} + \sigma'_{min}}{2} + c' \cot \phi'_p \right) \sin \phi_m \tag{4.4}$$

The duration of an earthquake is very short in comparison with other types of behaviour like consolidation. During the relatively slow process of consolidation, the pore water in sand layers is able to dissipate. However, due to the short duration of the rapid cyclic loading of an earthquake, the pore water is not able to dissipate; although the properties of the sand layer are still the same. Since the pore water is not able to dissipate during an earthquake, the behaviour is assumed to be undrained.

Undrained behaviour is often associated with no volumetric strain, because the stiff water precludes volumetric strains (Beaty & Perlea, 2011). However, the bulk modulus of water K_w is large, but not infinite. Hence, very small volumetric strains can occur as a consequence of cyclic behaviour. The change in excess pore water pressure p_w in undrained behaviour is related to the change in volumetric strain ε_v as given in equation (4.5) (Petalas & Galavi, 2013). Significant excess pore water pressures can develop since these pressures are the related to the product of these very small volumetric strains and the very large K_w.

$$dp_w = \frac{K_w}{n} d\varepsilon_v \tag{4.5}$$

In reality, the excess pore water pressure will decrease after some time, as a result of dissipation. However, PLAXIS is not able to include dissipation of pore pressure in dynamic calculations.

The UBC3D-PLM model has three major limitations or disadvantages (Brinkgreve, 2014b):

- it does not include compaction hardening;
- cyclic loading behaviour and liquefaction are not always realistic;
- damping in dynamics calculations is overestimated.

The absence of compaction hardening is caused by the fact that this model does not contain a so-called cap to introduce plastic strains in case of large isotropic stresses in combination with no or low shear stresses. Hence, it is theoretically possible to have only elastic strains with extremely large normal stresses; whereas in practice also plastic strain will occur. However, earthquakes are always associated with significant shear stresses, so the influence of this problem is not significant for this particular purpose.

Since cyclic loading behaviour and liquefaction are not always modelled realistically, it is recommended to have a critical view to the results and not fully rely on the model. One of the purposes of this report is to elaborate on the applicability and accuracy of the model. Hence, the results and conclusion in chapter 6 and, 7 respectively provide more detailed information on this point.

Consequence of the damping overestimation is that dissipation of energy in the model is larger than in reality. It might happen that the amount of energy that is able to reach a certain point according to the model is less than in reality; resulting in non-conservative results.

4.3.2 Model parameters

The model parameters of UBC3D-PLM are given in Table 4.1. Both friction angles and the cohesion can be obtained from triaxial or direct simple shear tests, the reference stress has a standard value of 100 kPa and the SPT value is based on in-situ testing and all other variables can also be obtained from series of laboratory tests (Petalas & Galavi, 2013). For practical reasons, Beaty and Byrne proposed correlations between the SPT value and several other parameters (Beaty & Byrne, 2011). These correlations are given in equation (5.5) to (5.9) in paragraph 5.3.1. Furthermore, they propose that *me, ne* and *np* should be equal to 0.5, 0.5 and 0.4 respectively.

Table 4.1 Model parameters of UBC3D-PLM (Galavi et al., 2013; Petalas & Galavi, 2013)

Parameter	Unit	Description
φ'_{cv}	^{o}	Friction angle at constant volume
φ'_{p}	^{o}	Peak friction angle
c'	kPa	Effective cohesion
k_G^e	-	Elastic shear modulus number
k_G^p	-	Plastic shear modulus number
k_B^e	-	Elastic bulk modulus number
me	-	Elastic bulk modulus power
ne	-	Elastic shear modulus power
np	-	Plastic shear modulus power
R_f	-	Failure ratio
P_A	kPa	Reference stress
σ_t	kPa	Tension cut-off
fac_{hard}	-	Fitting parameter to adjust densification rule
$(N_1)_{60}$	-	Corrected SPT blow counts
fac_{post}	-	Fitting parameter to adjust post liquefaction behaviour

4.4 Hypoplastic model

PLAXIS' implementation of hypoplasticity is based on the von Wolffersdorff version (Von Wolffersdorff, 1996), with the intergranular strain extension of Niemunis and Herle (Niemunis & Herle, 1997). The model is characterised by its tensorial formulation with non-linear stress rate – strain rate formulation (Brinkgreve, 2014a). This paragraph provides a qualitative description of the Hypoplastic model; for the complete mathematical background, it is recommended to read:

- A hypoplastic relation for granular materials with a predefined limit state surface (Von Wolffersdorff, 1996);
- Hypoplastic model for cohesionless soils with elastic strain range (Niemunis & Herle, 1997);
- Extended Hypoplastic models for Soils (Niemunis, 2003)
- Hypoplasticity Investigated – Parameter Determination and Numerical Simulation (Anaraki, 2008);
- Evaluation of Material Models for Liquefaction (Tsegaye, 2009);
- PLAXIS implementation of HYPOPLASTICITY (Mašín, 2014)

4.4.1 Model

The Hypoplastic model is a path-dependent and rate-independent constitutive model (Niemunis, 2003), which is available as user defined soil model for PLAXIS. This (in)dependency means that the accumulated stress is influenced by the sequence of deformation increments, while it is not influenced by the duration of the deformation processes or the individual increments. Hence, the model does not include time-dependent effects like creep or relaxation. Since the equations are based on experimental data, considering relevant principles of physics, instead of being derived from the fundamental laws of physics; it is a so-called phenomenological model (Niemunis, 2003).

According to Niemunis, "*Hypoplasticity describes the behaviour of soil in terms of macro variables like stress or void ratio treating soil as a continuum, without detailed description of movement of individual particles and so it is a macro mechanical approach."* Id est, the model considers the behaviour of the soil sample in general, without calculating the displacement of individual grains. A typical property of the model is that it does not decompose the strains into elastic and plastic components; whereas elasto-plastic models like UBC3D-PLM do. Hence the notions of the yield surface and plastic potential surface are not explicitly used in the model (Bauer & Wu, 1993; Mašín, 2010; Niemunis, 1993).

The Hypoplastic model is void ratio dependent. This means that the stiffness and strength of the soil model depend on void ratio and stress level. It uses pressure-dependent critical state void ratio e_c and two pressure-dependent limit void ratios: maximum void ratio e_i for the loosest possible state and minimum void ratio e_d for the densest possible state. Figure 4.3 depicts the relation between the three void ratios and the ratio pressure p over granular hardness, which is controlling the stiffness. Under shearing, the sample tries to reach the critical state line of e_c at any stress level; resulting in contractive behaviour for loose samples (void ratio $e > e_c$) and dilative behaviour for dense samples (void ratio $e < e_c$). Starting points of the lines and also the input values in PLAXIS are void ratios at zero pressure. The figure also illustrates that the critical and limiting void ratios decrease for larger effective pressures normalised by the granulate hardness.

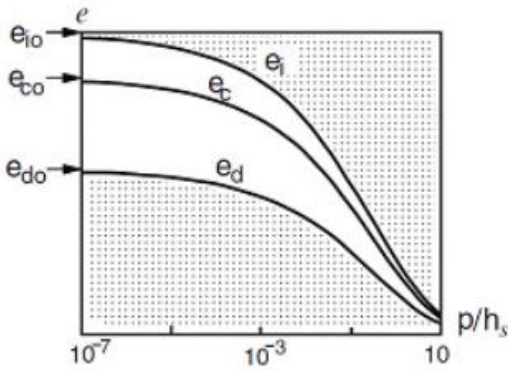

Figure 4.3 Relation between void ratios e_i, e_c, e_d and ratio p/h_s (Brinkgreve, 2014a)

In contrast to UBC3D-PLM, which has a Mohr-Coulomb failure criterion, the Hypoplastic model has a Matsuoka-Nakai failure criterion (Brinkgreve, 2014a; Niemunis, 2003; Tsegaye, 2009), as illustrated in Figure 4.4. This failure criterion *"has a concept of averaging the Mohr-Coulomb criterion, in such a way that the Mises criterion has a concept of averaging the Tresca criterion"* (Matsuoka & Nakai, 1985). The main advantage of the Matsuoka-Nakai failure criterion over the Mohr-Coulomb is that it has smooth corners, instead of the sharp hexagon corners. Principally, sharp corners are numerically difficult to handle (Bocchi, 2014) and require more computing power (Sarathchandran, 2014).

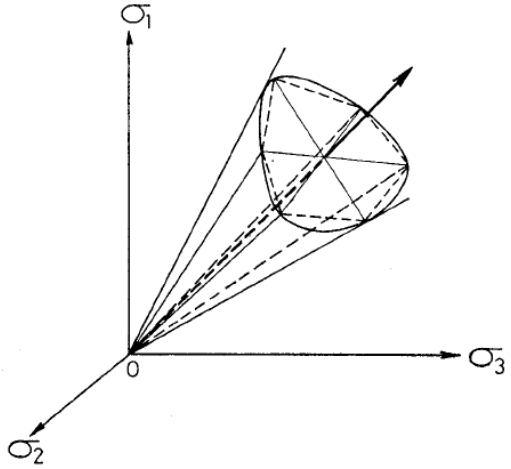

Figure 4.4 Shapes of the Mohr-Coulomb (dashed lines) and Matsuoka-Nakai (continuous lines) failure criteria (Matsuoka & Nakai, 1985)

The mathematical formulation of the Matsuoka-Nakai failure criterion is given in equation (4.6), including the invariants I_1, I_2 and I_3 of equation (4.7), (4.8) and (4.9) (Hicher & Shao, 2008; Tsegaye, 2009).

$$f_{M-N} = -\frac{I_1 I_2}{I_3} - \frac{9-\sin^2\varphi_c}{1-\sin^2\varphi_c} = 0 \tag{4.6}$$

$$I_1 = \sigma_{xx} + \sigma_{yy} + \sigma_{zz} \tag{4.7}$$

$$I_2 = \sigma_{xx}\sigma_{yy} + \sigma_{xx}\sigma_{zz} + \sigma_{yy}\sigma_{zz} - \sigma_{xy}^2 - \sigma_{xz}^2 - \sigma_{yz}^2 \tag{4.8}$$

$$I_3 = \sigma_{xx}\sigma_{yy}\sigma_{zz} - \sigma_{xx}\sigma_{yz}^2 - \sigma_{yy}\sigma_{xz}^2 - \sigma_{zz}\sigma_{xy}^2 + 2\sigma_{yx}\sigma_{xz}\sigma_{yz} \tag{4.9}$$

The original Hypoplastic model performs very well for deformations related to rearrangements of the grain skeleton. However, the results for cyclic loading are not satisfying (Bauer & Wu, 1993; Niemunis & Herle, 1997). Main problem is that the development of excess pore water pressure is overestimated in undrained loading (Niemunis, 1993; Niemunis & Herle, 1997).

During loading, the soil stiffness increases. This increase of stiffness is larger when the direction of loading is changed, for example reversed, than in case of continuous loading in one direction. To include this in the model, Niemunis and Herle proposed the intergranular strain extension. It contains a new state parameter; the so-called intergranular strain tensor δ (Niemunis & Herle, 1997). This parameter is controlled by the recent history of deformation (Niemunis, 2003) and it includes the increase in incremental stiffness when the direction of deformation is changed (Meier, 2012a). The intergranular strain extension is essential when modelling earthquake loading; because earthquakes are in fact a combination of rapidly reversing loads.

4.4.2 Model parameters

The model parameters for the Hypoplastic model are given in Table 4.2. Most parameters do not have a physical meaning, which makes them difficult to determine (Brinkgreve, 2014a). The model uses two critical state parameters: critical friction angle φ_c and critical void ratio at zero pressure e_{c0}. In case of non-cohesive soils like sand, φ_c can be estimated from the angle of repose φ_{rep} (Anaraki, 2008; Brinkgreve, 2014a; Herle, 1997; Miura, Maeda, & Toki, 1997); as illustrated in Figure 4.5 and Figure 4.6. This is not possible for materials that have grain sizes below 0.1 mm, since that would result in an increase of φ_{rep} because of capillary water resulting from air humidity (Mašín).

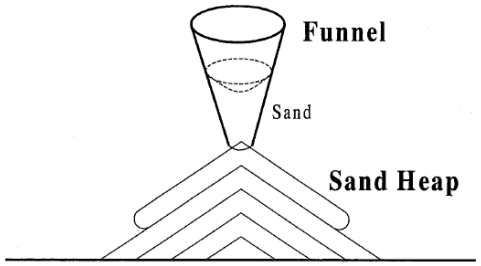

Figure 4.5 Method of measurement for the minimum density of sand proposed by Japanese Geotechnical Society (JGS) (Miura et al., 1997)

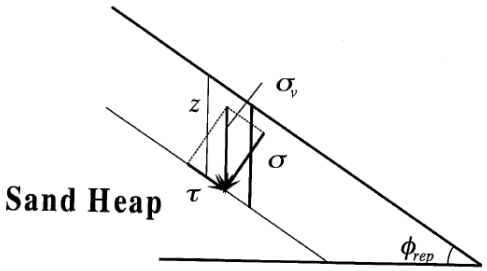

$$\sigma = \rho g z \cos^2 \phi_{rep}$$
$$\tau = \rho g z \sin \phi_{rep} \cos \phi_{rep}$$
$$\tan \phi = \tau / \sigma = \tan \phi_{rep}$$

Figure 4.6 Stability analysis of an infinite slope (Miura et al., 1997)

It is not possible to measure the void ratios directly, since they are defined at zero pressure. However, it is assumed that critical void ratio e_{c0} is equal to maximum void ratio e_{max} (Anaraki, 2008; Herle, 1997; Tsegaye, 2009). In addition, minimum void ratio at zero pressure e_{d0} can be taken equal to the minimum void ratio e_{min} (Anaraki, 2008; Herle, 1997; Meier, 2012a; Tsegaye, 2009) and the maximum void ratio at zero pressure e_{i0} is related to e_{max}, as shown in equation (4.10) (Anaraki, 2008; Herle, 1997; Meier, 2012a; Tsegaye, 2009).

$$e_{i0} = 1.15 * e_{max} \tag{4.10}$$

The stiffness is determined by granulate hardness h_s and exponent n. Both parameters can be obtained from oedometer compression tests (Brinkgreve, 2014a; Mašín, s.a.; Meier, 2012a). Factor α is related to the transition between peak and critical stress and can be retrieved from drained triaxial shear tests, as well as β which represents the change of stiffness at current density (Mašín, s.a.). Another possibility is to determine α by means of a shear test, whereas β can be determined with an oedemeter test (Meier, 2012b). The complete set of mathematical equations that can be used to obtain these values is provided by Tsegaye (Tsegaye, 2009).

Tsegaye also provides the mathematical background for the intergranular strain parameters. Factors m_T and m_R, representing the stiffness increase for 90^o and 180^o change of strain path direction, can be determined with cyclic shear tests and biaxial tests respectively. The other three intergranular strain parameters, R (radius of elastic range), β_R and χ (both controlling stiffness degradation) can be obtained from cyclic triaxial tests (Brinkgreve, 2014a) or cyclic shear tests (Tsegaye, 2009). Another option, instead of cyclic tests, is to use the unloading/reloading cycle from the oedometer test (Meier, 2012b). Consequently, no cyclic laboratory tests are required. In case cyclic laboratory tests are available, they can be used to check the quality of the obtained parameter set in cyclic behaviour, or to fine tune the parameters.

Table 4.2 Model parameters of Hypoplastic model (Brinkgreve, 2014a; Mašín; Meier, 2012a; Tsegaye, 2009)

Parameter	Unit	Description
φ_c	^{o}	Critical state friction angle
p_t	kPa	Shift of the mean stress due to cohesion
h_s	kPa	Granulate hardness, controls the overall slope in the compression curve
n	-	Parameter controlling the curvature in the compression curve
e_{d0}	-	Minimum void ratio at zero pressure
e_{c0}	-	Critical state void ratio at zero pressure
e_{i0}	-	Maximum void ratio at zero pressure
α	-	Parameter controlling the dependency of the peak friction angle on the relative density
β	-	Parameter controlling the dependency of the soil stiffness on the relative density
m_R	-	Parameter controlling the initial (very-small-strain) shear modulus upon 180^o strain path reversal and in the initial loading
m_T	-	Parameter controlling the initial shear modulus upon 90^o strain path reversal
R	-	Parameter controlling the elastic range size (in the strain space)
β_r	-	Parameter controlling the degradation rate of the stiffness with strain
χ	-	Parameter controlling the degradation rate of the stiffness with strain
e_0 or e	-	Initial void ratio corresponding to the zero mean stress or initial void ratio
δ (δ_{11}, δ_{22}, δ_{33}, $2\delta_{12}$, $2\delta_{13}$, $2\delta_{23}$)	-	Initial values of the intergranular strain tensor (in Voight notation)

5 Parameter calibration and sensitivity

This chapter elaborates on how the model parameters are determined, for both UBC3D-PLM and the Hypoplastic model. This is done with a calibration on cyclic laboratory tests in order to obtain a set of model parameters that describes the soil behaviour as good as possible. In this calibration, the results of cyclic direct simple shear test (DSS) calculations in the SoilTest facility of PLAXIS are compared to laboratory cyclic DSS tests performed by University of British Columbia. The derived model parameters are adjusted to obtain the best possible fit with the laboratory results. Fraser River Sand is used for both the calibration and the validation; which is elaborated in chapter 6. A calibration is only valid for its specific circumstances. Another calibration is required in case of a different situation; for instance another type of soil.

5.1 Fraser River Sand

The soil used for the centrifuge test, Fraser River sand, has been dredged in the Lower Mainland of British Columbia, Canada. Because of its judged susceptibility to liquefaction and its presence in the Fraser River delta, it has been selected to directly support and complement both the centrifuge tests and the numerical modelling (Wijewickreme, Sriskandakumar, & Byrne, 2005). Table 5.1 gives the properties that University of British Columbia obtained from index tests. The soil has an uniformity coefficient c_u of 1.6 (Wijewickreme et al., 2005); Figure 5.1 depicts the particle size distribution curve.

Table 5.1 Properties Fraser River sand (University of British Columbia, 2003a; Wijewickreme et al., 2005)

Specific Gravity, G_s	D_{50} [mm]	D_{10} [mm]	e_{min}	e_{max}
2.71	0.26	0.17	0.62	0.94

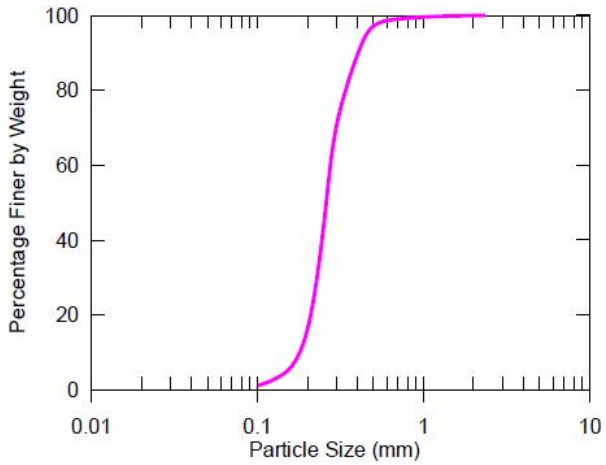

Figure 5.1 Particle size distribution curve (University of British Columbia, 2003a)

5.2 Undrained Cyclic Direct Simple Shear Test

In order to simulate cyclic loading conditions on the soil sample, Norwegian Geotechnical Institute (NGI) type undrained cyclic direct simple shear (DSS) tests have been conducted at the University of British Columbia. Constant volume tests are done, since this type of testing is less complex than truly undrained testing.

The testing consists of two phases. Firstly, a consolidation phase in which the vertical stress is incrementally increased to its desired value and secondly the actual shearing phase. For undrained conditions, both the top and bottom specimen boundary are fixed in the vertical direction during the shearing phase; by adjusting the vertical stress continuously. Since a steel-wire reinforced rubber membrane constrains the specimen in lateral direction, the volume of the

specimen is kept constant ($\varepsilon_x = \varepsilon_y = \varepsilon_z = 0$) (Dabeet, 2014; Wijewickreme et al., 2005). It is assumed that the change in vertical stress is equal to the change in pore water pressure that would have occurred in a real undrained test; which is a valid assumption (Norwegian Geotechnical Institute; Wijewickreme et al., 2005). Figure 5.2 shows a schematic cross-section of the specimen during the shearing phase of a DSS test. A schematic of the device used by University of British Columbia is given in Figure 5.3.

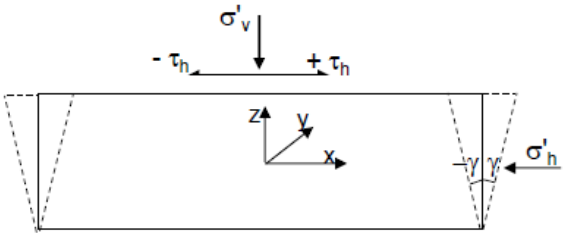

Figure 5.2 Schematic cross-section of a DSS specimen during the shearing phase (Dabeet, 2014)

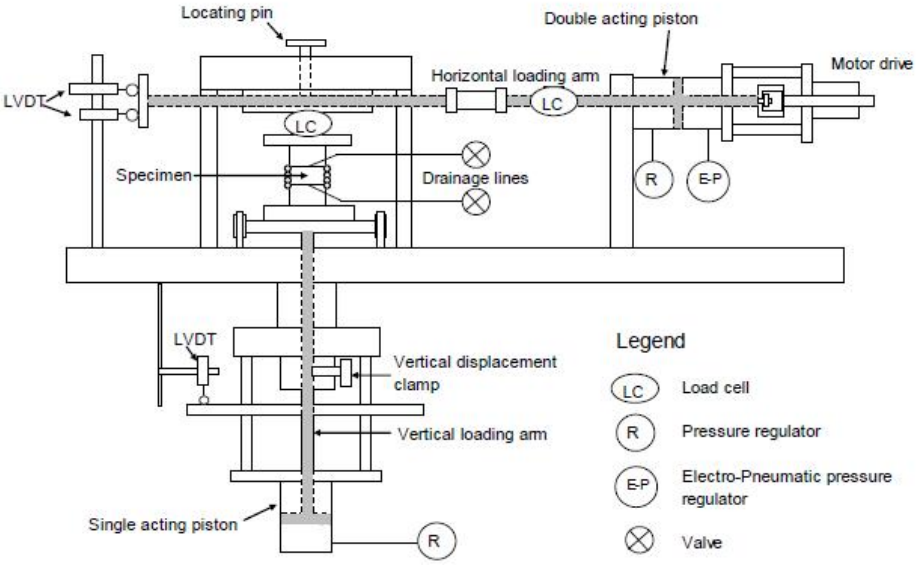

Figure 5.3 Schematic of the DSS device used by University of British Columbia (Dabeet, 2014)

University of British Columbia conducted tests for effective consolidation pressures σ'_{vc} of 100 kPa and 200 kPa, for different relative densities (University of British Columbia). In addition, some tests with initial static shear were conducted. The initial static shear is expressed in terms of initial static shear ratio α, which is the ratio of static shear stress τ_{st} over σ'_{vc} as shown in equation (5.1).

$$\alpha = \frac{\tau_{st}}{\sigma'_{vc}} \tag{5.1}$$

An overview of the Cyclic Stress Ratios (*CSR*) that are relevant for this research is given in Table 5.2 for both loose soil (D_r = 40%) and dense soil (D_r = 80%); all of them have been conducted with an effective consolidation pressure of 100 kPa. The *CSR* is given as the ratio of cyclic shear stress τ_{cyc} over σ'_{vc}, as shown in equation (5.2). Hence, a *CSR* of 0.08 corresponds with a shear stress amplitude of 8 kPa.

$$CSR = \frac{\tau_{cyc}}{\sigma'_{vc}} \tag{5.2}$$

It was considered that liquefaction was triggered when the single-amplitude horizontal shear strain γ reached 3.75%. However, the tests continued till horizontal shear strain γ was approximately 10%, to obtain data for research regarding post-liquefaction behaviour.

Table 5.2 Cyclic Stress Ratios for loose and dense soil

Relative density D_r [%]	Cyclic Stress Ratio (*CSR*)			Initial static shear
40	0.08	0.10	0.12	0
40	0.06	0.08	0.10	0.10
80	0.25	0.30	0.35	0

5.3 UBC3D-PLM

In 2013, Antonia Makra conducted a calibration for the same laboratory tests with Fraser River sand with UBC3D-PLM (Makra, 2013). It was therefore decided to use the values Makra obtained and check if results with UBC3D-PLM are similar to the results of Makra; for both her starting parameters and her final parameters.

5.3.1 Starting parameters

The starting parameters used by Makra are given in Table 5.3. They are based on the generic input parameters for UBCSAND 904aR (Beaty & Byrne, 2011), that are given in equation (5.5) to (5.7). These equation relate the parameters to SPT results in terms of normalised blow count $(N_1)_{60}$. When no information is available about the $(N_1)_{60}$, it can be estimated with relative density D_r. Which correlation should be applied is still subject of debate; this research uses the one proposed by Meyerhof (1957) as given in equation (5.3) (Makra, 2013). For instance, another option is the correlation that is used by Petalas and Galavi in the UBC3D-PLM documentation (Petalas & Galavi, 2013), as given in equation (5.4). This correlation gives slightly different values. A calibration constant C_d of 46 is used initially; this will be adjusted after the calibration. Which value should be applied is also subject of debate; for instance Meyerhof suggested a value of 41 in 1957; whereas Skempton states that the values ranges from 25 for fine sands in laboratory tests to 55 in natural deposits and even 65 for coarse sands (Idriss & Boulanger, 2015). This method to determine $(N_1)_{60}$ is not so accurate, owing to the fact that both the choice for a specific relation and its input parameters are uncertain. Hence, this relation should only be used to get a first estimate of $(N_1)_{60}$; it may be required to revise this estimation after the calibration procedure.

For practical situations, it is advantageous to measure $(N_1)_{60}$ in the field with a standard penetration test (SPT) to reduce the inaccuracy. However, many countries like the Netherlands are used to the cone penetration test (CPT) instead of the SPT. Hence, CPT results should be converted into $(N_1)_{60}$ values. In the past, many different correlations have been proposed (Shahri, Juhlin, & Malemir, 2014). Consequently, relating measured CPT values to SPT values in order to use the correlations proposed by Beaty and Byrne is associated with significant uncertainties.

$$D_r = \sqrt{\frac{(N_1)_{60}}{C_d}} \tag{5.3}$$

$$(N_1)_{60} = \frac{(D_r^2 * 100)}{15^2} \tag{5.4}$$

$$k_G^e = 21.7 * 20.0 * (N_1)_{60}^{0.333} \tag{5.5}$$

$$k_B^e = k_G^e * 0.7 \tag{5.6}$$

$$k_G^p = k_G^e * (N_1)_{60}^{2} * 0.003 + 100.0 \tag{5.7}$$

Besides, Beaty and Byrne say that φ_p can be determined by equation (5.8); this equation shows that an additional increase is required for values of $(N_1)_{60}$ larger than 15. R_f is given by equation (5.9).

$$\varphi_{pi} = \varphi_{cv} + \frac{(N_1)_{60}}{10.0} + \max\left(0.0, \frac{(N_1)_{60} - 15.0}{5.0}\right) \quad (5.8)$$

$$R_f = \min\left(1.1 * (N_1)_{60}^{-0.15}, 0.99\right) \quad (5.9)$$

Table 5.3 UBC3D-PLM starting parameters for loose and dense Fraser River sand (Makra, 2013)

	φ_{cv}	φ_p	k_G^e	k_G^p	k_B^e	R_f	fac_{hard}	$(N_1)_{60}$	fac_{post}
Loose	33.00	33.7	845.2	238.8	591.6	0.81	0.45	7.4	0.02
Dense	33.00	38.9	1339.5	3597.1	937.6	0.66	0.45	29.5	0.02

Furthermore, Beaty and Byrne state that parameters *me*, *ne* and *np* are 0.5, 0.5 and 0.4 respectively; an assumption that is adopted by Makra and also used by other researchers for undrained cyclic shear (Galavi et al., 2013; Park, 2005; Petalas, 2012; Petalas & Galavi, 2013).

5.3.2 Calibration

The calibration was in fact more a comparison with the results of Makra, comparing the available graphs from her report with the graphs obtained for this research. At first, the results with the starting parameters from Table 5.3 were compared; checking three types of graphs for *CSR* values of 0.08, 0.10 and 0.12 for $(N_1)_{60}$ = 7.4 and *CSR* values of 0.25, 0.30 and 0.35 for $(N_1)_{60}$ = 29.5. The considered graphs are:

- pore pressure ratio as function of the number of cycles;
- shear stress as function of shear strain;
- shear stress as function of the vertical effective stress.

Appendix B provides the graphs that compare the results of UBC3D-PLM with the laboratory tests, for these input values. In all cases, the pore pressure ratio graphs were exactly the same. The second type of graph gave some minor deviations, especially where the failure contour was reached. This is caused by small numerical differences between both versions of the constitutive models and PLAXIS. This is not considered to be a problem. The graphs of the third type fitted perfectly, except for the one with *CSR* = 0.08. This one had a minor difference, caused by small numerical differences. It is concluded that the results of this research are equal or at least sufficiently similar to the results that Antonia Makra obtained; which mean that the assumption that the same parameters can be used is valid.

After the calibration, Makra concluded that, regarding the amount of cycles to liquefaction, more accurate results were obtained if the values for $(N_1)_{60}$ were changed to 6.5 and 24.5 for loose and dense sand respectively and the other parameters were determined again according to the relations mentioned in equations (5.5) to (5.9) of paragraph 5.3.1. The final parameters are given in Table 5.4 in paragraph 5.3.4. The only available graphs in Makra's report regarding these parameters are the pore pressure ratio as function of the number of cycles. All graphs of this research had a perfect fit with her graphs. The graphs comparing the final results of the calibration with the laboratory tests are given in appendix C.

5.3.3 Static shear

With embankments, the sloping ground causes static shear stresses in the initial stress conditions; affecting the cyclic resistance of the soil (Stedman, 1997). One of the main disadvantages of UBC3D-PLM is that the model is not able to take this effect into account with the same soil parameters (Makra, 2013; Petalas, 2012). To include the effect of static shear, it is recommended to perform another calibration, with cyclic DSS tests that do include static shear. In general, this would lead to two (or even more) parameter sets for the same soil; one for the soil nearby the slope and one for soil further away. For more accurate calculations it might be necessary to use more different parameter sets, with decreasing influence of static shear. Afterwards, during the validation or calculation, one assumes a certain area that is affected by

static shear. One should, based on his expertise, decide whether the assumption is valid. For instance, when the chosen area is not sufficiently large, the results might show flow liquefaction instead of cyclic mobility. In that case, another calculation is required with a larger area. This procedure makes dynamic calculations on sloping grounds more complicated. Moreover, it takes more time since several calculations might be required to get the right static shear area.

Because of this problem, Makra used initially two parameter sets for the loose layer; one calibrated on normal cyclic DSS tests and one on the same tests including static shear. During the validation she found out that the entire loose layer was affected by static shear. Hence, only the parameter set that was calibrated with static shear was used for the loose layer. This set is similar to the one without static shear, except for fac_{hard} and fac_{post}. Both are increased to a value of 1.0. The graphs comparing the final results with this dataset to the laboratory tests are given in appendix D.

5.3.4 Parameters after calibration

Because the results of Makra's calibration are similar to the ones conducted for this research, it was decided to adopt Makra's parameters. As mentioned in paragraph 5.3.2, Makra concluded that the best fit with the laboratory tests was obtained with $(N_1)_{60}$ = 6.5 and $(N_1)_{60}$ = 24.5 for loose and dense sand respectively. The other final parameters are obtained by implementing the new $(N_1)_{60}$ values in the relations that are given in equations (5.5) to (5.9) of paragraph 5.3.1.

The results are given in Table 5.4. After the validation process, Makra concluded that fac_{hard} and fac_{post} should be equal to 1.0 for the entire loose sand layer. Therefore, these values are used during the validation instead of 0.45 and 0.02 respectively. In addition, parameters *me*, *ne* and *np* are 0.5, 0.5 and 0.4 respectively for both types of sand.

Table 5.4 UBC3D-PLM parameters after calibration for loose and dense Fraser River sand (Makra, 2013)

	φ_{cv}	φ_p	k_G^e	k_G^p	k_B^e	R_f	fac_{hard}	$(N_1)_{60}$	fac_{post}
Loose	33.00	33.65	809.45	202.60	566.61	0.83	1.0	6.50	1.0
Dense	33.00	37.35	1259.2	2387.4	881.4	0.68	0.45	24.5	0.02

5.3.5 Sensitivity analysis

The purpose of the sensitivity analysis is to show the response of the model results to minor changes in parameter input and to see which parameters are most influential. This research focusses on the development of excess pore water pressures; the amount of cycles to liquefaction is therefore used as criterion. All parameters have been observed individually, comparing the amount of cycles to liquefaction during cyclic DSS tests for 10 and 20 per cent higher and lower values to the ones obtained with the original value. The original amount of cycles is 6.3 and 8.8 for loose and dense soil respectively. However, it is not possible to change φ_{cv} and φ_p separately, so it was decided to do the analysis for these parameters in two ways. Firstly, both parameters were changed at the same time and secondly φ_p was changed in such a way that the difference between the two parameters increased and decreased with 10 and 20 per cent. Furthermore, the influence of $(N1)_{60}$ has been investigated in two ways. Firstly, $(N1)_{60}$ was changed individually. Secondly, $(N1)_{60}$ was changed, as well as φ_p, k_G^e, k_G^p, k_B^e and R_f according to the proposed relations by Beaty & Byrne of equation (5.5) to (5.9). The results of the latter are given by parameter $(N1)_{60,bb}$. The sensitivity analysis for loose soil has been conducted at *CSR* = 0.10, for dense soil *CSR* = 0.30 was used. The results of the analysis are given in Table 5.5 and appendix G. This appendix provides also an overview in a tornado diagram.

Table 5.5 Sensitivity of liquefaction response to variation of UBC3D-PLM input parameters

	φ_{cv} & φ_p	φ_{cv} - φ_p	k_G^e	k_G^p	k_B^e	me	ne	np	R_f	fac_{hard}	$(N_1)_{60}$	fac_{post}	$(N_1)_{60,bb}$
Loose	+	None	-	+	-	-	-	-	+	+	+	None	++
Dense	-	+	-	+	-	-	None	-	+	-	None	None	++
++ Highly influential, + Influential, - Hardly influential													

The conclusion of the sensitivity analysis is that $(N1)_{60,bb}$ is the only parameters that is highly influential. The effect of the associated uncertainties may even be larger, when $(N1)_{60}$ is obtained from a correlation with the relative density or the result of a CPT test; as mentioned in paragraph 5.3.1. Principally, the more correlations are used consecutively, the larger the uncertainty of the final product is; because each correlation has its uncertainty, which is included in the next one.

Some other parameters did not show any deviation at all. This is obvious for fac_{post}, since this parameter determines post liquefaction behaviour. Furthermore, it turned out that the difference between φ_{cv} and φ_p did not influence the amount of cycles to liquefaction for loose sand, while for dense sand small changes in *ne* and $(N_1)_{60}$ did not result in less or more cycles to liquefaction. In conclusion, the input parameters of the UBC3D-PLM model are not so influential when they are slightly changed, which makes this model more robust.

In 2012, Alexandros Petalas conducted also a sensitivity analysis for UBC3D-PLM (Petalas, 2012), based on the results of triaxial tests. He concluded that φ_{cv} is very critical for the prediction of the evolution of excess pore water pressures. Furthermore, Petalas reports that the undrained conditions are also influenced by large sensitivity of the model to the used linear simplified flow rule, because of the effective stress approach of the model.

Moreover, he concluded that more excess pore pressures are generated in case of lower k_G^p values and that the accuracy of the final magnitude of the excess pore pressures is more accurate. However, Petalas noticed that the performance of the model becomes worse, due to a decrease of the mobilised shear stress in case of lower k_G^p values. Unfortunately, it is not reported in which way and to which extent the performance becomes worse.

Lastly, Petalas concluded that for undrained behaviour of loose sands the influence of R_f is very critical. If R_f has a value of almost 1, say 0.99, the stress path is able to develop; passing the instability point and goes towards zero. In case of lower values, for instance 0.95, the stress path stops at a lower strain level, not crossing the instability point. In that case, the maximum shear stress is constant with the ultimate value.

5.4 Hypoplastic model

5.4.1 Starting parameters

The only laboratory tests that are available for Fraser River sand are cyclic shear tests; no oedometer tests or triaxial tests have been conducted by University of British Columbia. In addition, it is difficult to obtain all parameters directly from such tests or by curve fitting. The limit void ratios are the only parameters that can be approximated easily with the available information. It has therefore been decided to compare the limit void ratios of Fraser River sand to the hypoplastic parameters of several other types of sand. The parameters of the type of sand with the largest similarity to Fraser River sand are used as starting parameters for the calibration process.

The limit void ratios are based on equation (5.10), (5.11) and (5.12) (Anaraki, 2008; Herle, 1997; Meier, 2012a; Tsegaye, 2009). Using the index parameters from Table 5.1, it results in the limit void ratios that are given in Table 5.6.

$$e_{d0} \approx e_{min} \tag{5.10}$$

$$e_{c0} \approx e_{max} \tag{5.11}$$

$$e_{i0} \approx 1.15 * e_{c0} \tag{5.12}$$

Table 5.6 Limit void ratios for Fraser River sand

e_{d0}	e_{c0}	e_{i0}
0.62	0.94	1.081

Table 5.7 gives an overview of the hypoplastic parameters for several types of sand. It shows that the limit void ratios in Table 5.6 fit accurately with the void ratios of Hostun sand. The parameters of this type of sand are therefore used as starting parameters.

Table 5.7 Hypoplastic parameters for several types of sand (Mašín)[1], (Mašín, 2014)[2], (Brinkgreve, 2014a)[3]

Sand type	φ_c [°]	h_s [GPa]	n	e_{d0}	e_{c0}	e_{i0}	α	β
Hochstetten[1,2,3]	33	1.5	0.28	0.55	0.95	1.05	0.25	1.5
Hostun[1,2,3]	31	1.0	0.29	0.61	0.96	1.09	0.13	2
Karlsruhe[1,2,3]	30	5.8	0.28	0.53	0.84	1	0.13	1
Lausitz[1,2,3]	33	1.6	0.19	0.44	0.85	1	0.25	1
Toyoura[1,2,3]	30	2.6	0.27	0.61	0.98	1.1	0.18	1.1
Zbraslav[1]	31	5.7	0.25	0.52	0.82	0.95	0.13	1
Baskarp[3]	30	4.0	0.42	0.548	0.929	1.018	0.12	0.13
Mai-Liao[3]	31.5	0.032	0.32	0.570	1.040	1.200	0.40	1.00
Bremerhaven[3]	30	4.1	0.20	0.490	0.830	0.996	0.05	1.50
Min	**30**	**0.032**	**0.19**	**0.44**	**0.82**	**0.95**	**0.05**	**0.13**
Mean	**31.06**	**2.93**	**0.28**	**0.54**	**0.91**	**1.04**	**0.18**	**1.14**
Max	**33**	**5.8**	**0.42**	**0.61**	**1.04**	**1.2**	**0.4**	**2**

Regarding intergranular strain, $R = 10^{-4}$ may be considered as material independent constant and $\chi = 1.0$ and $\beta_r = 0.1$ are good values to start the calibration (Meier, 2012a). In addition, $m_R = 5$ and $m_T = 2$ is recommended for sands. On the contrary, intergranular strain parameters for Hochstetten sand consist of $\beta_\chi = 0.5$ and $\chi = 6$ (Mašín, 2014). The latter values are adopted as starting parameters for the Fraser River sand calibration. The total set of starting parameters is given in Table 5.8, for an e_0 of 0.820 and 0.698 for loose sand and dense sand respectively (Brinkgreve, 2014a).

Table 5.8 Starting parameters for Fraser River sand in the Hypoplastic model

φ_c [°]	h_s [GPa]	n	e_{d0}	e_{c0}	e_{i0}	α	β	m_R	m_T	R_{max}	β_r	χ
31	1.0	0.29	0.61	0.96	1.09	0.13	2	5	2	10^{-4}	0.5	6

5.4.2 Calibration

After the first run with loose sand, it turned out that liquefaction occurred in more cycles than in the lab. For *CSR* = 0.08, liquefaction was not triggered at all within a reasonable amount of cycles. This means that liquefaction should be triggered more easily than with the current parameters. In order to achieve this, the sand should be a little less dense. This resulted in an e_0 value of 0.860 instead of 0.820. After this change, the amount of cycles to liquefaction fit almost perfectly. The results are shown in appendix E.

When using one type of sand with different densities, e_0 should be the only parameter that needs to be modified (Brinkgreve, 2014a). However, it turned out that liquefaction for dense sand occurred in much fewer cycles than in the laboratory. In order to make a better fit between the laboratory test and the Hypoplastic model, e_0 of dense sand has been decreased from 0.698 to 0.678. Furthermore, α and β were increased slightly and intergranular strain parameters m_R, R_{max} and β_r were changed. The final Hypoplastic model parameters for loose and dense Fraser River sand are given in Table 5.9 and Table 5.11.

During the calibration, it was observed that the maximum excess pore water pressure that was reached in the dense sand is significantly lower than in the laboratory test. As a result of that, the effective vertical stress remains larger. The excess pore water pressure ratio r_u that was reached in the dense sand after the calibration was 0.81, 0.78 and 0.75 for *CSR* is 0.25, 0.30 and 0.35 respectively; whereas in the laboratory test r_u was 0.99 for all three *CSR* values. Consequently, the residual vertical effective stress predicted by the Hypoplastic model was 19, 22 and 25 kPa for *CSR* is 0.25, 0.30 and 0.35 respectively; whereas vertical effective stress in the laboratory test was almost zero. Nevertheless, it was clearly shown that the failure contour was reached and liquefaction occurred, despite the larger minimum vertical effective stress.

In addition, it turned out that the dense sand acts too stiff compared to the laboratory tests. The shear strain obtained with the Hypoplastic model is smaller than 0.5% for all three *CSR* values; whereas in the laboratory the shear strain increased significantly to several per cent after the onset of liquefaction. However, the shear strain for loose sand is predicted accurately with the Hypoplastic model.

Besides, another calibration was done on the laboratory tests that included static shear. It appeared that, similarly to UBC3D-PLM, the parameters that were calibrated on the laboratory tests without static shear were not satisfactory for the ones with static shear. In all cases, more cycles to liquefaction were required than in the laboratory. Decreasing χ to 1 and increasing n to 0.36 resulted in satisfactory results. Unfortunately, the results are less accurate for different *CSR* values; as depicted by the results of this calibration in appendix F. The final Hypoplastic parameters for loose sand, including static shear, are given in Table 5.10.

5.4.3 Parameters after calibration

The final Hypoplastic parameters for loose Fraser River sand without and with static shear are given in Table 5.9 and Table 5.10 respectively. The final parameters for dense Fraser River sand are given in Table 5.11.

Table 5.9 Hypoplastic parameters after calibration for loose Fraser River sand

φ_c [°]	h_s [GPa]	n	e_{d0}	e_{c0}	e_{i0}	α	β	m_R	m_T	R_{max}	β_r	χ	e_0
31	1.0	0.29	0.61	0.96	1.09	0.13	2	5	2	10^{-4}	0.5	6	0.86

Table 5.10 Hypoplastic parameters after calibration for loose Fraser River sand, including static shear

φ_c [°]	h_s [GPa]	n	e_{d0}	e_{c0}	e_{i0}	α	β	m_R	m_T	R_{max}	β_r	χ	e_0
31	1.0	0.36	0.61	0.96	1.09	0.13	2	5	2	10^{-4}	0.5	1	0.86

Table 5.11 Hypoplastic parameters after calibration for dense Fraser River sand

φ_c [°]	h_s [GPa]	n	e_{d0}	e_{c0}	e_{i0}	α	β	m_R	m_T	R_{max}	β_r	χ	e_0
31	1.0	0.29	0.61	0.96	1.09	0.20	2,5	5,8	2	$1.15*10^{-4}$	0.4	6	0.678

5.4.4 Sensitivity analysis

The purpose of the sensitivity analysis is to show the response of the model results to minor changes in parameter input. This research focusses on the development of excess pore water pressures; the amount of cycles to liquefaction is therefore used criterion. All parameters have been observed individually, comparing the amount of cycles to liquefaction during cyclic DSS tests for 10 and 20 per cent higher and lower values to the ones obtained with the original value. The original amount of cycles is 5.2 and 10.5 for loose and dense soil respectively and the sensitivity analysis for loose soil has been conducted at *CSR* = 0.10, for dense soil *CSR* = 0.30 was used. The figures with the results are given in appendix H; a summary of the results is given in Table 5.12. Appendix H provides also an overview in a tornado diagram.

Table 5.12 Sensitivity of liquefaction response to variation of Hypoplastic model input parameters

	φ_c	h_s	n	e_{d0}	e_{c0}	e_{i0}	α	β	m_R	m_T	R_{max}	β_r	χ	e_0
Loose	++	-	++	-	-	++	-	+	+	None	+	+	+	++
Dense	++	++	++	+	++	-	-	++	++	None	++	++	+	++
++ Highly influential, + Influential, - Hardly influential														

The sensitivity analysis had some limitations. For instance, some combinations of parameters were impossible or liquefaction did not occur. For this analysis, it should be noted that:

- for loose soil, liquefaction did not occur within 40 cycles for e_0 -20%, an additional step of e_0 = 0.70 (approximately e_0 -19%) was added to take this into account;
- for dense soil, e_{d0} +20% was not possible because of the consistency requirement $e_{d0} \leq e_0 \leq e_{c0}$;
- for dense soil, liquefaction did not occur within 62 cycles for e_{i0} +20%;
- for dense soil, liquefaction did not occur within 62 cycles for e_0 -10% and e_0 -20%, an additional step of e_0 -5% was added to take into account a decrease of e_0.

The overall conclusion of the sensitivity analysis is that the liquefaction response with the Hypoplastic model is sensitive to variation of several parameters. Particularly φ_c, n and e_0 are highly influential for both loose and dense soils; whereas α and m_T are hardly influential. The latter did not show any deviation at all. Furthermore, it should be noted that the deviations of plus and minus 20% for φ_c are large, resulting in unrealistic values; in practice this value will not deviate so much.
Another conclusion is that the degree of influence of some parameters depends on the density of the soil. For instance, h_s is highly influential for dense soils, while it is not so important for loose soils. In addition, e_{d0}, β and intergranular strain parameters m_R, R_{max} and β_r show a higher influence for dense soils. Lastly, it was shown that e_{c0} is not influential at all for loose soils, while it is highly influential for dense soils. The opposite is true for e_{i0}.

In 2008, Kambiz Elmi Anaraki conducted a sensitivity analysis for Baskarp sand on oedometric and triaxial response, also by increasing and decreasing each individual parameter by 10 and 20 per cent. The original Baskarp sand parameters used by Anaraki are given in Table 5.13.

Table 5.13 Hypoplastic parameters for Baskarp sand (Anaraki, 2008)

φ_c [°]	h_s [GPa]	n	e_{d0}	e_{c0}	e_{i0}	α	β
31	4.0	0.42	0.55	0.93	1.08	0.12	0.96

The initial axial loading of the oedometric tests was 3.25 kPa and it increased to 6 MPa, for initial void ratios of 0.823 and 0.657 for loose and dense samples respectively. The results are given in Table 5.14.

Table 5.14 Sensitivity of oedometric response to parameter variation (Anaraki, 2008)

	φ_c [°]	h_s [GPa]	n	e_{d0}	e_{c0}	e_{i0}	α	β
Loose	-	+	++	-	+	+	-	-
Dense	-	+	++	+	-	+	-	+
++ Highly influential, + Influential, - Hardly Influential								

The triaxial test was conducted at an effective confining pressure of 200 kPa for a dense soil with an initial void ratio of 0.60. During this test, e_{d0} and e_{c0} were only varied 10%, because of the consistency requirement $e_{d0} \leq e \leq e_{c0}$.The results are given in Table 5.15.

Table 5.15 Sensitivity of triaxial response to parameter variation (Anaraki, 2008)

	φ_c [°]	h_s [GPa]	n	e_{d0}	e_{c0}	e_{i0}	α	β
Stiffness	++	-	+	-	-	-	-	-
Peak strength	++	-	+	+	++	-	++	-
Residual strength	++	-	-	-	++	-	-	-
Dilatancy	+	-	-	+	++	-	++	-
++ Highly influential, + Influential, - Hardly influential								

Concluding, the influence of a specific parameter depends on the type of test. For instance h_s, n and, in case of dense sand, β are influential in the oedometric test; whereas their influence in the triaxial test is limited. This is not peculiar, since these three parameters are determined with oedometer tests. The triaxial response, on the other hand, is mainly influenced by the parameters that describe the critical state, φ_c, e_{c0} and α. It was shown that φ_c, n and e_{c0} are the most sensitive parameters, taking into account the three types of laboratory tests.

5.5 Comparison and conclusion

Comparing both constitutive models, it is concluded that both have advantages and disadvantages. Firstly, obtaining input parameters is easier with the UBC3D-PLM model, since most input parameters can be related to SPT values. When such a relation would be also available for the Hypoplastic model, the input parameters could be obtained much easier; since the current method is complicated. However, one can obtain starting parameters for the calibration by determining the void ratios at zero pressure, which can be related to the minimum and maximum void ratios measured in an index test. These void ratios at zero pressure can be compared to other Hypoplastic parameter sets mentioned in literature. For Fraser River sand, this method resulted in useful starting parameters. However, further research is required to ensure that this method provides reliable input parameters for other types of sand. Even more, it would be beneficial to have a relation between the input parameters of both constitutive models and CPT values.

Secondly, it is not possible to conclude whether one of the two models is more accurate, based on the calibration results. Considering the amount of cycles to liquefaction for loose sand, with *CSR* values of 0.08, 0.10 and 0.12, it turned out that the Hypoplastic model predicted the amount of cyclic to liquefaction more accurate. While the results of UBC3D-PLM show large deviations with the laboratory results in case of altered *CSR* values, the results of the Hypoplastic model fit almost perfectly.

Furthermore, both constitutive models require another parameter set in case of initial static shear. Surprisingly, the results of UBC3D-PLM and the Hypoplastic model are similar for loose sand. When static shear is included, the Hypoplastic model is not capable to predict the amount of cycles to liquefaction accurately for different *CSR* values; whereas it is able to do so without static shear. The predicted amount of cycles to liquefaction is similar for both constitutive models for *CSR* is 0.08 and 0.10. The amount of cycles with *CSR* is 0.06 is predicted more accurate with the Hypoplastic model; although both constitutive models predict significant fewer cycles to liquefaction than in the laboratory test.

Looking at the calibration for dense sand with *CSR* values of 0.25, 0.30 and 0.35, it was shown that UBC3D-PLM has a more gradual development of excess pore water pressure; more or less following the curved line of the laboratory tests. On the other hand, the Hypoplastic model predicts that the development of excess pore water pressure is linear instead of curved, till the point where the maximum excess pore water pressure is reached. Furthermore, the maximum excess pore water pressure is lower than in the laboratory, resulting in larger minimum vertical

effective stresses. Despite these residual vertical effective stresses, liquefaction occurs. Besides, the Hypoplastic model is able to simulate the oscillations from the first cycle, while UBC3D-PLM only shows oscillations after a few cycles.

An important limitation is that both UBC3D-PLM and the Hypoplastic model act too stiff in case of dense sand; resulting in too little strains. This effect is larger for the Hypoplastic model; however, both models came up with significantly less strains than the laboratory tests.

Regarding sensitivity, it was shown that the predicted amount of cycles to liquefaction deviated much more with the Hypoplastic model than with UBC3D-PLM, when the input parameters were slightly changed. Moreover, the amount of parameters that turned out to be (highly) influential is much larger for the Hypoplastic model. This makes, in combination with the complex parameter determination of the Hypoplastic model, the UBC3D-PLM model more robust.

Concluding, it is not possible to say which model performs best; based on the calibration. Principally, loose sands are more vulnerable to liquefaction than dense sands. This would make the Hypoplastic model more favourable; in situations without static shear. However, the sensitivity of its model parameters and its complex calibration process might make UBC3D-PLM more applicable.

6 Validation of models

The goal of the validation is to determine to which extent the UBC3D-PLM and the Hypoplastic constitutive model are able to simulate the generation of excess pore water pressure under cyclic loading and to obtain their accuracy. The optimal validation would be to compare the results of the models with measurements in real embankments. Since earthquakes are unpredictable and soil is inhomogeneous, it is very difficult and costly to obtain such data. Therefore centrifuge tests were performed in laboratories to simulate earthquakes, since the soil in such tests can be prepared under controlled conditions, the input horizontal acceleration can be controlled and the complete test can be measured extensively. The main advantage of centrifuge tests is that by increasing the centrifugal accelerations, the geometrical scale of a model can be decreased (Tobita, Iai, & Noda, 2008).

Three different centrifuge tests were considered for the validation:

- VELACS (Verification of Liquefaction Analysis by Centrifuge Studies). This is a cooperative research performed by eight universities (University of California at Davis and Berkeley, California Institute of Technology (Caltech), Cambridge University, University of Colorado at Boulder, Massachusetts Institute of Technology (MIT), Princeton University and Rensselaer Polytechnic Institute (RPI)) and funded by the National Science Foundation (NSF) (Arulanandan & Scott, 1993). It was performed in 1992, which made it difficult to obtain the data and to contact the researchers.
- University of Davis. Between 2000 and 2004, this university conducted centrifuge tests in their 9 m centrifuge facility (National Science Foundation, 2000). Unfortunately, these tests included soil models with multiple layers, resulting in a more complicated simulation than necessary for the purposes in this study.
- C-CORE. This research institute conducted eight centrifuge tests for a cooperative research project with the University of British Columbia and the Memorial University of Newfoundland, to *"optimize soil liquefaction treatment using numerical and centrifuge testing, and so reducing the cost associated with soil liquefaction"* (C-CORE, 2004).

Due to the disadvantages of the VELACS project and the project conducted by the University of Davis and the extensive amount of data available for the C-CORE project, it was decided to use the latter. The best way to compare the results of UBC3D-PLM and the Hypoplastic model is to use the actual data files of the laboratory tests. These files were obtained by contacting project manager Ryan Phillips of C-CORE. Furthermore, it was required to obtain the results of cyclic simple shear tests on this specific type of sand for the calibration of the model parameters. Those results were provided by the University of British Columbia, which conducted these tests.

Although it is currently the best method to evaluate the accuracy of constitutive models, centrifuge tests are not able to simulate a practical situation perfectly. One of the major drawbacks of a centrifuge test is that the soil model is placed in a rigid box and thus has rigid boundaries; whereas in reality soil is continuous. Moreover, the soil used in the centrifuge test is homogenous, while in reality soil is heterogeneous.

6.1 Centrifuge test

C-CORE was founded in 1975 as Centre for Cold Ocean Resources Engineering, focussing on the challenges of offshore oil and gas development in the presence of ice and icebergs (C-CORE, s.a.-b). The corporation *"creates value in the private and public sectors by undertaking applied research and development, generating knowledge, developing technology solutions and driving innovation"* (C-CORE, s.a.-a). The geotechnical facility of C-CORE has a 5.5 metre radius centrifuge with a maximum payload capacity of 200g, as shown in Figure 6.1, and an advanced Actidyn earthquake simulator (C-CORE, s.a.-c).

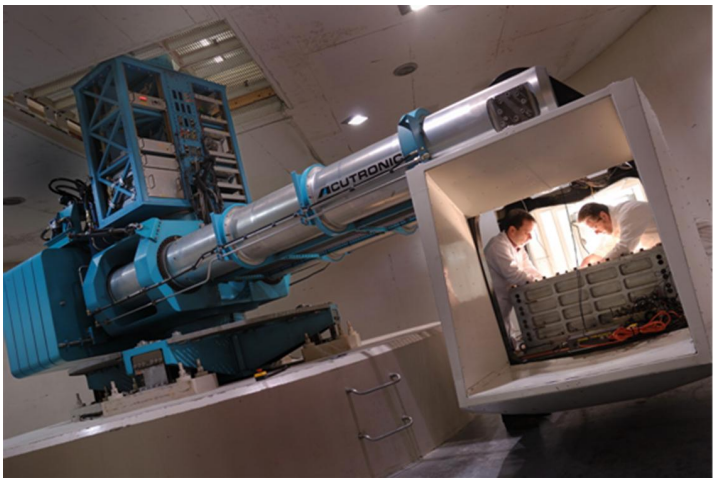

Figure 6.1 C-CORE's 5.5m-radius, 200g payload capacity Actidyn centrifuge (C-CORE, s.a.-d)

The project was a cooperative research project in which C-CORE was responsible for conducting the centrifuge tests, University of British Columbia conducted the laboratory element tests and both University of British Columbia and Memorial University of Newfoundland carried out numerical analyses (C-CORE, 2004). In addition, some industrial partners contributed their practical experience to the project.

The objective of the research program was *"to investigate the effectiveness of mitigation measures used for slope stability against earthquake-induced pore pressure generation"* (C-CORE, 2004). Therefore, eight different tests were done, including different soil models. Only the first test, CT1, is considered during this research; since this configuration with the homogeneous sand suits best to the requirements for the validation. The test was conducted on April 14th, 2004.

6.1.1 Soil model

The geometry used during the tests consists of a drainage layer, a layer of dense sand and a loose liquefiable sand layer with a 2:1 slope; as illustrated in Figure 6.2. The hatched "dyke" had different properties in other tests, but it was exactly the same as the loose sand layer for the CT1 test. The water level is 1 metre above the surface, at Z = 25 m, to ensure the model is virtually fully saturated.

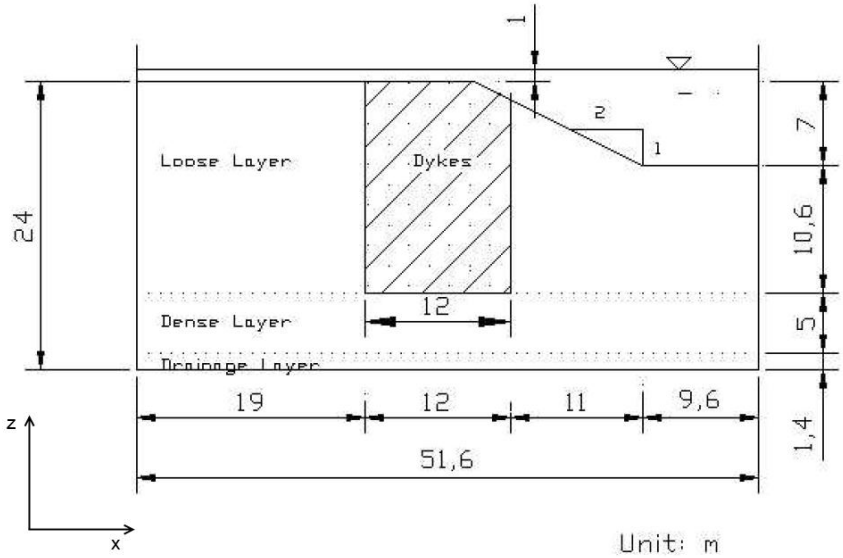

Figure 6.2 Geometry of the model slope (C-CORE, 2004)

Fraser River sand has been used for this research; the particle size distribution is shown in Figure 5.1 and the index properties are given in Table 5.1. The loose and dense layer consists of Fraser

River sand with relative densities of about 40 and 80 per cent respectively. This used to be 32 and 78 per cent, but it increased because of compression during model saturation and mechanical handling (C-CORE, 2004).

The drainage layer is used to create a one-dimensional saturation front and consists of a coarse sand material, with a specific gravity of 2.67 (C-CORE, 2004). The minimum and maximum void ratios of this sand are 0.62 and 0.81 respectively and the hydraulic conductivity of this sand was estimated with Hazen's formula to be 0.040 m/s. For comparison, the hydraulic conductivity of Fraser River sand at a relative density of 40 per cent is $4.3*10^{-4}$ m/s. The scaling factors that are applied in this experiment are given in appendix I, in Table I.1.

In order to maintain scaling laws, a mixture of methylcellulose powder with 1.76% to water in weight was used to obtain the required viscosity (C-CORE, 2004).

6.1.2 Input signal

Two different input signals were used during the validation to increase the robustness of the validation; viz. A475 and A2475. Both are depicted in Figure 6.3. A475 is based on a 10 per cent exceedance limit in 50 years, matching the firm ground target spectrum for the building code earthquake for Vancouver that was in force in 2004; whereas A2475 is based on a 2 per cent exceedance limit in 50 years (C-CORE, 2004). Both signals have been modified to pass the 40 to 200 Hz band pass filter (0.57 to 2.86 Hz in prototype) of the earthquake simulator. Furthermore, Ernie Naesgaard used a 10^{th} order polynomial to modify the signal for the baseline correction.

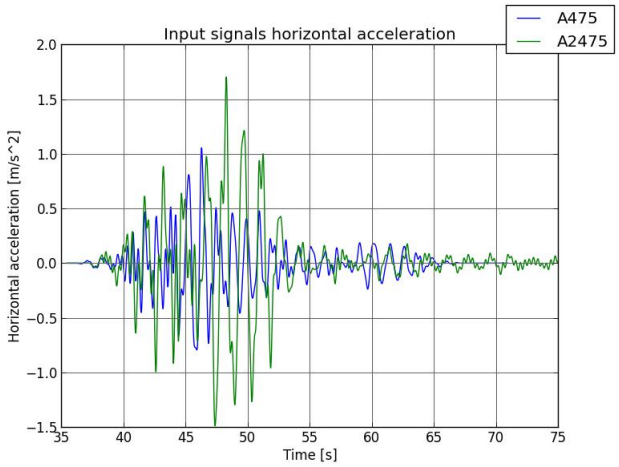

Figure 6.3 The horizontal acceleration input signals

6.1.3 Measuring equipment

Four types of instruments were used during the centrifuge tests (C-CORE, 2004):

- pore pressure transducers, to measure the development of the pore water pressure;
- accelerometers, to measure the horizontal acceleration;
- Linear Variable Differential Transformers (LVDT), to measure the vertical displacement;
- one laser transducer, to measure the horizontal displacement of the model container.

The locations of the used pore pressure transducers (P#), accelerometers (A#) and LVDT's (L#) are given in Table 6.1, as well as the locations of the points in the numerical model. Most points in the numerical model do not correspond exactly to the points in the centrifuge test, due to the location of the nodes and stress points in the numerical model. Figure 6.4 gives an overview of these points. Transducers P3 and A10 were not placed due to limited availability of transducers. The same holds for the LVDTs, were only four of the five planned LVDTs were placed. Besides, A9 and P9 were accidentally pulled out during saturation of the soil model and P6 did not work properly.

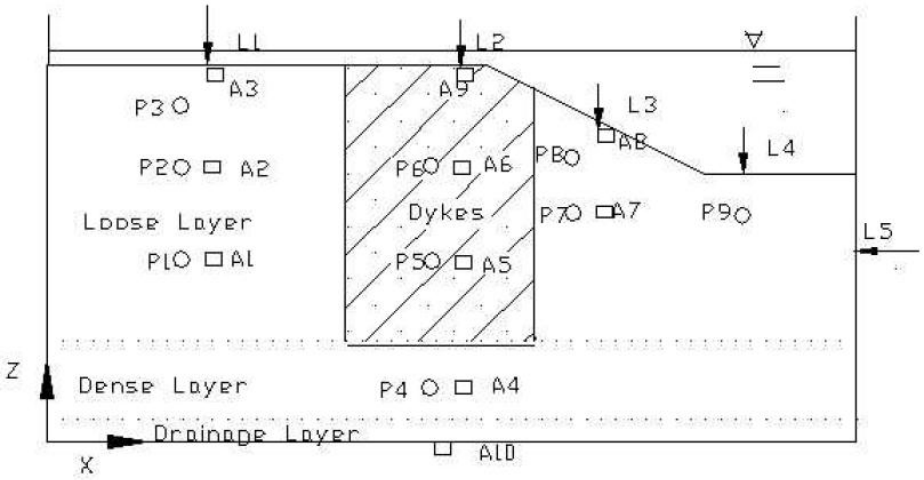

Figure 6.4 Locations of pore pressure transducers (P#) and accelerometers (A#) (C-CORE, 2004)

Table 6.1 Locations of pore pressure transducers (P#) and accelerometers (A#) in both centrifuge test (C-CORE, 2004) and the numerical model

Transducer	$X_{centrifuge}$	$Z_{Centrifuge}$	$X_{numerical}$	$Z_{numerical}$
A1	11.0	12.5	11.34	12.62
A2	11.0	18.0	11.06	17.76
A3	11.0	23.5	10.77	23.25
A4	25.5	3.9	25.80	3.75
A5	25.5	12.5	25.85	12.44
A6	25.5	18.0	25.40	17.84
A7	34.0	15.0	33.65	15.14
A8	34.0	20.5	33.96	20.63
P1	10.0	12.5	10.13	12.51
P2	10.0	18.0	9.84	18.38
P4	24.5	3.9	24.68	3.80
P5	24.5	12.5	24.45	12.66
P7	33.0	15.0	33.12	14.98
P8	33.0	19.0	32.74	19.08
L1	11.0	24.0	10.87	24.00
L2	25.0	24.0	24.73	24.00
L3	35.0	20.5	35.00	20.50
L4	45.0	17.0	44.91	17.00

6.2 Model input

6.2.1 Geometry

The geometry of the model in PLAXIS is shown in Figure 6.5; the dimensions are the same as the dimensions of the centrifuge prototype, as given in Figure 6.2. The locations of the points that are used to compare the horizontal accelerations and the development of pore water pressure in PLAXIS with the results of the transducers during the centrifuge tests are given in Table 6.1 of paragraph 6.1.2. These nodes and stress points are chosen in such a way that they are, according to PLAXIS, as close as possible to the actual location of the transducers in the centrifuge test.

The horizontal acceleration input signal described in paragraph 6.1.2 and depicted in Figure 6.3 is applied as prescribed line displacement in x-direction, as illustrated by the purple right pointing arrows in Figure 6.5. The displacement is, besides on the base, also applied on both vertical

sides; since the physical model was placed in a rigid box. This is contrary to practical applications, which would only have a signal at the base.

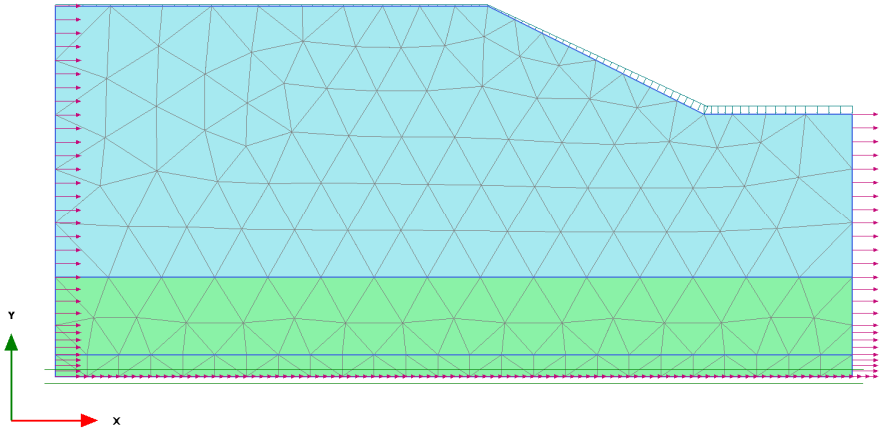

Figure 6.5 The geometry used in PLAXIS; including soil stratification, principle load and mesh.

6.2.2 Model parameters

The applied model parameters for UBC3D-PLM are given in Table 5.4 and the model parameters for the loose and dense layer in the Hypoplastic model are given in Table 5.10 and Table 5.11 respectively. As mentioned in paragraph 5.3.3 and 5.4.2, it is required to use different input parameters when soil is influenced by static shear; for instance nearby a slope. Based on the research of Makra, it is assumed that the entire loose sand layer is affected by static shear caused by the slope (Makra, 2013). Hence, the parameter set that is obtained with static shear is applied to the entire loose sand layer.

The specific weight of both the loose and dense layer are estimated with the minimum and maximum densities; which are 1400 kg/m^3 and 1670 kg/m^3 respectively (C-CORE, 2004). The minimum and maximum void ratios are 0.62 and 0.94 respectively and the specific gravity G_s is 2.71 (University of British Columbia, 2003a). The saturated and dry density of the soil is determined by equation (6.1) and (6.2) respectively (Liu). The upper and lower boundaries for the specific weight are obtained by calculating the densities for the minimum and maximum void ratio and multiplying that by *g*.

$$\rho_{sat} = \frac{\rho_w (e + G_s)}{1 + e} \tag{6.1}$$

$$\rho_d = \frac{G_s \rho_w}{1 + e} \tag{6.2}$$

The initial specific weights that are used in PLAXIS during the validation are based on the obtained boundary values. After the first calculations to determine the initial stresses, it turned out that these stresses were too low; probably caused by underestimation of the densities. Hence, the densities are increased slightly. An overview of these weights is given in Table 6.2. The specific weight of the drainage layer is assumed to be the same as the dense layer.

Table 6.2 Specific weight of the soil used in PLAXIS

		Loose [kN/m^3]	Dense [kN/m^3]
γ_{unsat}	Dry	17.0	19.0
γ_{sat}	Saturated	20.0	22.0

6.2.3 Initial stresses

Gravity loading is used to determine the initial stresses for both UBC3D-PLM and Hypoplastic model. This is a plastic calculation, generating the initial stresses based on the volumetric weight of the soil and considering equilibrium (PLAXIS, 2014).

Although Makra reported that *"no significant differences exist"* (Makra, 2013) between initial stresses with Mohr-Coulomb and UBC3D-PLM, is it recommended to use another model to determine the initial stresses (Galavi et al., 2013); for instance Mohr-Coulomb or Hardening Soil. The initial stresses with UBC3D-PLM gave reliable initial stresses for the part where the soil layers are perfectly parallel. However, the initial stresses beneath the slope contain some fluctuations. Hence, Mohr-Coulomb was used to determine the initial stresses, with soil densities that are similar to the ones in the dynamic phase in UBC3D-PLM and the Hypoplastic model. The stiffness is of minor importance, since the deformations are reset after the gravity procedure.

For the Hypoplastic model, it turned out that the gravity loading procedure was not applicable. This is caused by the fact that strength in the Hypoplastic model is mainly based on friction, requiring stresses; while most other models also include cohesive strength that does not require stresses. Since the stresses in gravity loading are built up from zero to their actual value, the soil has hardly any strength at the start of the procedure in the Hypoplastic model. Due to this lack of strength, the model is close to failure. For that reason, Mohr-Coulomb was also used for this calculation.

6.3 Results

This paragraph gives the results of the validation with UBC3D-PLM and Hypoplastic model, in paragraphs 6.3.1 and 6.3.2 respectively. As mentioned in paragraph 6.1.2, two different signals are used for the horizontal acceleration: A475 and A2475. The paragraphs below elaborate on the results for A475. In addition, the paragraphs contain a qualitative interpretation of the A2475 results. The appurtenant figures for UBC3D-PLM and Hypoplastic model are given in appendix J and K respectively.

The horizontal accelerations and development of excess pore water pressure are compared with data of the centrifuge tests, provided by C-CORE. This is done at three different locations; viz. further away from the slope (A1-3 and P1-2), close to the slope (A4-6 and P4-5) and beneath the slope (A7-8 and P7-8); at different depths. Furthermore, the settlement of the surface is compared.

6.3.1 UBC3D-PLM

In all points, the excess pore water pressure starts developing too early; while there is hardly any dynamic loading. This is caused by initialisation of the model and it is the main reason of inaccuracies in the excess pore water pressure development. Furthermore, excess pore water pressure dissipated in the centrifuge test after the largest peaks at t is 50 s. This is depicted by the decreasing excess pore water pressure line in the graphs. Since PLAXIS is not able to include dissipation in a dynamic calculation, this effect is not shown in the model results.

Considering the accelerations in Figure 6.6, it is shown that the results are moderate. The accelerations with UBC3D-PLM are comparable to the ones from the centrifuge test. One of the most significant differences is that the amplitude in A2 and A3 are slightly lower with UBC3D-PLM. This is caused by the fact that the model is overdamped, since this effect mainly occurs further away from the bottom and hardly in A1. Another difference is the spurious rapid oscillations in the model results, which are caused numerically. Furthermore, the large negative peak in A3, which is caused by dilative behaviour, is not captured by UBC3D-PLM.

The results of the excess pore water pressure development are appropriate in P1 and moderate in P2, as depicted in Figure 6.7. The maximum excess pore water pressure that is reached is in both cases almost exactly the same. However, the model predicts that the maximum in P2 is reached earlier than happened during the centrifuge tests.

The results for the accelerations closer to the slope are similar to the ones further away. It is notable that the amplitudes in case of A4 are larger in the model; which illustrates that the accelerations are affected by the dense sand layer. Besides, the results show the same overdamped behaviour resulting in smaller amplitudes closer to the surface, in A5 and A6. In addition, the same small spurious oscillations occur.

The excess pore water pressure developments in P4 and P5, as illustrated in Figure 6.9, are decent. In P4, UBC3D-PLM and the centrifuge test show a similar result, although the maximum value is reached earlier in UBC3D-PLM. However, this point is of minor importance since this measurement took place in the dense sand layer and it is unlikely that liquefaction will occur in this layer. P5 is more important, but its result is less accurate. The graph shows a negative peak after seven seconds, which was not expected. Furthermore, the maximum excess pore water pressure is reached earlier in the model, analogous to the other results. Moreover, the maximum value is slightly overestimated.

The accelerations beneath the slope, A7 and A8, are shown in Figure 6.10. At these points, the model gives also an adequate result. Again, the maximum amplitudes are somewhat smaller and spurious rapid oscillations occur, comparable to the other points. Besides, only one of the two large negative peaks at A8 is captured by the model.

Figure 6.11 displays the excess pore water pressure development in points P7 and P8, beneath the slope; which are probably the most important points in the embankment. Unfortunately, the results at these points are not satisfactory. The maximum predicted excess pore water pressure in P7 is close to the one of the centrifuge test. However, the development is much faster. The excess pore water pressure in P8, on the other hand, has a significantly lower maximum of only half the initial effective vertical stress. Based on the fact that large deformations occur in this point and the effective vertical stress is decreasing towards zero, it is concluded that liquefaction occurred in point P8. The decreasing effective stress is the result of excess pore water pressure development and decreasing vertical stresses. It is concerning that this is not visible in the results of UBC3D-PLM in Figure 6.11, whereas it is clearly visible in the centrifuge results.

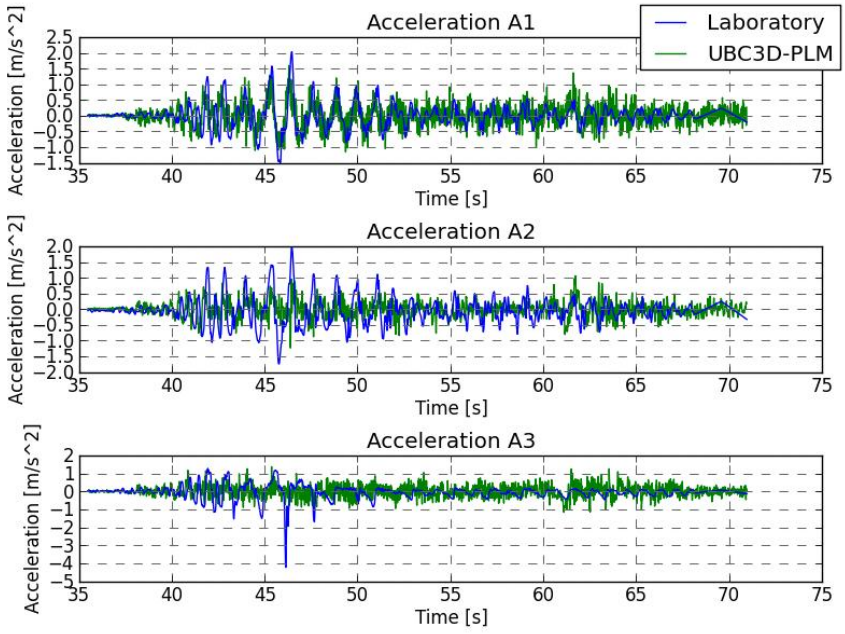

Figure 6.6 Horizontal accelerations for UBC3D-PLM in points A1, A2 and A3 for A475

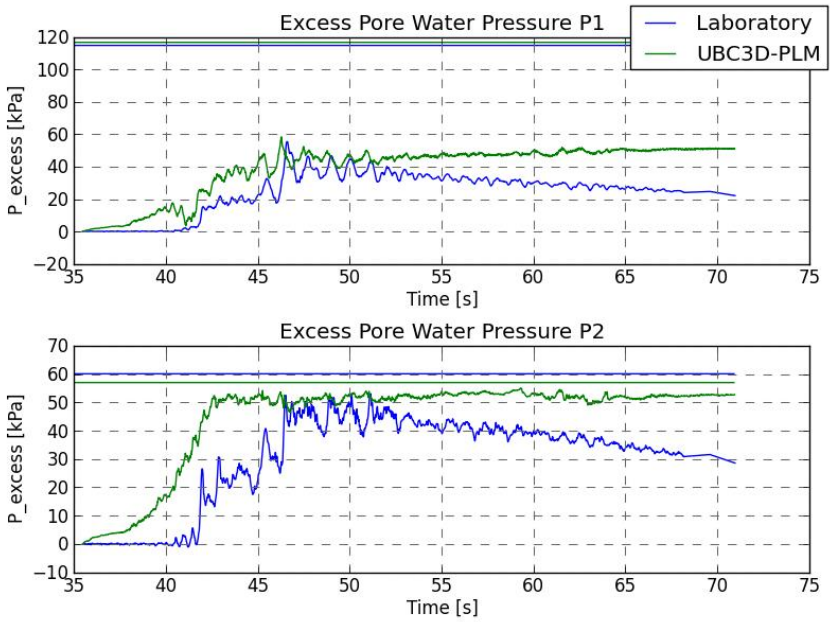

Figure 6.7 Excess pore water pressures for UBC3D-PLM in points P1 and P2 for A475. The horizontal lines represent the initial effective vertical stress.

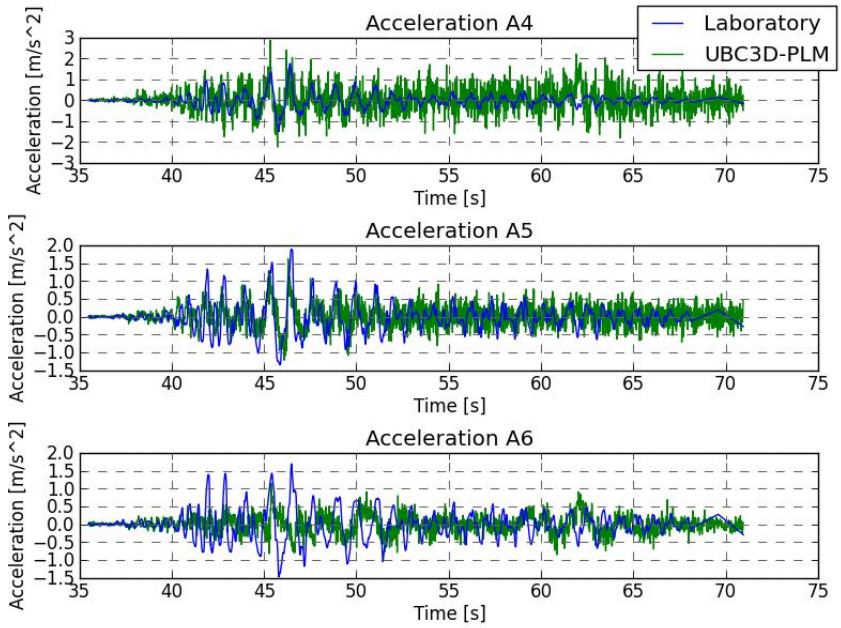

Figure 6.8 Horizontal accelerations for UBC3D-PLM in points A4, A5 and A6 for A475

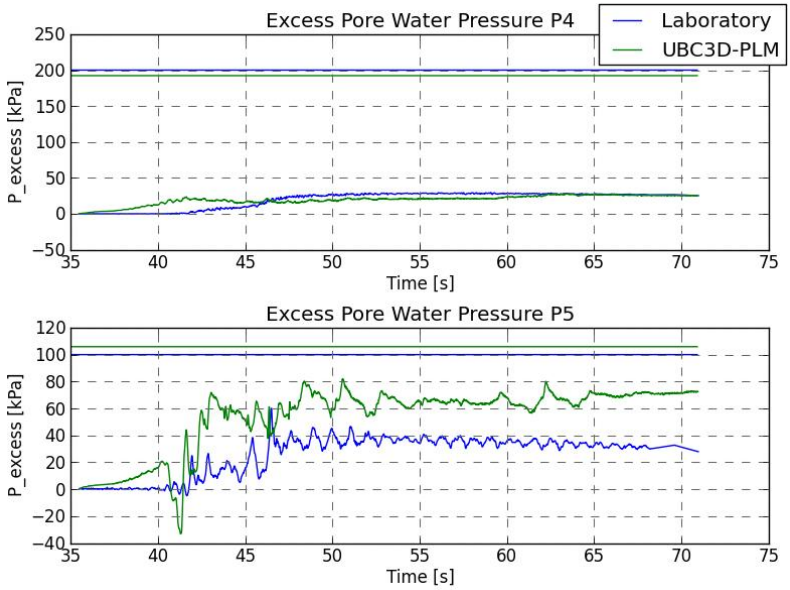

Figure 6.9 Excess pore water pressures for UBC3D-PLM in points P4 and P5 for A475. The horizontal lines represent the initial effective vertical stress.

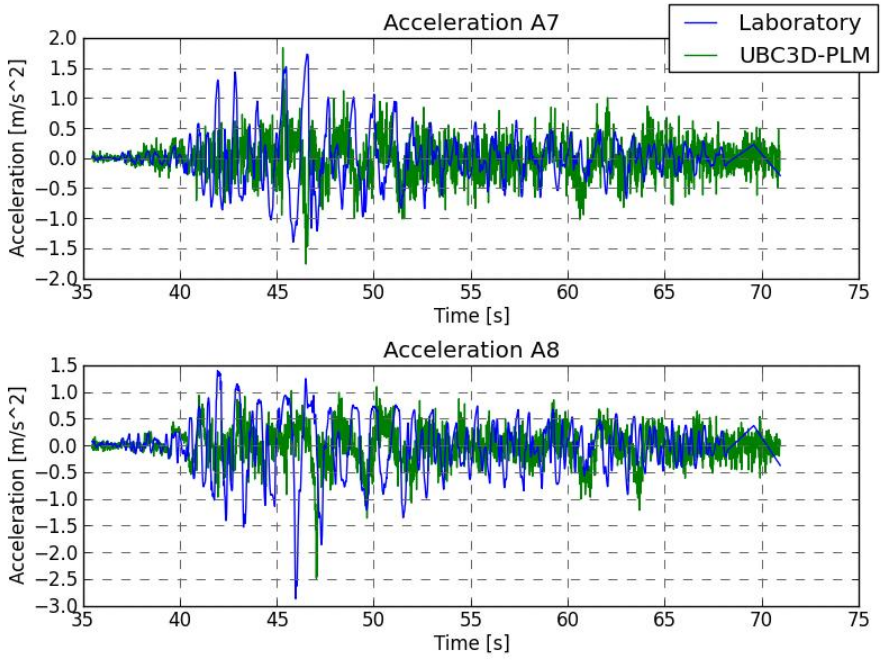

Figure 6.10 Horizontal accelerations for UBC3D-PLM in points A7 and A8 for A475

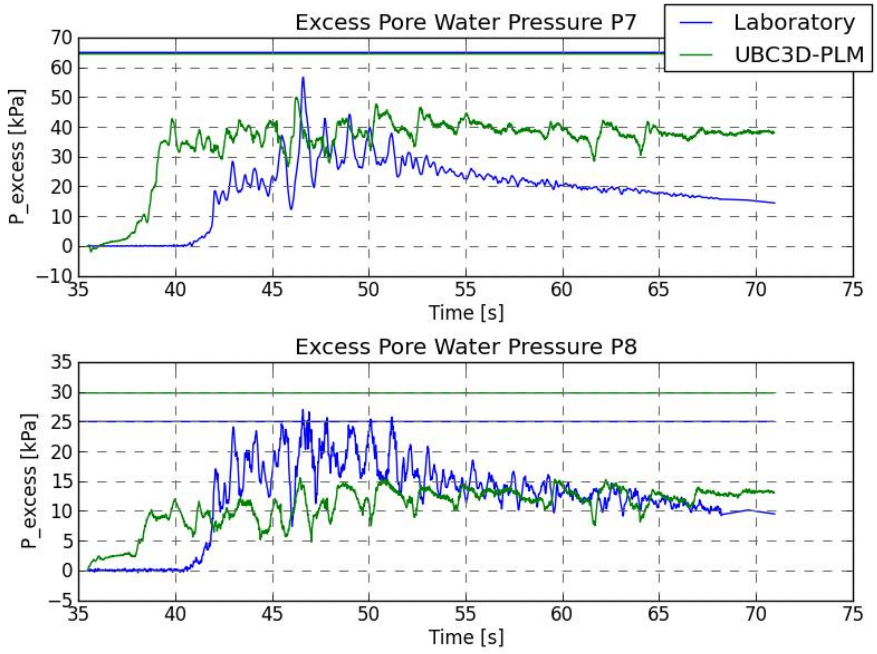

Figure 6.11 Excess pore water pressures for UBC3D-PLM in points P7 and P8 for A475. The horizontal lines represent the initial effective vertical stress.

The displacement direction and magnitude are depicted in Figure 6.12 and Figure 6.13 respectively. The direction of the predicted displacement is plausible. As expected, the soil displaces in downward direction of the slope; resulting in settlements on the top and an increasing surface level at toe. This was also expected to happen during the centrifuge test, but it turned out that the surface level at the toe also moved downward. This is probably caused by absence of significant lateral displacement of the slope during the earthquake (C-CORE, 2004). The magnitude of the settlements is extremely overestimated, which makes the model not suitable for post-liquefaction behaviour. Furthermore, the predicted settlement still increases after fifty to fifty-five seconds; while the soil in the centrifuge test became more or less stable once the largest accelerations are gone and dissipation starts to set in.

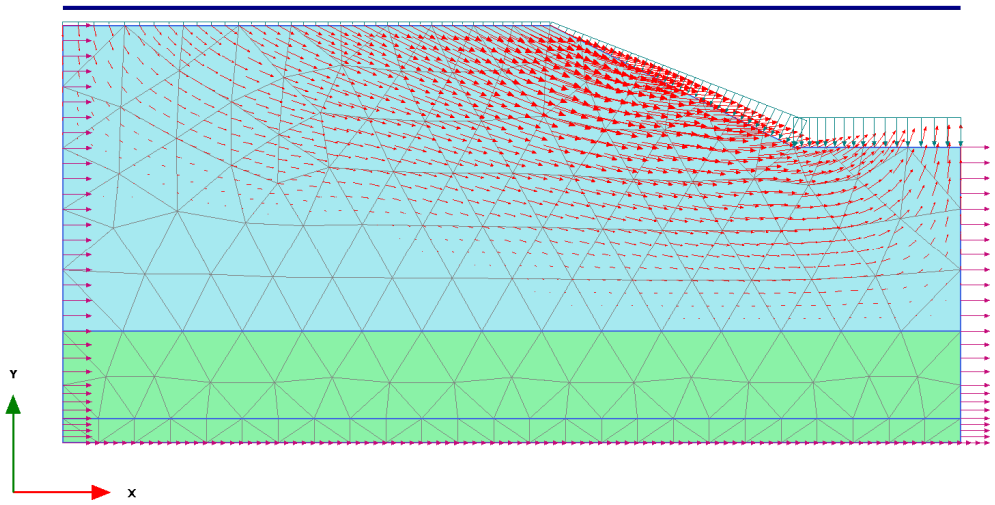

Figure 6.12 Total displacement |u|

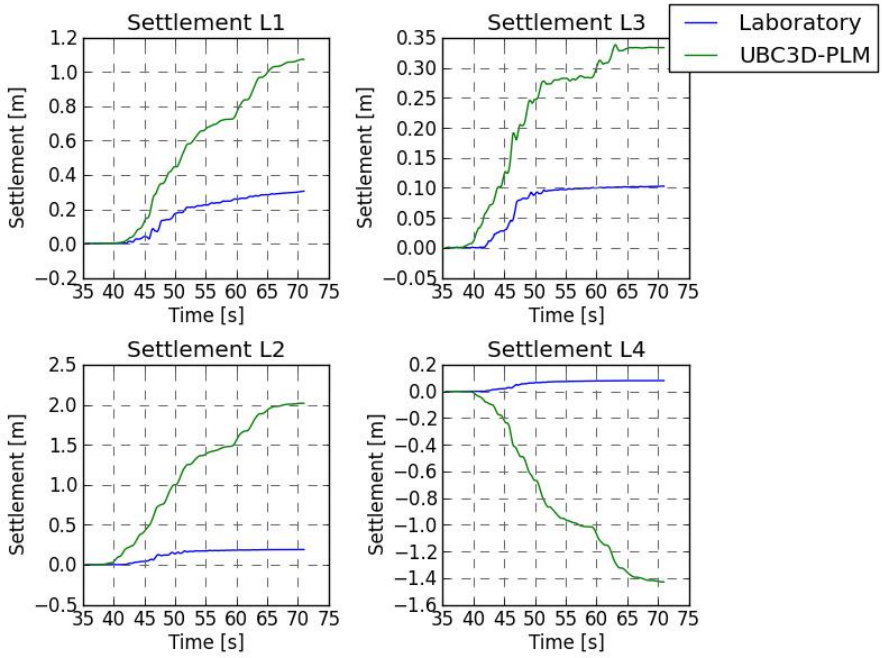

Figure 6.13 Settlements for UBC3D-PLM in points L1, L2, L3 and L4

The results for the A2475 signal are given in appendix J. Considering accelerations; the results are similar to the ones of A475. The maximum amplitude at smaller depths is less and rapid numerical oscillations occur, especially in the second half of the signal. The amplitude in A4 is

overestimated after the largest peaks; similarly to A4 in the A475 signal. Furthermore, the dilative behaviour that is illustrated by the large negative peaks in A3, A6 and A8 is not captured by the model; as it was not captured in A3 for the A475 signal.

The results of the excess pore water pressure development are also similar to the ones of A475. The development of excess pore water pressure is slightly overestimated in P1, but P2 is predicted almost perfectly. The same holds closer to the slope for P4 and P5; P4 is slightly overestimated, whereas P5 is captured accurately. The result in P7 is in a way contrary to the one of A475. For A2475, the development is predicted adequate, but the peak is underestimated; whereas it is the other way around for A475. P8 shows the same problem as it had during the A475 signal: liquefaction occurs, although the excess pore water pressure does not go towards the line of the initial vertical stress. Unfortunately, the effective vertical stress does not approach zero in P7. In P8, it does approach zero; but much later. This makes it difficult to predict liquefaction based on the results. As in the A475 analysis, dissipation is not taken into account by the model.

The settlements results of A2475 are similar to the ones of A475. The settlements are overestimated and the settlements continue after t = 47 seconds, whereas the soil in the laboratory was more or less stable. The only difference is that in L3 the settlement prediction decreases after this point, which was not seen with the A475 signal.

6.3.2 Hypoplastic model

The accelerations further away from the slope, A1, A2 and A3 are depicted in Figure 6.14. The prediction in A1 is accurate, up till fifty seconds. Hereafter, the amplitude becomes significantly larger and the line shows spurious rapid oscillations. It is assumed that this is caused by the complications that are associated with P waves in undrained behaviour. The predictions in A2 and A3, which are closer to the surface, are inaccurate. They have lower amplitude; similarly to the results of UBC3D-PLM. Especially the larger peaks in A2 are not captured by the model. This suggests overdamping. Lastly, the dilative behaviour in A3, represented by the large negative peak, is not captured by the model.

Figure 6.15 depicts the development of excess pore water pressure in P1 and P2. The development in P1 is extremely overestimated. This indicates that the assumption that the loose sand layer is affected completely by static shear is not valid. Two other calculations were done, in order to check this assumption. In the first calculation, the input parameters that were obtained including static shear were only applied in the region close to the slope. However, the development of excess pore water pressure in P1 was almost exactly the same. In the second calculation, the input parameters without static shear were applied in the entire loose sand layer. The complete results of this calculation are given in appendix L. As depicted in Figure 6.20, this calculation predicted the excess pore water pressure in P1 much more accurately. The development in P2 starts accurately, but it starts overestimating after a few seconds. The maximum value is reached earlier and its value is slightly larger than in reality. After some time, dissipation is perceptible in the centrifuge test results. However, this was not captured by the constitutive model.

The accelerations in A4, A5 and A6 are illustrated in Figure 6.16. The acceleration prediction starts accurately in all three points. However, the results of A4 and A5 start to oscillate rapidly after ten to fifteen seconds, with larger amplitude. This effect is larger in A4, which is in the dense sand layer.

The development of excess pore water pressure in P4 and P5 are given in Figure 6.17. It is remarkable that in the dense layer, in P4, suction is predicted by means of negative excess pore water pressures; whereas in reality small positive pressures occurred. However, this point is of minor importance, since the dense layer is unlikely to liquefy. The prediction in P5 is, similar to P1, extremely overestimated. The prediction is much more accurate when the input parameters without static shear are applied on the complete loose sand layer, as shown in Figure 6.21.

Figure 6.18 displays the accelerations beneath the slope, in point A7 and A8. These predictions are similar to the ones in former points. The beginning is accurate, but after some time it starts

oscillation rapidly with larger amplitude. Furthermore, the large negative spike in A8 is not captured.

The development of excess pore water pressure beneath the slope, in point P7 and P8, is depicted in Figure 6.19. Both graphs show that the prediction is not accurate at all. This is disturbing, since both points are of major importance. Negative excess pore water pressures are predicted in P7 and P8, whereas in reality significant positive ones occurred. Even more, the excess pore water pressures in the centrifuge test did approach the initial effective vertical stress. Consequently, the effective vertical stress decreased; whereas it remains more or less constant in the results of the Hypoplastic model. Based on the model predictions, one would expect no reduction in strength and certainly no liquefaction; while the excess pore water pressure in the centrifuge test is close the initial effective vertical stress. The predicted effective vertical stress is decreasing in both points. However, it is not approaching towards zero. It is concerning that based on the development of excess pore water pressure and the effective vertical stress predicted by the model, one would overestimate the strength of the soil significantly. The same problem occurred in the calculation using the parameters that were determined without static shear.

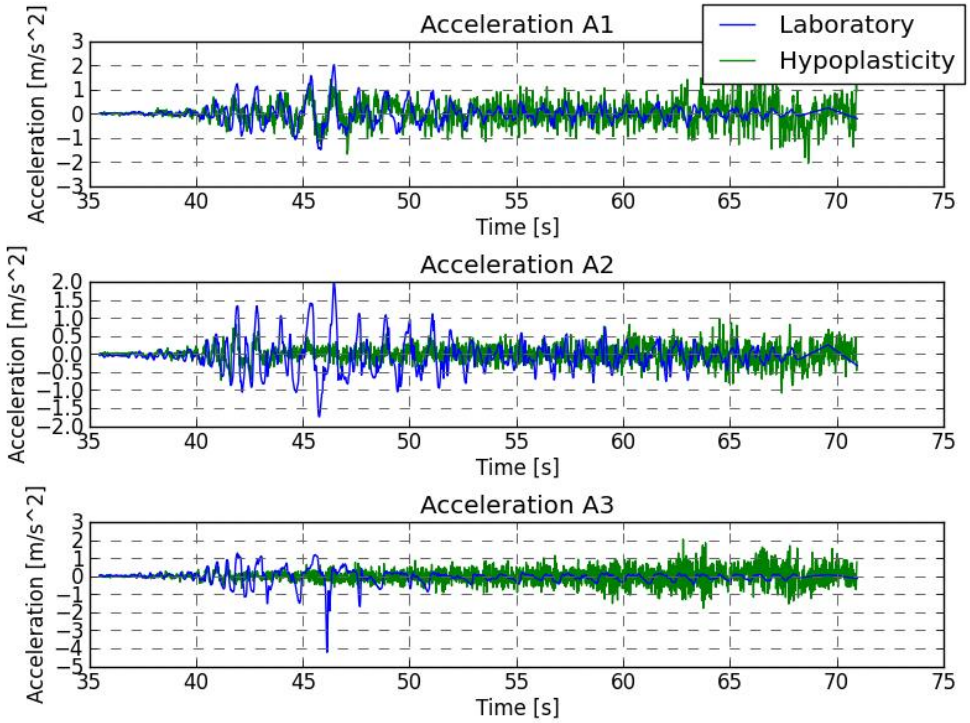

Figure 6.14 Horizontal accelerations with Hypoplastic model in points A1, A2 and A3 for A475

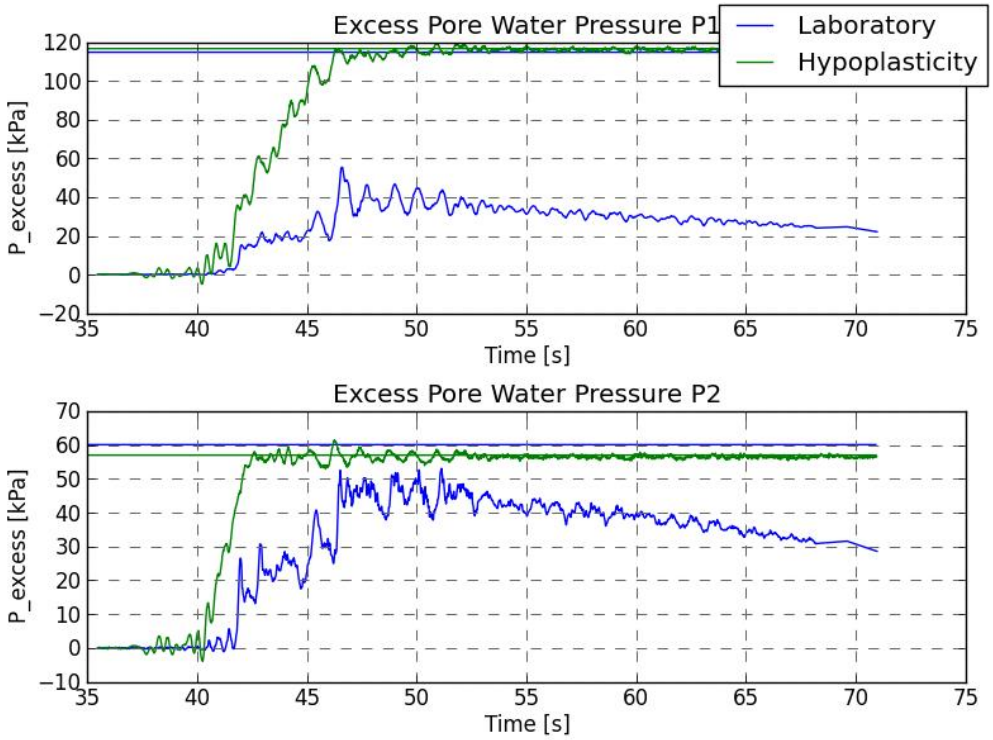

Figure 6.15 Excess pore water pressures with Hypoplastic model in points P1 and P2 for A475. The horizontal lines represent the initial effective vertical stress.

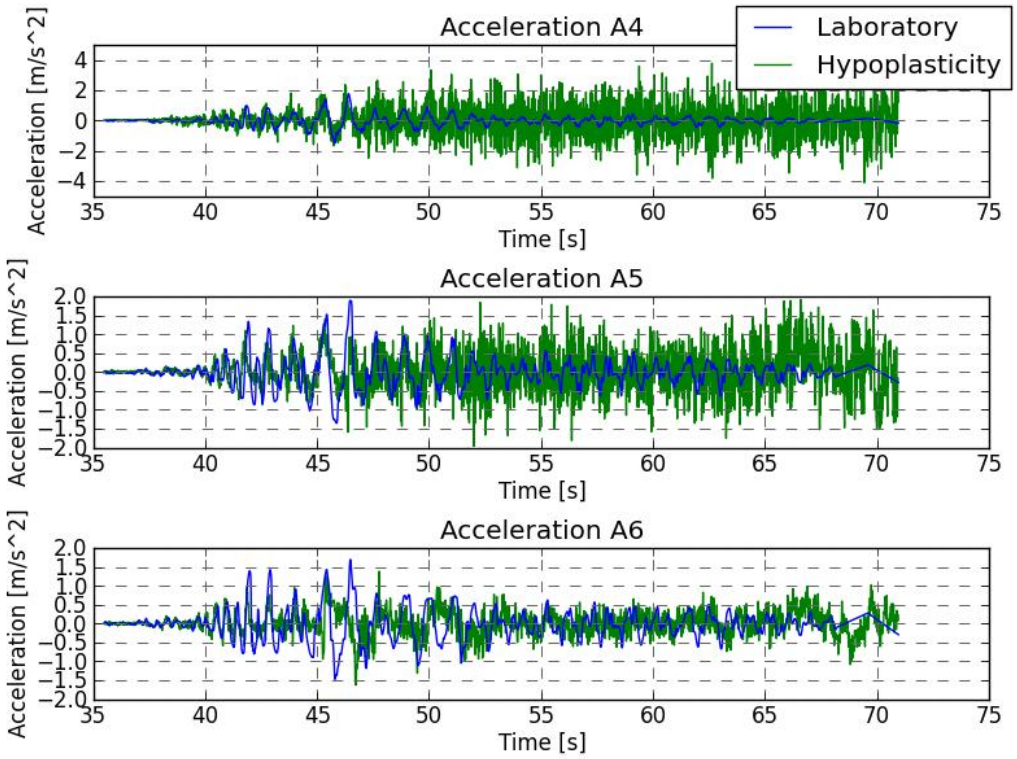

Figure 6.16 Horizontal accelerations with Hypoplastic model in points A4, A5 and A6 for A475

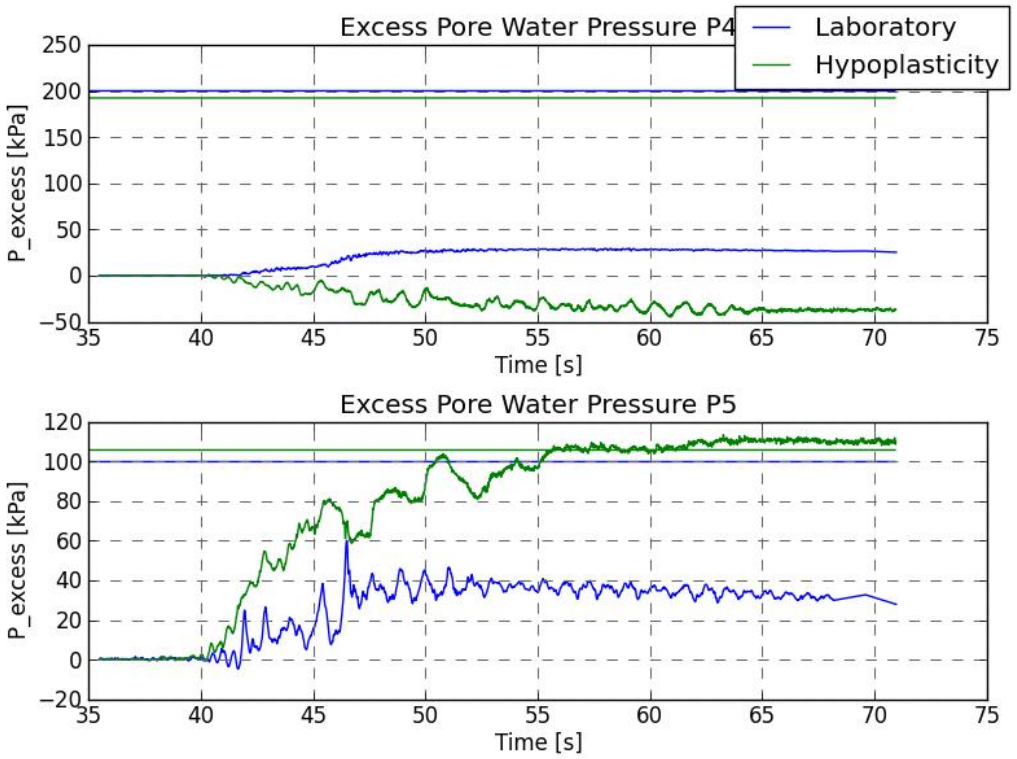

Figure 6.17 Excess pore water pressures with Hypoplastic model in points P4 and P5 for A475. The horizontal lines represent the initial effective vertical stress.

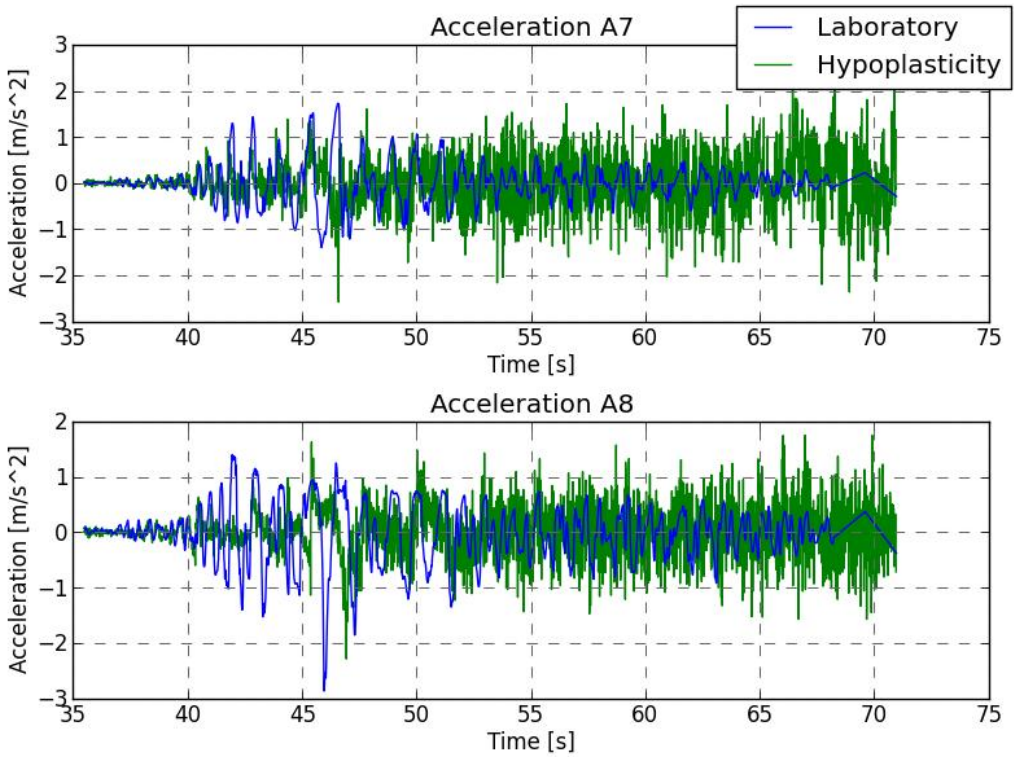

Figure 6.18 Horizontal accelerations with Hypoplastic model in points A7 and A8 for A475

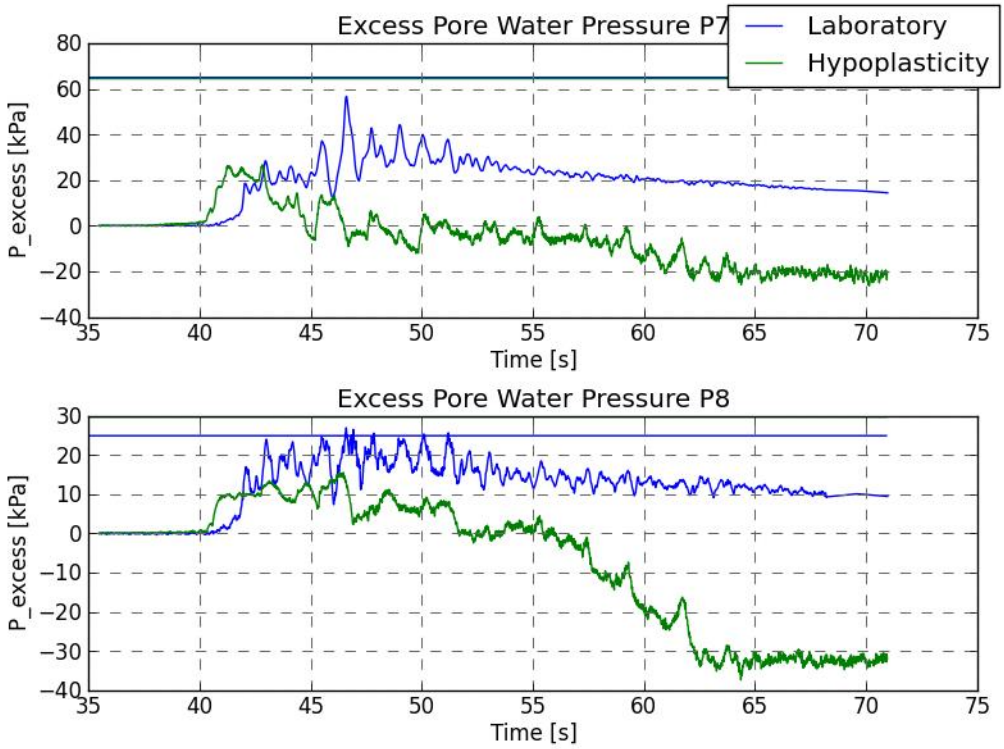

Figure 6.19 Excess pore water pressures with Hypoplastic model in points P7 and P8 for A475. The horizontal lines represent the initial effective vertical stress.

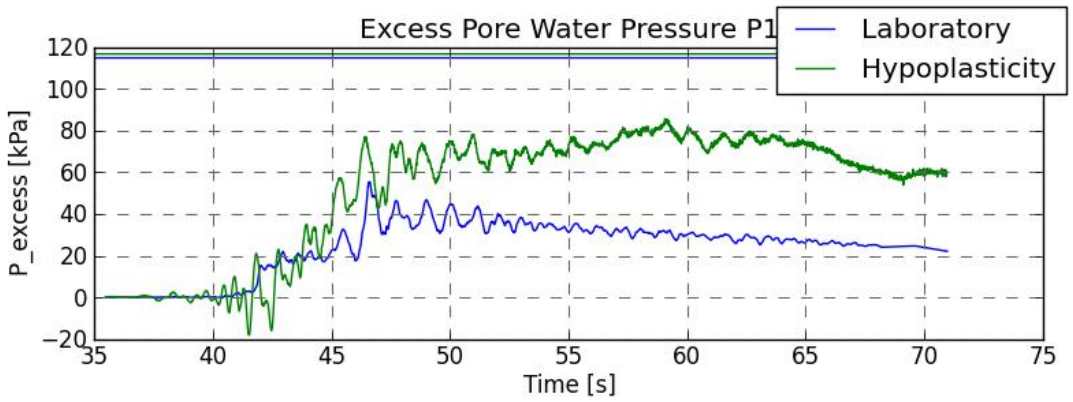

Figure 6.20 Excess pore water pressure development in P1, when the input parameters are determined without static shear

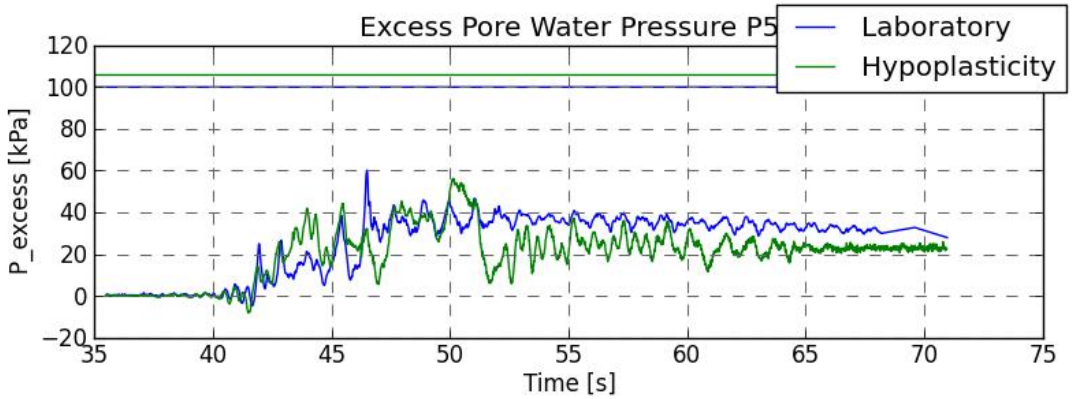

Figure 6.21 Excess pore water pressure development in P5, when the input parameters are determined without static shear

As mentioned before, the development of excess pore water pressure in P1 and P5 were predicted much more accurate in the calculation where the input parameters were determined without static shear were applied on the complete loose sand layer. The results of this calculation are provided in appendix L. The development of excess pore water pressure further away from the slope is affected by the application of input parameters that are obtained including static shear; even if these parameters are only applied nearby the slope.

Figure 6.22 and Figure 6.23 illustrate the settlements that occurred during the earthquake. Figure 6.22 shows that the settlements are captured poorly, with locally extremely high or low values at some points. Moreover, the direction of the displacements is, in most cases, unrealistic. As shown in Figure 6.23, the magnitudes of the settlements are overestimated. Although the overestimation is not particularly large in these graphs, Figure 6.22 shows that at some points extremely large settlements are predicted. The main problem is that the settlement of the model continues after t = 50 s, whereas it in the centrifuge test became more or less stable after some time. It is assumed that the unrealistically large settlements are caused by the rapid large amplitude oscillations of the horizontal accelerations. Because of this, the model is not applicable for post-liquefaction behaviour.

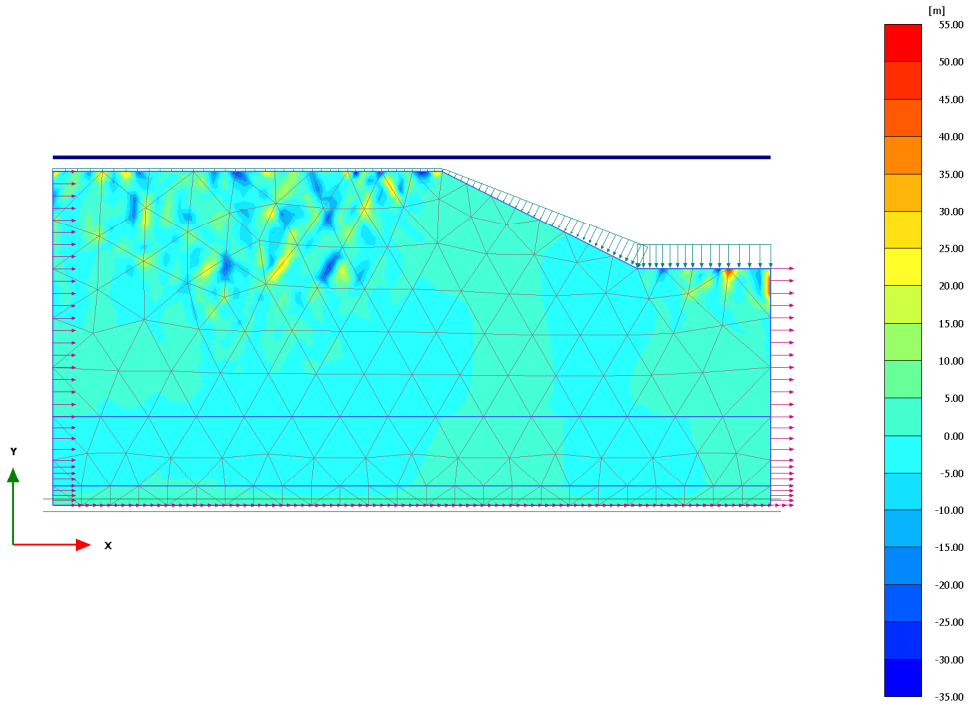

Figure 6.22 Settlements for Hypoplastic model for A475

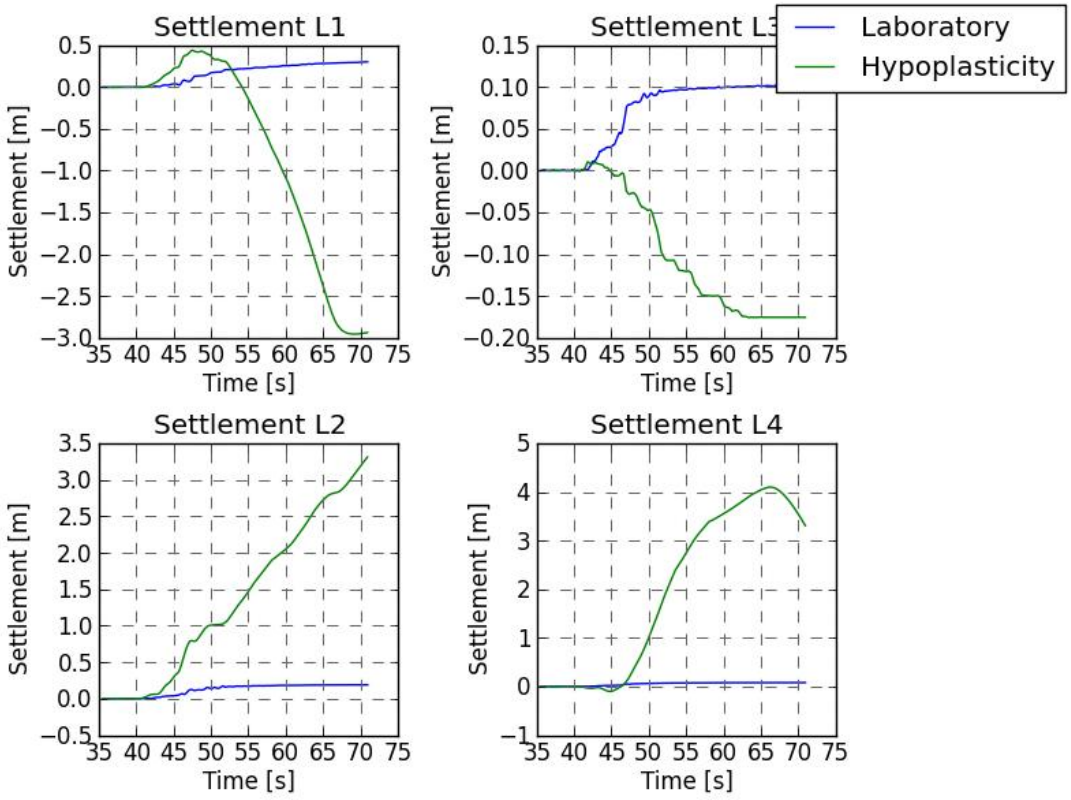

Figure 6.23 Settlements for Hypoplastic model in points L1, L2, L3 and L4

The development of excess pore water pressure depends on the shear stresses, caused by the horizontal acceleration. The inaccurate prediction of horizontal acceleration and the unrealistic

displacements make the reliability and usefulness of the results questionable; also with respect to the development of excess pore water pressure. However, a closer look to the results showed that the remarkable displacement pattern arises after the largest acceleration peaks; so, with other words, after the development of excess pore water pressure. Figure 6.24 illustrates the displacements at *t* is 45 seconds; which, besides a few outliers, corresponds to the displacement pattern one would initially expect. Moreover, the predicted horizontal accelerations were accurate till at least *t* is 45 seconds in most points. Concluding, the large spurious oscillations in the horizontal acceleration do affect the displacements, but the development of excess pore water pressure is not influenced. Appendix L provides similar figures as Figure 6.24, at different points in time.

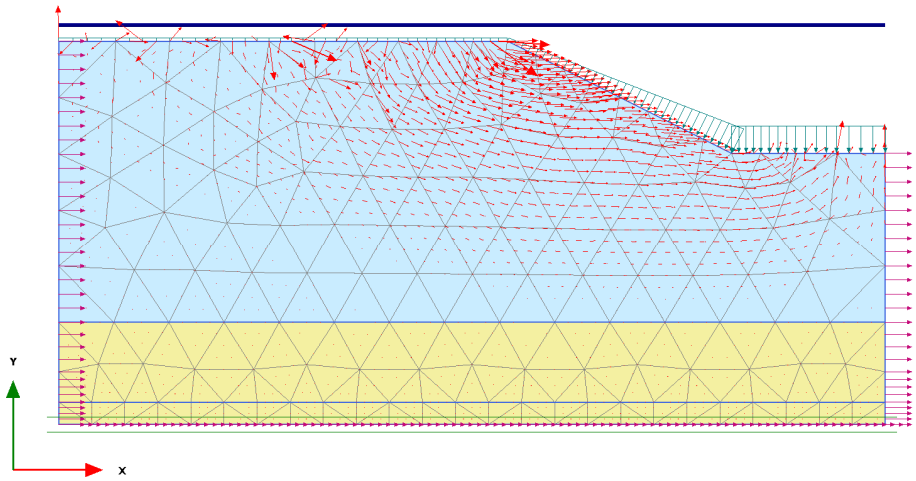

Figure 6.24 Displacements at t = 45 s; maximum displacement is 2.51 metres

The results for the A2475 signal are given in appendix M. The acceleration results are similar to the ones of A475. In A2 and A3, smaller amplitudes are predicted in the beginning. Furthermore, dilative behaviour that occurred in A3, A6 and A8 is not captured by the model. Lastly, these results also contain the rapid oscillations with larger amplitudes and again this effect is largest in the dense layer, in A4.

Considering the excess pore water pressure development, the quality of the results is varying. The results in P2 and P5 are promising. Both are very accurate, although P5 is slightly overestimating. The development of excess pore water pressure in P1 is overestimated, although it is not so much as in P1 with the A475 signal. The influence of the application of input parameters that have been obtained including static shear is much less than with the A475 signal. Similarly to the A475 signal, P4 shows a small negative development of excess pore water pressures. Contrary to the A475 signal, in P7 and P8 are predicts positive excess pore water pressures predicted. Although this is a more accurate result; it is still not satisfactory. The prediction of excess pore water pressure is underestimated and purely based on these graphs; one would expect larger soil strength.

The results for the settlements with A2475 are different than to the ones of A475. With the A2475 signal, settlements are predicted in each point; whereas with the A475 signal a rise of the surface level was predicted in L1 and L3. Again, the settlements are overestimated. Figure 6.22 shows that the settlements for A475 had locally extremely large peaks; this was also the case for A2475.

6.4 Comparison and conclusion

UBC3D-PLM is able to give moderate predictions regarding accelerations. Overdamping causes that the maximum amplitudes are slightly lower at locations closer to the surface and small numerical oscillations occur at the second half of the signal. The predicted accelerations with Hypoplastic model are moderate in the first few seconds, but poor after the first large peaks. After these peaks, the accelerations start to oscillate rapidly, with larger amplitude. It is expected that this is caused by the complications that are associated with P waves in undrained behaviour. However, it did not influence the development of excess pore water pressure. The accuracy of the

Hypoplastic model is much lower than UBC3D-PLM when considering acceleration predictions. In addition, both models were not able to capture dilative behaviour that occurred in the centrifuge test.

The quality of the excess pore water pressure predictions varies; although it is satisfactory in most cases. Appendix N provides six graphs comparing the predicted development of excess pore water pressure for both models with the actual development from the centrifuge test. UBC3D-PLM overestimates the development in the first few seconds, till the first large accelerations take place. This is caused by initialisation of the model; which is the main reason of inaccuracies. Considering the prediction of liquefaction onset, this might lead to too conservative results. Generally, the maximum excess pore water pressure is predicted correctly in points P1, P2 and P5. Hence, these results are sufficiently satisfactory to predict whether liquefaction occurs. The results in the Hypoplastic model are affected by the application of input parameters that have been determined when static shear stress was included. When the loose sand layer is modelled with input parameters that have been determined without static shear stress, the development of excess pore water pressure is estimated accurately in P1, P2 and P5.

The prediction of the Hypoplastic model in P4 is not accurate, since it predicts negative pore excess pressures instead of positive ones. The result of UBC3D-PLM in this point is relatively accurate. However, this point is in the dense sand layer, so it is unlikely that liquefaction will occur at this point. Therefore, this point is of minor importance.

The predicted excess pore water pressures below the slope, in point P7 and P8 are disappointing. Liquefaction occurs, but the development of excess pore water pressure is probably supressed by the displacements in both models; presumably due to the influence of static shear. The only satisfactory result is shown in P7 with the A475 signal in UBC3D-PLM; although this result predicts liquefaction much earlier than in reality.

At last, both models are not suitable to predict post-liquefaction behaviour, since deformations are extremely overestimated. Part of this overestimation is caused by the fact that dissipation is not taken into account; resulting in pursuing deformations while the largest accelerations are over. Besides, the extreme overestimation in the Hypoplastic model is also caused by the spurious large amplitude oscillations in the accelerations. Although the deformations predicted by UBC3D-PLM are overestimated, they might be useful for an indication of the deformations. However, they show exactly what one would expect based on his or her geotechnical knowledge and experience. The deformation magnitude and pattern predicted by the Hypoplastic model is only reasonable till the first large peaks; hereafter both become unrealistic.

Concluding, both models give satisfactory results for the excess pore water pressure development where the soil is layered horizontally and static shear stresses are not involved. Hence, both models could be useful to predict liquefaction in similar situations. However, when static shear stresses are involved, for instance beneath the slope, the results are less accurate. When also considering the development of effective vertical stress and settlement; one might recognise liquefaction. Generally, when one of both models predicts liquefaction, the model is right and relatively accurate; except for the Hypoplastic model when the input parameters are determined including static shear stresses. However, when one of both models does not predict liquefaction, it does not necessarily mean that liquefaction will not occur. It might be the case that the models did not show liquefaction clearly, whereas it is clear in the results of the centrifuge test. With other words, it is possible to see that liquefaction occurs; but it is not possible to see liquefaction will not occur. This is problematic when the models are used for the design or safety assessment of a dyke and one needs to be absolutely sure liquefaction will not occur. It is, beneath the slope, not possible to exclude liquefaction with either UBC3D-PLM or Hypoplastic model. Finally, the accuracy of the Hypoplastic model and UBC3D-PLM with respect to excess pore water pressure development is comparable. Although the Hypoplastic model had more accurate results during the calibration was it not able to distinguish itself during the validation. The most striking conclusion is that in the Hypoplastic model application of input parameters that have been determined including static shear stresses did not result in a better prediction beneath the slope. However, it did affect the development of excess pore water pressure further away from the slope in a negative way.

7 Conclusion

7.1 How can finite element models be applied within the Dutch design approach?

The possible consequences of earthquake loading on earthen dykes are divided in three mechanisms:

- Squeezing, caused by squeezing of a liquefied soil layer beneath a dyke; resulting in settlements or deformations.
- Densification, caused by dissipation of excess pore pressures in liquefied soils; resulting in settlements.
- Macro instability. Reduction of soil strength when the effective stress is reduced by the development of excess pore pressures can result in sliding of either inner or outer slope of a dyke. Liquefaction is not required for this component.

The focus of this research is on the prediction of excess pore water pressure development and the onset of liquefaction. This is required to investigate if liquefaction occurs; which means that the dyke is vulnerable to squeezing and densification. Furthermore, the developed excess pore water pressure is used to determine the soil strength reduction for the macro instability calculation. In addition, the accuracy of the predicted displacements is evaluated to see if this can be used for macro instability.

Unfortunately, the deformation was overestimated with both the UBC3D-PLM and Hypoplastic constitutive model and the deformation pattern that was predicted by the Hypoplastic model after the first large acceleration peaks was unrealistic. However, this did not affect the predicted development of excess pore water pressure. Furthermore, the excess pore water pressure development beneath the slope was not realistic in both constitutive models; the development was suppressed by the displacements. Hence, both models are not suitable for densification and macro instability analyses with integrated pore water pressure generation.

The only locations where both models provided promising results were beneath the horizontal surface; although the development of excess pore water pressure was slightly overestimated in comparison with the results of the centrifuge test. This results in more conservative designs, since liquefaction was predicted earlier in the model than actually occurred in the centrifuge test.

Since the results of both models below the horizontal surface were promising, the models may be suitable to model the development of excess pore water pressure and the onset of liquefaction in loose sand layers beneath a dyke or other flood defence structures. This is affirmed by PLAXIS for UBC3D-PLM, reporting: *"the UBC3D-PLM model can be considered capable of modelling the accumulation of excess pore water pressures in saturated loose sands subjected to cyclic loading"* (PLAXIS, 2015); after performing calculations with a horizontally layered soil model in UBC3D-PLM. In this way, the constitutive models may be used to identify liquefiable layers and to investigate their susceptibility to liquefaction. However, this is a very limited application which should be validated before it can be applied in practice. The validation should also provide insight in the accuracy of predicted deformations in such analyses, since this is still unknown. Figure 7.1 depicts how to set up a finite element model for earthquake modelling.

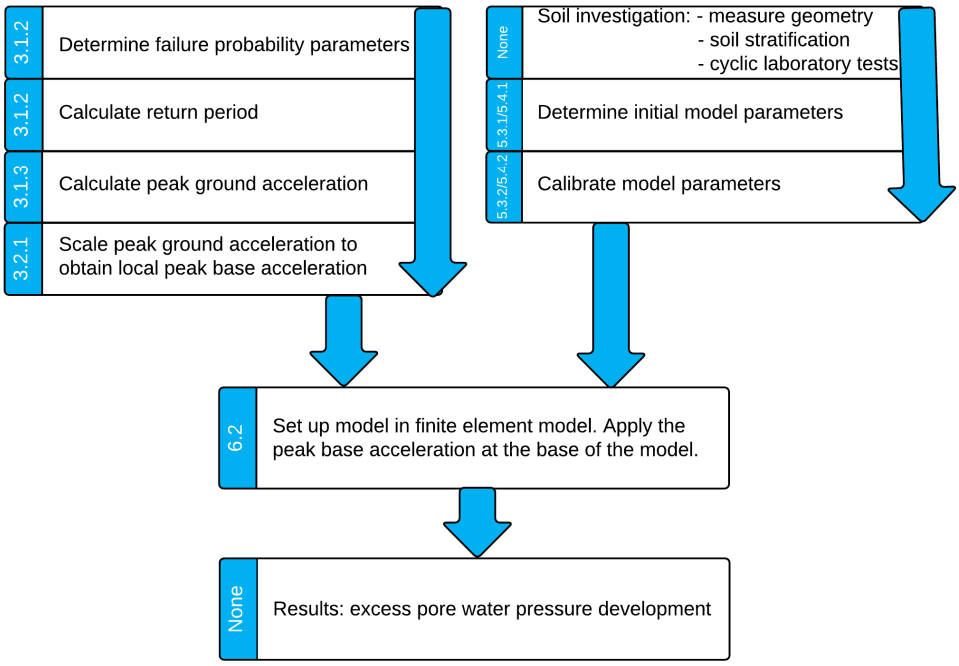

Figure 7.1 Flowchart how to set up a finite element model for earthquake modelling. The numbers in the blue box refer to the accessory paragraph in this report.

7.2 How to determine the earthquake load according to the Dutch standards?

The design Peak Ground Acceleration of the earthquake depends on the following parameters:

- norm, by means of design probability per year P_d;
- contribution to the failure probability budget ω;
- Influence factor α;
- length effect, depending on three parameters:
  - constant that indicates which fraction of the trajectory's length is sensitive to earthquakes a;
  - length of trajectory considered L_t;
  - length of a typical section for failure mechanism L_j.

The calculation steps that are required to determine the *PGA* are given in Figure 7.2.

There are still a lot of ongoing discussions on which values should be applied to obtain the design peak acceleration; mainly due to the fact that earthquake loading, especially in combination with flood defences, is still an uncharted territory in the Netherlands. The most dominant parameters is α; especially for higher values. With a larger contribution to the failure probability budget and a shorter recovery time is it possible to reduce the return period and consequently the *PGA*.

Moreover, the discussion about an upper boundary for the peak ground acceleration *PGA* might even be more important. The determination of the return period in combination with the absence of a physical upper boundary results in unrealistically high *PGA*s. It is expected that there is an upper boundary, since soft soil is not able to transfer large accelerations. However, it is not trivial to determine such an upper boundary for Groningen. This problem will be irrelevant in case the earthquake signals are provided at the base instead of surface level. In that case, the finite element calculation takes the confined shear strength of soft soils into account and therewith the maximum physically possible accelerations at surface level.

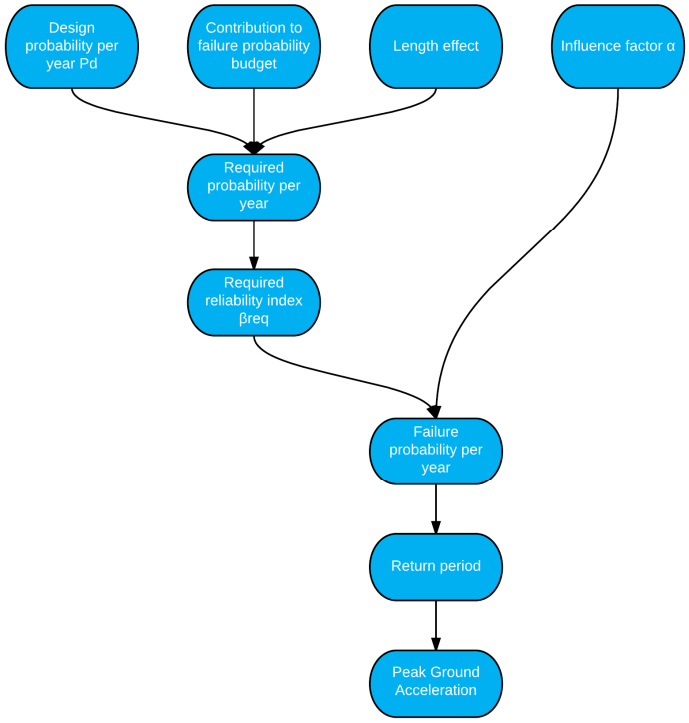

Figure 7.2 Flowchart depicting the procedure to determine the design PGA

7.3 How to obtain model parameters from the laboratory tests?

The most accurate way to obtain model parameters of both models requires several types of (cyclic) laboratory tests required like triaxial, oedometer and direct simple shear; which are mostly not available. It is therefore recommended to use another method to obtain the model parameters.

For the UBC3D-PLM model, the relation proposed by Beaty and Byrne between the normative SPT blowcount $(N_1)_{60}$ and most of the other parameters (Beaty & Byrne, 2011) can be used. The parameters that cannot be related to $(N_1)_{60}$ are mostly standard values. The obtained values are used as initial values for calibration on cyclic DSS tests. During the calibration, these values were adjusted to obtain a more accurate fit on the results of the DSS tests.

Unfortunately, no correlation between SPT or CPT results and Hypoplastic parameters is available; consequently the parameters for this model are more difficult to determine. The initial model parameters for the Hypoplastic model were obtained by comparing the critical void ratios, which are related to the minimum and maximum void ratio from the index test, to several known parameters sets of similar types of sand. It was concluded that Fraser River Sand has the most similarity with Hostun sand; so the Hypoplastic parameters of Hostun sand were adopted as initial values for the calibration. Again, the initial values were adjusted to get a more accurate fit on the results of the DSS tests. This method can also be applied for other types of sand, although one should always compare the results with cyclic laboratory tests, to be sure that the obtained model parameters are valid.

Lastly, both constitutive models required a separate set of model parameters in case of static shear stress; calibrated on cyclic DSS tests with static shear.

7.4 How is the behaviour of UBC3D-PLM and the Hypoplastic model in comparison with centrifuge tests?

The results of both models were in most cases rather disappointing, as reported in paragraph 6.3. UBC3D-PLM is able to model horizontal accelerations relatively accurate in most points. However, the fact that the model is overdamped results in slightly lower amplitudes closer to the surface. Furthermore, small numerical oscillations occur in the signal. The accelerations predicted by the Hypoplastic model start accurate. However, spurious rapid oscillations with large amplitudes occur after the first large peaks, continuing till the end of the signal. Hence, UBC3D-PLM gave better results for the accelerations. In addition, both models did not capture the dilative behaviour that occurred in the centrifuge test.

Considering the predicted development of excess pore water pressure, the accuracy of the results is diverse. In the loose layer beneath the horizontal surface, in P1, P2 and P5, the results of both models are relatively accurate, when the model parameters for the Hypoplastic model were determined without static shear stress. In case the model parameters that have been determined including static shear stress were applied on the loose sand layer, the excess pore water pressure was largely overestimated. This was also the case when these model parameters only were applied nearby the slope. In general, the development of excess pore water pressure in P1, P2 and P5 is slightly overestimated; which would result in conservative estimations. The excess pore water pressure in the dense layer, in P4, is also predicted accurately by UBC3D-PLM, whereas the Hypoplastic model predicts suction, by means of negative development of excess pore water pressure. However, this point is of minor influence since it is unlikely that the dense layer will liquefy.

In the slope, in P7 and P8, the results are unreliable; although this might be the most important location. It appears that the development of excess pore water pressure in some cases is suppressed by the occurring deformations. In some cases it is possible to detect liquefaction based on the development of the effective vertical stress and the deformations, but in other cases it is not possible. This problem occurred with both UBC3D-PLM and the Hypoplastic model. In case one of the models predicted liquefaction, it was right. However, it was not possible to exclude liquefaction, based on the model results. This is concerning since one might assume that a soil structure is safe; whereas in reality liquefaction might occur.

To summarise, both models are able to predict the development of excess pore water pressure accurately, as long as there are no or hardly any deformations. Beneath sloping ground, the results become unreliable.

Finally, both models overestimated the deformations; making them unsuitable for modelling post-liquefaction behaviour. This effect was much larger for the Hypoplastic model, which predicted extremely large deformations. However, this application of the models is of minor interest.

7.5 To what extent are UBC3D-PLM and Hypoplastic model applicable to dyke design with earthquake loading?

Based on the comparison with centrifuge tests, it is concluded that the applicability of both constitutive models is limited. It should be noted that, although it is currently the best method to evaluate the accuracy of constitutive models, centrifuge tests are not able to simulate a practical situation perfectly.

Both UBC3D-PLM and the Hypoplastic model give promising results for the excess pore water pressure development in points P1, P2 and P5; which are beneath the horizontal surface. At these locations, hardly any deformation occurs. This signifies that both models are suitable to predict liquefaction in loose sand layers beneath a dyke or other flood defence structure. In this way, both models can be used to identify liquefiable layers and to investigate their susceptibility to liquefaction. However, this should be validated more extensively before it can be applied in practice; for instance by validating on similar centrifuge tests as used for this research, but then with a horizontally layered soil profile.

Based on the results beneath the slope, in P7 and P8, is concluded that both models are not sufficiently accurate in reproducing the centrifuge test. The models are correct when they predict liquefaction, but liquefaction cannot be excluded when the models do not predict liquefaction. This is concerning and one should be aware of this limitation when using constitutive models to predict liquefaction.

Although the results are not completely satisfactory, there are some positive points. The model parameters could be obtained relatively easily. Moreover, it was possible with both models to reproduce the cyclic DSS tests relatively accurately during the calibration procedure. Especially the results of the loose sand without static shear were extremely accurate with the Hypoplastic model, whereas UBC3D-PLM was less able to handle different cyclic stress ratios. Surprisingly, the Hypoplastic model gave similar results as UBC3D-PLM for loose sand during the validation and was not able to be more accurate than UBC3D-PLM. However, the Hypoplastic model could not be calibrated accurately for dense sand; which clearly had its repercussion on the result of the validation in P4.

The fact that the model parameters can be obtained relatively easily and the cyclic DSS tests can be simulated accurately forms a solid base for future development of both models. However, significant improvement is required to obtain reliable and applicable results. The most important improvement that is required for practical situations is the implementation of static shear stresses in combination with excess pore water pressure development.

8 Recommendations for further research

This research forms a very small part in a substantial research campaign related to earthquake engineering in the Netherlands. Since this subject is only a few years at issue now, a significant amount of research is still to be done. This chapter provides recommendations for further research.

8.1 Return period

The design peak ground acceleration PGA_{design} is based on the return period. Currently, there are hardly any earthquake specific values for the required parameters to determine the return period; since this topic is relatively new in the Netherlands. Mostly, parameters of other fields are adopted; like the stability parameters in the length effect. More research on these parameters is required to:

- check the validity of the currently applied values;
- investigate if more favourable values may be used, which would result in less conservative designs.

Currently, most parameters are adopted from the static stability calculations, since that is the best what is available. However, earthquakes are significantly different. For instance, the magnitude of an earthquake decreases when the distance to the epicentre increases. Hence, it is unlikely that a few kilometres of dyke will fail due to an earthquake. Consequently, the parameters that are related to the length effect might be changed to more favourable ones.

8.2 Peak ground and base acceleration

The current method to determine PGA_{design} results in extremely large accelerations; which are physically not realistic because of the confined shear strength of soils. Hence, it is required to define an upper boundary for the *PGA*. A few different methods have been proposed over the last year:

- defining a fixed value as upper limit;
- apply a new non-linear transfer function for soft soils;
- use base accelerations, instead of accelerations at surface level, in combination with site response analyses.

It is currently expected that the latter is the most promising solution; since the site response analysis can take the confined shear strength of soft soils into account. Furthermore, the design peak base acceleration PBA_{design} can be applied in finite element calculations, so there is no need to determine PGA_{design}. However, further research and discussion with involved parties is required to settle a standard method for an upper boundary.

8.3 Calibration

Firstly, more research is required on the way the initial Hypoplastic model parameters were determined during this research; by comparing the critical void ratios to other known Hypoplastic parameter sets. In this case, the results for loose Fraser River Sand were extremely accurate. However, it cannot be concluded that this method works perfectly in any case, based on this research only. If, after several other calibrations, can be proved that this method works; it would simplify the calibration procedure significantly.

Secondly, one of the main advantages of UBC3D-PLM over the Hypoplastic model is that the initial model parameters can be estimated with SPT value $(N_1)_{60}$, by the relation of Beaty and Byrne. A similar relation between $(N_1)_{60}$ and the Hypoplastic model parameters would simplify the calibration procedure and thereby improve the applicability of the model significantly.

Finally, it would be useful to have a relation between CPT values and the model parameters of both models. The relation of Beaty and Byrne for UBC3D-PLM is based on SPT values, whereas in Europe mostly CPTs are used. This would simplify the calibration procedure enormously. In that case, the model parameters for soil profiles with several different sand layers can obtained much quicker; since then it is not required to perform a time-consuming calibration for each individual sand layer.

8.4 Static shear stress

As mentioned in paragraph 6.4 and 7.4, both models were not able to predict the development of excess pore water pressure accurately in combination with static shear stress. Further research on this topic is required, because this would be a valuable addition to the models. For instance, when the development of excess pore water pressure can be predicted accurately in the slope, the strength reduction that is required for macro instability calculations can be determined.

8.5 Finite element model

PLAXIS is not able to include dissipation in dynamic calculations; whereas during the centrifuge tests dissipation occurred after the large peaks in horizontal acceleration. Consequently, the development of excess pore water pressure is overestimated and the settlements continue, whereas they become more or less stable in reality. This is one of the causes of the settlement overestimation. More accurate results might be obtained when dissipation can be taken into account; hence further research on this topic is required.

9 References

Akkar, S., Sandikkaya, M. A., & Bommer, J. J. (2013). Empirical Ground-Motion Models for Point- and Extended-Source Crustal Earthquake Scenarios in Europe and the Middle East. *Bulletin of Earthquake Engineering, 12*(1), 359-387.

Anaraki, K. E. (2008). *Hypoplasaticity Investigated.* (Master of Science thesis), Delft University of Technology, Delft, The Netherlands.

Arulanandan, K., & Scott, R. F. (1993). Project VELACS - Control Test Results. *Journal of Geotechnical Engineering, 119*, 1276-1292.

Ashford, S. A., Jakrapiyanun, W., & Lukkunaprasit, P. (2000). *Amplification of Earthquake Ground Motion in Bangkok*. Paper presented at the 12th World Conference on Earthquake Engineering, Auckland, New Zealand.

Bauer, E., & Wu, W. (1993). A Hypoplastic Model for Granular Soils under Cyclic Loading. In D. Kolymbas (Ed.), *Modern Approaches to Plasticity* (pp. 247-258). Amsterdam: Elsevier.

Beaty, M. H., & Byrne, P. M. (2011). UBCSAND Constitutive Model Version 904aR.

Beaty, M. H., & Perlea, V. G. (2011). *Several Observations on Advanced Analyses with Liquefiable Materials*. Paper presented at the 31st USSD Annual Meeting and Conference, San Diego.

Begeleidingscommissie Onderzoek Aardbevingen. (1993). Eindrapport Multidisciplinair Onderzoek naar de Relatie tussen Gaswinning en Aardbevingen in Noord-Nederland.

Bocchi, F. (2014, 16 October). Yield Surfaces and Plastic Flow Rules in Geomechanics. Retrieved 11 May, 2015, from http://www.comsol.nl/blogs/yield-surfaces-plastic-flow-rules-geomechanics/

Bommer, J. J., Abrahamson, N. A., Strasser, F. O., Pecker, A., Bard, P. Y., Bungum, H., . . . Studer, J. (2004). The Challenge of Defining Upper Bounds on Earthquake Ground Motions. *Seismological Research Letters, 75*(1), 82-95.

Booth, E., & Key, D. (2006). *Earthquake Design Practice for Buildings* (Second ed.). London: Thomas Telford Publishing.

Brinkgreve, R. B. J. (2014a). *Hypoplasticity*. PowerPoint Presentation retrieved from http://blackboard.tudelft.nl/webapps/portal/frameset.jsp?tab_tab_group_id=_10_1&url=%2Fwebapps%2Fblackboard%2Fexecute%2Flauncher%3Ftype%3DCourse%26id%3D_49105_1%26url%3D, viewed 13 January 2015. Delft University of Technology, Delft, The Netherlands

Brinkgreve, R. B. J. (2014b). *UBCSAND model*. PowerPoint Presentation retrieved from http://blackboard.tudelft.nl/webapps/portal/frameset.jsp?tab_tab_group_id=_10_1&url=%2Fwebapps%2Fblackboard%2Fexecute%2Flauncher%3Ftype%3DCourse%26id%3D_49105_1%26url%3D, viewed 13 January 2015. Delft University of Technology, Delft, The Netherlands

Brinkgreve, R. B. J. (2015). *Possiblities and Limitations of Material Models for Soil and Rock*. PowerPoint Presentation retrieved from http://blackboard.tudelft.nl/webapps/portal/frameset.jsp?tab_tab_group_id=_10_1&url=%2Fwebapps%2Fblackboard%2Fexecute%2Flauncher%3Ftype%3DCourse%26id%3D_49105_1%26url%3D, viewed 13 January 2015. Delft University of Technology, Delft, The Netherlands

C-CORE. (2004). Earthquake Induced Damage Mitigation from Soil Liquefaction. Data Report - Centrifuge Test CT1. Contract Report Prepared for University of British Columbia. St. John's, NL.

C-CORE. (s.a.-a). About C-CORE. Retrieved March, 9th, 2015, from http://www.c-core.ca/aboutus

C-CORE. (s.a.-b). Corporate History. Retrieved March, 9th, 2015, from http://www.c-core.ca/corporatehistory

C-CORE. (s.a.-c). Facilities & Resources. Retrieved March, 9th, 2015, from http://www.c-core.ca/facilities

C-CORE. (s.a.-d). Geotechnical Centrifuge Modeling. Retrieved March, 9th, 2015, from http://www.c-core.ca/CentrifugeModeling

California Geological Survey. (2008). Guidelines for Evaluating and Mitigating Seismic Hazards in California.

CIRIA. (2013). *International Levee Handbook (IHL)*. London: CIRIA.
CUR. (1997). Kansen in de Civiele Techniek Deel 1: Probabilistisch Ontwerpen in Theorie: Stichting CUR, Gouda, The Netherlands.
Dabeet, A. (2014). *Discrete Element Modeling of Direct Simple Shear Response of Granular Soils and Model Validation Using Laboratory Tests.* (PhD thesis), University of British Columbia, Vancouver, Canada.
De Crook, T., Haak, H. W., & Dost, B. (1998). Seismisch Risico in Noord-Nederland. De Bilt, The Netherlands: KNMI.
Delft University of Technology. (s.a.). Glossary Hydraulic Engineering Terms. Retrieved 5 July, 2015, from http://www.kennisbank-waterbouw.nl/Glossary/printUK.php?subject=@
Deltares. (2013a). Effecten Geïnduceerde Aardbevingen op het Gasunie-netwerk in Groningen. Delft, The Netherlands.
Deltares. (2013b). Effecten Geïnduceerde Aardbevingen op Kritische Infrastructuur Groningen - Quick Scan naar de Sterkte van de Infrastructuur. Delft, The Netherlands.
Deltares. (2014). Groningse Kades en Dijken bij Geïnduceerde Aardbevingen. Delft, The Netherlands.
Deltares. (2015). Aardbevingsbestendige Waterkeringen - Opties voor een Haalbaar en Betaalbaar Ontwerp. Delft, The Netherlands.
Dost, B., Van Eck, T., & Haak, H. (2004). Scaling of Peak Ground Acceleration and Peak Ground Velocity Recorded in the Netherlands. *Bollettino di Geofisica Teorica ed Applicata, 45*(3), 153-168.
ENW. (2014). *Advies Aardbevingsbestendige Zeedijk Eemshaven - Delfzijl*. Letter retrieved from http://enwinfo.nl/index.php/adviezen2014, viewed 18 May 2015
ENW. (2015). *Verzoek Advies Ontwerpuitgangspunten Dijkverbetering Eemshaven-Delfzijl*. Letter retrieved from http://enwinfo.nl/index.php/adviezen-2015, viewed 26 May 2015
European Committee for Standardization. (2003). Eurocode 8: Design of Structures for Earthquake Resistance - Part 1: General Rules, Seismic Actions and Rules for Buildings. Brussels, Belgium.
Galavi, V., Petalas, A., & Brinkgreve, R. B. J. (2013). Finite Element Modelling of Seismic Liquefaction in Soils. *Geotechnical Engineering Journal of the SEAGS & AGSSEA, 44*(3), 55-64.
Geotechnical Info .Com. (s.a.). Geotechnical Glossary. Retrieved 5 July, 2015, from http://www.geotechnicalinfo.com/geotechnical_glossary.html
Grasso, J.-R. (1992). Mechanics of Seismic Instabilities Induced by the Recovery of Hydrocarbons. *Pure and Applied Geophysics, 139*(3), 507-534.
Green, C. A., Styles, P., & Baptie, B. J. (2012). Preese Hall Shale Gas Fracturing - Review & Recommendation for Induced Seismic Mitigation. London, United Kingdom: Department of Energy and Climate Change.
Heijn, K. (2014). Hoogwaterbeschermingsprogramma - Ontwerpinstrumentarium 2014 (IO2014). Retrieved October 20th, 2014, from http://www.hoogwaterbeschermingsprogramma.nl/Documenten+openbaar/Kennis+en+Innovatie/274378.aspx?t=Ontwerpinstrumentarium+2014+%28OI2014%29
Helpdesk Water. (2014, October 8th). WTI2017 in Ontwikkeling. Retrieved October 20th, 2014, from http://www.helpdeskwater.nl/onderwerpen/waterveiligheid/primaire/toetsen/wti2017-ontwikkeling/
Herle, I. (1997). *Hypoplastizität und Granulometrie Einfachter Korngerüste* (Vol. 142). Karlsruhe, Germany: Insitut für Boden- und Felsmechanik der Universität.
Hicher, P. Y., & Shao, J. F. (2008). *Constitutive Modeling of Soils and Rocks*. London, United Kingdom and Hoboken, United States of America: ISTE Ltd and John Wiley & Sons, Inc.
Idriss, I. M., & Boulanger, R. W. (2008). Soil Liquefaction during Earthquakes (EERI Monograph MNO-12): Earthquake Engineering Research Institute.
Idriss, I. M., & Boulanger, R. W. (2015). 2nd Ishihara Lecture: SPT- and CPT-based Relationships for the Residual Shear Strength of Liquefied Soils. *Soil Dynamics and Earthquake Engineering, 68*, 57-68.
International Code Council. (2000). International Building Code. United States of America.
Ishihara, K., & Yoshimine, M. (1992). Evaluation of Settlements in Sand Deposits Following Liquefaction During Earthquakes. *Soils and Foundations, 32*(1), 173-188.
Jibson, R. W. (2011). Methods for Assessing the Stability of Slopes During Earthquakes - A Retrospective. *Engineering Geology, 122*, 43-55.

Jongejan, R. (2014). De Overschrijdingskans van de Ontwerpbelasting - Nadere Toelichting op het Ontwerpinstrumentarium 2014.

Jonkman, S. N., & Schweckendiek, T. (2015). *Flood Defences - Lecture Notes CIE5314*. Delft, The Netherlands: Delft University of Technology.

Kamp, H. G. J. (2014). *Gaswinning in Groningen*. 's-Gravenhage, The Netherlands: Retrieved from http://www.rijksoverheid.nl/documenten-en-publicaties/kamerstukken.

KNMI. (2013a). The August 16, 2012 Earthquake near Huizinge (Groningen). De Bilt, The Netherlands.

KNMI. (2013b). Report on the Expected PGV and PGA Values for Induced Earthquakes in the Groningen Area. De Bilt, The Netherlands.

KNMI. (2014, 13 March). Geïnduceerde Aardbevingen in Nederland. Retrieved June, 24th, 2015, from http://www.knmi.nl/seismologie/geinduceerde-bevingen-nl

Lindenberg, J. (1996). Aardbevingen in Nederland - Een Gevaar voor de Waterkeringen? Delft, The Netherlands: Rijkswaterstaat.

Liu, L. (s.a.). *CE 240 Soil Mechanics & Foundations Lecture 2.2 - Weight - Volume Relationships*. PowerPoint presentation retrieved from http://www.engr.uconn.edu/~lanbo/courses.html, viewed 21 May 2015. University of Connecticut, Storrs, United States of America

Liyanapathirana, D. S., & Poulos, H. G. (2002). A Numerical Model for Dynamic Soil Liquefaction Analysis. *Soil Dynamics and Earthquake Engineering, 22*(9), 1007-1015.

Logan, J. M., Higgs, N. G., & Rudnicki, J. W. (1997). Seismicity Risk Assessment of a Possible Gas Storage Project in the Bergermeer field, Bergen Concession.

Makra, A. (2013). *Evaluation of the UBC3D-PLM Constitutive Model for Prediction of Earthquake Induced Liquefaction on Embankment Dams.* (Master of Science thesis), Delft University of Technology, Delft, The Netherlands.

Mašín, D. (2010). PLAXIS Implementation of Hypoplasticity. Delft, The Netherlands: Plaxis bv.

Mašín, D. (2014). PLAXIS Implementation of Hypoplasticity.

Mašín, D. (s.a.). *Hypoplasticity for Practical Applications - Part 4: Determination of Material Parameters*. PowerPoint Presentation retrieved from http://web.natur.cuni.cz/uhigug/masin/hypocourse/, viewed 13 March 2015. Charles University, Prague, Czech Republic

Matsuoka, H., & Nakai, T. (1985). Relationship among Tresca, Mises, Mohr-Coulomb and Matsuoka-Nakai Failure Criteria. *Soil and Foundations, 25*(4), 123-128.

Meier, T. (2012a). *Application of Hypoplastic and Viscohypoplastic Constitutive Models for Geotechnical Problems.* (PhD thesis), Universität Karlsruhe, Karlsruhe, Germany.

Meier, T. (2012b). *Hypoplastic Constitutive Equation: Basic Concept, Calibration of Parameters and Application for Liquefaction Analyses*. PowerPoint Presentation retrieved from Hypoplasticity Workshop @ Deltares, viewed 6 July 2015

Ministerie van Infrastructuur en Milieu. (2014). Synthesedocument Deelprogramma Veiligheid. 's-Gravenhage, The Netherlands.

Ministerie van Verkeer en Waterstaat. (2007). Voorschrift Toetsen op Veiligheid Primaire Waterkeringen. 's-Gravenhage, The Netherlands.

Miura, K., Maeda, K., & Toki, S. (1997). Method of Measurement for the Angle of Repose of Sands. *Soil and Foundations, 37*(2), 89-96.

Mulders, F. M. M. (2003). *Modelling of Stress Development and Fault Slip in and around a Producing Gas Reservoir.* (PhD thesis), Delft University of Technology, Delft, The Netherlands.

Muntendam-Bos, A. G., & De Waal, J. A. (2013). Reassessment of the Probability of Higher Magnitude Earthquakes in the Groningen Gas Field. 's-Gravenhage, The Netherlands: Staatstoezicht op de Mijnen.

NAM. (2013). Technical Addendum to the Winningsplan Groningen 2013 - Subsidence, Induced Earthquakes and Seismic Hazard Analysis in the Groningen Field. Assen, The Netherlands.

National Research Council. (1985). *Liquefaction of Soils During Earthquakes*. Washington, D.C., United States of America: National Academy Press.

National Science Foundation. (2000). Award Abstract #0070111 - Effects of Void Redistribution on Liquefaction Flow of Layered Soils. Retrieved March, 5th, 2015, from http://www.nsf.gov/awardsearch/showAward?AWD_ID=0070111&HistoricalAwards=false

Nederlands Normalisatie Instituut. (2005). NEN-EN 1998-5 (en) - Eurocode 8 - Ontwerp en Berekening van Aardbevingsbestendige Constructies - Deel 5: Funderingen, Grondkerende Constructies en Geotechnische Aspecten.

Nederlands Normalisatie Instituut. (2014). Voorlopige Ontwerpuitgangspunten voor Nieuwbouw en Verbouw onder Aardbevingsbelasting ten Gevolge van de Gaswinning in het Groningenveld. Delft, The Netherlands.

NEN. (s.a.). Veilige Constructies bij Aardbevingen. Retrieved 26 May, 2015, from http://www.nen.nl/NEN-Shop/Vakgebieden/Bouw/Eurocodes/Veilige-constructies-bij-aardbevingen.htm

Newmark, N. M. (1965). Effects of Earthquakes on Dams and Embankments. *Geotechnique, 15*(2), 139-160.

Niemunis, A. (1993). Hypoplasticity vs. Elastoplasticity. In D. Kolymbas (Ed.), *Modern Approaches to Plasticity* (pp. 277-305). Amsterdam, The Netherlands: Elsevier.

Niemunis, A. (2003). *Extended Hypoplastic Models for Soils.* (Habilitation thesis), Ruhr University Bochum, Bochum, Germany.

Niemunis, A., & Herle, I. (1997). Hypoplastic Model for Cohesionless Soils with Elastic Strain Range. *Mechanics of Cohesive-Frictional Materials, 2*, 279-299.

Norwegian Geotechnical Institute. (s.a.). Direct Simple Shear Test - DSS. Retrieved January, 1st, 2015, from http://www.ngi.no/no/Innholdsbokser/Referansjeprosjekter-LISTER-/Beskrivelse-av-labforsok/test1/

Onderzoeksraad voor Veiligheid. (2015). Aardbevingsrisico's in Groningen - Onderzoek naar de Rol van Veiligheid van Burgers in de Besluitvorming over de Gaswinning (1959-2014). 's-Gravenhage, The Netherlands.

Ottemöller, L., Nielsen, H. H., Atakan, K., J.Braunmiller, & Havskov, J. (2005). The 7 May 2001 Induced Seismic Event in the Ekofisk Oil Field, North Sea. *Journal of Geophysical Research, 110*.

Park, S. S. (2005). *A Two Mobilized-Plane Model and its Application for Soil Liquefaction Analysis.* (PhD thesis), University of British Columbia, Vancouver, Canada.

Petalas, A. (2012). *Validation and Verification of a Practical Constitutive Model for Soil Liquefaction in PLAXIS.* (Master of Science thesis), Delft University of Technology, Delft, The Netherlands.

Petalas, A., & Galavi, V. (2013). Plaxis Liquefaction Model UBC3D-PLM. Delft, The Netherlands: Plaxis bv.

PLAXIS. (2014). PLAXIS 2D Reference Manual Anniversary Edition Build 6972. Delft, The Netherlands: Plaxis bv.

PLAXIS. (2015). Site Reponse Analysis and Liquefaction Evaluation. Delft, The Netherlands: Plaxis bv.

Puzrin, A. M. (2012). *Constitutive Modelling in Geomechanics*. Dordrecht, The Netherlands; London, United Kingdom; New York, United States of America: Springer-Verlag Berlin Heidelberg.

Rauch, A. F. (1997). *EPOLLS: An Empirical Method for Predicting Surface Displacements Due to Liquefaction-Induced Lateral Spreading in Earthquakes.* (PhD thesis), Virginia Polytechnic Institute and State University, Blacksburg, United States of America.

Rijkswaterstaat. (2013). Achtergrondrapport Ontwerpinstrumentarium 2014. 's-Gravenhage, The Netherlands.

Rijkswaterstaat. (2014). Handreiking Ontwerpen met Overstromingskansen. 's-Gravenhage, The Netherlands.

Sarathchandran, A. (2014). *Three Dimensional Numerical Modelling of Coal Mine Roadways Under High Horizontal Stress Fields.* (Master of Science thesis), University of Exeter, Exeter, United Kingdom.

Schultz van Haegen, M. H. (2014). *Waterveiligheid*. 's-Gravenhage. http://www.hoogwaterbeschermingsprogramma.nl/Documenten+openbaar/Kennis+en+Innovatie/274378.aspx, viewed 15 March 2015

Seed, H. B. (1987). Design Problems in Soil Liquefaction. *Journal of Geotechnical Engineering, 113*, 827-845.

Segall, P. (1989). Earthquakes Triggered by Fluid Extraction. *Geology, 17*, 942-946.

Shahri, A. A., Juhlin, C., & Malemir, A. (2014). A Reliable Correlation of SPT-CPT Data for Southwest of Sweden. *The Electronic Journal of Geotechnical Engineering, 19*(E), 1013-1032.

Staf deltacommissaris. (2014). Deltaprogramma 2015 - Werk aan de Delta. 's-Gravenhage, The Netherlands: Ministerie van Economische Zaken &

Ministerie van Infrastructuur en Milieu.

Stedman, J. D. (1997). *Effects of Confining Pressure and Static Shear on Liquefaction Resistance of Fraser River Sand.* (Master of Applied Science thesis), University of British Columbia, Vancouver, Canada.

Stewart, J. P., & Seyhan, E. (2013). Semi-Empirical Nonlinear Site Amplification and its Application in NEHRP Site Factors. Berkeley, United States of America: Pacific Earthquake Engineering Research Center.

Subramani, T., Sakthi Kumar, D., & Badrinarayanan, S. (2014). Fem Modelling and Analysis of Reinforced Concrete Section with Light Weight Blocks Infill. *International Journal of Engineering Research and Applications, 4*(6), 142-149.

Sun, J. I., Chang, S. W., Bray, J. D., & Mejia, L. H. (1993). *Damage Patterns/Response of Deep Stiff Clay in Oakland.* Paper presented at the Third International Conference on Case Histories in Geotechnical Engineering, St. Louis, United States of America.

Tobita, T., Iai, S., & Noda, S. (2008). Generalized Scaling Relations for Level Ground Response. *Annuals of the Disaster Prevention Research Institute, Kyoto University, 51B*, 315-321.

Tsegaye, A. B. (2009). *Evaluation of Material Models for Liquefaction.* (Master of Science thesis), Delft University of Technology, Delft, The Netherlands.

Tsegaye, A. B. (2010). Plaxis Liquefaction Model. Delft, The Netherlands: Plaxis bv.

U.S. Geological Survey. (s.a.-a). Earthquake Glossary. Retrieved 5 July, 2015, from http://earthquake.usgs.gov/learn/glossary/

U.S. Geological Survey. (s.a.-b). The Los Angeles Dam Story. Retrieved 5 July, 2015, from http://earthquake.usgs.gov/learn/publications/la-damstory/

U.S. Geological Survey. (s.a.-c). Soil Type and Shaking Hazard in the San Francisco Bay Area. Retrieved December, 15th, 2014, from http://earthquake.usgs.gov/regional/nca/soiltype/

University of British Columbia. (2003a). Fraser River Sand Index Tests - Final Vancouver, Canada.

University of British Columbia. (2003b). Lab and Centrifuge Tests Data and Reports. Retrieved January 15th, 2015, from http://liquefaction-civil.sites.olt.ubc.ca/about/laboratory-testing/lab-and-centrifuge-tests-data-and-reports/

University of Luxembourg. (2015, 20 January). Constitutive Soil Modeling. Retrieved 3 July, 2015, from http://wwwen.uni.lu/research/fstc/research_unit_in_engineering_science_rues/members/stefan_van_baars/research/constitutive_soil_modeling

Van Eck, T., Goutbeek, F., Haak, H., & Dost, B. (2004). Seismic Hazard due to Small Shallow Induced Earthquakes. De Bilt, The Netherlands: KNMI.

Van Eck, T., Goutbeek, F., Haak, H., & Dost, B. (2006). Seismic Hazard due to Small-Magnitude, Shallow-source, Induced Earthquakes in The Netherlands. *Engineering Geology, 87*, 105-121.

Van Eck, T., Goutbeek, F. H., & Dost, B. (2007). Site Specific Hazard Estimates for the NUON Energy Plant in the Eemshaven. De Bilt, The Netherlands: KNMI.

Van Eijs, R. M. H. E., Mulders, F. M. M., Nepveu, M., Kenter, C. J., & Scheffers, B. C. (2006). Correlation Between Hydrocarbon Reservoir Properties and Induced Seismicity in the Netherlands. *Engineering Geology, 84*, 99-111.

Verheij, H. J., Diermanse, F., van Eck, T., de Lange, G., Lindenberg, J., Simmelink, H. J., & Weerts, H. J. T. (2002). Invloed van Aardbevingen op Overstromingsrisico's. Delft, The Netherlands: WL | delft hydraulics.

Volkskrant. (2014, 16 January). 'Stoppen met boren helpt tegen aardbevingen, maar niet meteen'. Retrieved 5 July, 2015, from http://www.volkskrant.nl/dossier-tyfoon-haiyan/stoppen-met-boren-helpt-tegen-aardbevingen-maar-niet-meteen~a3578620/

Von Wolffersdorff, P.-A. (1996). A Hypoplastic Relation for Granular Materials with a Predefined Limit State Surface. *Mechanics of Cohesive-Frictional Materials, 1*(3), 251-271.

Wassing, B. B. T., Maljers, D., Westerhoff, R. S., Bosch, J. H. A., & Weerts, H. J. T. (2003). Seismisch Hazard van Geïnduceerde Aardbevingen - Rapportage Fase 1. Utrecht, The Netherlands: TNO.

Waterman, D. (2015). *Modelling Liquefaction in PLAXIS*. PowerPoint presentation retrieved from PLAXIS Course on Dynamic Analysis, viewed 8 May 2015. Plaxis bv, Delft, The Netherlands

Waterschap Noorderzijlvest. (s.a.). Aardbevingen. Retrieved May, 22th, 2015, from http://www.noorderzijlvest.nl/organisatie/over-ons/onze-taken/waterveiligheid/aardbevingen/

Weijers, J., & Tonneijck, M. (2009). *Lecture Notes CT5314 - Flood Defences*. Delft, The Netherlands: Delft University of Technology.

Wiersum, E. (2014). *Lucht Foto Groninger Dijk*. Photo retrieved from https://www.flickr.com/photos/116132348@N06/14958662770/

Wijewickreme, D., Sriskandakumar, S., & Byrne, P. M. (2005). Cyclic Loading Response of Loose Air-pluviated Fraser River Sand for Validation of Numerical Models Simulating Centrifuge Tests. *Canadian Geotechnical Journal, 42*(2), 550-561.

A Results design peak ground acceleration

The design value for the *PGA* is related to the failure probability requirement, as shown in paragraph 3.1 of the report. This requirement depends on four factors:

- Design probability per year P_d;
- contribution to the failure probability budget ω;
- Influence factor α;
- length effect, depending on three parameters:
  - constant that indicates which fraction of the trajectory's length is sensitive to earthquakes *a;*
  - length of trajectory considered L_t;
  - length of a typical section for failure mechanism L_j.

Furthermore, it depends on whether the earthquake load is considered to be dominant with respect to the hydraulic load or not dominant. In case the earthquake load is not dominant, the calculation is done with a value of 0.4*α (CUR, 1997). Figure A.1 till Figure A.6 show the influence of P_d, ω and α on the *PGA*; since those three parameters are still subject to debate. Two parameters are plotted on the horizontal and vertical axes, the third parameter is constant; its value is given in Table A.1. The *PGA* is depicted in the figures by the different colours and contour lines.

Table A.1 Values used to determine the peak ground acceleration

Parameter	Value	Unit
P_d	1/5000	year^{-1}
ω	0.24	-
α	0.9	-

In addition, a distinction is made between a situation in which the earthquake load is dominant and a situation where it is not. Based on the figures, it is concluded that α is the most influential parameter; especially for larger values of α. Parameters P_d and ω are much less influential.

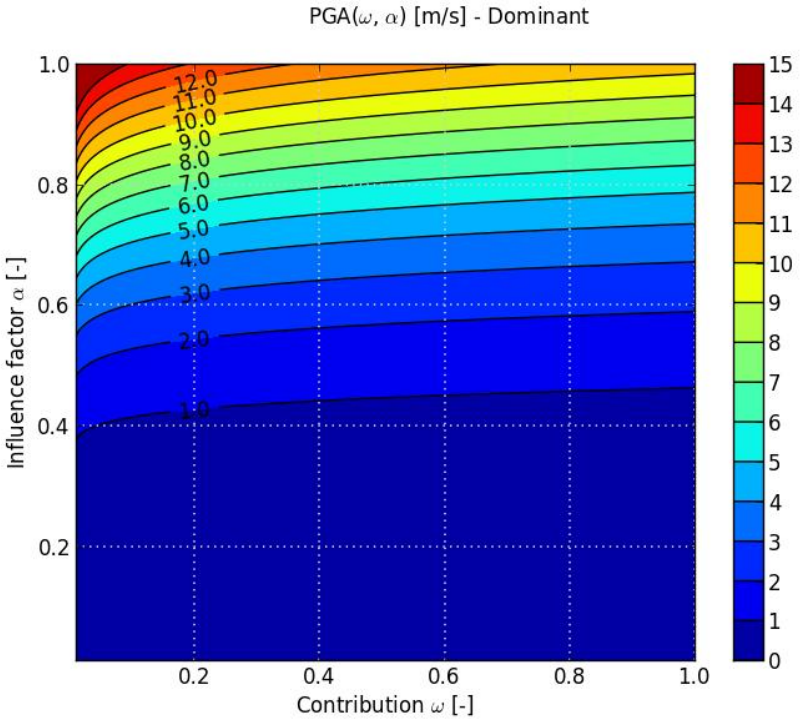

Figure A.1 PGA as function of ω and α; dominant

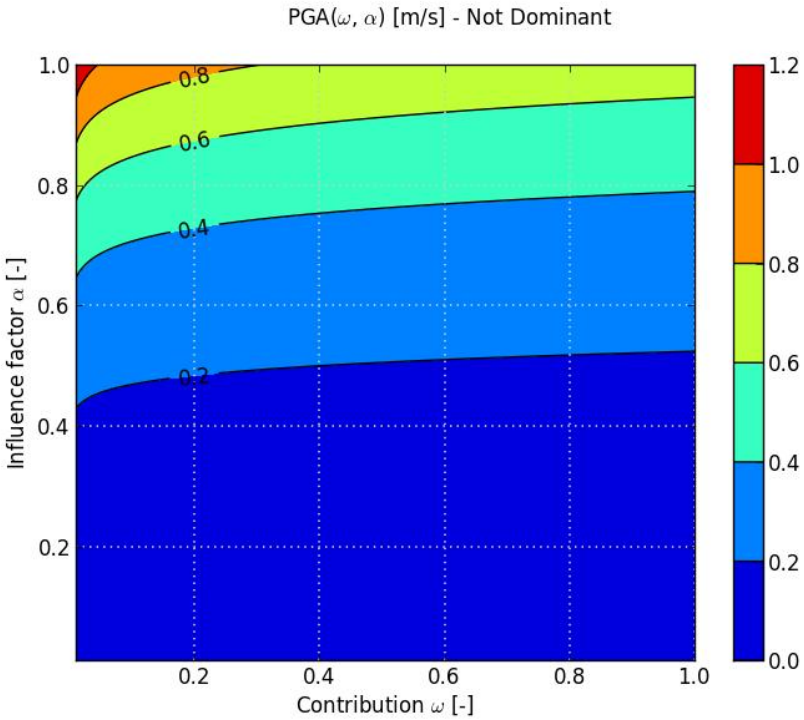

Figure A.2 PGA as function of ω and α; not dominant

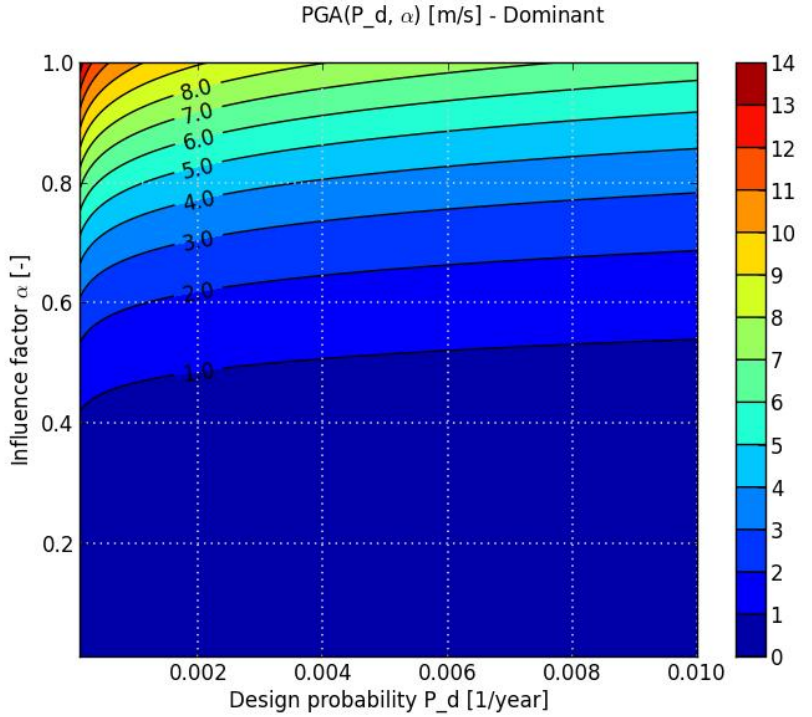

Figure A.3 PGA as function of P_d and α; dominant

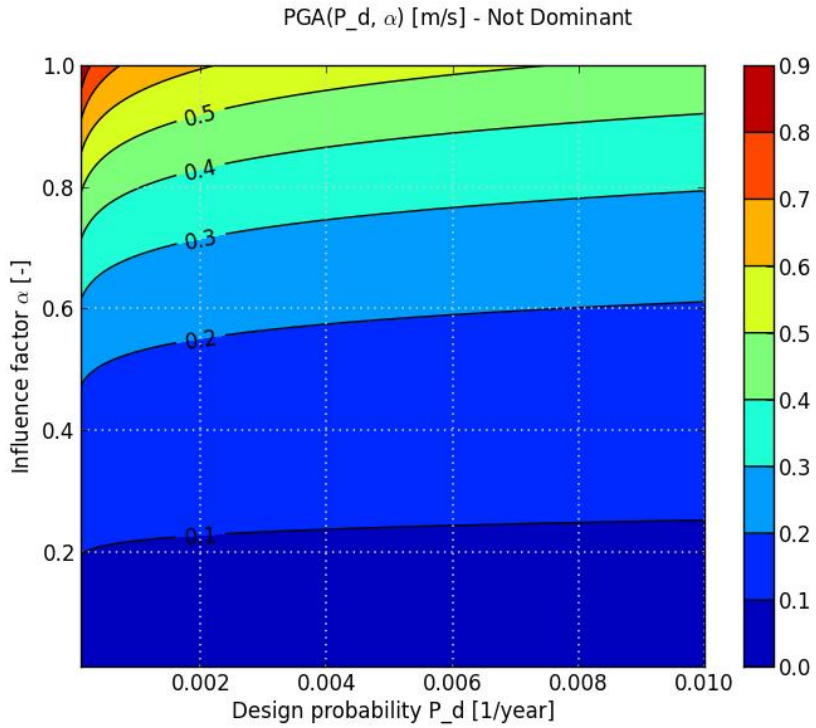

Figure A.4 PGA as function of P_d and α; not dominant

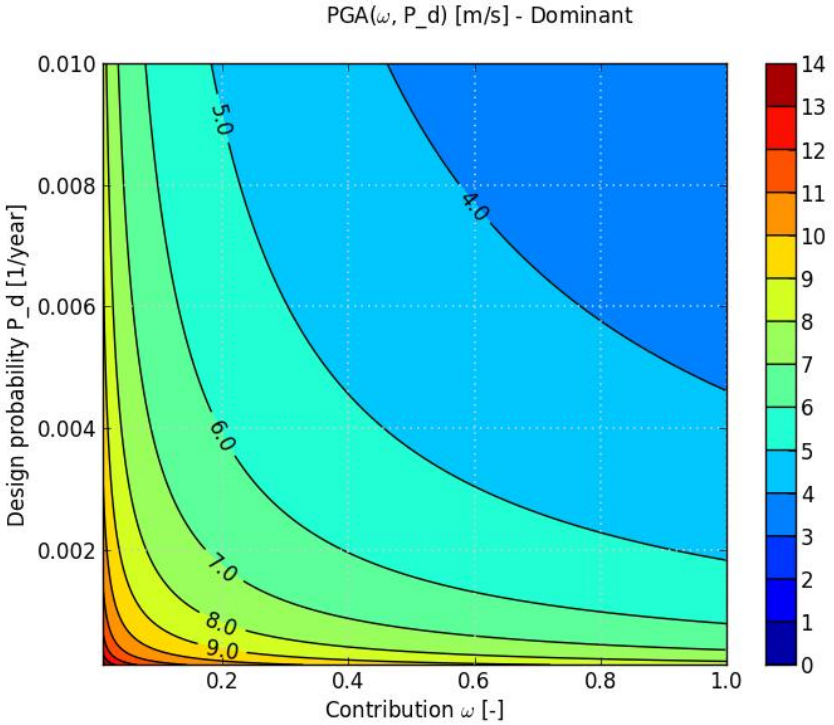

Figure A.5 PGA as function of ω and P_d; dominant

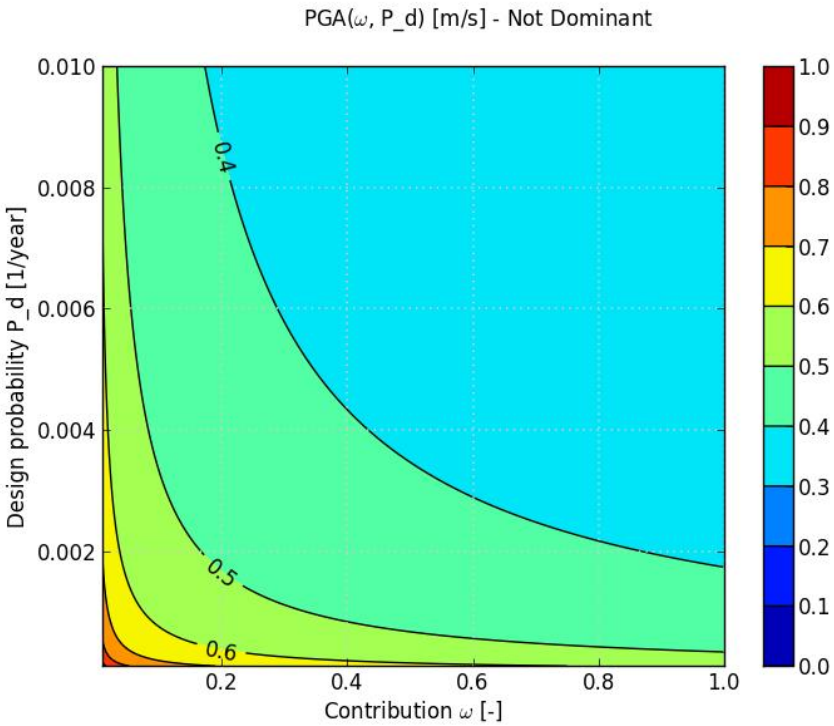

Figure A.6 PGA as function ω and P_d; not dominant

B Initial calibration results UBC3D-PLM

This appendix depicts the graphs that compare the results of UBC3D-PLM with those of laboratory tests in Figure B.1 to Figure B.6. The laboratory tests were conducted with *CSR* values of 0.08, 0.10 and 0.12 for loose sand (D_r = 40%) and 0.25, 0.30, 0.35 for dense sand (D_r = 80%). The input parameters for UBC3D-PLM are given in Table B.1.

Please note that these figures do not depict the final results of the calibration; they are only used to compare the results obtained with the initial parameters to the results of Makra (Makra, 2013). This is done to check if the current versions of UBC3D-PLM and PLAXIS give the same results; in order to see if the assumption that Makras parameter sets can be used for this research is valid. The conclusion is indeed that the assumption is valid, since there are only really small differences.

Table B.1 UBC3D-PLM input parameters for loose and dense Fraser River sand (Makra, 2013)

	φ_{cv}	φ_p	k_G^e	k_G^p	k_B^e	R_f	fac_{hard}	$(N_1)_{60}$	fac_{post}
Loose	33.00	33.7	845.2	238.8	591.6	0.81	0.45	7.4	0.02
Dense	33.00	38.9	1339.5	3597.1	937.6	0.66	0.45	29.5	0.02

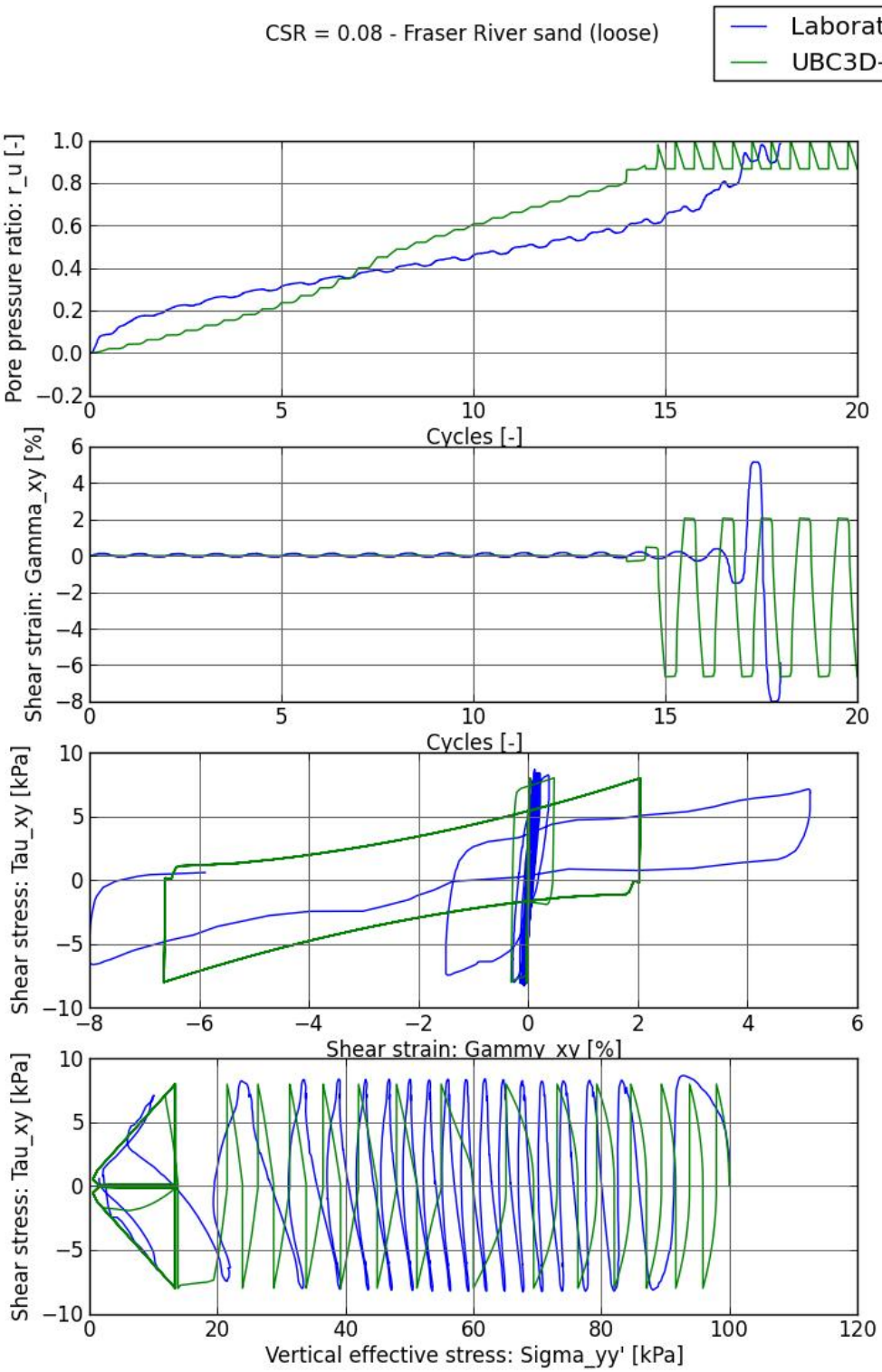

Figure B.1 Initial calibration results UBC3D-PLM, for loose sand and CSR = 0.08

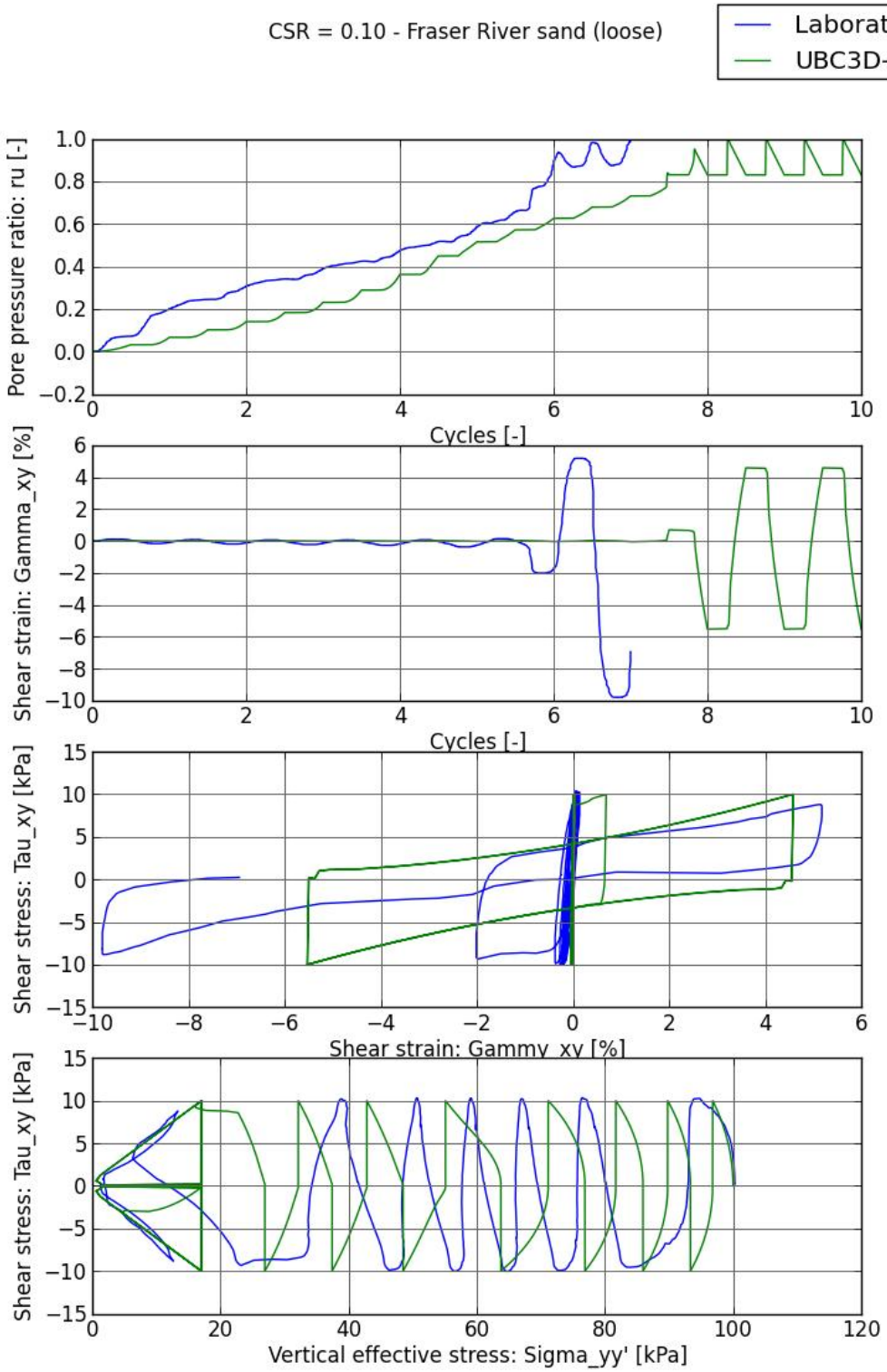

Figure B.2 Initial calibration results UBC3D-PLM, for loose sand and CSR = 0.10

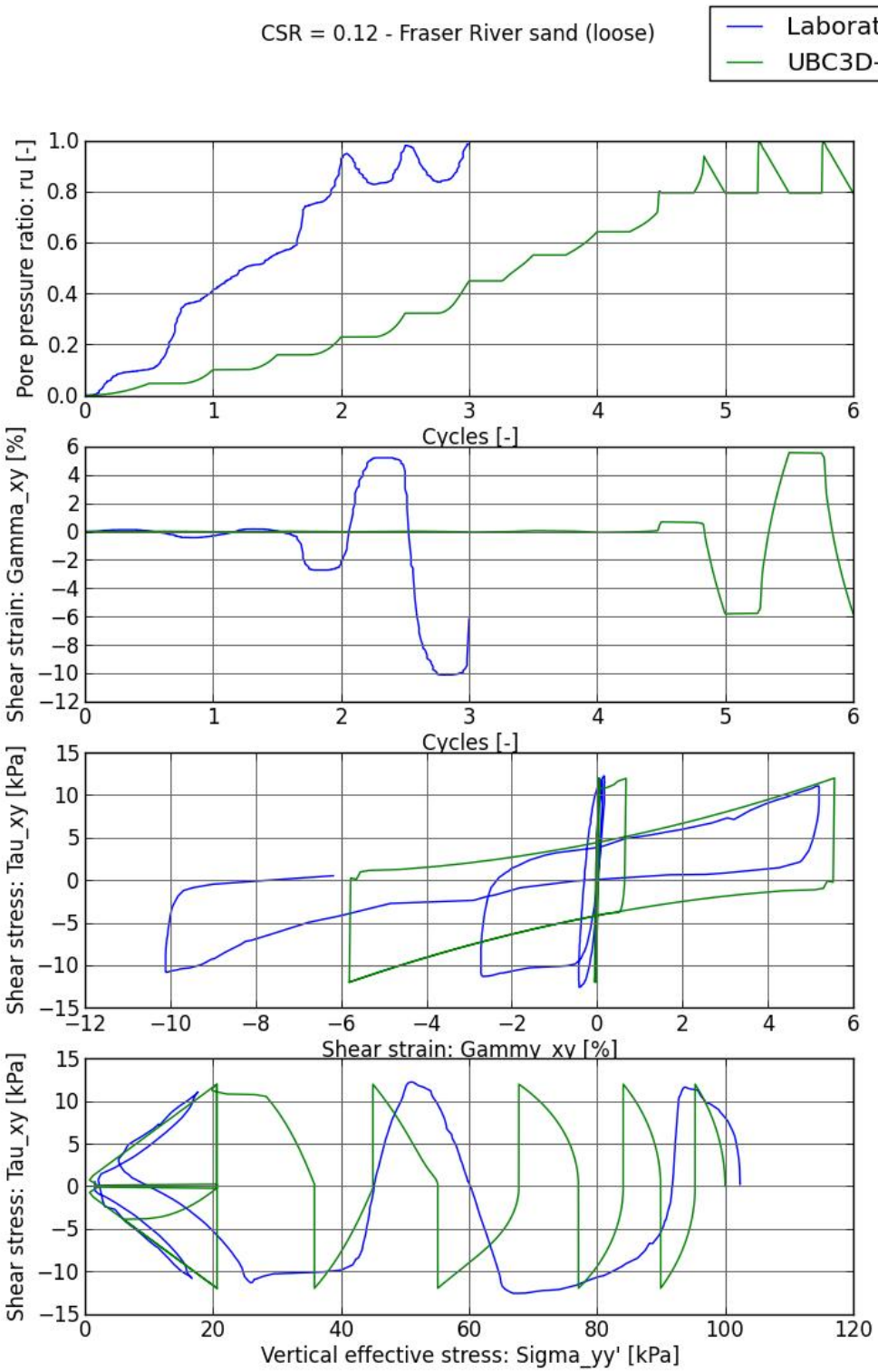

Figure B.3 Initial calibration results UBC3D-PLM, for loose sand and CSR = 0.12

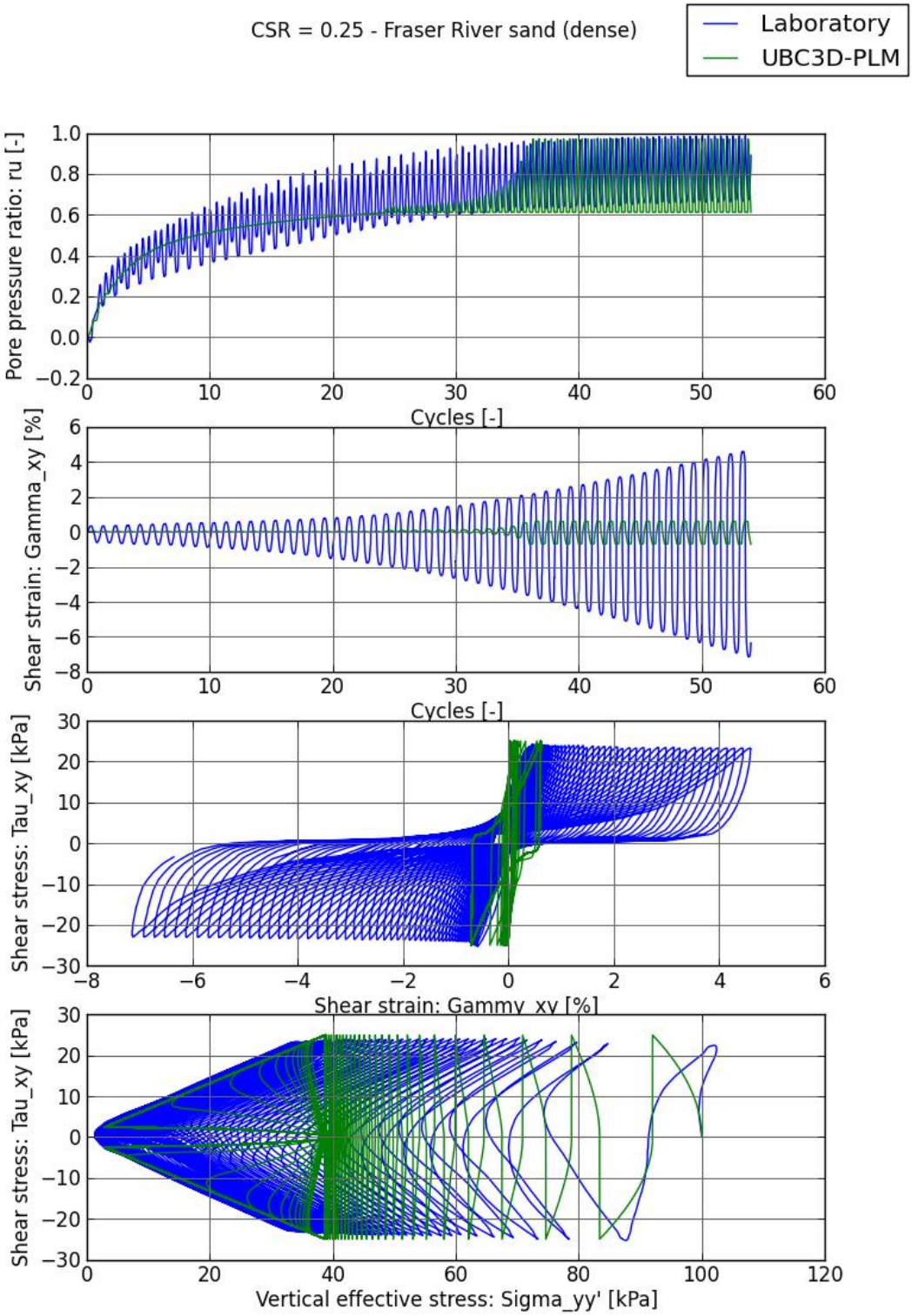

Figure B.4 Initial calibration results UBC3D-PLM, for dense sand and CSR = 0.25

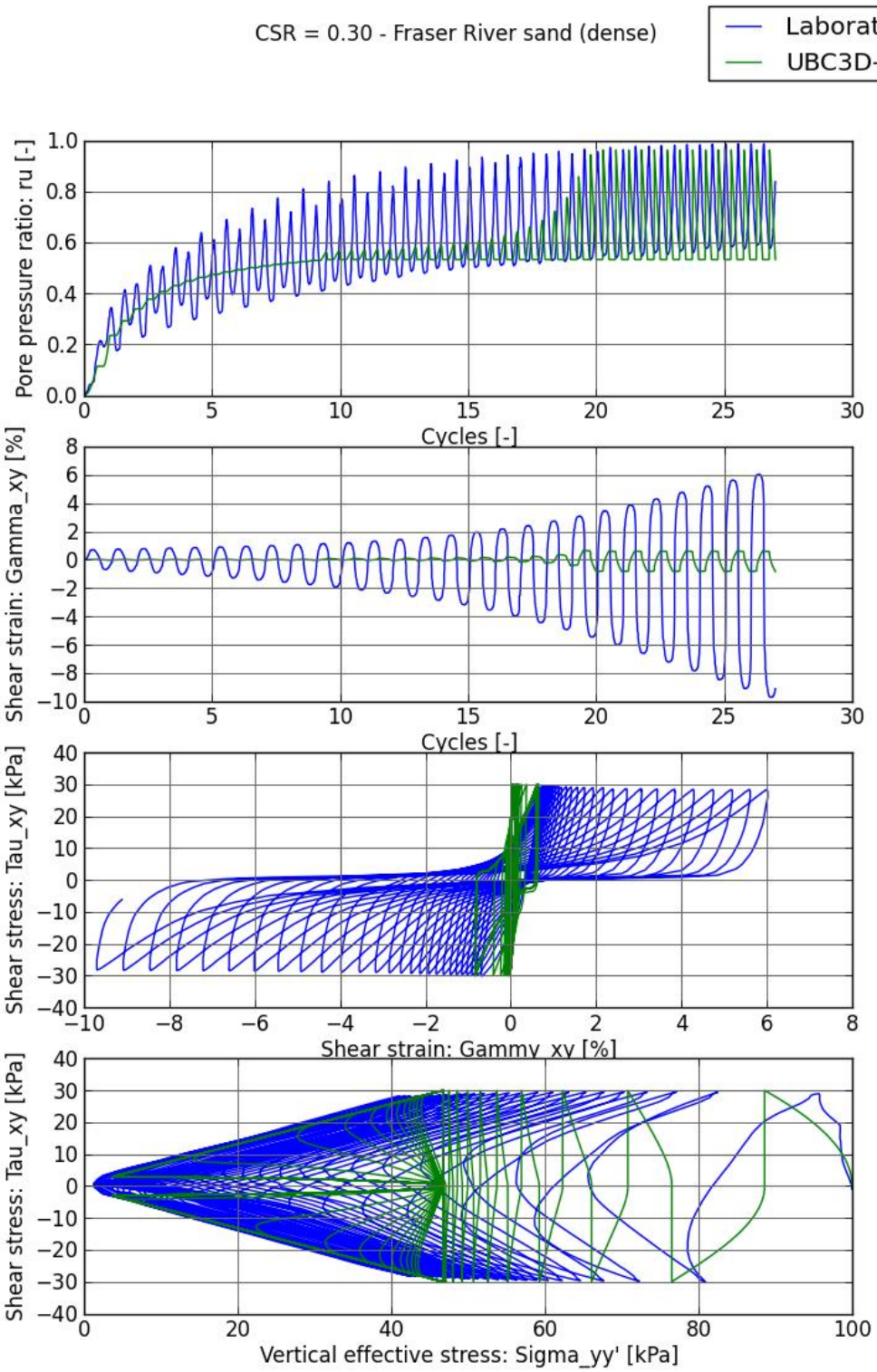

Figure B.5 Initial calibration results UBC3D-PLM, for dense sand and CSR = 0.30

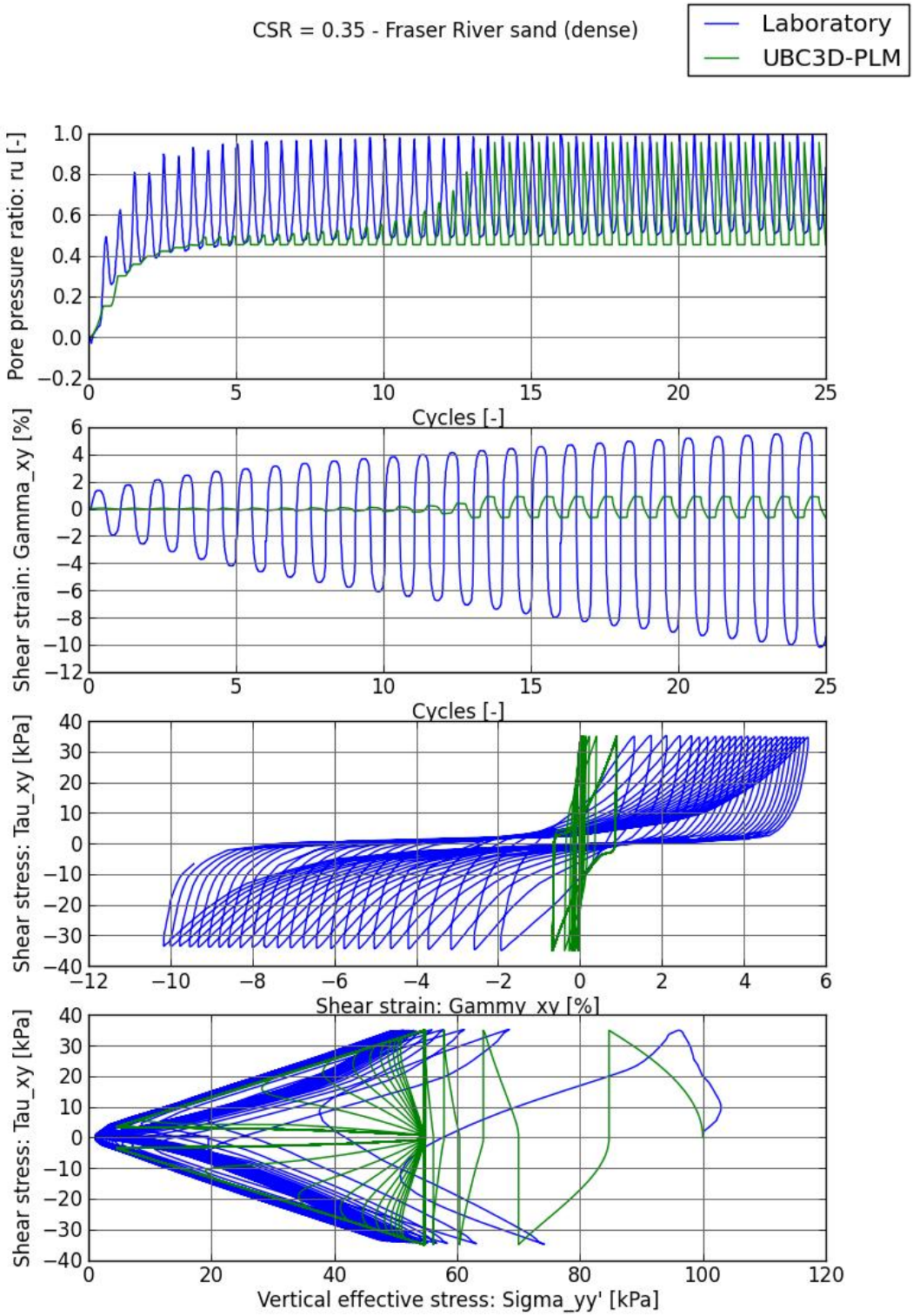

Figure B.6 Initial calibration results UBC3D-PLM, for dense sand and CSR = 0.35

C Final calibration results UBC3D-PLM

These graphs depict the final results of the calibration for UBC3D-PLM, comparing them to the results of laboratory tests in Figure C.1 to Figure C.6. The laboratory tests were conducted with *CSR* values of 0.08, 0.10 and 0.12 for loose sand (D_r = 40%) and 0.25, 0.30, 0.35 for dense sand (D_r = 80%). The final input parameters for UBC3D-PLM after calibration are given in Table C.1.

Table C.1 Input parameters UBC3D-PLM after calibration

	φ_{cv}	φ_p	k_G^e	k_G^p	k_B^e	R_f	fac_{hard}	$(N_1)_{60}$	fac_{post}
Loose	33.00	33.65	809.45	202.60	566.61	0.83	0.45	6.50	0.02
Dense	33.00	37.35	1259.2	2387.4	881.4	0.68	0.45	24.5	0.02

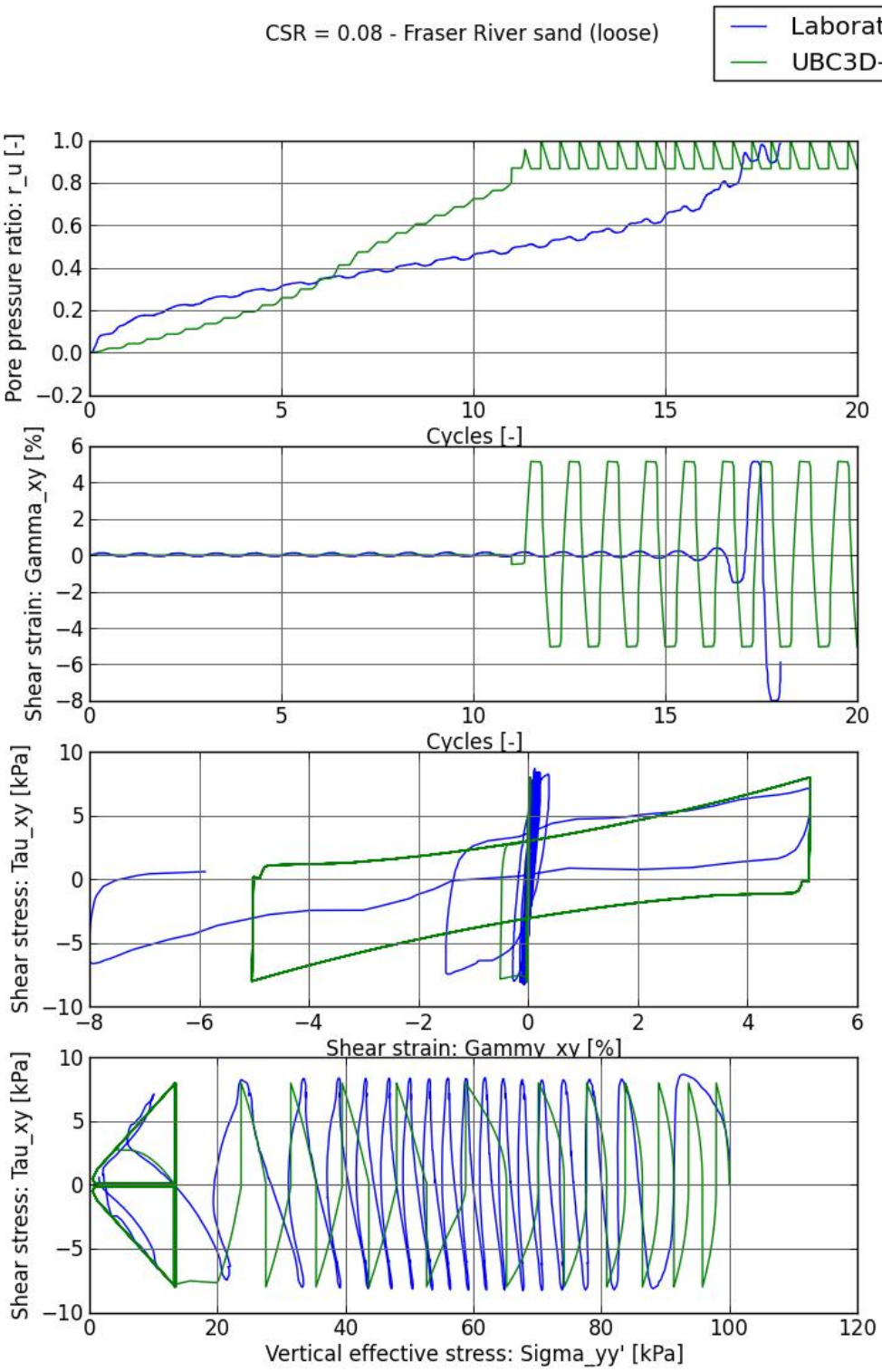

Figure C.1 Final calibration results UBC3D-PLM, for loose sand and CSR = 0.08

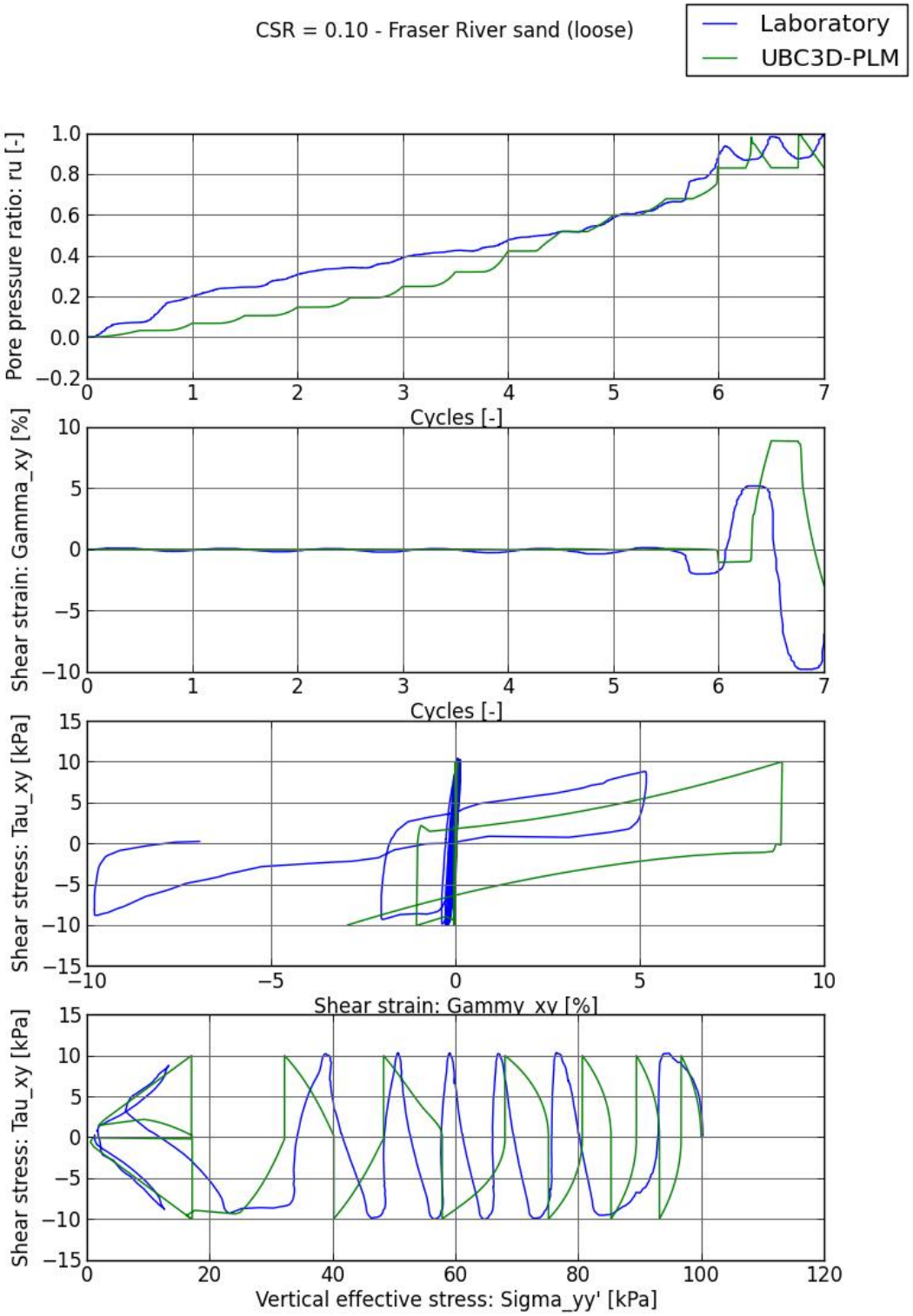

Figure C.2 Final calibration results UBC3D-PLM, for loose sand and CSR = 0.10

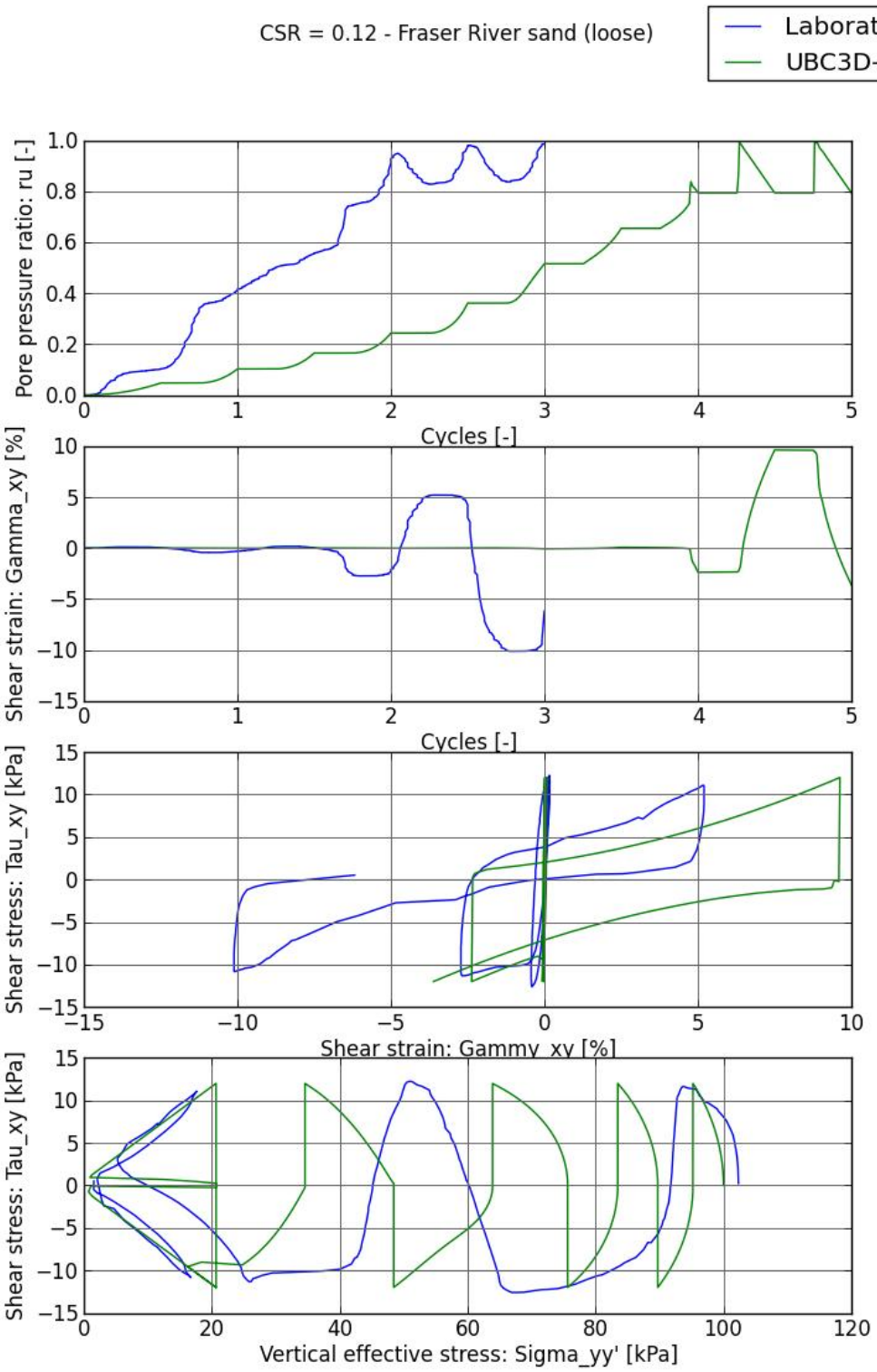

Figure C.3 Final calibration results UBC3D-PLM, for loose sand and CSR = 0.12

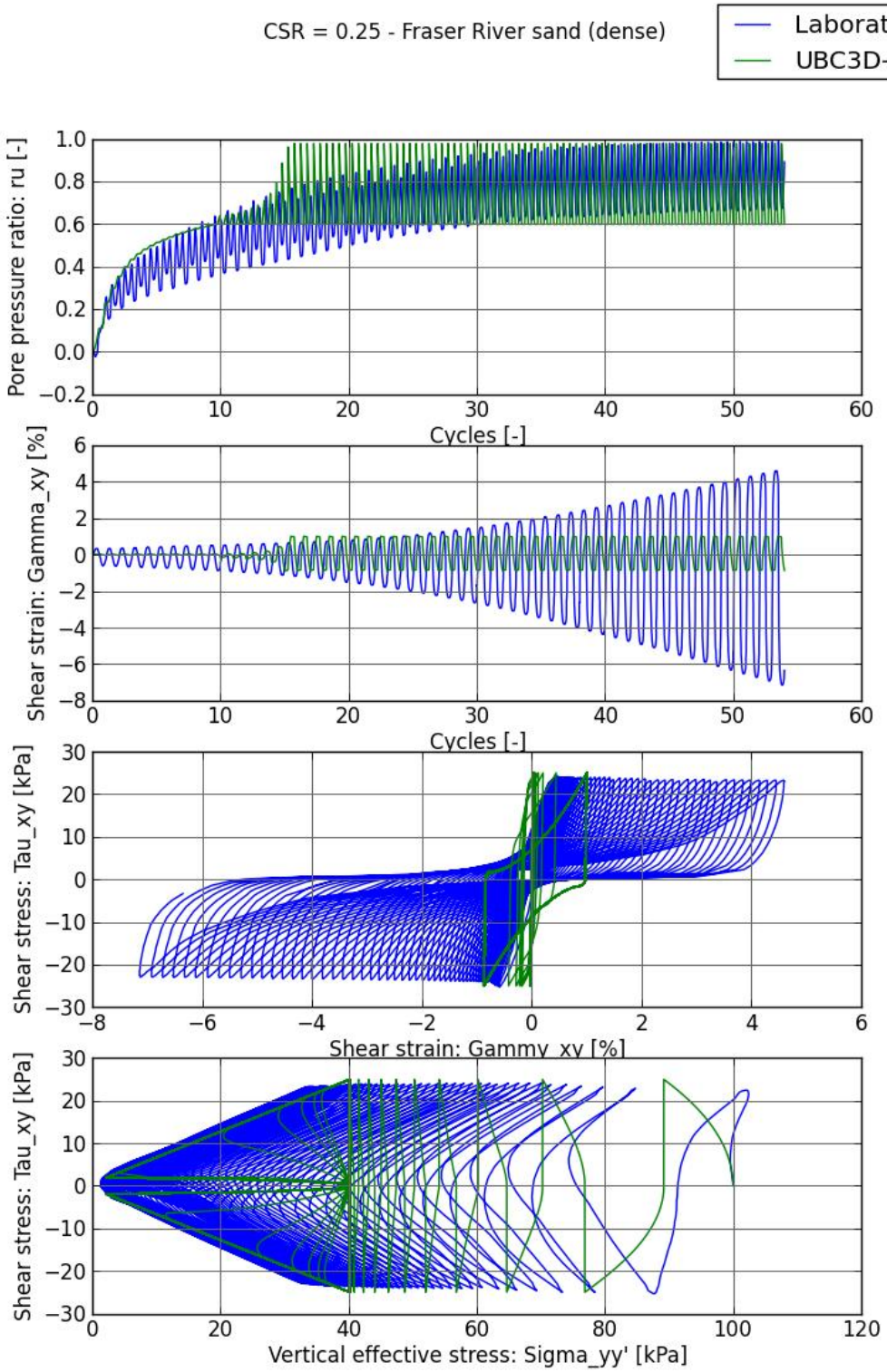

Figure C.4 Final calibration results UBC3D-PLM, for dense sand and CSR = 0.25

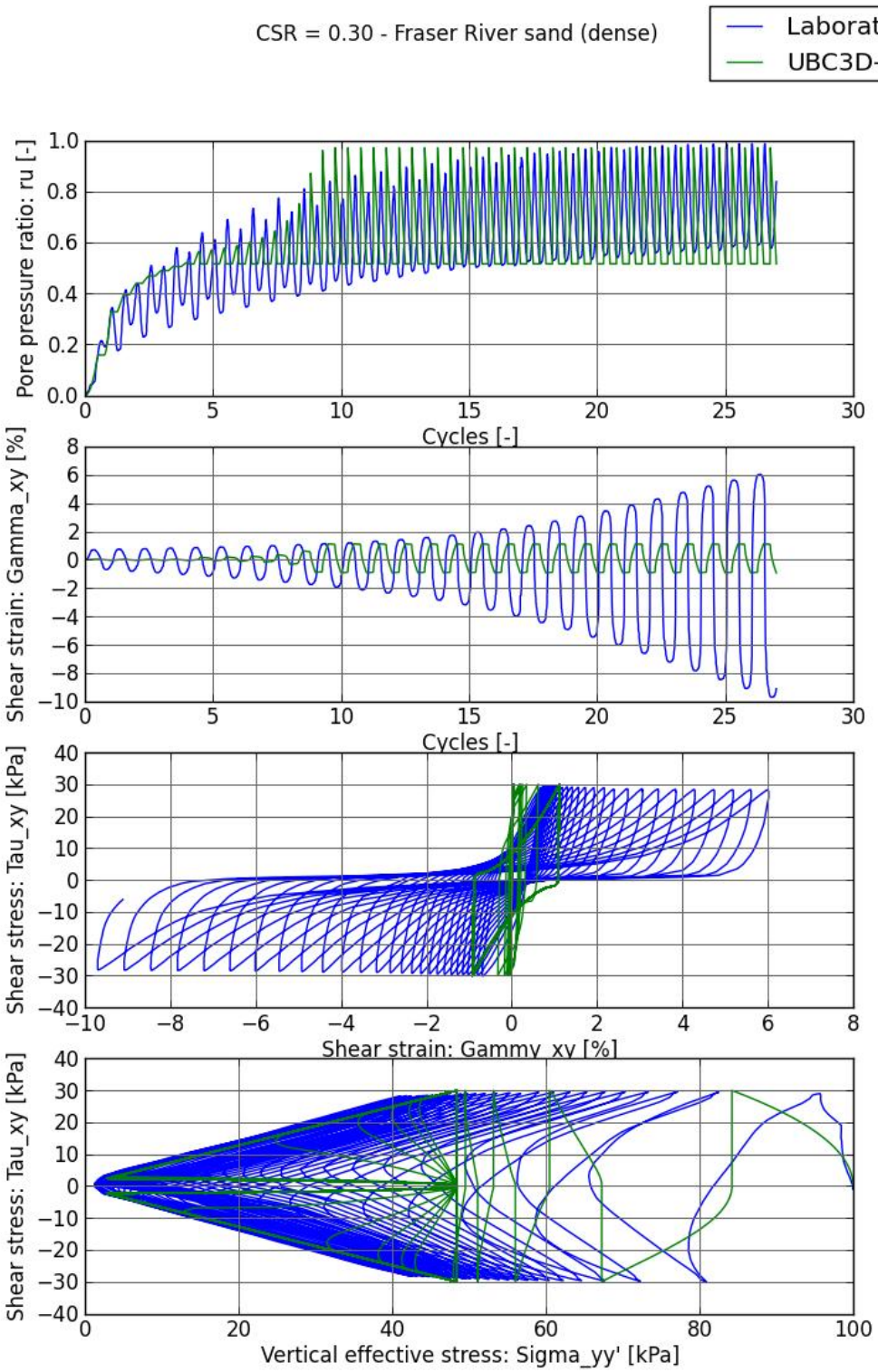

Figure C.5 Final calibration results UBC3D-PLM, for dense sand and CSR = 0.30

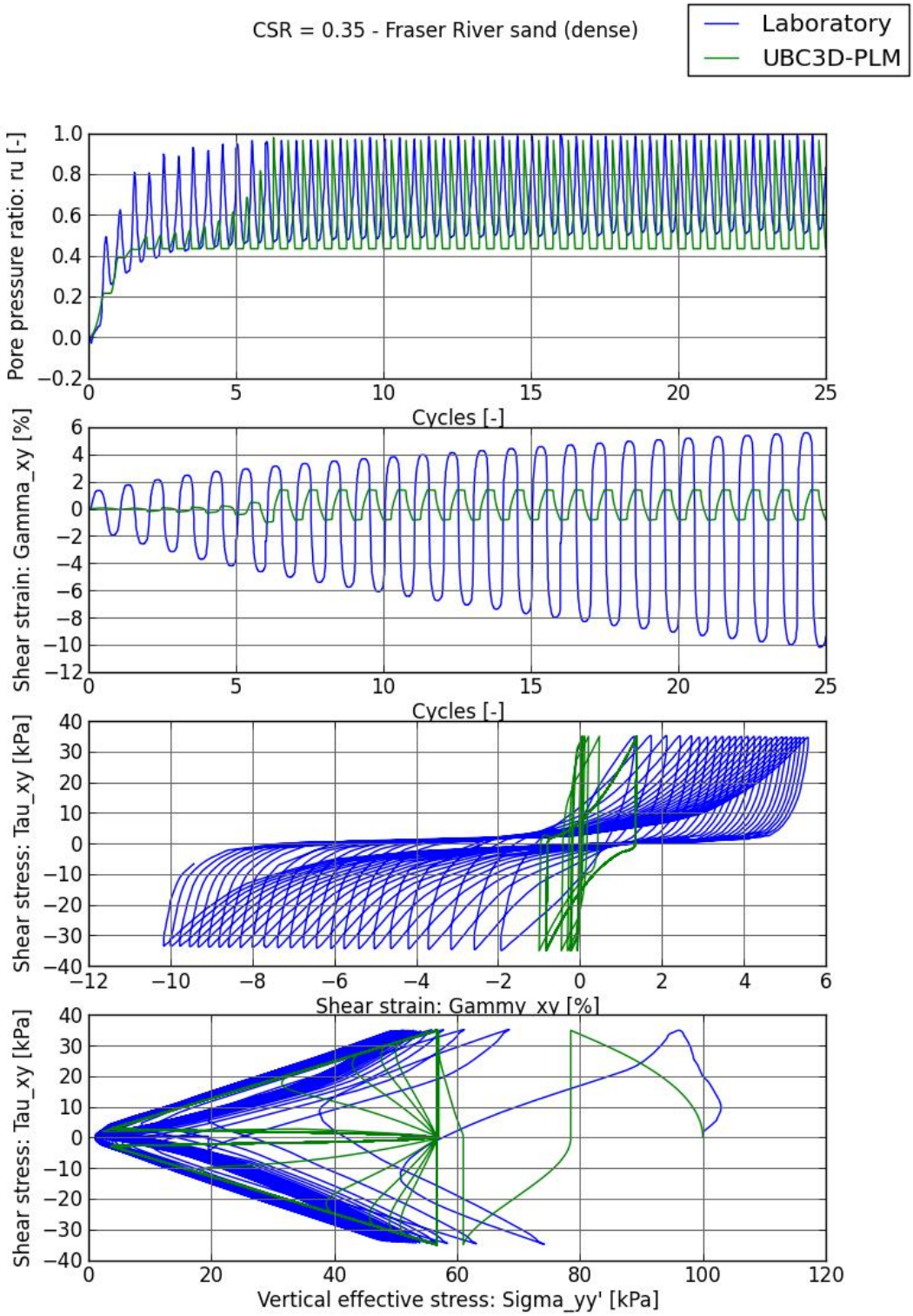

Figure C.6 Final calibration results UBC3D-PLM, for dense sand and CSR = 0.25

D Final calibration results UBC3D-PLM with static shear

This appendix depicts the graphs that compare the results of the UBC3D-PLM calibration with static shear with those of laboratory tests in Figure D.1 to Figure D.3. The laboratory tests were conducted with *CSR* values of 0.06, 0.08 and 0.10 for loose sand (D_r = 40%). Furthermore, the tests were conducted with an initial static shear ratio of 0.1. The input parameters for UBC3D-PLM are given in Table D.1.

Table D.1 Input parameters UBC3D-PLM after calibration, including static shear

	φ_{cv}	φ_p	k_G^e	k_G^p	k_B^e	R_f	fac_{hard}	$(N_1)_{60}$	fac_{post}
Loose	33.00	33.65	809.45	202.60	566.61	0.83	1.0	6.50	1.0

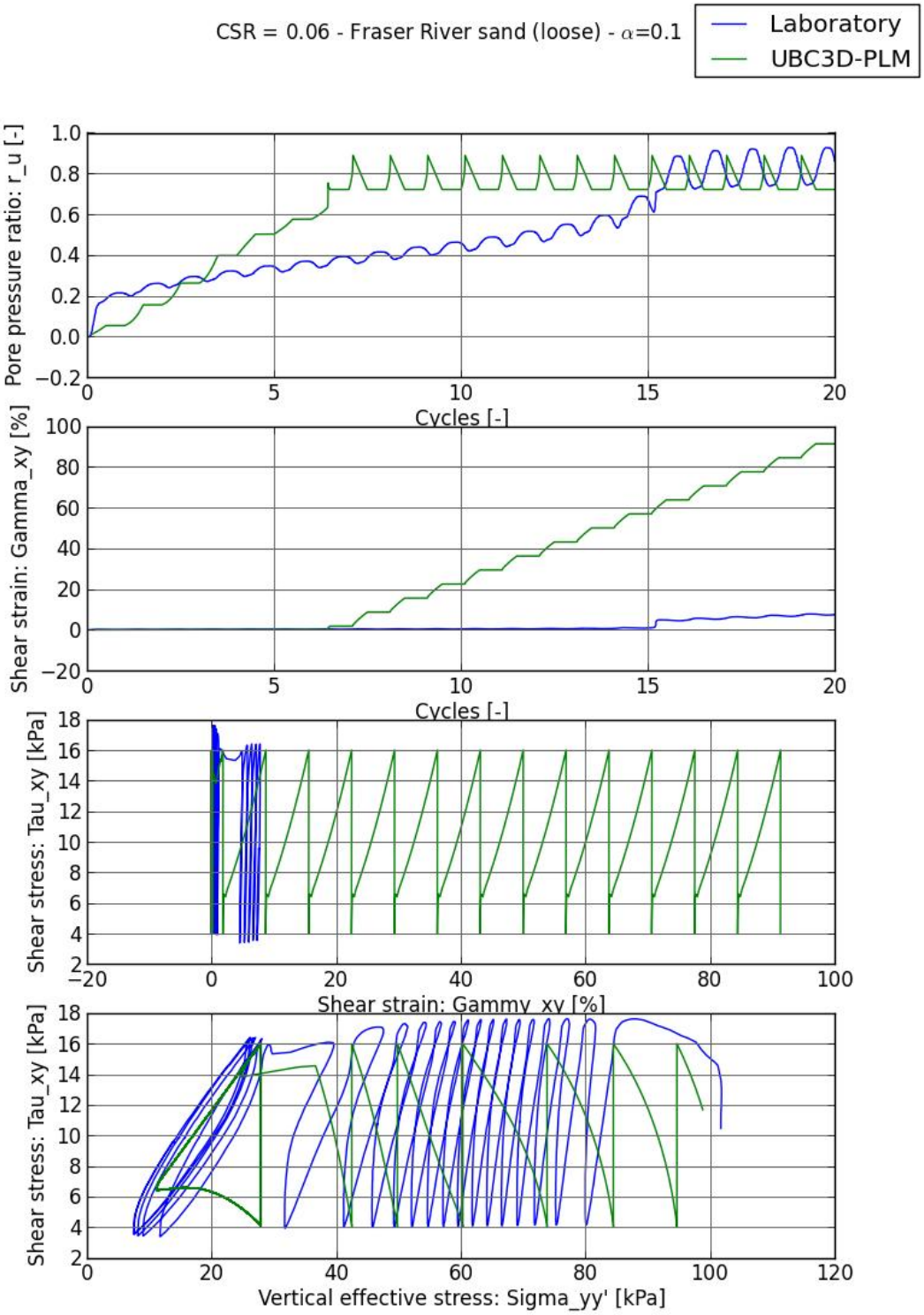

Figure D.1 Final calibration results UBC3D-PLM, for loose sand, CSR = 0.06 and α = 0.1

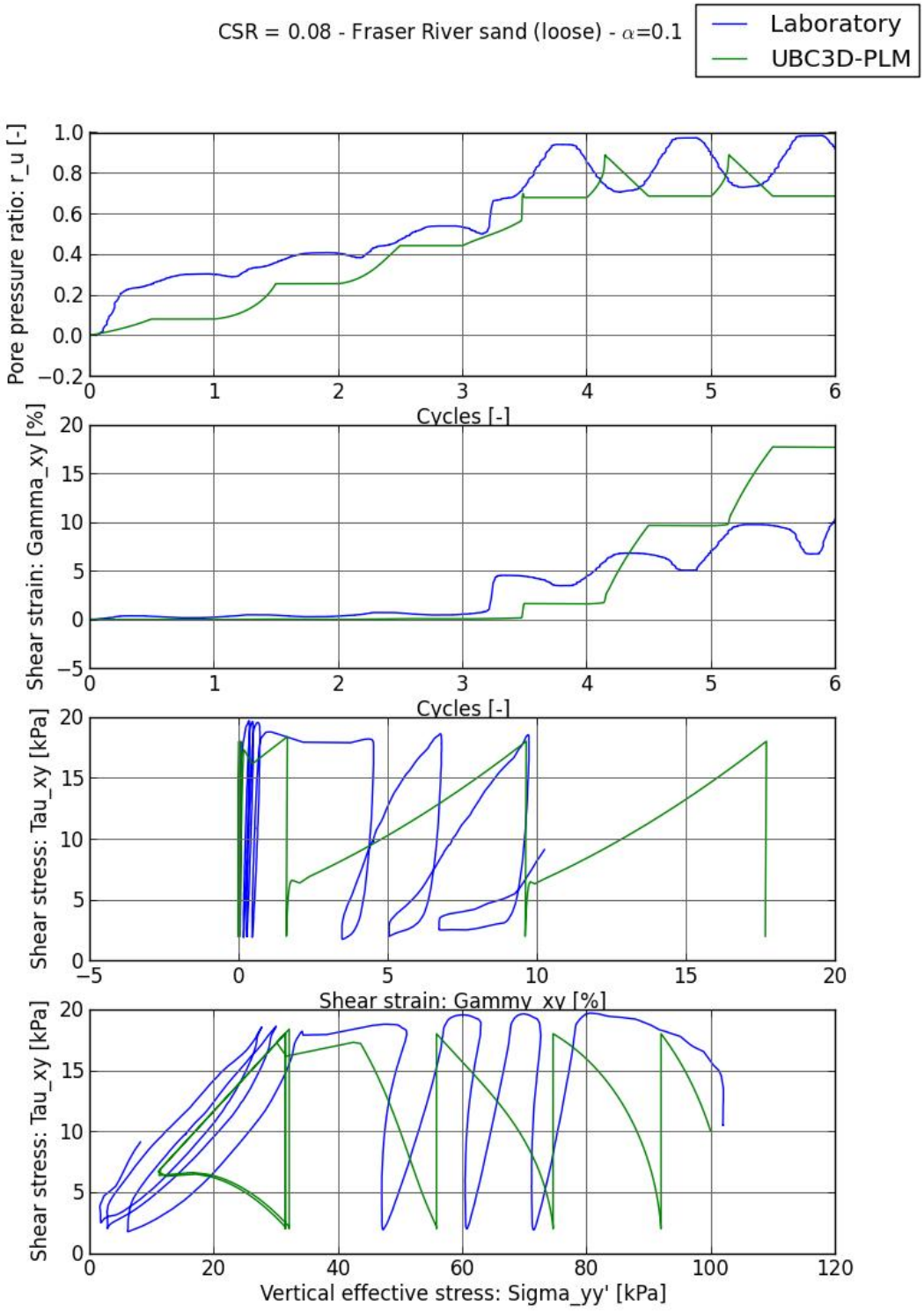

Figure D.2 Final calibration results UBC3D-PLM, for loose sand, CSR = 0.08 and α = 0.1

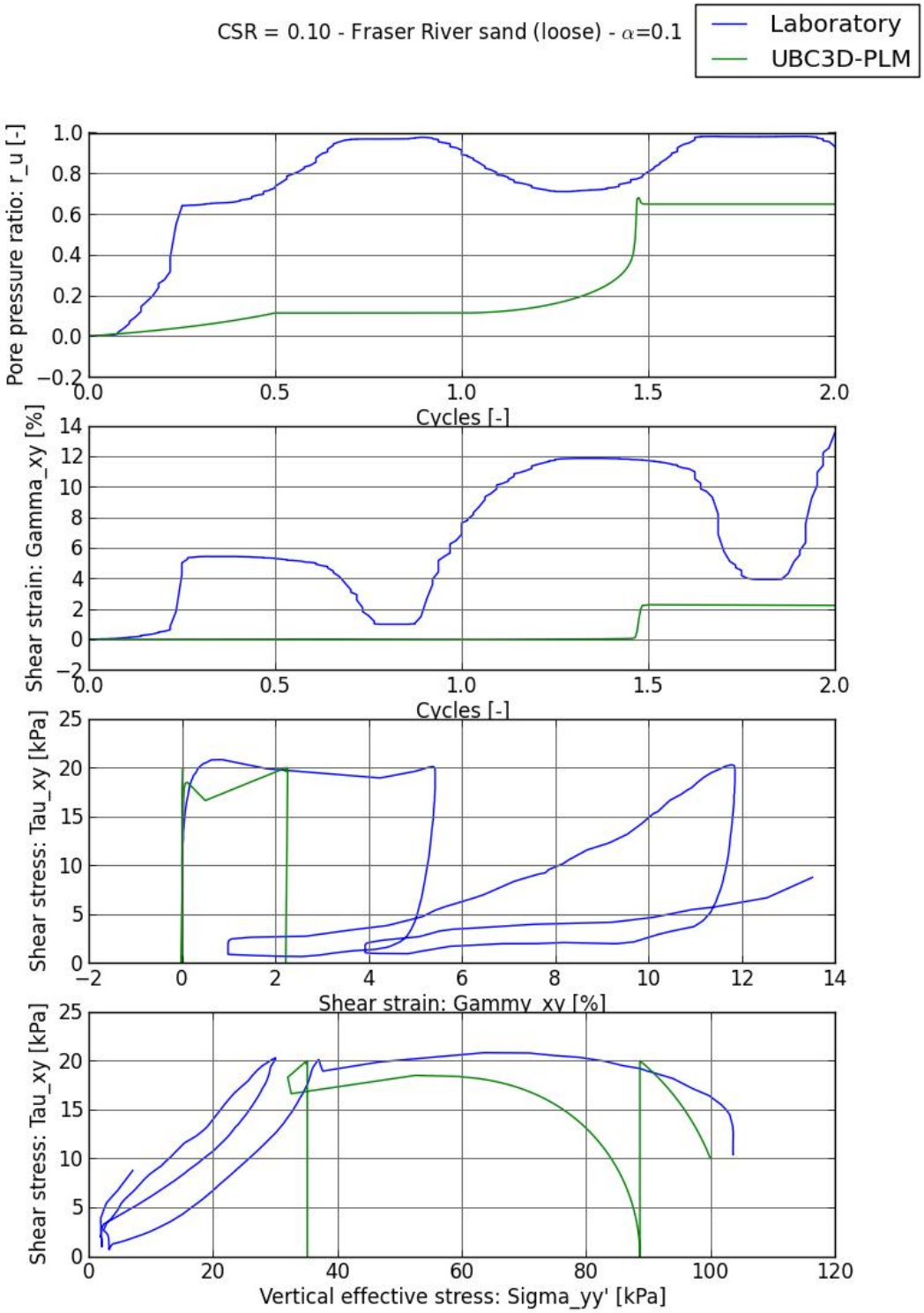

Figure D.3 Final calibration results UBC3D-PLM, for loose sand, CSR = 0.10 and α = 0.1

E Calibration results Hypoplastic model

These graphs depict the final results of the calibration for the Hypoplastic model, comparing them to the results of the laboratory tests in Figure E.1 to Figure E.6. The laboratory tests were conducted with *CSR* values of 0.08, 0.10 and 0.12 for loose sand (D_r = 40%) and 0.25, 0.30, 0.35 for dense sand (D_r = 80%). The input parameters for UBC3D-PLM are given in Table E.1 and Table E.2 for loose and dense Fraser River sand, respectively.

Table E.1 Hypoplastic parameters after calibration for loose Fraser River sand

φ_c [°]	h_s [GPa]	n	e_{d0}	e_{c0}	e_{i0}	α	β	m_R	m_T	R_{max}	β_r	χ	e_0
31	1.0	0.29	0.61	0.96	1.09	0.13	2	5	2	10^{-4}	0.5	6	0.86

Table E.2 Hypoplastic parameters after calibration for dense Fraser River sand

φ_c [°]	h_s [GPa]	n	e_{d0}	e_{c0}	e_{i0}	α	β	m_R	m_T	R_{max}	β_r	χ	e_0
31	1.0	0.29	0.61	0.96	1.09	0.20	2,5	5,8	2	$1.15*10^{-4}$	0.4	6	0.678

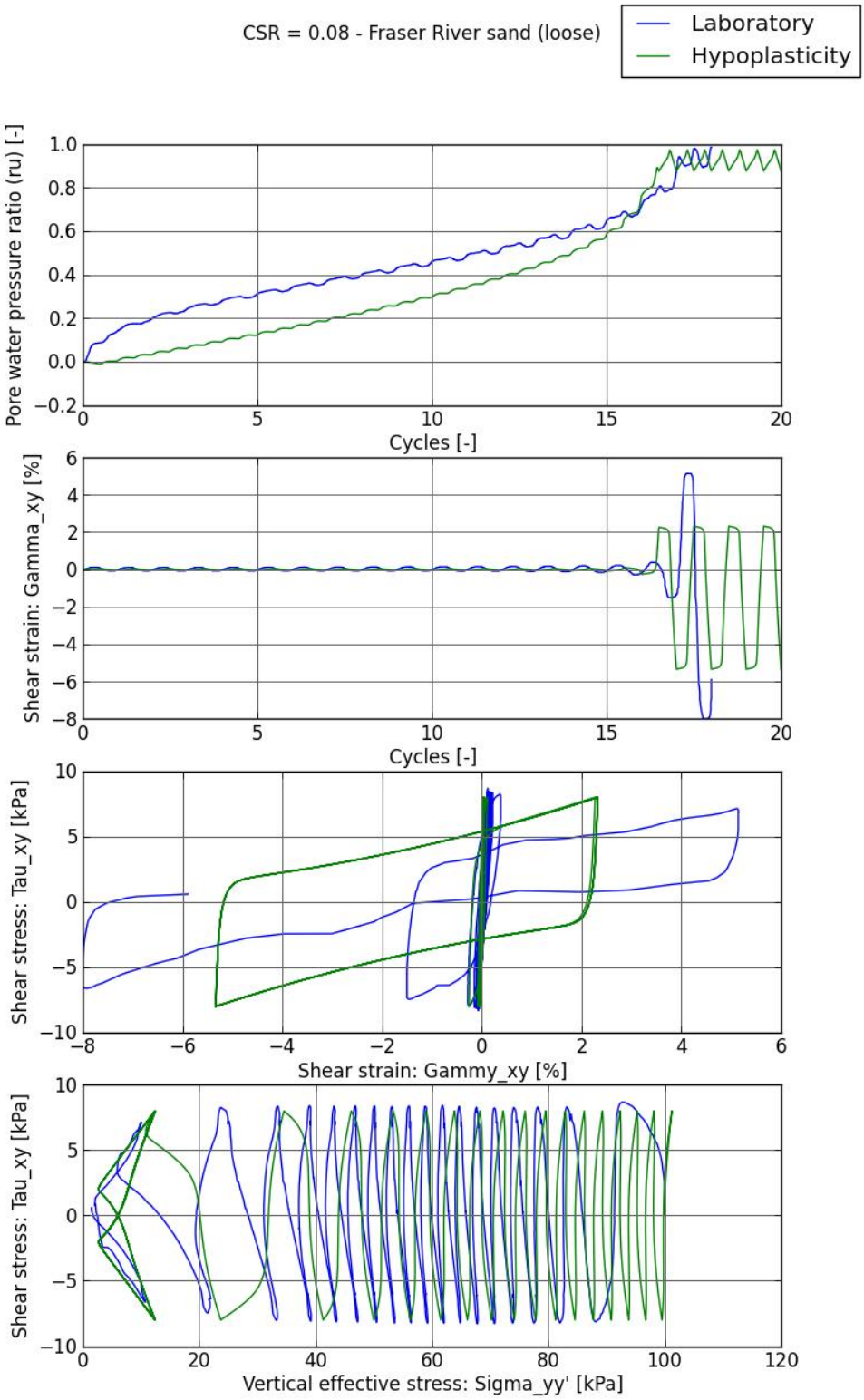

Figure E.1 Final calibration results Hypoplastic model, for loose sand and CSR = 0.08

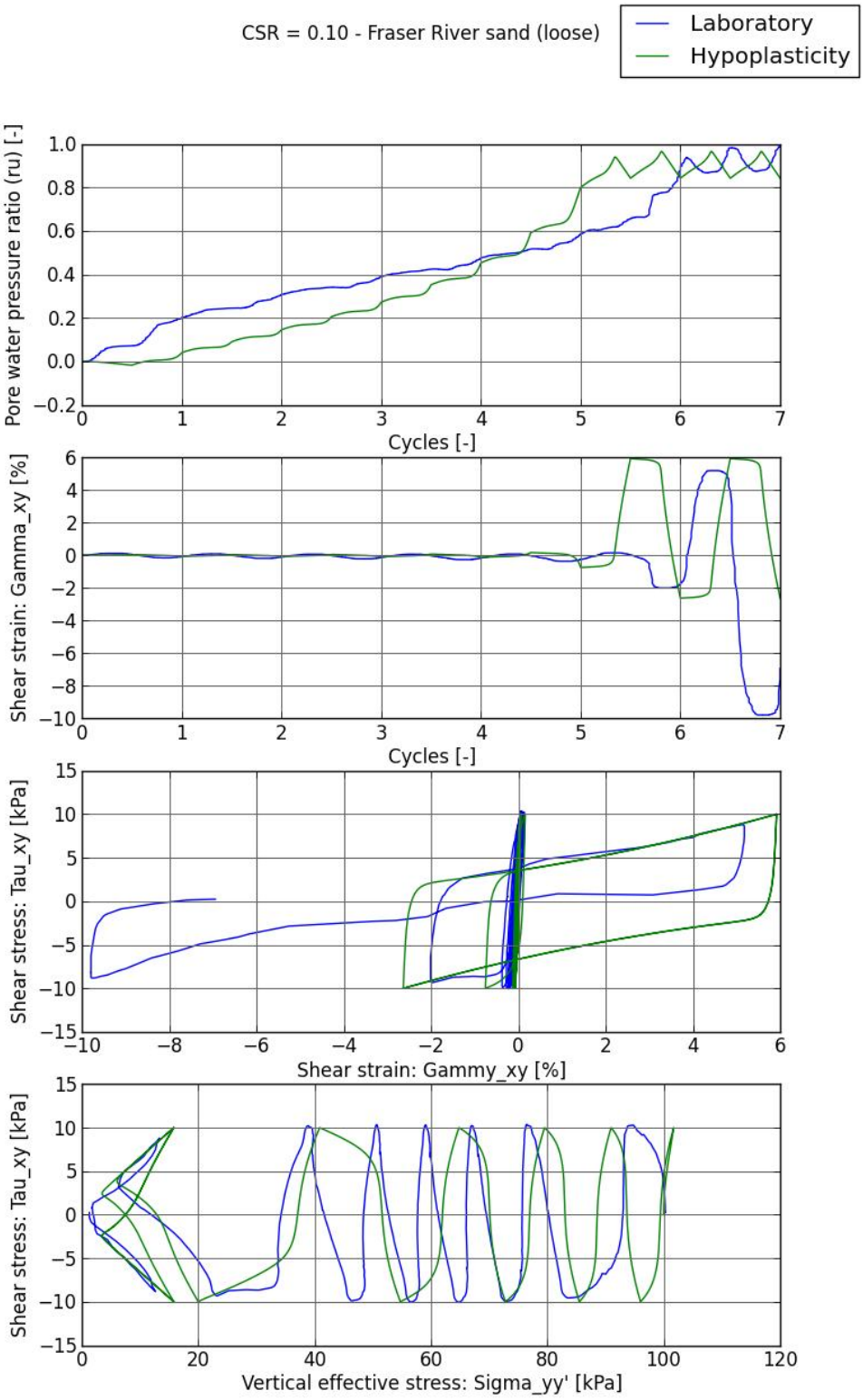

Figure E.2 Final calibration results Hypoplastic model, for loose sand and CSR = 0.10

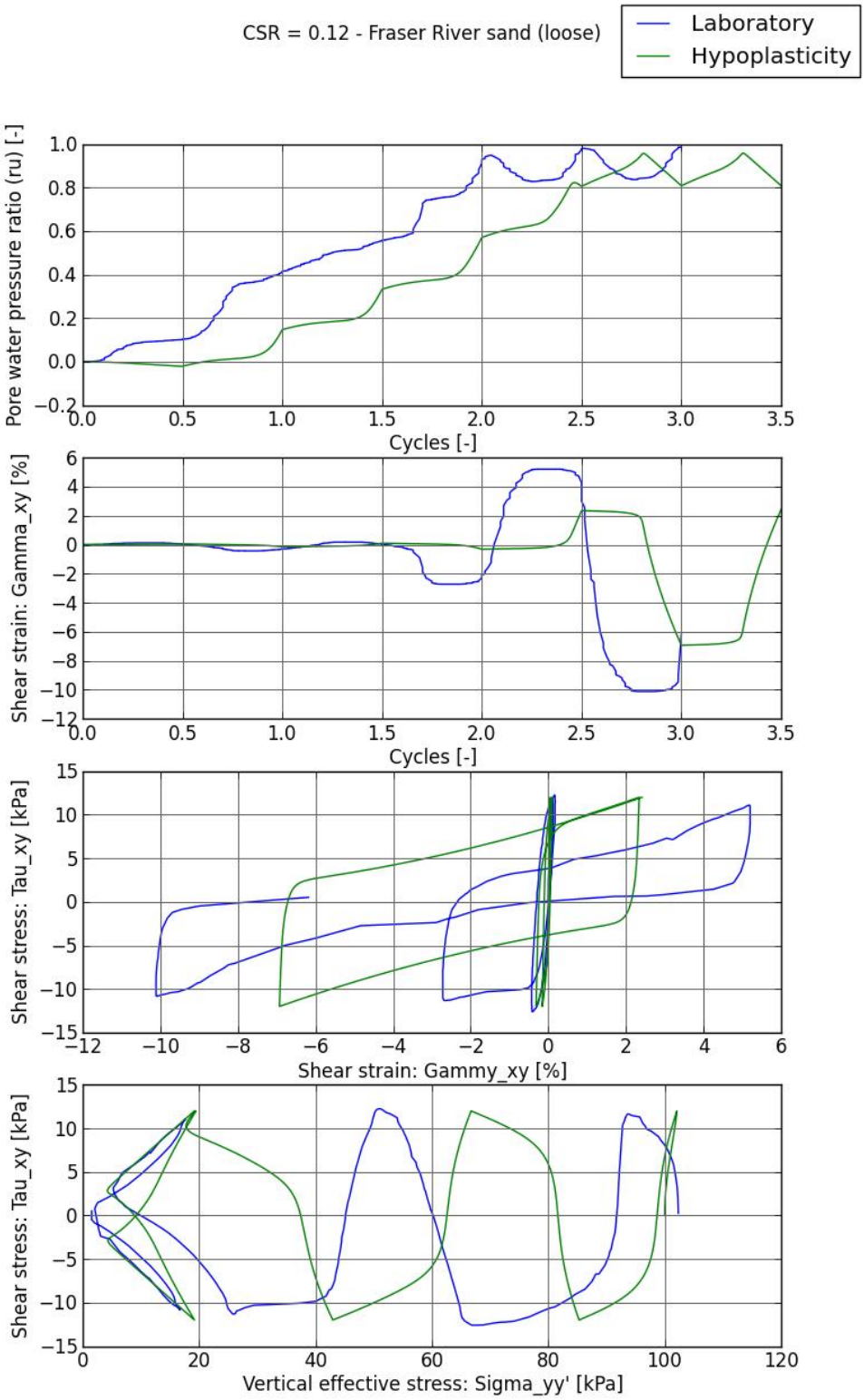

Figure E.3 Final calibration results Hypoplastic model, for loose sand and CSR = 0.12

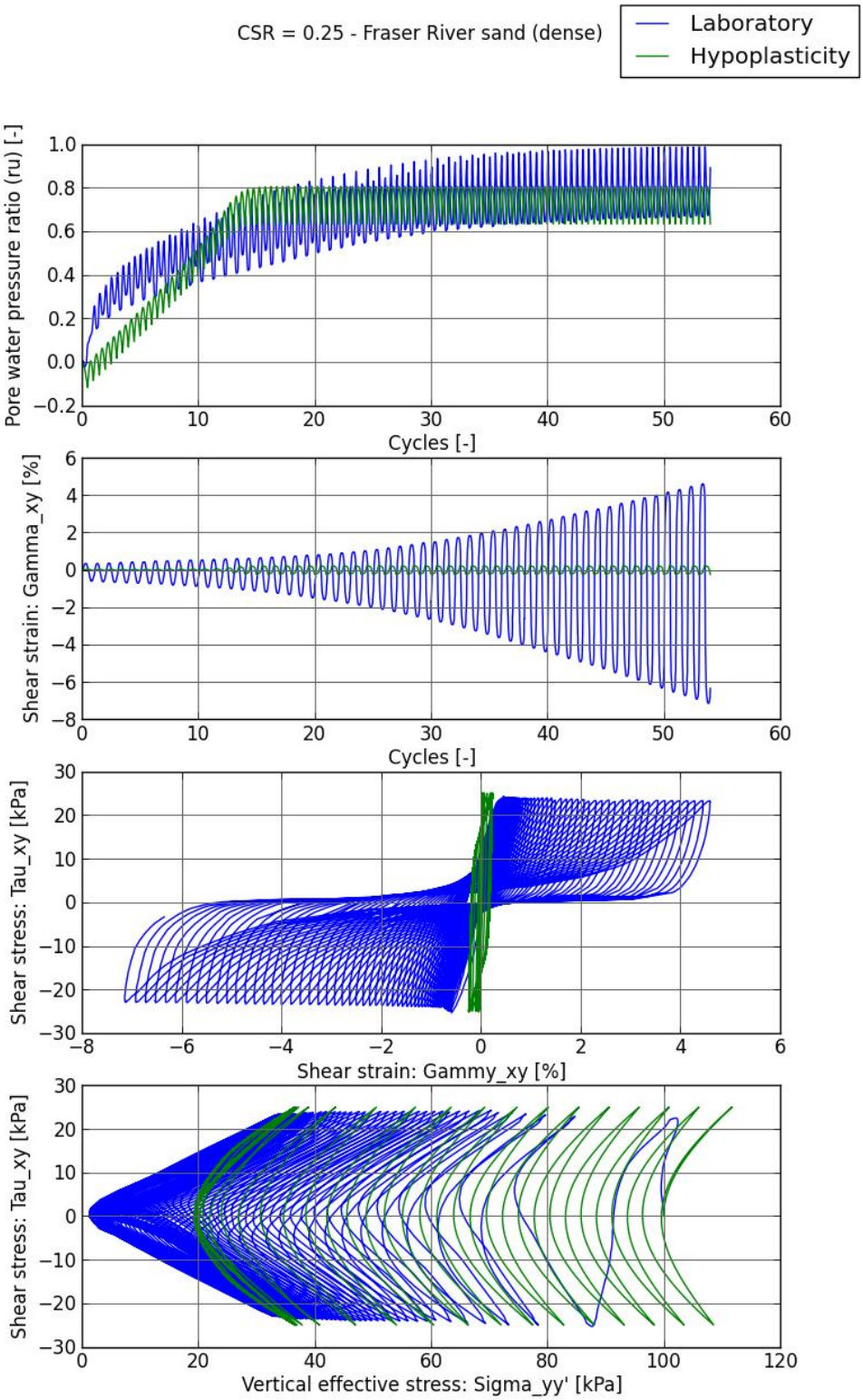

Figure E.4 Final calibration results Hypoplastic model, for dense sand and CSR = 0.25

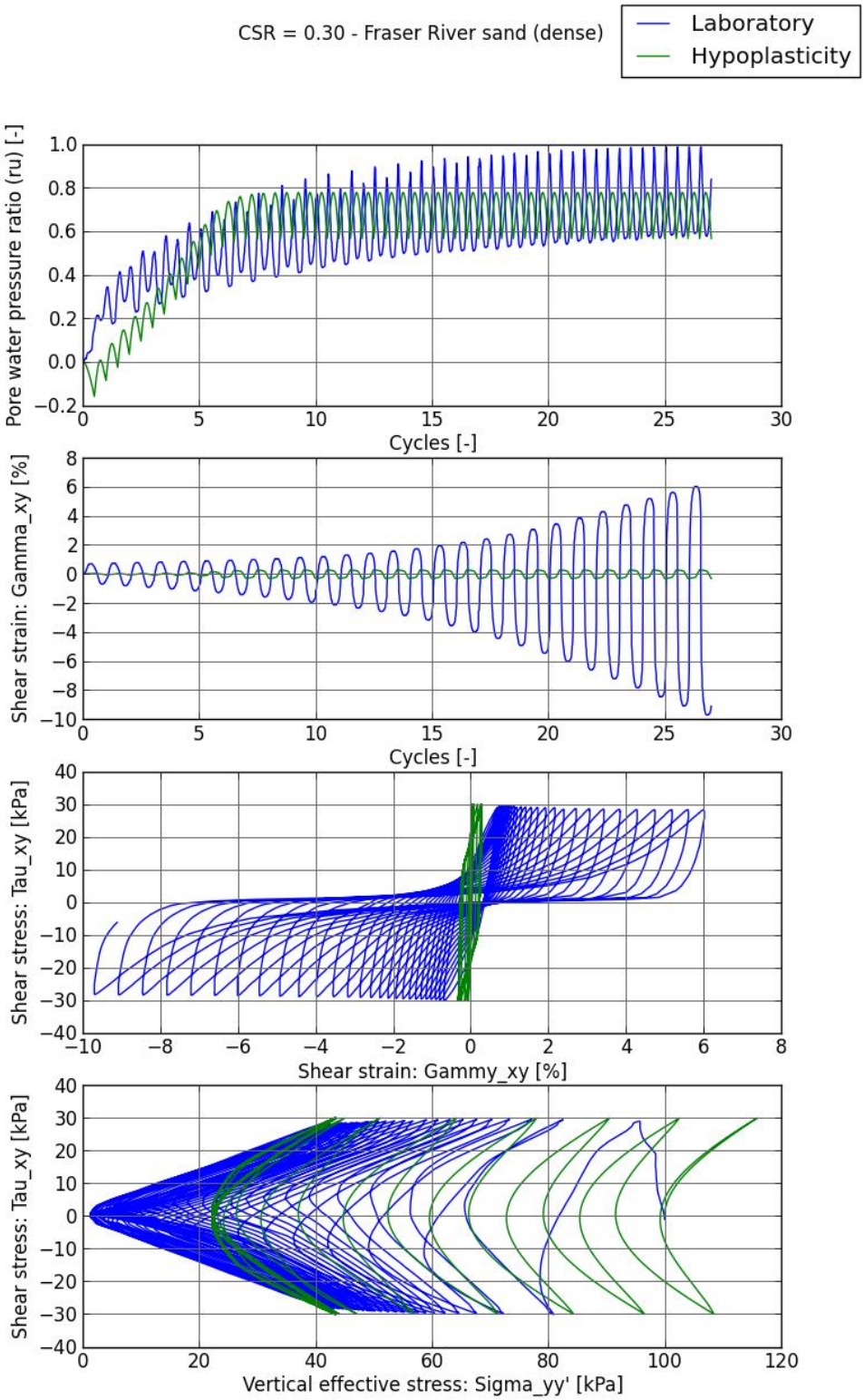

Figure E.5 Final calibration results Hypoplastic model, for dense sand and CSR = 0.30

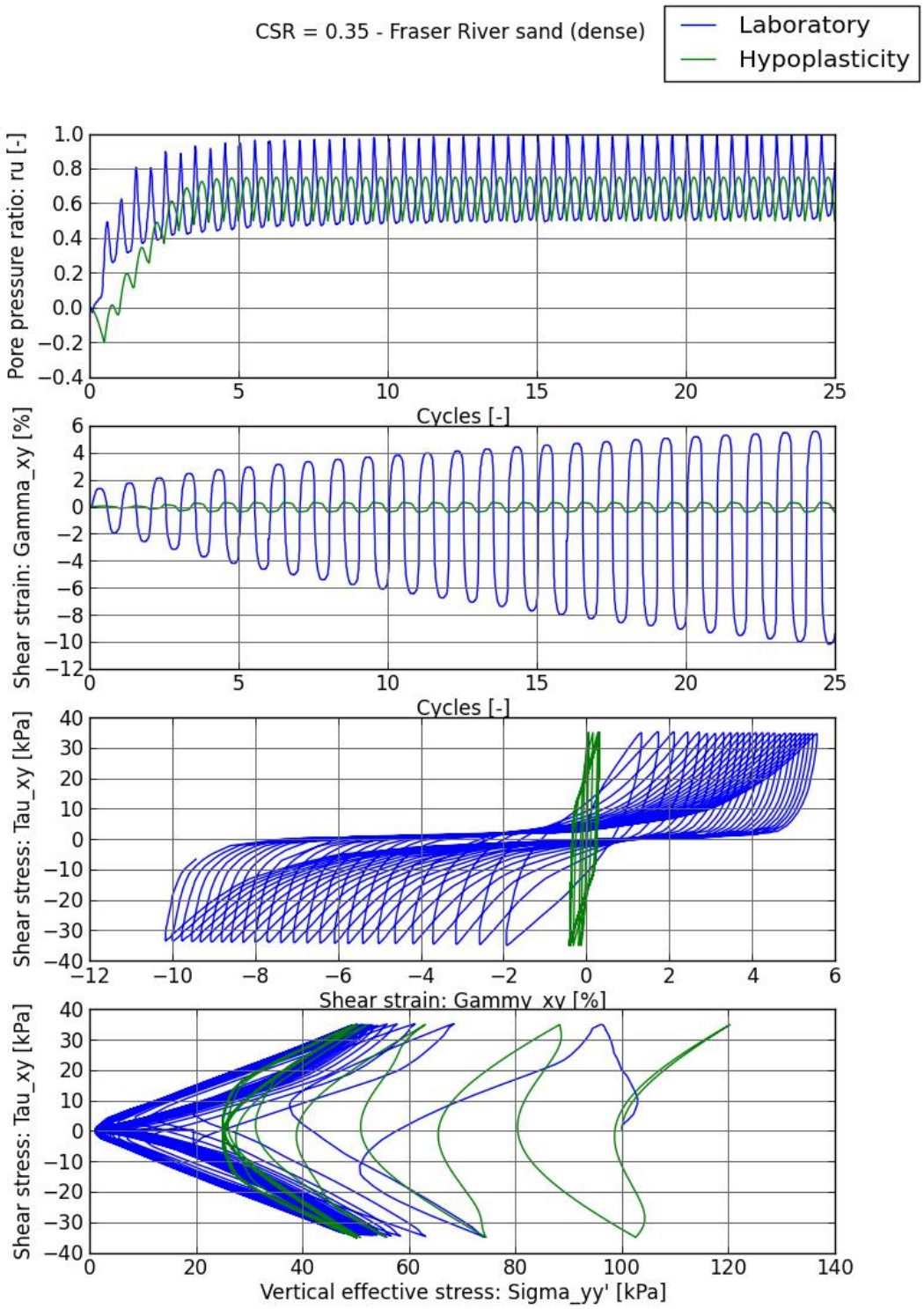

Figure E.6 Final calibration results Hypoplastic model, for dense sand and CSR = 0.35

F Calibration results Hypoplastic model with static shear

This appendix depicts the graphs that compare the results of the Hypoplastic model calibration with static shear with those of laboratory tests in Figure F.1 to Figure F.3. The laboratory tests were conducted with *CSR* values of 0.06, 0.08 and 0.10 for loose sand (D_r = 40%). Furthermore, the tests were conducted with an initial static shear ratio of 0.1. The input parameters for the Hypoplastic model are given in Table F.1.

Table F.1 Hypoplastic parameters after calibration for loose Fraser River sand, including static shear

φ_c [°]	h_s [GPa]	n	e_{d0}	e_{c0}	e_{i0}	α	β	m_R	m_T	R_{max}	β_r	χ	e_0
31	1.0	0.36	0.61	0.96	1.09	0.13	2	5	2	10^{-4}	0.5	1	0.86

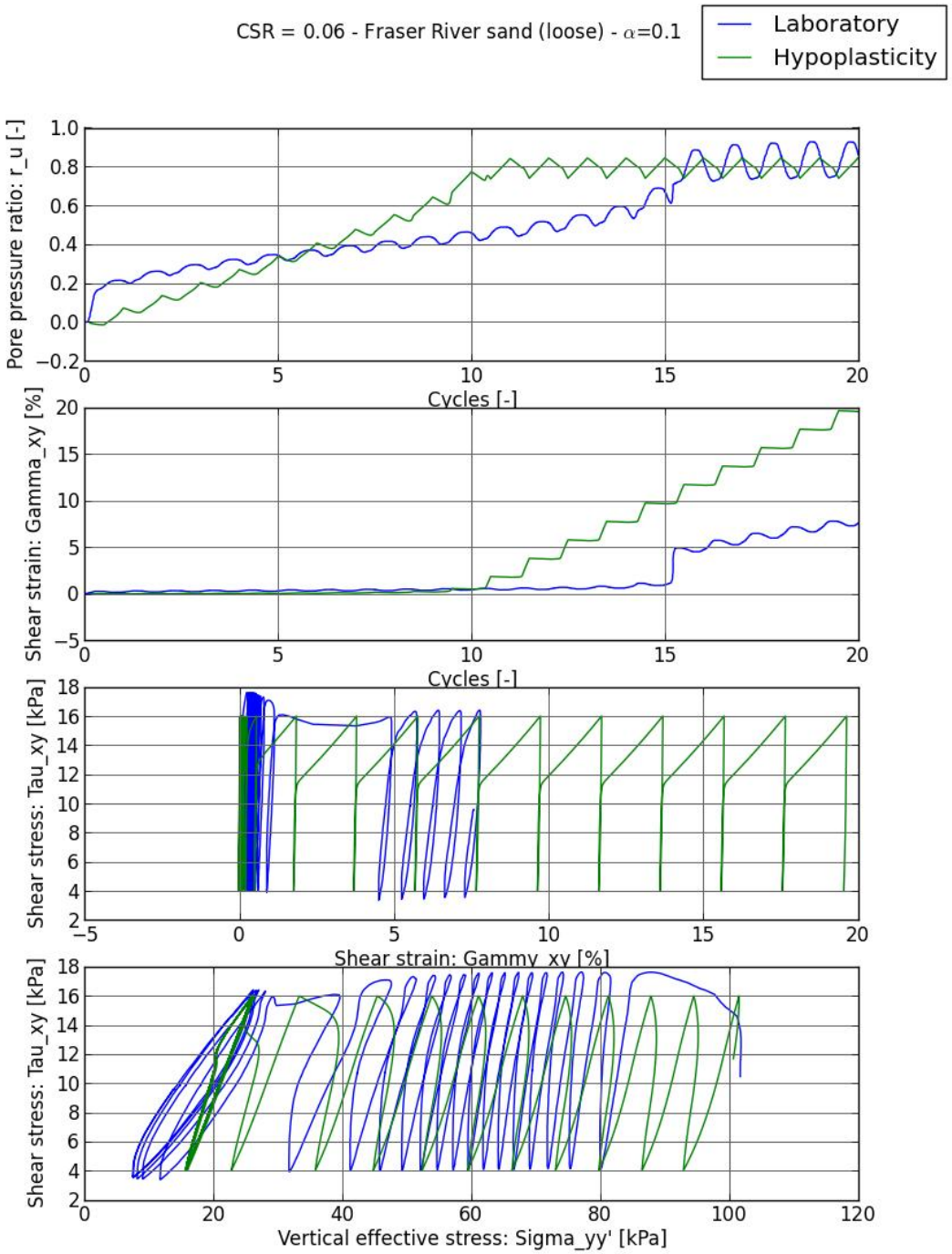

Figure F.1 Final calibration results Hypoplastic model, for loose sand, CSR = 0.06 and α = 0.1

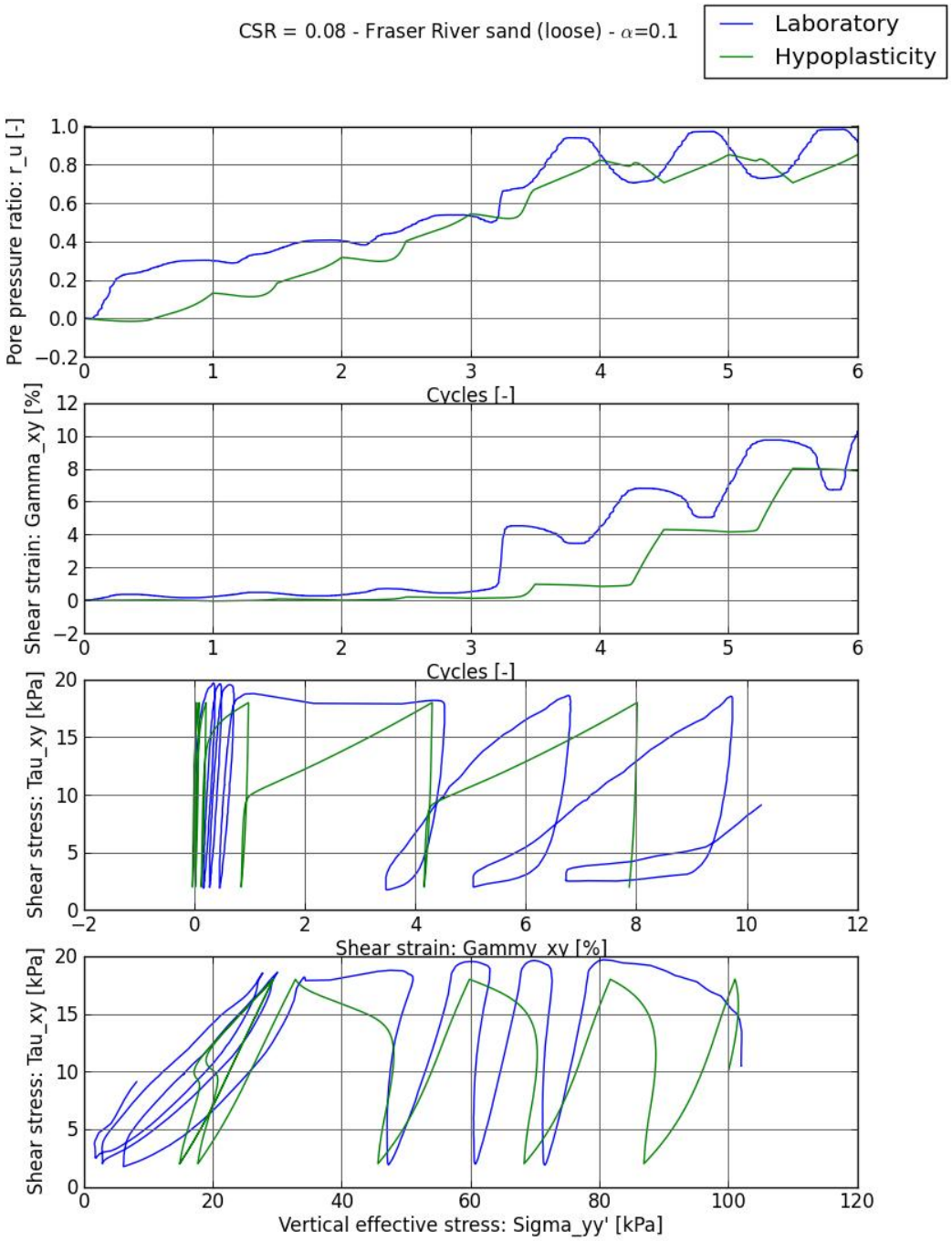

Figure F.2 Final calibration results Hypoplastic model, for loose sand, CSR = 0.08 and α = 0.1

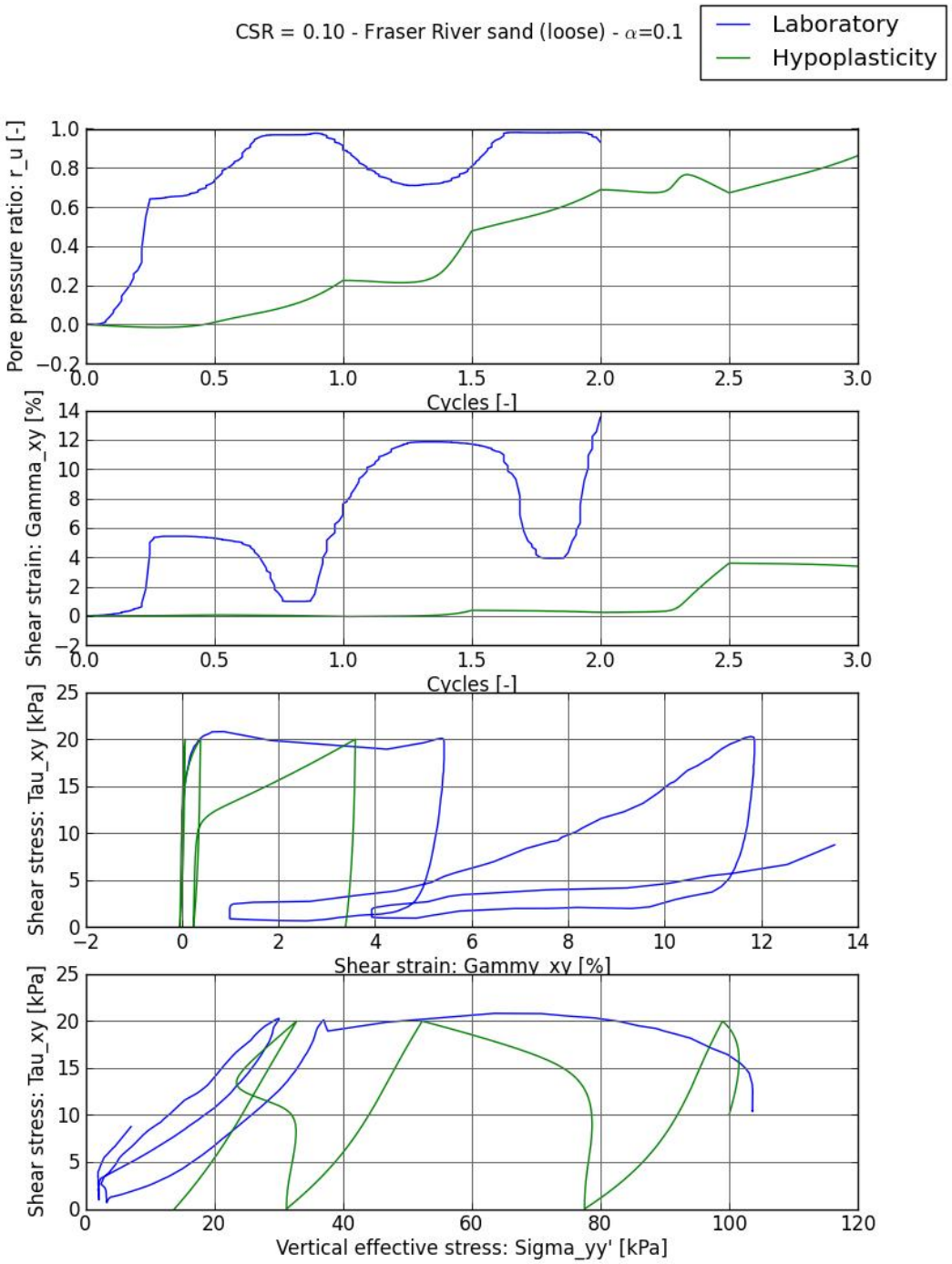

Figure F.3 Final calibration results Hypoplastic model, for loose sand, CSR = 0.10 and α = 0.1

G Results sensitivity analysis UBC3D-PLM

This appendix contains the graphs depicting how influential individual parameters for UBC3D-PLM, when considering the amount of cycles to liquefaction. Figure G.1 and Figure G.2 provide a tornado diagram depicting the results for loose and dense sand respectively; whereas Figure G.3 and Figure G.4 illustrate the individual graphs. The sensitivity analysis was conducted by changing each individual parameter to values of 10% and 20% smaller and larger.

It was not possible to vary φ_{cv} and φ_p separately with this model, hence the sensitivity of both parameters was analysed in two ways. Firstly, both parameters were varied simultaneously (first bar in the tornado diagram and top left graph in the overview) and secondly by varying the difference between both parameters (second bar in the tornado diagram and top right graph in the overview). Table G.1 gives the combinations of both parameters that are used in the sensitivity analysis.

Table G.1 Combinations of φ_{cv} and φ_p used in the sensitivity analysis

φ_{cv}	26.4	29.7	33	36.3	39.6
φ_p (loose)	26.96	30.33	33.7	37.07	40.44
φ_p (dense)	31.12	35.01	38.9	42.79	46.68

Furthermore, the sensitivity of $(N_1)_{60}$ was tested in two ways. Firstly, $(N_1)_{60}$ was changed individually and afterwards another analysis was done changing $(N_1)_{60}$ together with the other parameters according to the relation of Beaty and Byrne. The first one is denoted in the tornado diagram and the graphs with $(N_1)_{60}$, while the one including the Beaty and Byrne relation is denoted by $(N_1)_{60\_bb}$.

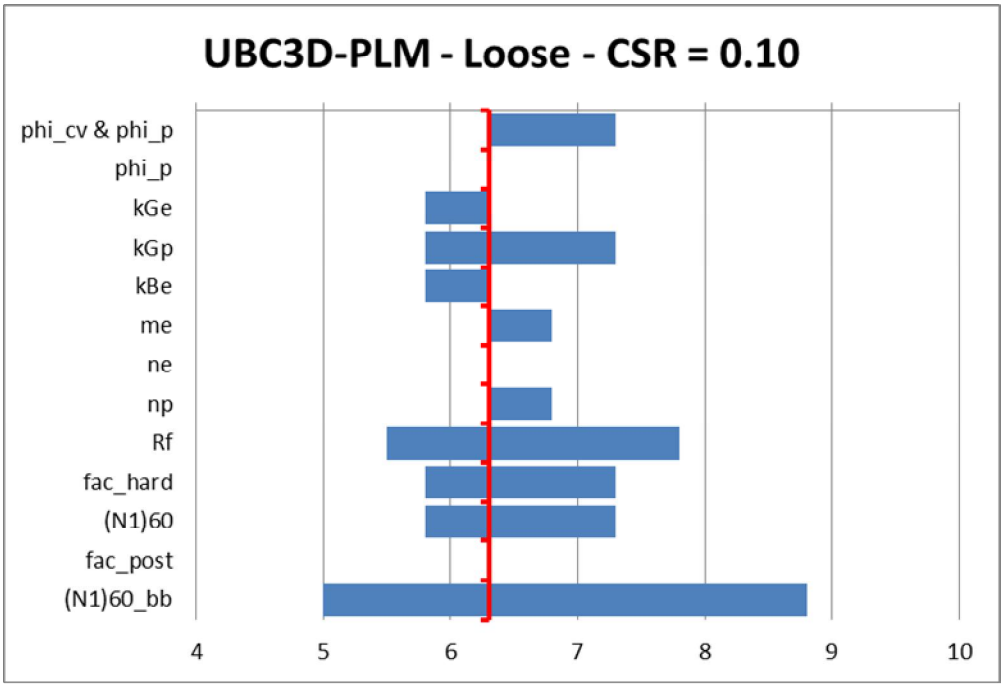

Figure G.1 Tornado diagram sensitivity UBC3D-PLM for loose sand at CSR = 0.10

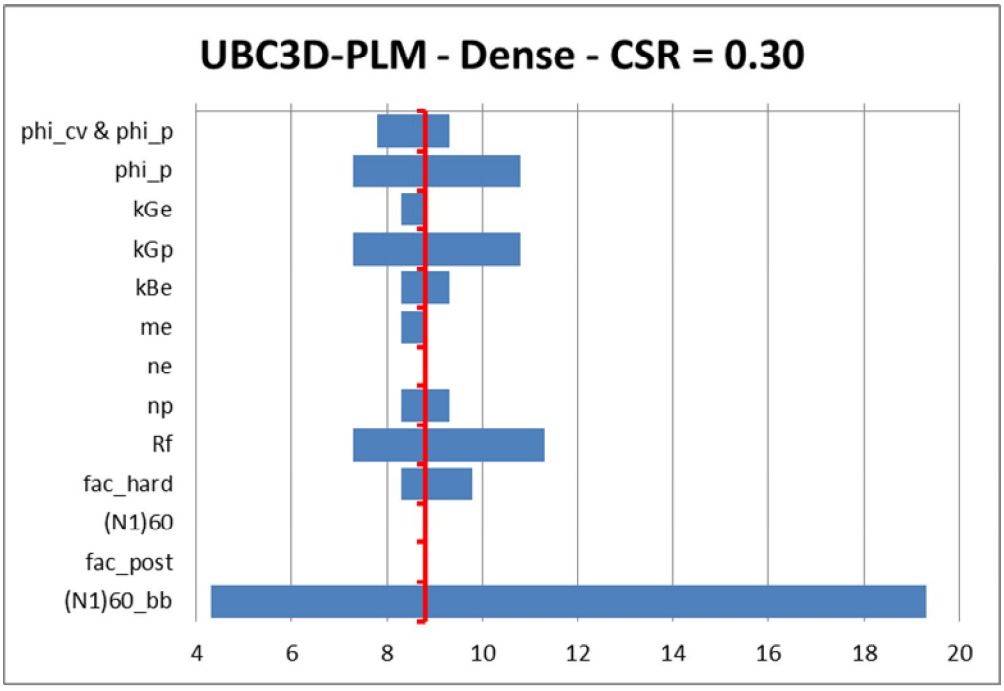

Figure G.2 Tornado diagram sensitivity UBC3D-PLM for dense sand at CSR = 0.30

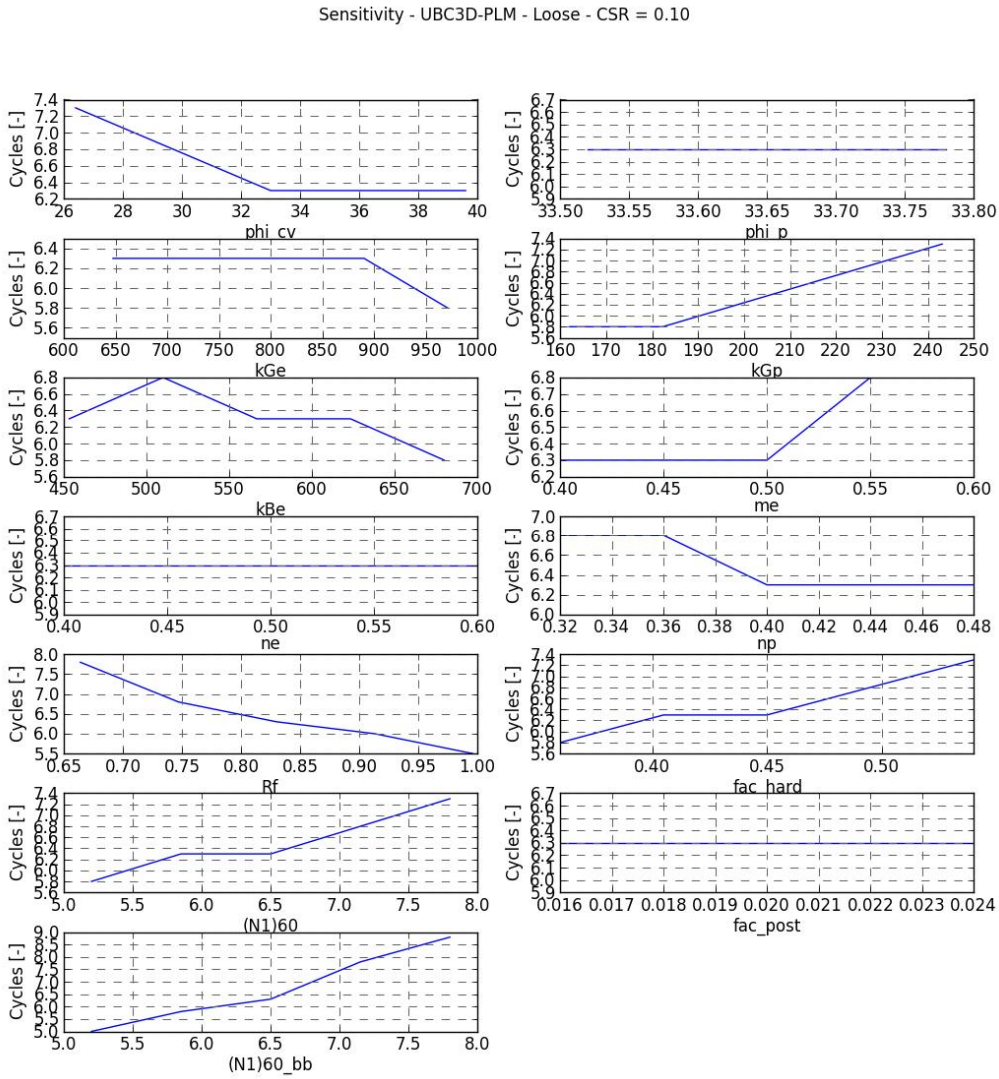

Figure G.3 Individual graphs sensitivity analysis UBC3D-PLM for loose sand at CSR = 0.10

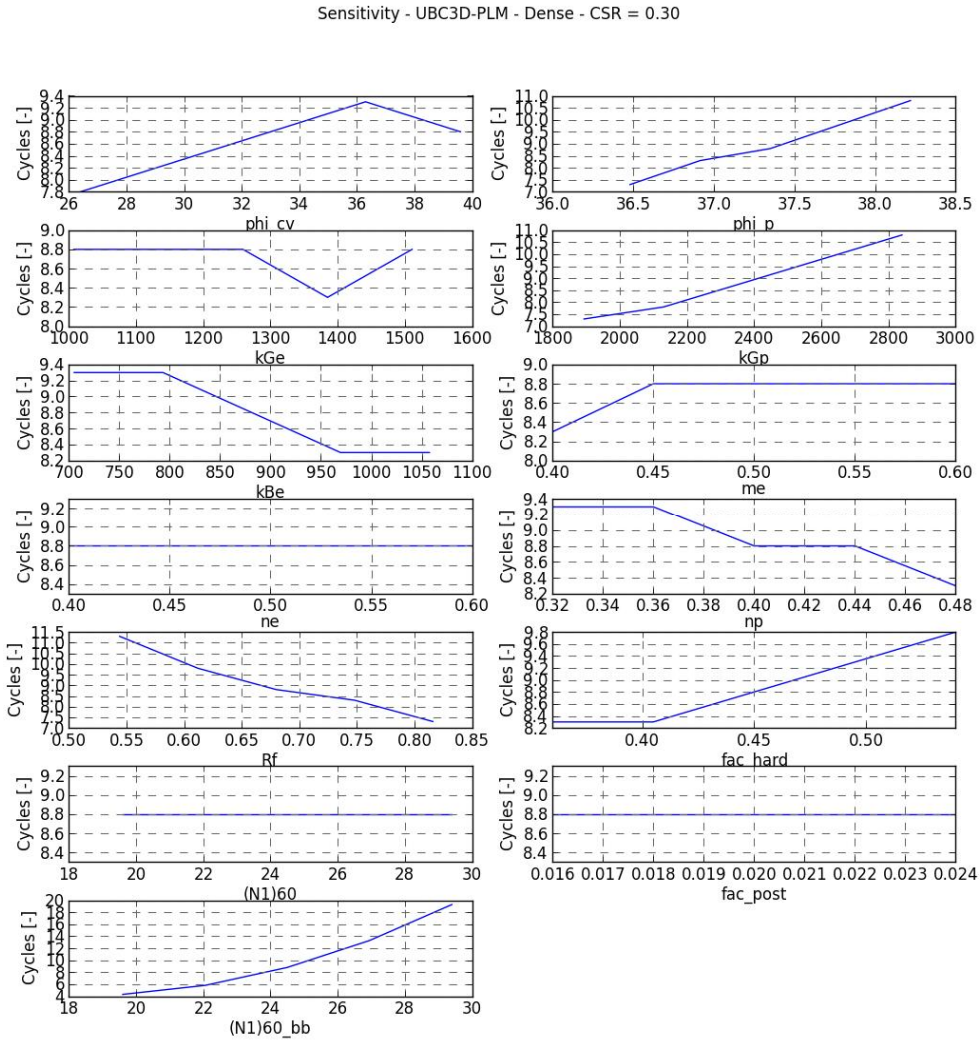

Figure G.4 Individual graphs sensitivity analysis UBC3D-PLM for dense sand at CSR = 0.30

H Results sensitivity analysis Hypoplastic model

This appendix contains the graphs depicting how influential individual parameters for the Hypoplastic, when considering the amount of cycles to liquefaction. Figure H.1 and Figure H.2 provide a tornado diagram depicting the results for loose and dense sand respectively; whereas Figure H.3 and Figure H.4 illustrate the individual graphs. The sensitivity analysis was conducted by changing each individual parameter to values of 10% and 20% smaller and larger.

The sensitivity analysis had some limitations. For instance, some combinations of parameters were impossible or liquefaction did not occur. For this analysis, it should be noted that:

- for loose soil, liquefaction did not occur within 40 cycles for e_0 -20%, an additional step of e_0 = 0.70 (approximately e_0 -19%) was added to take this into account;
- for dense soil, e_{d0} +20% was not possible because of the consistency requirement $e_{d0} \leq e_0 \leq e_{c0}$;
- for dense soil, liquefaction did not occur within 62 cycles for e_{i0} +20%;
- for dense soil, liquefaction did not occur within 62 cycles for e_0 -10% and e_0 -20%, an additional step of e_0 -5% was added to take into account a decrease of e_0.

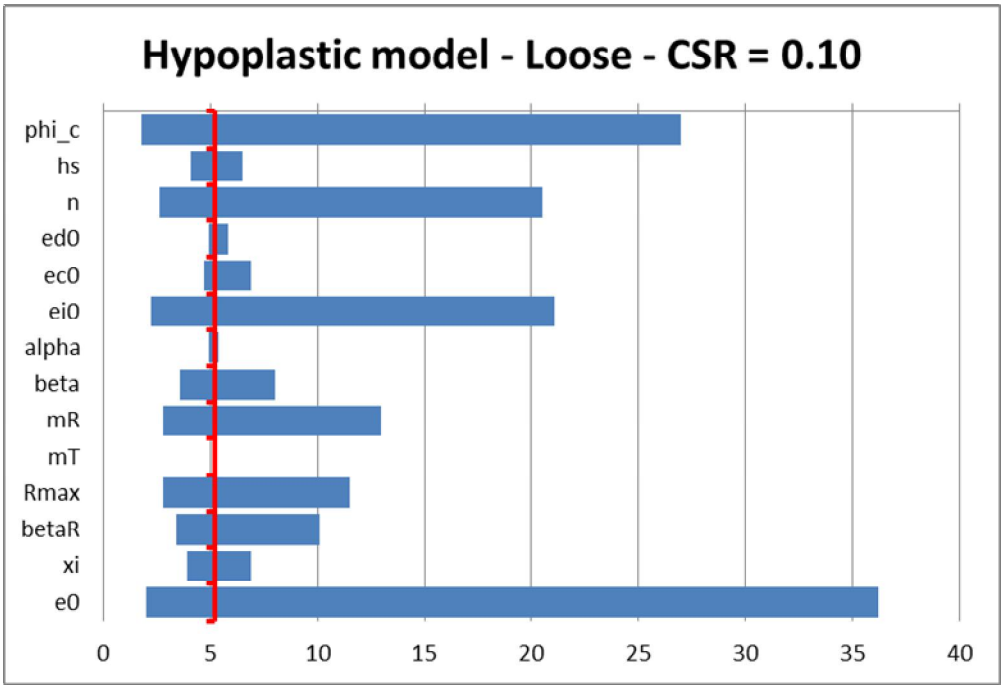

Figure H.1 Tornado diagram sensitivity Hypoplastic model for dense sand at CSR = 0.10

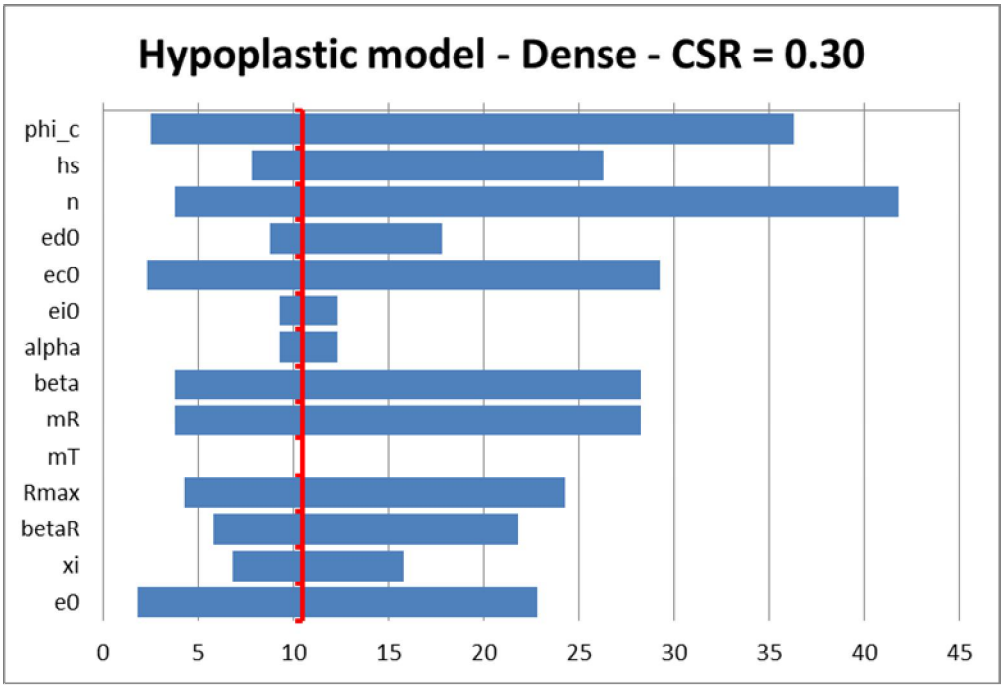

Figure H.2 Tornado diagram sensitivity Hypoplastic model for dense sand at CSR = 0.30

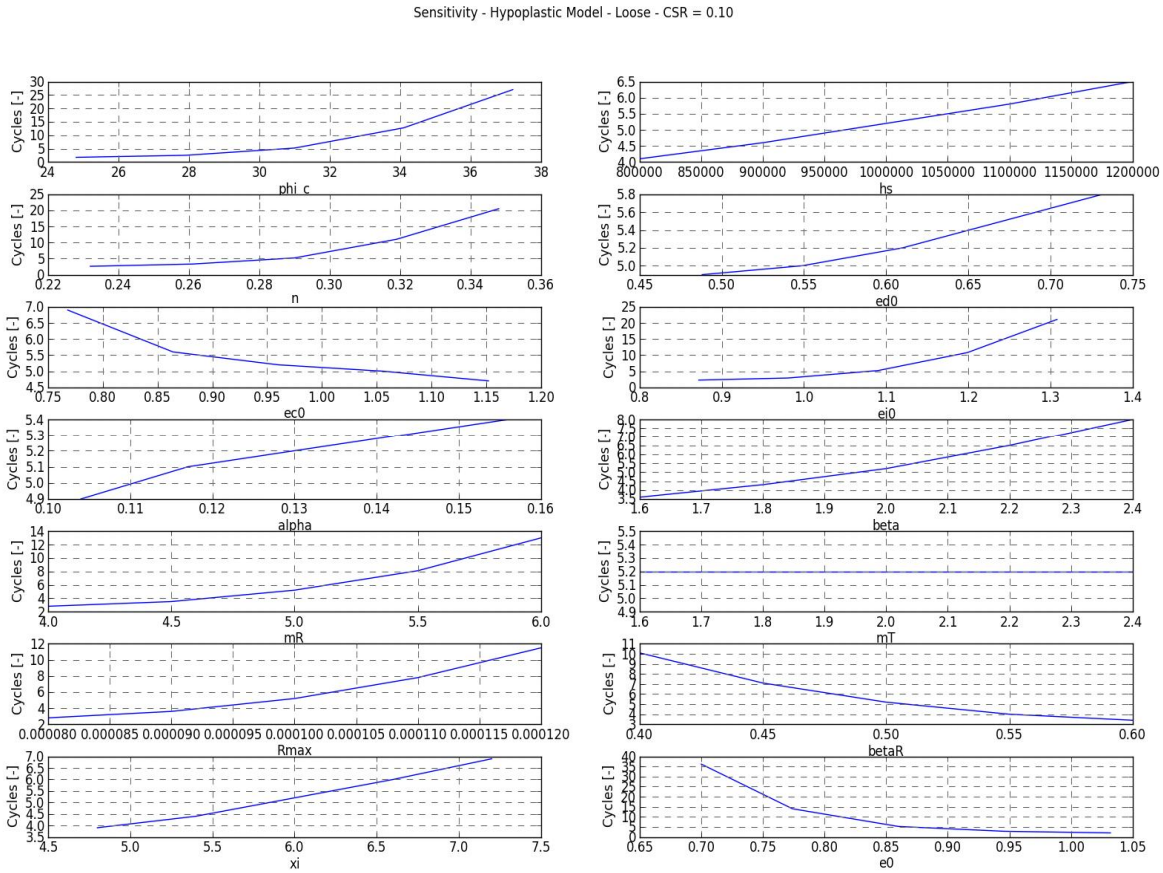

Figure H.3 Individual graphs sensitivity analysis Hypoplastic model for loose sand at CSR = 0.10

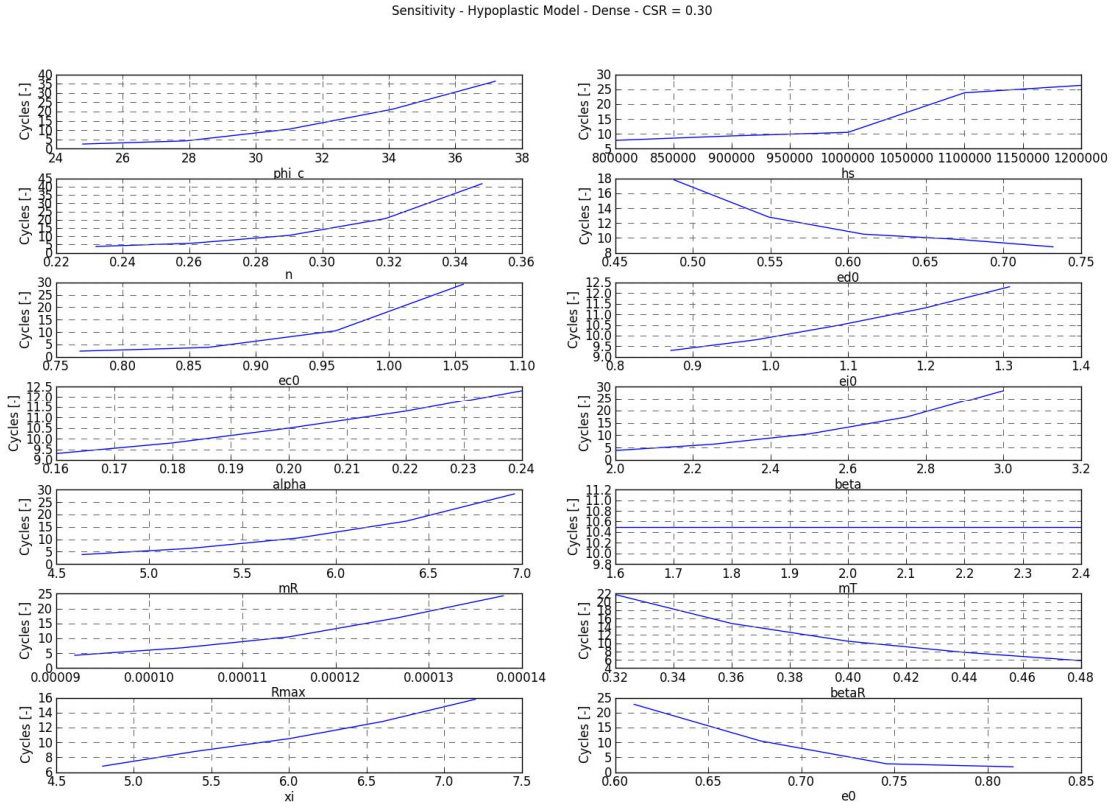

Figure H.4 Individual graphs sensitivity analysis Hypoplastic model for dense sand at CSR = 0.30

I Scaling factors centrifuge test

Scaling factors give the relation between the physical model and the prototype for physical quantities. The generalised scaling factors for centrifuge model tests are given in Table I.1; the scaling factor is the ratio between the prototype (desired model) and the physical model (the actual model in the centrifuge) as shown in equation (I.1). The centrifuge tests was flown at 70g, with an actual inertia acceleration of 69.96g (C-CORE, 2004), so η is 70 (Tobita et al., 2008).

$$Scaling\ \ factor = \frac{\text{Prototype}}{\text{Physical model}} \tag{I.1}$$

Table I.1 Generalised scaling factors for centrifuge model tests (Tobita et al., 2008)

Physical quantity	Scaling factor
Length	η
Density	1
Time	η
Stress	1
Pore water pressure	1
Displacement	η
Particle velocity	1
Shear wave velocity	1
Acceleration	$1/\eta$
Strain	1
Bending moment	$\eta^{3.0}$
Flexial rigidity	$\eta^{4.0}$

J Validation results UBC3D-PLM for A2475 signal

This appendix contains the results for the A2475 signal, obtained with UBC3D-PLM. Figure J.1 to Figure J.6 depict the comparison of the predicted accelerations and excess pore water pressures with the results of the centrifuge test; whereas Figure J.7 provides the comparison of the predicted settlements.

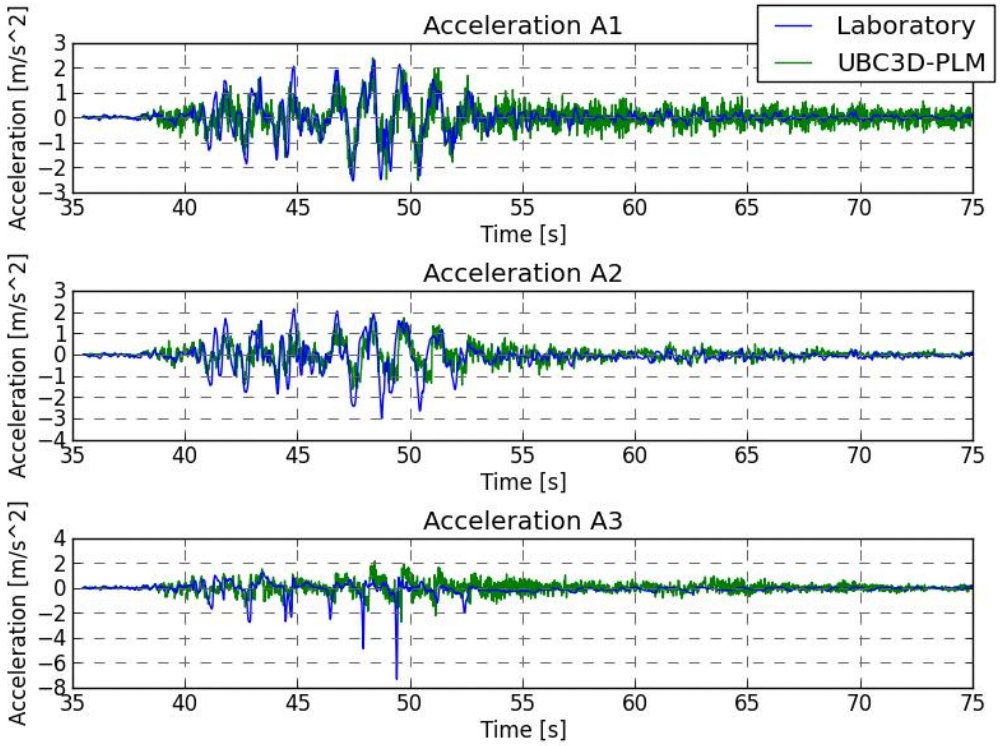

Figure J.1 Horizontal accelerations with UBC3D-PLM in points A1, A2 and A3 for A2475

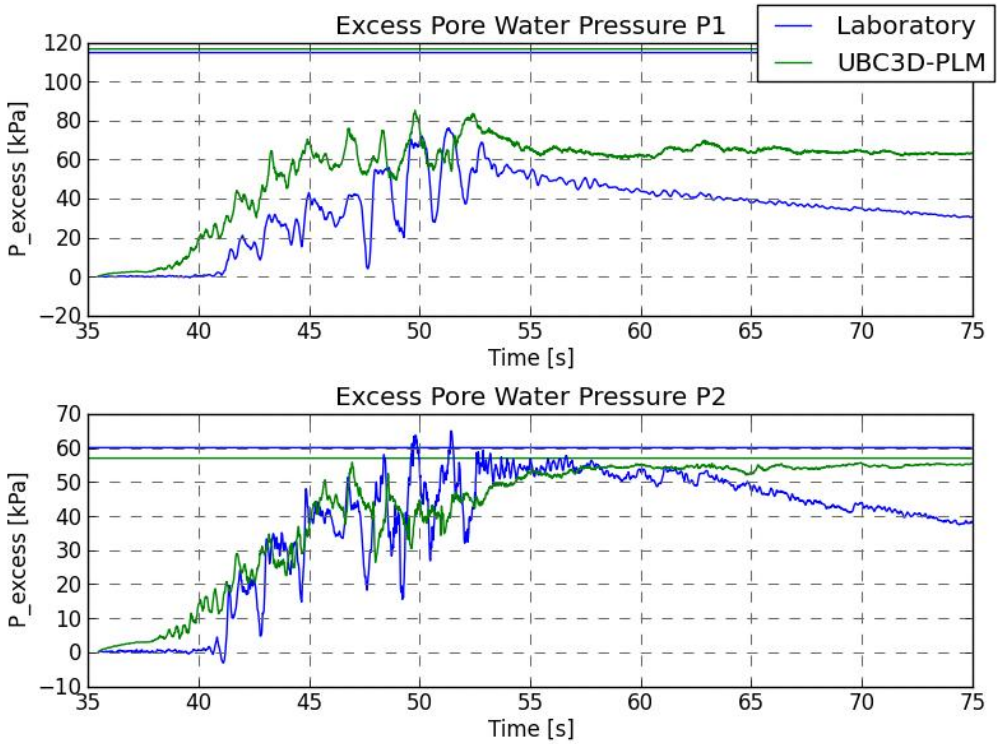

Figure J.2 Excess pore water pressures for UBC3D-PLM in points P1 and P2 for A2475. The horizontal lines represent the initial effective vertical stress.

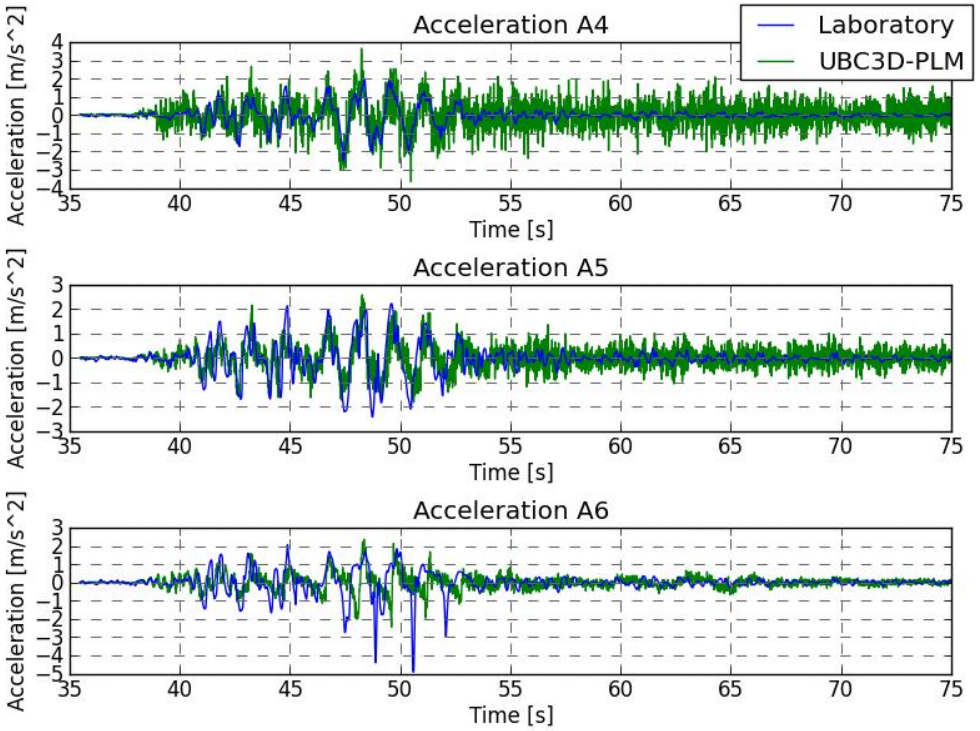

Figure J.3 Horizontal accelerations with UBC3D-PLM in points A4, A5 and A6 for A2475

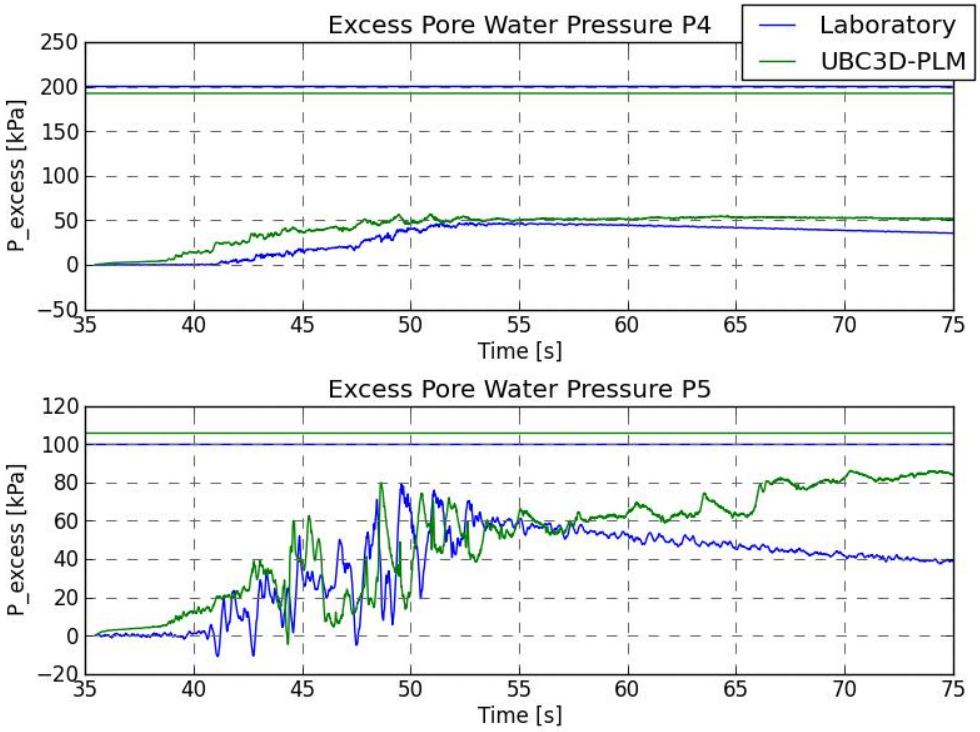

Figure J.4 Excess pore water pressures for UBC3D-PLM in points P4 and P5 for A2475. The horizontal lines represent the initial effective vertical stress.

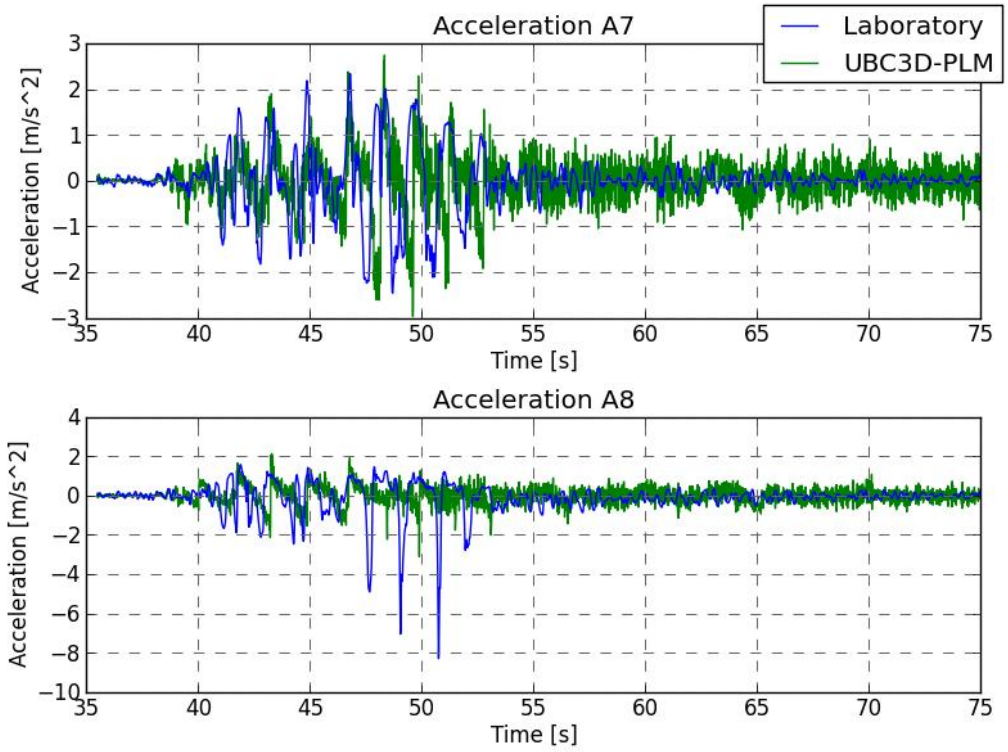

Figure J.5 Horizontal accelerations with UBC3D-PLM in points A7 and A8 for A2475

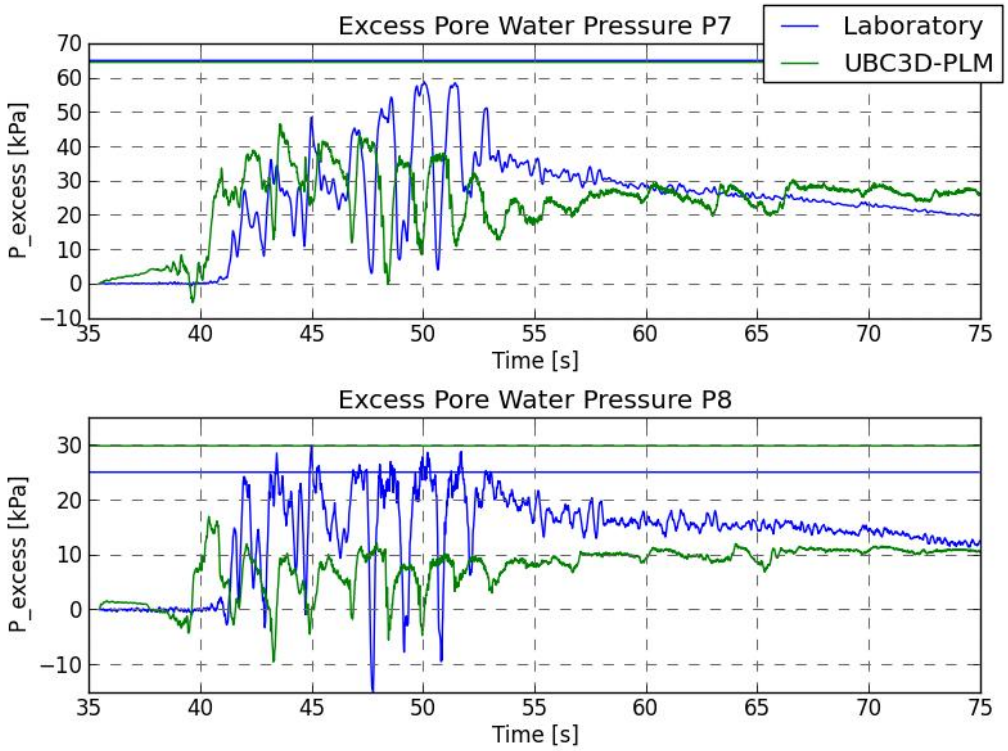

Figure J.6 Excess pore water pressures for UBC3D-PLM in points P7 and P8 for A2475. The horizontal lines represent the initial effective vertical stress.

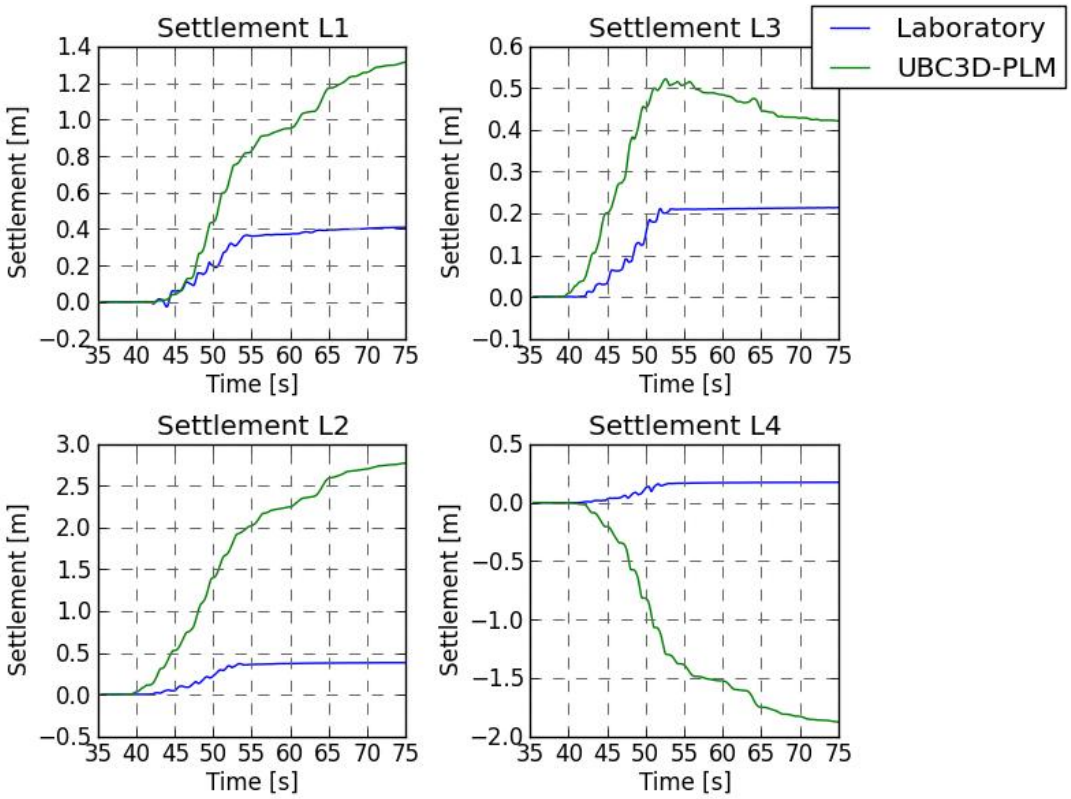

Figure J.7 Settlements for UBC3D-PLM in points L1, L2, L3 and L4

K Validation results Hypoplastic model for A2475 signal

This appendix contains the results for the A2475 signal, obtained with the Hypoplastic model. Figure K.1 to Figure K.6 depict the comparison of the predicted accelerations and excess pore water pressures with the results of the centrifuge test; whereas Figure K.7 provides the comparison of the predicted settlements.

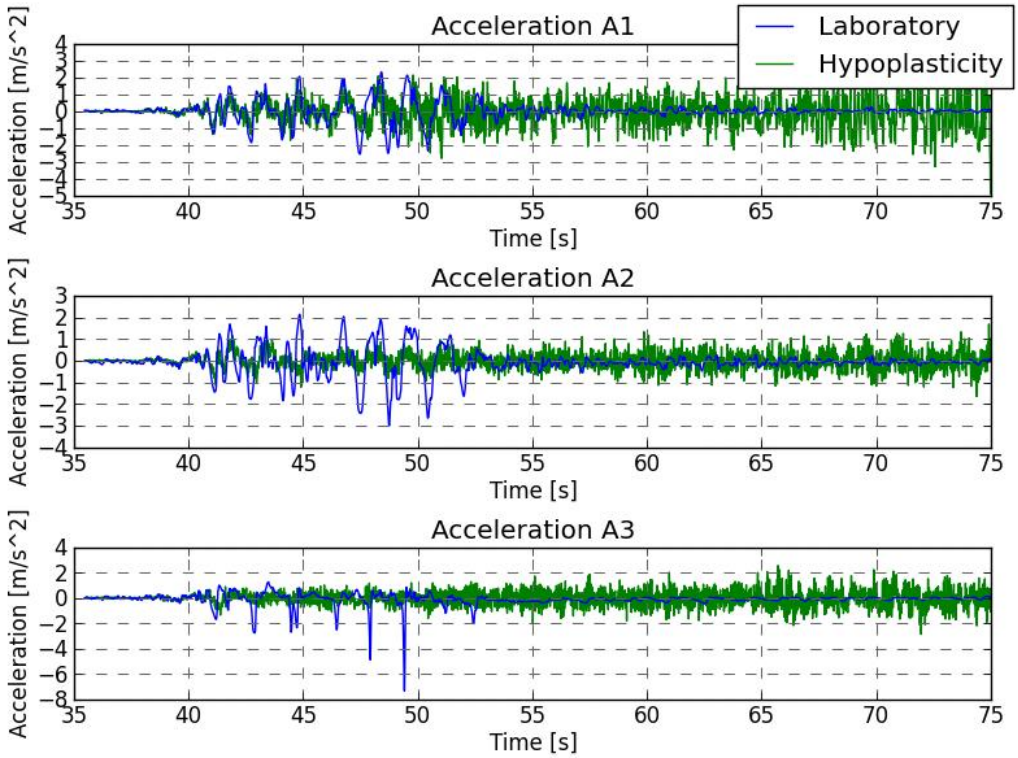

Figure K.1 Horizontal accelerations with Hypoplastic model in points A1, A2 and A3 for A2475

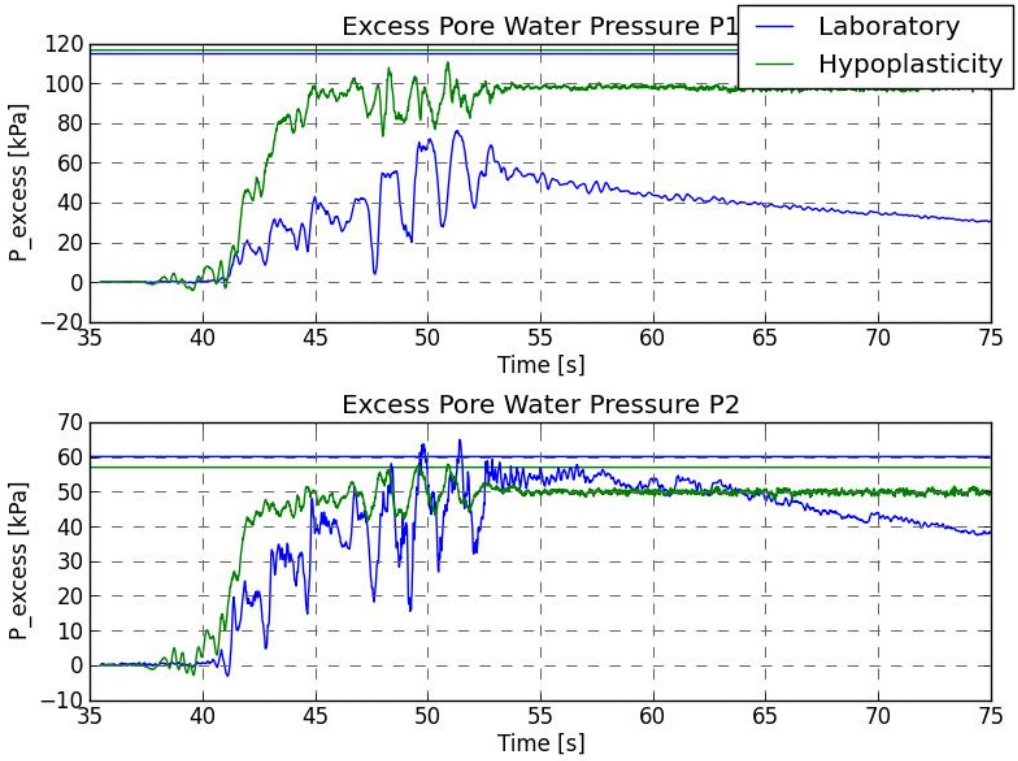

Figure K.2 Excess pore water pressures for Hypoplastic model in points P1 and P2 for A2475. The horizontal lines represent the initial effective vertical stress.

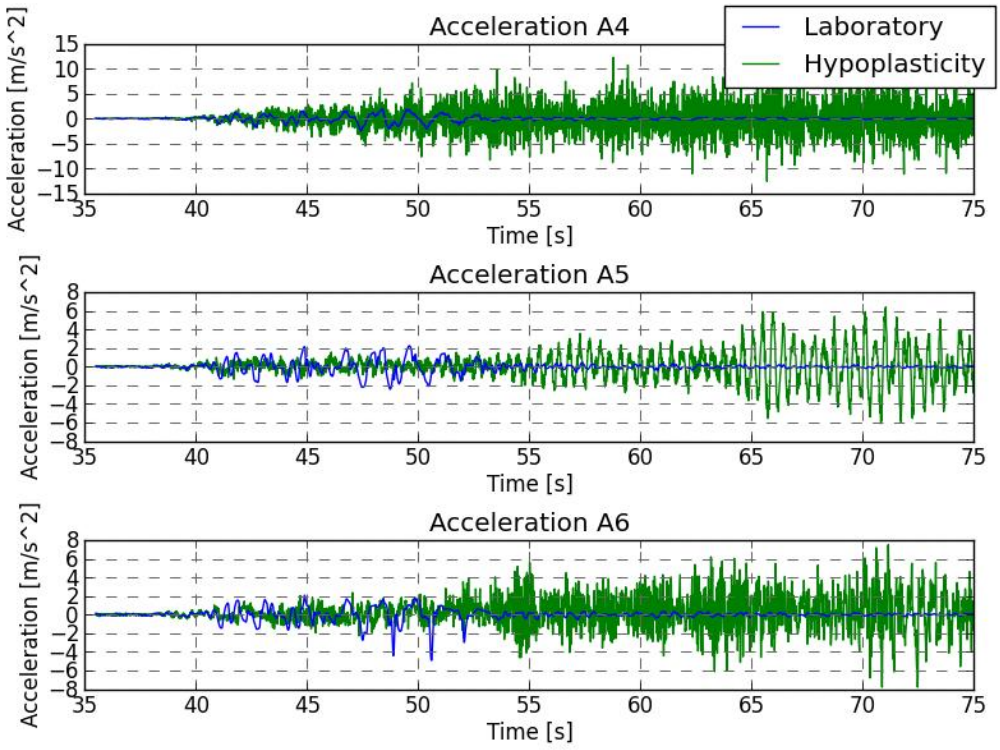

Figure K.3 Horizontal accelerations with Hypoplastic model in points A4, A5 and A6 for A2475

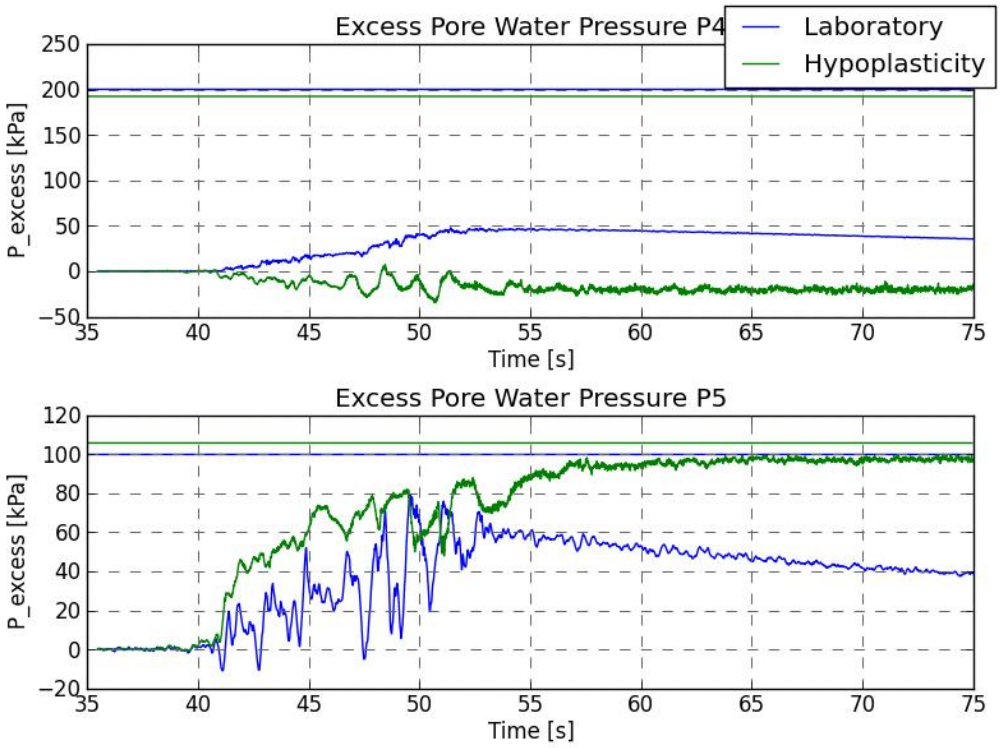

Figure K.4 Excess pore water pressures for Hypoplastic model in points P4 and P5 for A2475. The horizontal lines represent the initial effective vertical stress.

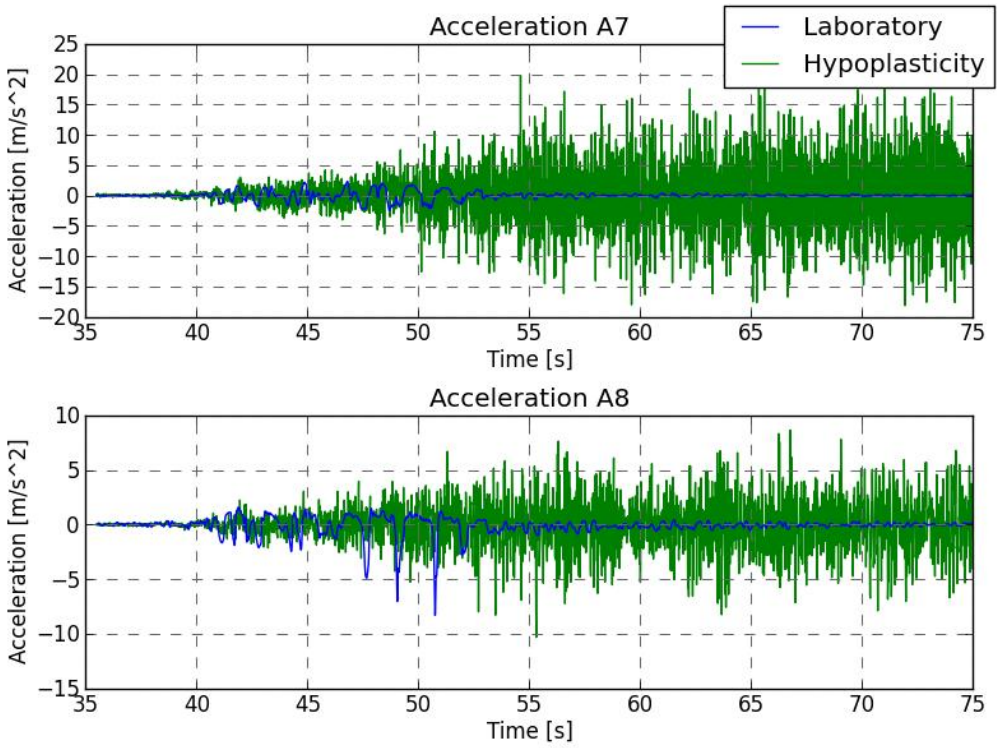

Figure K.5 Horizontal accelerations with Hypoplastic model in points A7 and A8 for A2475

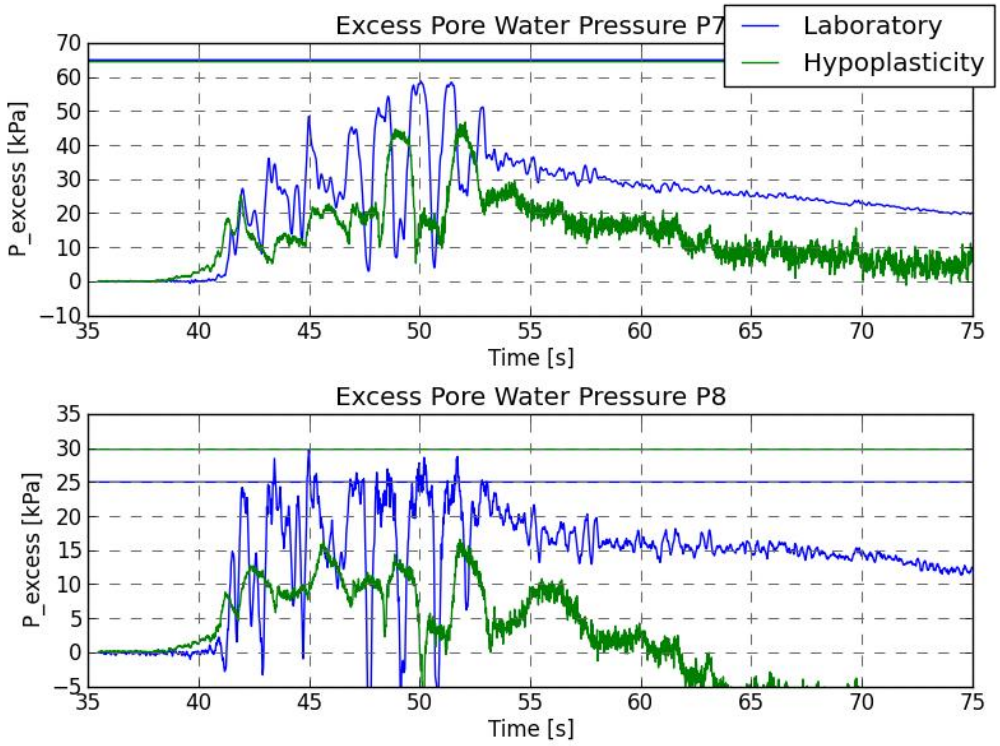

Figure K.6 Excess pore water pressures for Hypoplastic model in points P7 and P8 for A2475. The horizontal lines represent the initial effective vertical stress.

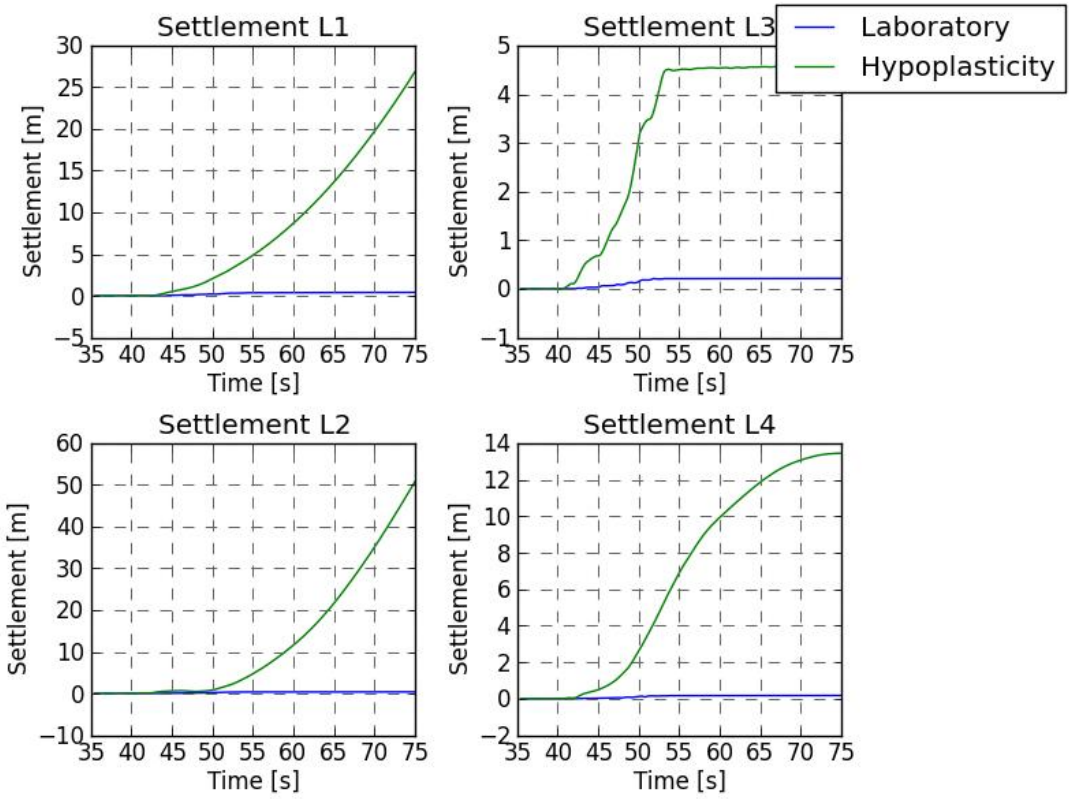

Figure K.7 Settlements for Hypoplastic model in points L1, L2, L3 and L4 for A2475

L Results Hypoplastic model for A475 signal; parameters without static shear

This appendix contains the results for the A475 signal, obtained with Hypoplastic model. For this calculation, the loose sand parameters that were obtained without static shear (provided in Table L.1) are used. Figure L.1 to Figure L.6 depict the comparison of the predicted accelerations and excess pore water pressures with the results of the centrifuge test; whereas Figure L.7 provides the comparison of the predicted settlements.

Table L.1 Hypoplastic parameters after calibration for loose Fraser River sand

φ_c [°]	h_s [GPa]	n	e_{d0}	e_{c0}	e_{i0}	α	β	m_R	m_T	R_{max}	β_r	χ	e_0
31	1.0	0.29	0.61	0.96	1.09	0.13	2	5	2	10^{-4}	0.5	6	0.86

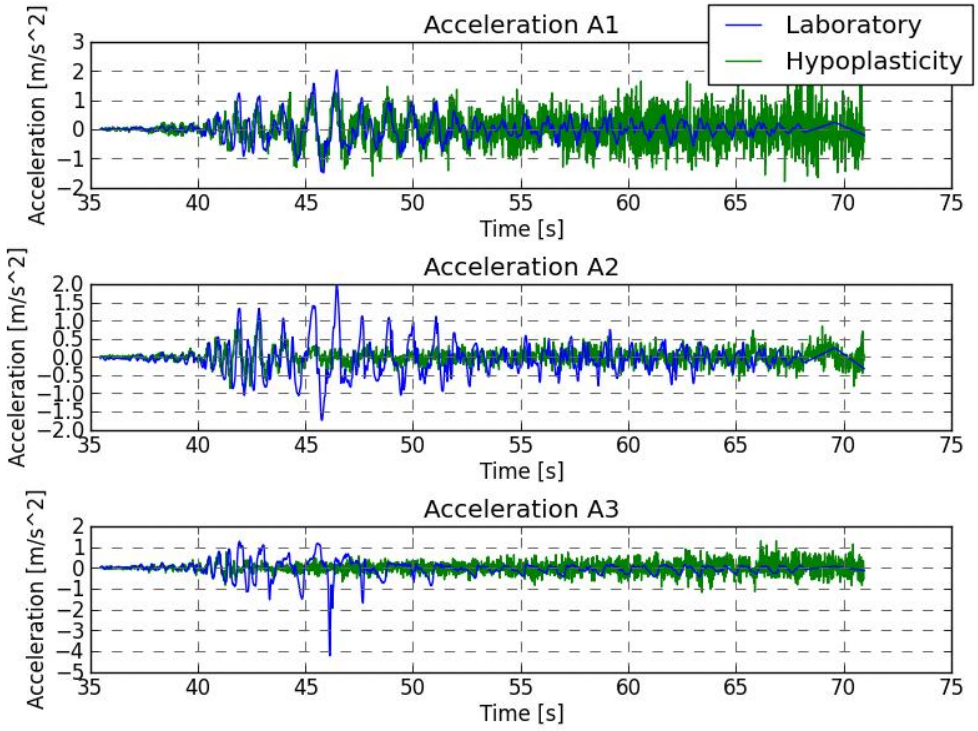

Figure L.1 Horizontal accelerations with Hypoplastic model in points A1, A2 and A3 for A475

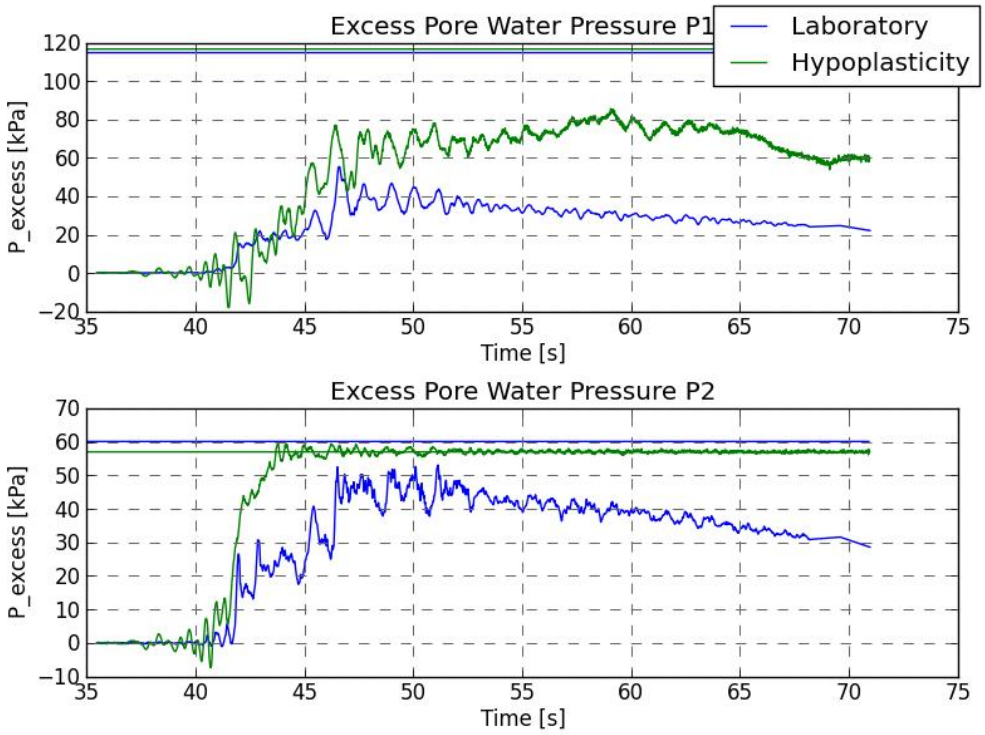

Figure L.2 Excess pore water pressures for Hypoplastic model in points P1 and P2 for A475. The horizontal lines represent the initial effective vertical stress.

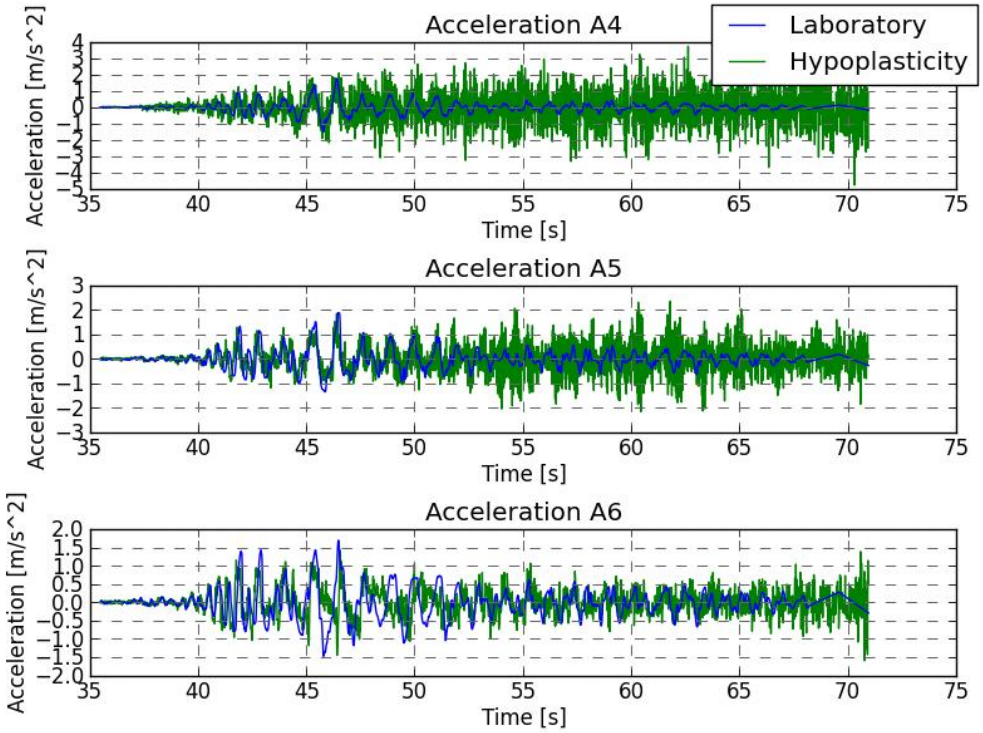

Figure L.3 Horizontal accelerations with Hypoplastic model in points A4, A5 and A6 for A475

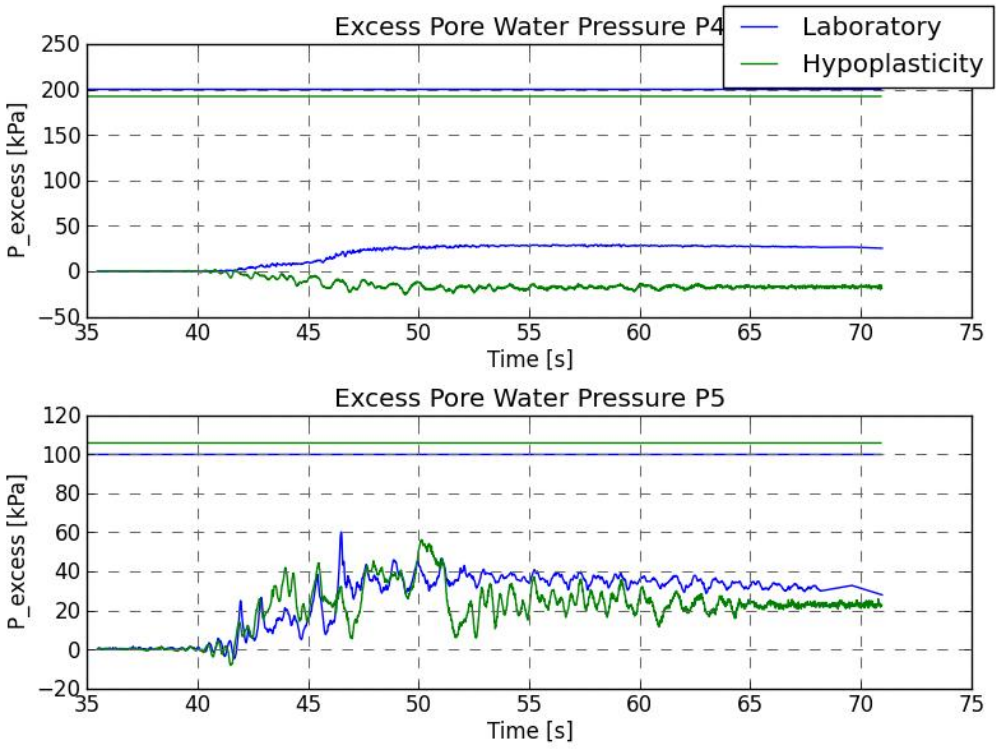

Figure L.4 Excess pore water pressures for Hypoplastic model in points P4 and P5 for A475. The horizontal lines represent the initial effective vertical stress.

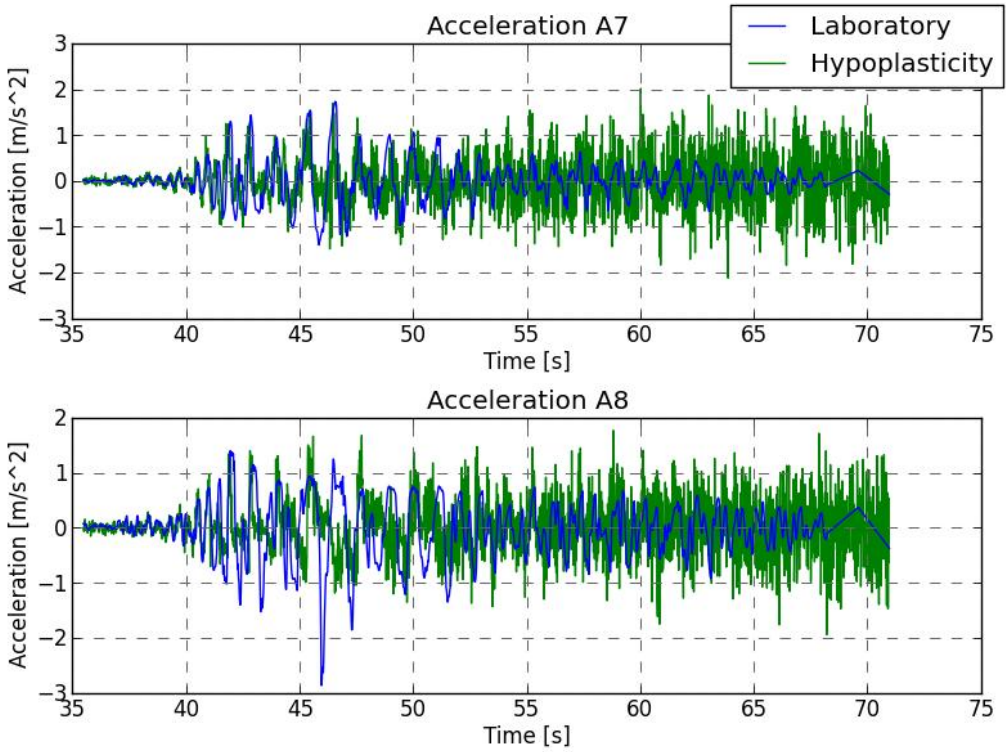

Figure L.5 Horizontal accelerations with Hypoplastic model in points A7 and A8 for A475

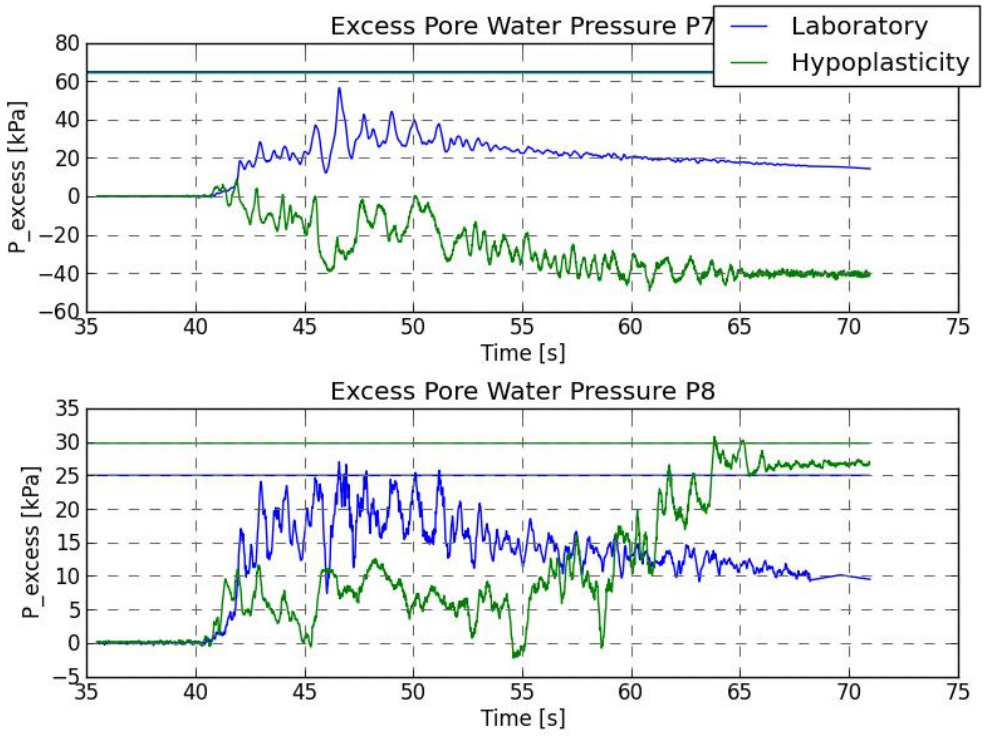

Figure L.6 Excess pore water pressures for Hypoplastic model in points P7 and P8 for A475. The horizontal lines represent the initial effective vertical stress.

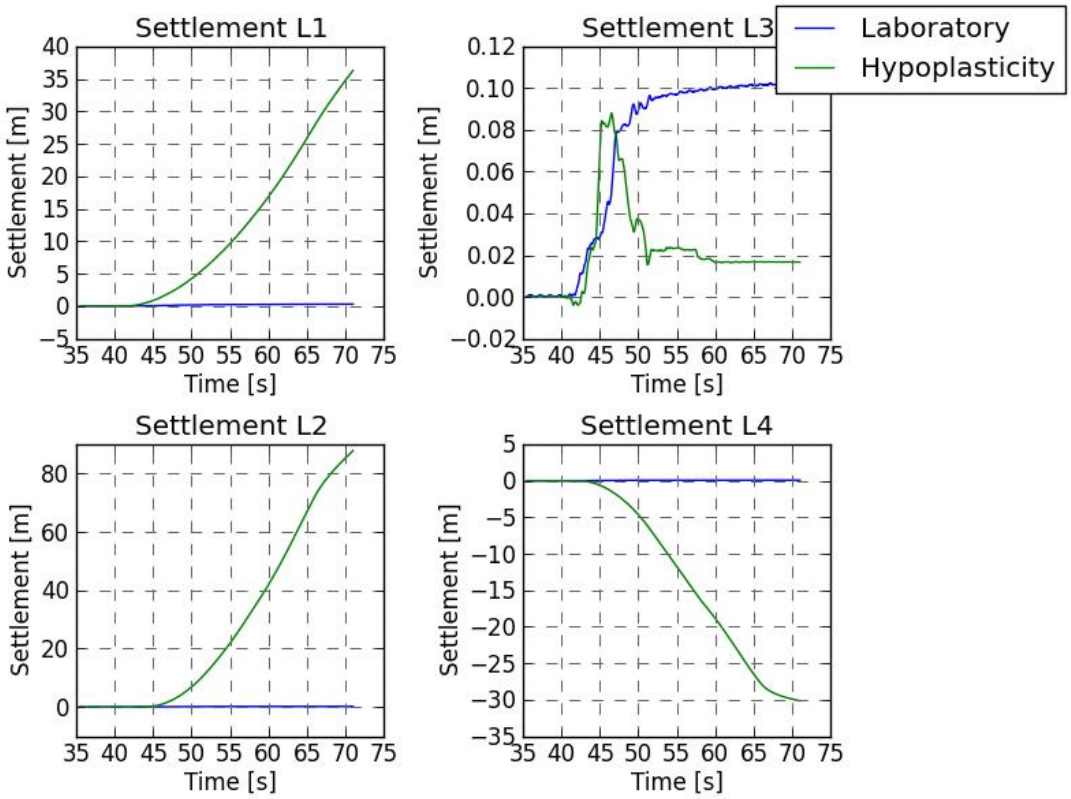

Figure L.7 Settlements for Hypoplastic model in points L1, L2, L3 and L4 for A475

M Displacements Hypoplastic model A475 signal

This appendix provides displacements predicted by the Hypoplastic model with the A475 signal at different points in time; depicted by Figure M.1 to Figure M.6. It is clearly shown that at the start the displacement pattern is realistic. However, after the first large peaks (45 to 50 seconds), outliers start to occur.

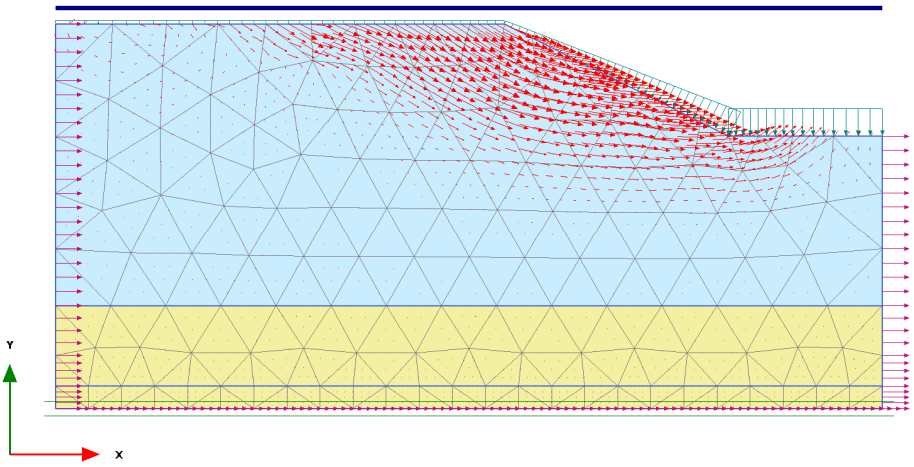

Figure M.1 Displacement Hypoplastic model at t = 41.0 s; maximum displacement is 0.11 m

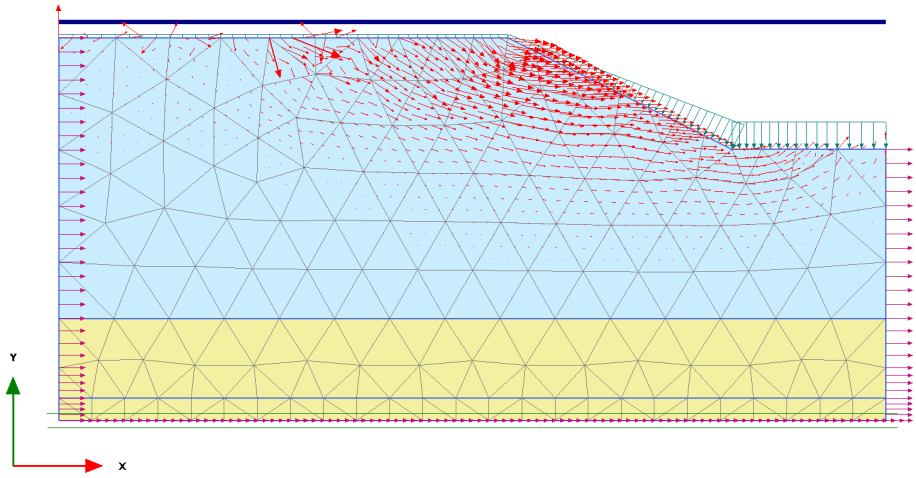

Figure M.2 Displacement Hypoplastic model at t = 43.0 s; maximum displacement is 0.68 m

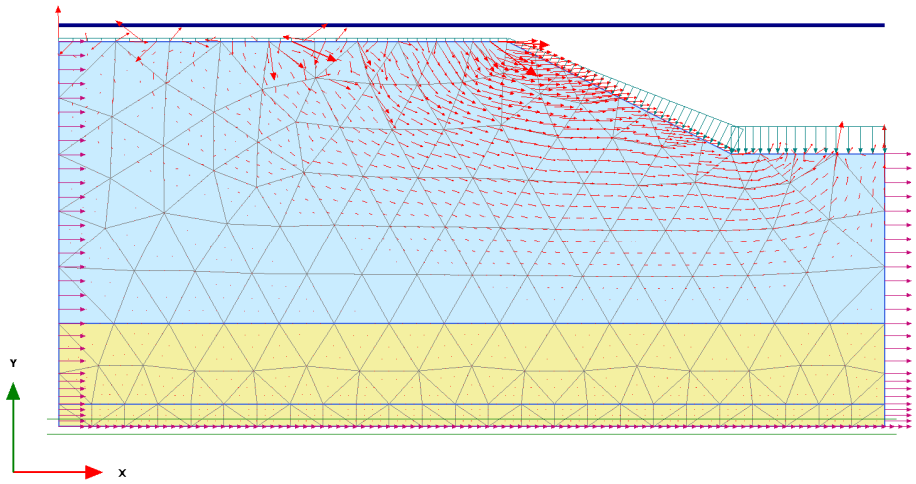

Figure M.3 Displacement Hypoplastic model at t = 45.0 s; maximum displacement is 2.51 m

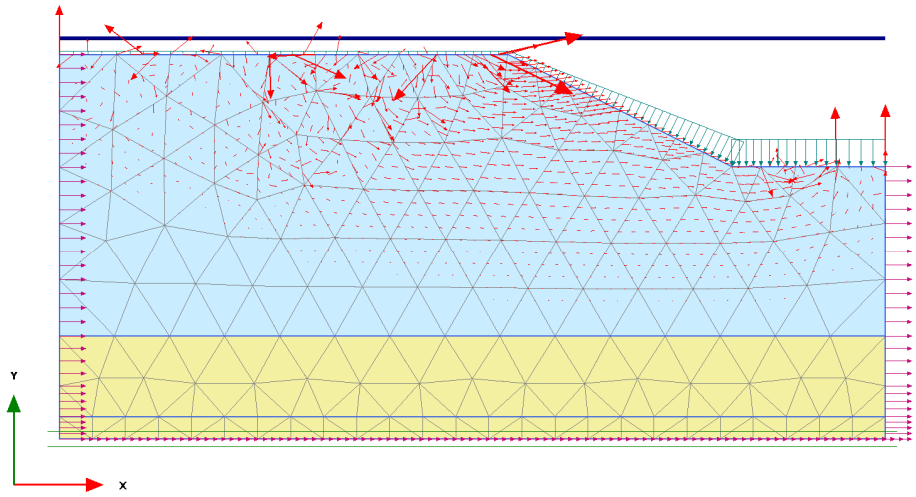

Figure M.4 Displacement Hypoplastic model at t = 50.0 s; maximum displacement is 14.60 m

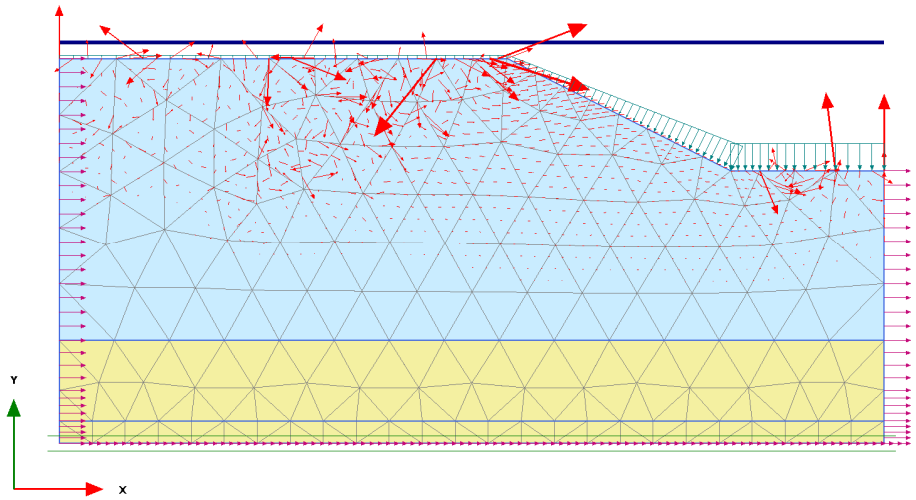

Figure M.5 Displacement Hypoplastic model at t= 55.0 s; maximum displacement is 33.23 m

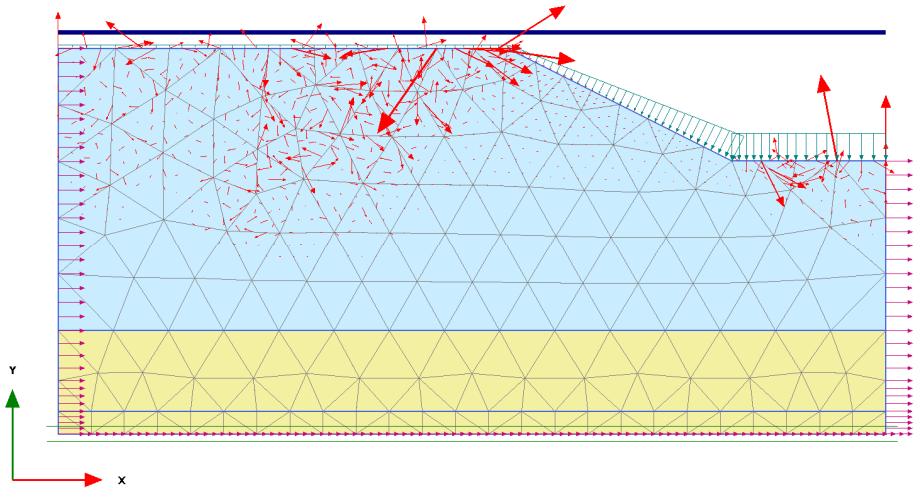

Figure M.6 Displacement Hypoplastic model at t = 70.50 s; maximum displacement is 109.1 m

N Comparison excess pore water pressure development

The figures in this appendix depict the development of the excess pore water pressure that was measured during the centrifuge test (blue line) and modelled by UBC3D-PLM (green line) and Hypoplastic model (red line). The results for the A475 signal are depicted in Figure N.1 to Figure N.3; the results for the A2475 signal are given in Figure N.4 to Figure N.6.

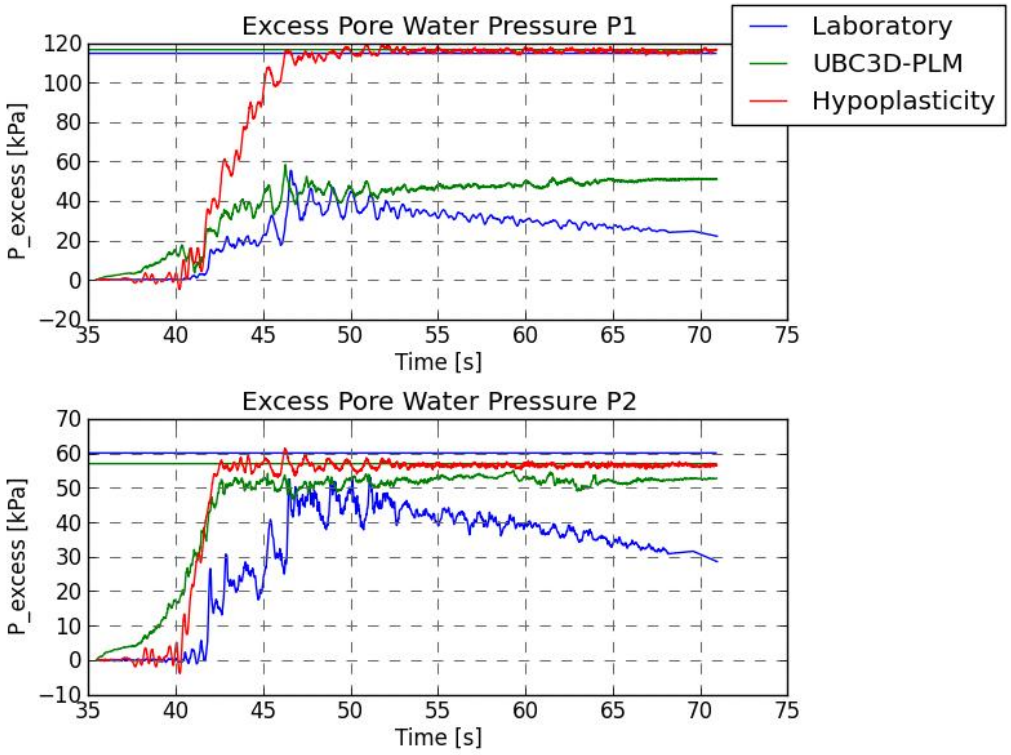

Figure N.1 Comparison excess pore water pressure development in P1 and P2 for A475

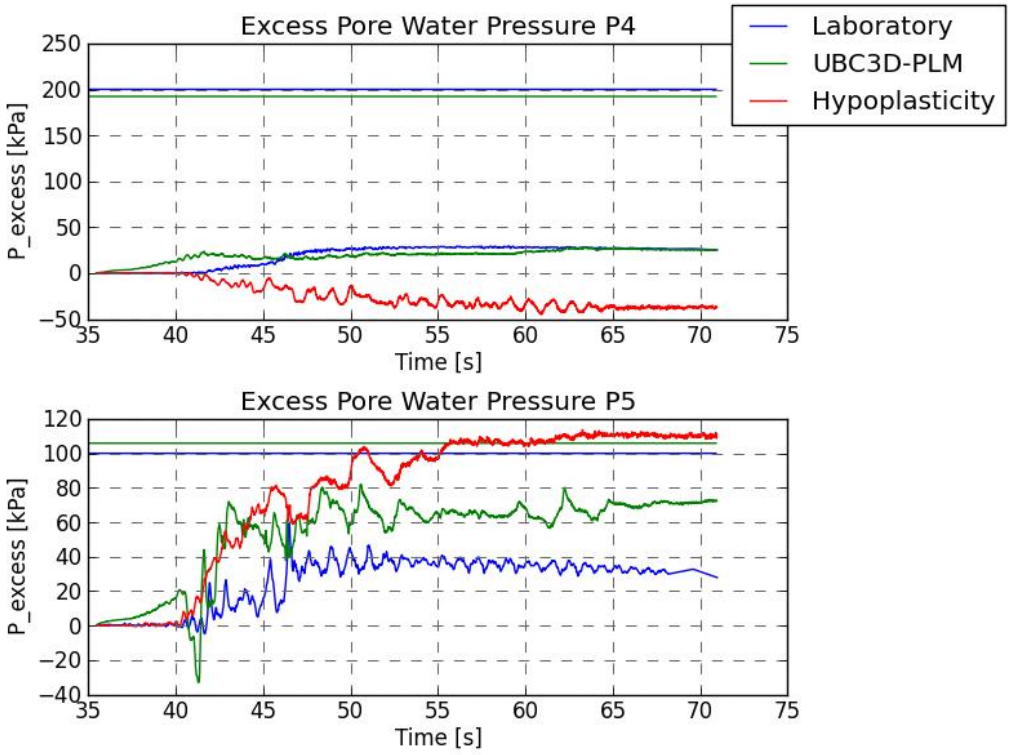

Figure N.2 Comparison excess pore water pressure development in P4 and P5 for A475

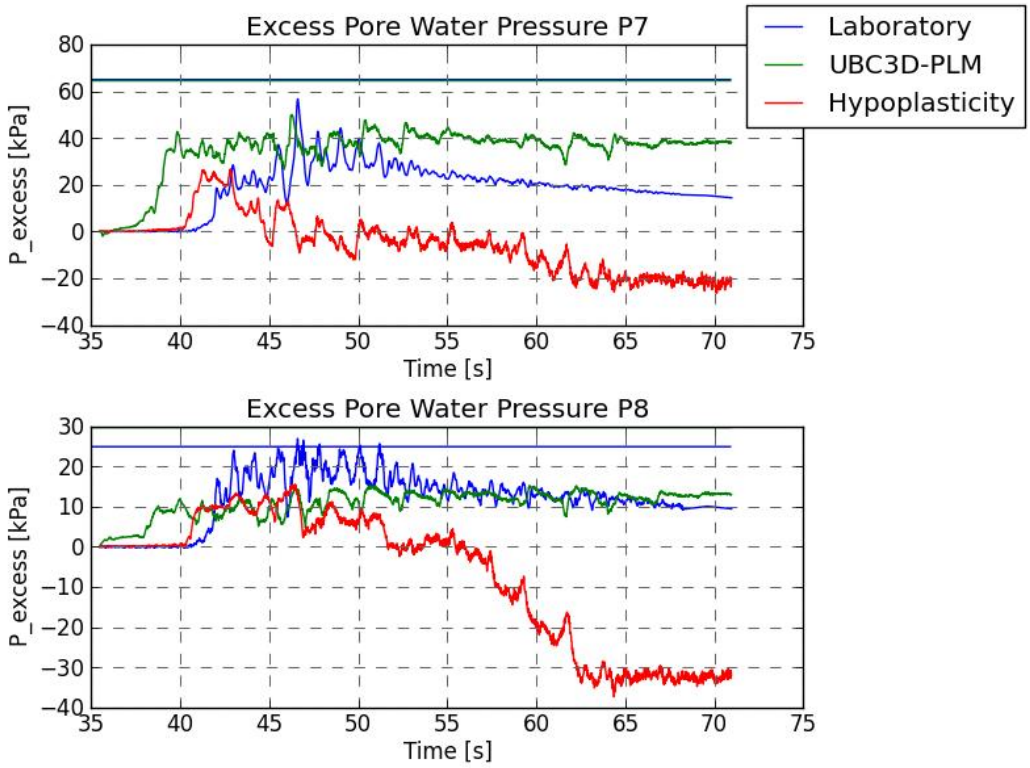

Figure N.3 Comparison excess pore water pressure development in P7 and P8 for A475

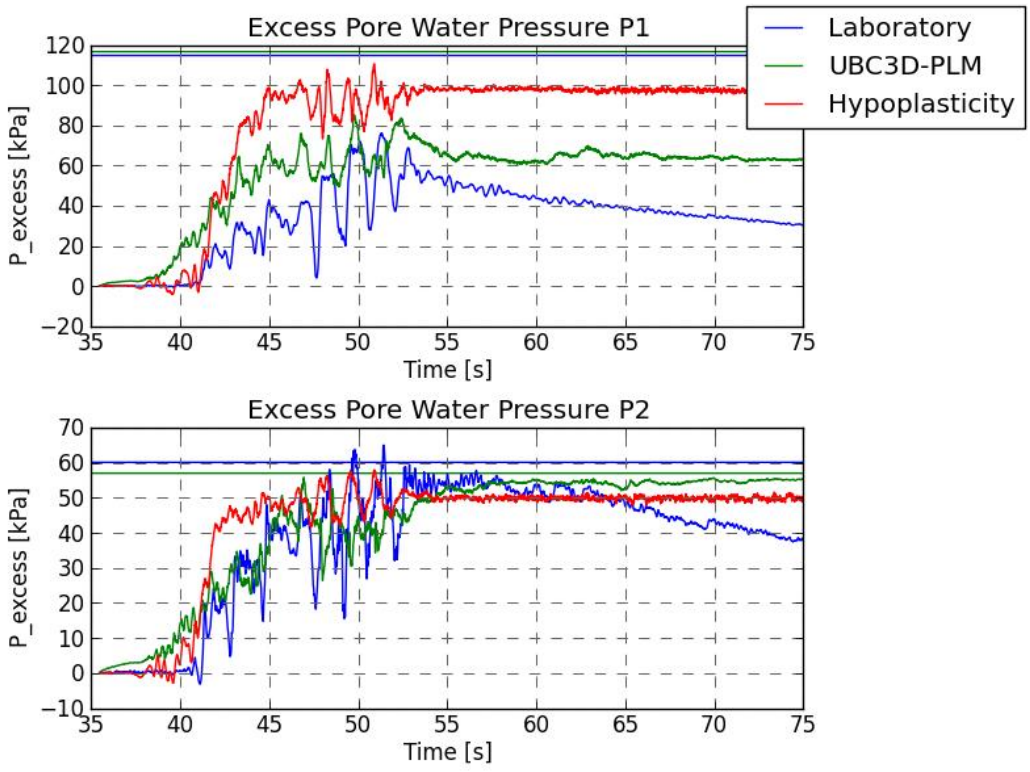

Figure N.4 Comparison excess pore water pressure development in P1 and P2 for A2475

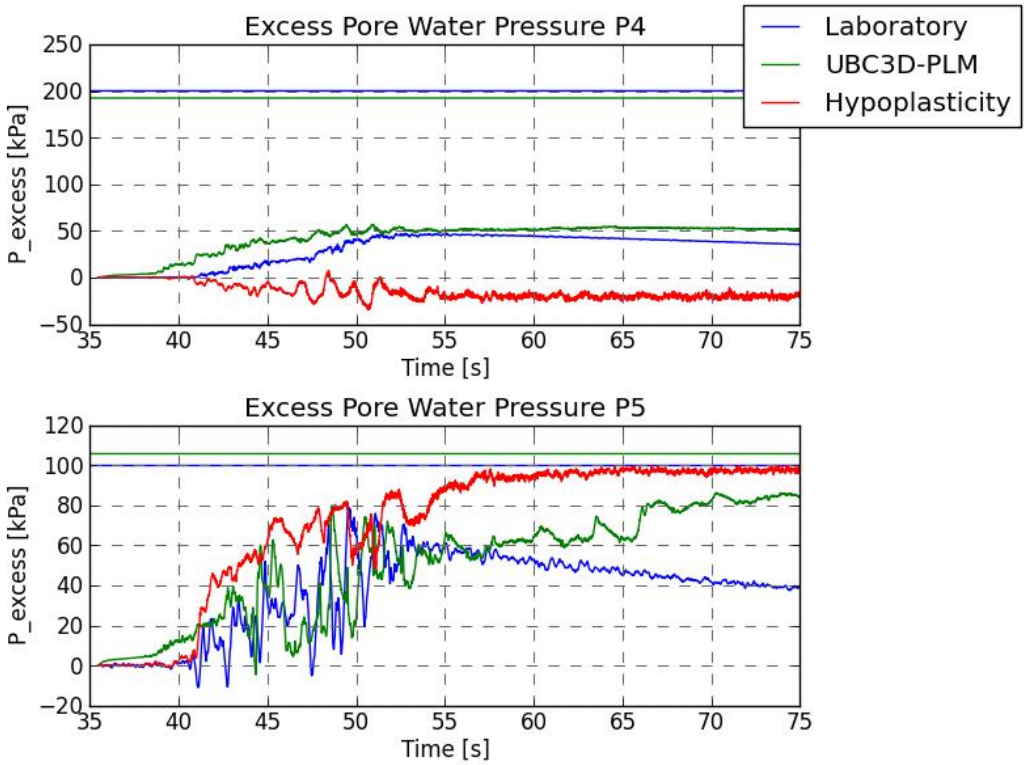

Figure N.5 Comparison excess pore water pressure development in P4 and P5 for A2475

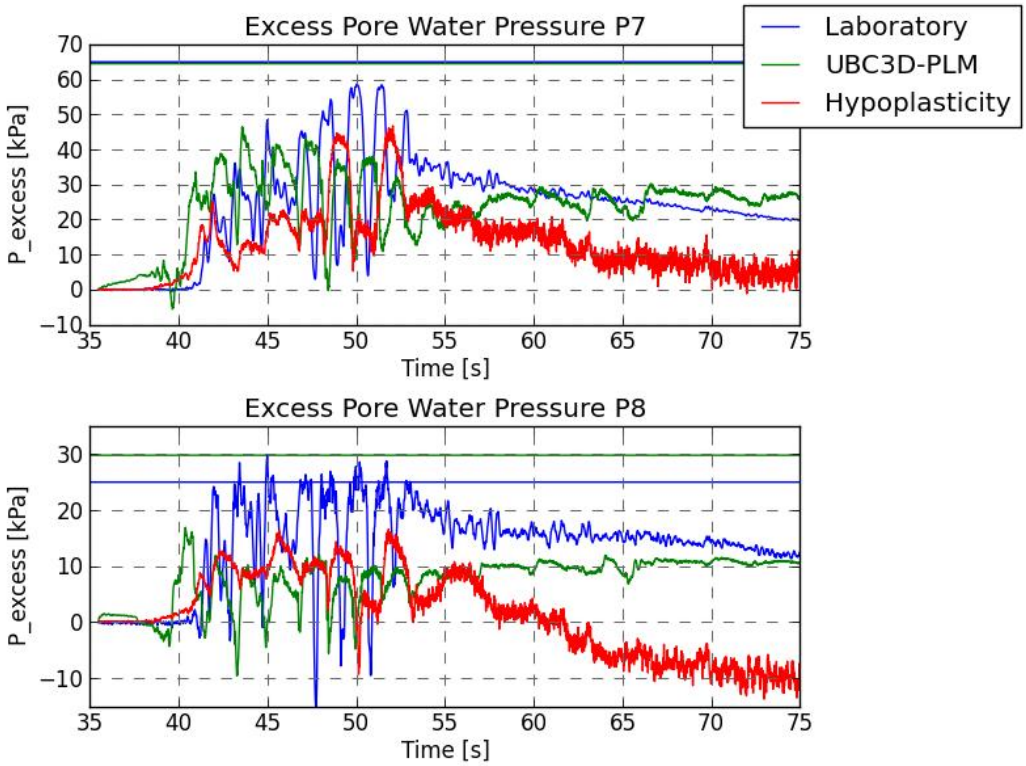

Figure N.6 Comparison excess pore water pressure development in P7 and P8 for A2475

List of Figures

List of Tables

List of Symbols

Symbol	Unit	Description
a	-	Constant for CRR
a	-	Length effect factor
a_g	m/s²	Design value *PGA*
a_{yield}	m/s²	Yield acceleration
b	-	Constant for CRR
c'	kPa	Effective cohesion
C_d	-	Calibration constant for relative density – blowcount relation
c_{red}	kPa	Reduced cohesion
CRR	-	Cyclic Resistance Ratio
CRR_{field}	-	*CRR*, in-situ for two-dimensional shaking
$CRR_{k0\neq1}$	-	*CRR* for anisotropically consolidated specimens
$CRR_{k0=1}$	-	CCR for isotropically consolidated specimens
CRR_{SS}	-	*CRR* from a simple shear test
CRR_{TX}	-	*CRR* from a ICU triaxial test
$CRR_{\sigma'c}$	-	*CRR* of a soil under a specific value of effective consolidation stress σ'_c
$CRR_{\sigma'c=1}$	-	*CRR* of the same soil as used for $CRR_{\sigma'c}$, but then for σ'_c = 1 atm
CSR	-	Cyclic Stress Ratio
c_u	-	Uniformity coefficient
d_{liq}	m	Thickness liquefied layer
d_{top}	m	Thickness top layer (layer between liquefied layer and the dyke)
D_r	%	Relative density
e	-	Void ratio
e_0	-	Initial void ratio corresponding to the zero mean stress
e_{c0}	-	Maximum critical state void ratio
e_{d0}	-	Minimum void ratio
e_{i0}	-	Maximum void ratio
f_{site}	Hz	Site eigen frequency
fac_{hard}	-	Fitting parameter to adjust densification rule
fac_{post}	-	Fitting parameter to adjust post liquefaction behaviour
FC	-	Fine content
F_H	kN	Horizontal design seismic inertia force
FS_{liq}	-	Safety factor against liquefaction
g	m/s²	Gravity acceleration
G	kPa	Shear modulus
h_{dyke}	m	Dyke height

h_s	kPa	Granulate hardness
I	-	Impedance ratio
K	kPa	Maximum bulk modulus
K_0	-	Coefficient of lateral earth pressure at rest
K_α	-	Correction factor, representing the effects of α on the cyclic strength
K_σ	-	Overburden correction factor
k^e_B	-	Elastic bulk modulus number
k^e_G	-	Elastic shear modulus number
k^p_G	-	Plastic shear modulus number
L_j	m	Length typical section for a certain failure mechanism
L_t	m	Length of the considered trajectory
me	-	Elastic bulk modulus power
M_L	-	Local magnitude
M_{max}	-	Maximum magnitude
m_R	-	Material constant
MSF	-	Magnitude Scaling Factor
m_T	-	Material constant
M_w	-	Moment magnitude
n	-	Parameter controlling the curvature in the compression curve
n	-	Porosity
ne	-	Elastic shear modulus power
np	-	Plastic shear modulus power
N	-	Measure for length effect
N	-	Number of loading cycles
$N_{(1,60)}$	-	Corrected blow count
OCR	-	Over Consolidation Ratio
P_a	kPa	Atmospheric pressure
P_c	$year^{-1}$	Centre probability per year
P_d	$year^{-1}$	Design probability per year
P_f	$year^{-1}$	Failure probability per year
P_{req}	$year^{-1}$	Failure probability requirement
p_t	kPa	Shift of the mean stress due to cohesion
PGA	m/s^2 (or g)	Peak Ground Acceleration
PGV	m/s	Peak Ground Velocity
q_{cyc}	kPa	Cyclic deviatoric stress stress
R	-	Parameter controlling the elastic range size (in the strain space)
R_{hyp}	km	Hypocentral distance
R_f	-	Failure ratio

S	-	Soil parameter
T_{piek}	s	Period between peaks for M or *PGA*
$T_{piek,ref}$	s	T_piek for the unscaled accelerogram
T_{site}	s	Site period
u	kPa	Pore water pressure
V_{REF}	m/s	Reference velocity
V_S	m/s	Shear wave velocity
V_{S30}	m/s	Shear wave velocity from 0 to 30 metres below surface level
W	kN	Weight of the sliding mass
x	m	Deformation
α	-	Constant, controls the influence of density on the peak friction angle
α	-	Initial static shear stress ratio
α	-	Ratio of α_g to g
α_a	-	Influence factor earthquake loads
α_g	m/s^2	Design ground acceleration on type A ground
α_H	-	Influence factor hydraulic loads
β	-	Constant, for the void ratio dependence of the stiffness
β	-	Damping ratio
β_{doel}	-	Reliability index (Dutch)
β_{req}	-	Required reliability index
β_{target}	-	Reliability index
β_r	-	Parameter controlling the degradation rate of the stiffness with strain
γ	-	Maximum shear strain
γ^p	-	Plastic shear strain
δ	-	Intergranular strain tensor
Δu	kPa	Excess pore water pressure
ε_v^p	-	Plastic volumetric strain
ρ	kg/m^3	Density
σ	kPa	Soil pressure
σ'	kPa	Effective soil pressure
σ'_{3c}	kPa	Minor effective consolidation stress
σ_t	kPa	Tension cut-off
σ'_{vc}	kPa	Vertical effective consolidation stress
τ	kPa	Shear stress
τ_{cyc}	kPa	Cyclic shear stress
τ_{st}	kPa	Static shear stress
φ	^{o}	Friction angle
φ_c	^{o}	Critical state friction angle

φ'_{cv}	^{o}	Constant volume friction angle
φ'_{p}	^{o}	Peak friction angle
φ_{red}	^{o}	Reduced friction angle
χ	-	Parameter controlling the degradation rate of stiffness with strain
ω	-	Failure probability budget factor

List of Acronyms

Acronym	Full name
CIRIA	Construction Industry Research and Information Association
CPT	Cone Penetration Test
DSS	Direct Simple Shear
EERI	Earthquake Engineering Research Institute
ENW	Expertise Netwerk Waterveiligheid
GMPE	Ground Motion Prediction Equation
KNMI	Koninklijk Nederlands Meteorologisch Instituut
LVDT	Linear Variable Differential Transformers
NAM	Nederlandse Aardolie Maatschappij
NEHRP	National Earthquake Hazards Reduction Program
NGI	Norwegian Geotechnical Institute
NPR 9998	Nationale Praktijkrichtlijn 9998
OI2014	Ontwerpinstrumentarium 2014
SPT	Standard Penetration Test
UBC	University of British Columbia
WTI2006	Wettelijk Toetsinstrumentarium 2006
WTI2017	Wettelijk Toetsinstrumentarium 2017

List of Definitions

Definition	Description
Accelerogram[1]	The recording of the ground acceleration during an earthquake.
Consolidation[3]	Volume change due to dissipation of excess pore pressure from static loads.
Densification[4]	Settlement caused by reconsolidation of the liquefied soil
Drained loading[3]	Loading which is slow enough for the water to drain from the soil as the total stresses increase. Pore pressure will not change, and volume will with loading.
Earthquake[1]	Sudden slip on a fault, and the resulting ground shaking and radiated seismic energy caused by the slip, or by volcanic or magmatic activity, or other sudden stress changes in the earth.
Effective stress[3]	The portion of the total stress that is supported through grain-to-grain contact of the soil. Effective stress = Total stress - Pore water pressure
Elastic deformation[3]	Deformation caused in a soil due to a change in loading, and the soil recovers completely when the load is removed.
Epicentre[1]	The epicentre is the point on the earth's surface vertically above the hypocentre.
Failure[5]	Gradual decline (deterioration) or sudden decline (break) of the structure of a levee or of its foundation, leading to the inability to achieve its function.
Failure probability[2]	The probability that a construction is no longer able to perform its function.
Fault[1]	A fault is a fracture along which the blocks of crust on either side have moved relative to one another parallel to the fracture.
Flood[5]	An inundation (by overflowing or overtopping) that comes from a river, a sea or other body of water and causes or threatens damage.
Flood defence system[5]	An asset that would by its failure increase the likelihood of flooding from any main river and/or the sea to people, property or infrastructure (e.g. levees, flood walls and other raised defences, closure structures, pumping stations).
Homogenous soil[3]	A mass of soil where the soil is of one characteristic having the same engineering and index properties.
Hypocentre[1]	The hypocentre is the point within the earth where an earthquake rupture starts.
Induced earthquake	Earthquakes caused by human activity, like extraction of gas or mining. Induced earthquakes mentioned in this research are related to the extraction of gas in Groningen.
Isotropic[3]	A soil mass having essentially the same properties in all directions. Primarily refers to permeability and stress-strain characteristics.
Liquefaction[1]	A process by which water-saturated sediment temporarily loses strength and acts as a fluid. This effect can be caused by earthquake shaking.
Lithosphere[1]	The lithosphere is the outer solid part of the earth, including the crust and uppermost mantle.
Macro instability	Sliding of soil mass along a slip circle.

Magnitude[1]	The magnitude is a number that characterizes the relative size of an earthquake.
Normal stress[1]	The normal stress is that stress component perpendicular to a given plane. Normal stress can either be compressional or tensional.
P wave[1]	A P wave, or compressional wave, is a seismic body wave that shakes the ground back and forth in the same direction and the opposite direction as the direction the wave is moving.
Peak Base Acceleration	Largest acceleration measured at base level (30 metres depth) during an earthquake.
Peak Ground Acceleration	Largest acceleration measured at surface level during an earthquake.
Piping[5]	The creation of flow channels within a levee or the underlying ground as a result of seepage and continuing internal erosion. Piping can lead to the development of boils or breaches.
Plastic deformation[3]	The distortion of soil resulting in a permanent and irrecoverable change in shape or volume.
Plastic strain[3]	Deformation of soil that is not recovered upon unloading.
Pore pressure[3]	The pressure exerted by the fluid (mostly water) within the pores or voids in a porous material; in saturated soil the pore pressure is the pore water pressure
Pore pressure ratio[3]	At a given depth of soil, the ratio of the pore water pressure to the vertical overburden pressure.
Primary flood defence	Flood defences that are part of a dyke ring; protecting against uncontrolled water levels of seas and rivers.
Residual strength	Remaining strength of a system after failure.
Return period[5]	For a given parameter (e.g. water level), the mean duration between two events where this parameter was observed. Inverse of the probability that a given event will occur in any one year.
S wave[1]	An S wave, or shear wave, is a seismic body wave that shakes the ground back and forth perpendicular to the direction the wave is moving.
Settlement[3]	The downward movement of soil or the downward movement of a foundation.
Shear modulus[3]	The ratio of the change in shear stress to the resulting change in shear strain.
Shear strain[3]	The angular distortion or change in shape of a mass of soil.
Shear strength[3]	The maximum shear stress which a soil can sustain under a given set of conditions.
Shear stress[1]	The stress component parallel to a given surface that results from forces applied parallel to the surface.
Site response	The phenomenon that properties of the earthquake are influenced by shallow soil layers.
Squeezing	Settlement or deformation caused by squeezing of a liquefied layer beneath a dyke
Stiffness[3]	Susceptibility to distortion or volume change under an applied load.
Strain[3]	A measure of the change in size or shape of a mass of soil relative to its original size or shape.

Stress[3]	The intensity of force per unit area; normal stress is applied perpendicularly to a surface or plane, shear stress is applied tangentially to a surface or plane.
Tectonic[1]	Tectonic refers to rock-deforming processes and resulting structures that occur over large sections of the lithosphere.
Total stress[3]	The stress acting on or within a soil mass due to surcharges, overlying weight, etc. Total stress = effective stress + pore water pressure.
Void ratio[3]	The ratio of the volume of voids to the volume of solids (soil grains).

Sources:

1	Earthquake Glossary	(U.S. Geological Survey, s.a.-a)
2	Glossary Hydraulic Engineering Terms	(Delft University of Technology, s.a.)
3	Geotechnical Glossary	(Geotechnical Info .Com, s.a.)
4	EERI Monograph MNO-12	(Idriss & Boulanger, 2008)
5	International Levee Handbook	(CIRIA, 2013)